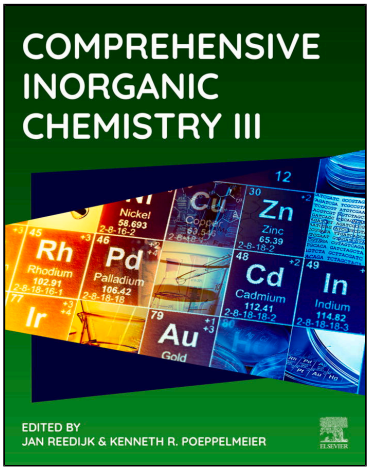

Pauleta, S. R.; Grazina, R.; Carepo, M. S. P.; Moura, J. J. G.; Moura, I. Iron-sulfur clusters – functions of an ancient metal site. In *Bioinorganic Chemistry and Homogeneous Biomimetic Inorganic Catalysis;* Pecoraro, V. L.; Guo, Z.; in Comprehensive Inorganic Chemistry III; Reedijk, J., Poeppelmeier, K. R., Eds.; Vol. 2, pp 105–173. Oxford: Elsevier. ©2023 Elsevier Ltd. ISBN 9780128231531. DOI: B978-0-12-823144-9.00116-3.
ISBN: 9780128231449

2.06 Iron-sulfur clusters – functions of an ancient metal site

Sofia R. Pauleta[a,b], Raquel Grazina[c], Marta S.P. Carepo[c], José J.G. Moura[c], and Isabel Moura[c], [a] Microbial Stress Lab, UCIBIO – Applied Molecular Biosciences Unit, Department of Chemistry, NOVA School of Science and Technology, Universidade NOVA de Lisboa, Caparica, Portugal; [b] Associate Laboratory i4HB - Institute for Health and Bioeconomy, NOVA School of Science and Technology, Universidade NOVA de Lisboa, Caparica, Portugal; and [c] LAQV, REQUIMTE, Department of Chemistry, NOVA School of Science and Technology, Universidade Nova de Lisboa, Caparica, Portugal

Abstract

Iron-sulfur clusters are ubiquitous and ancient prosthetic groups that are present in all kingdoms of life. In the 1960s, they were recognized to play a role in electron-transfer reactions, but since then several other functions were identified, which can be attributed to their flexible coordination and redox properties. In here, the canonical iron-sulfur clusters, as well as the ones with other coordinating ligands will be described. The chapter has also been updated to account for the advances in the knowledge of complex iron-sulfur clusters of nitrogenase and hydrogenases.

In addition, the role of iron-sulfur clusters in metabolic regulation, as sensors of gases (nitric oxide, oxygen), iron and cellular content of iron-sulfur clusters, cellular redox status, and redox cycling compounds, as well as their role in DNA processing enzymes, and their involvement in catalysis of a wide range of reactions will be described.

Iron-sulfur clusters also participate in their biosynthetic and repair pathways. The knowledge in this field as evolved tremendously in recent years, which would require a complete chapter devoted to it by itself, reason why the authors have decided not to include this subject in this chapter.

The chapter is an update of the one published in the previous edition, focusing on the recent advances mostly on the iron-sulfur clusters involved in new catalytic functions, sensor mechanisms and DNA processing.

Comprehensive Inorganic Chemistry III, Third Edition, 2023, 105–173

2.06.1 Introduction

Iron-sulfur clusters are ubiquitous and evolutionary ancient prosthetic groups that are required by all living organisms.[1–4] Their primary role is electron transfer as they can delocalize electron density over both Fe and S atoms.[5,6] Iron-sulfur clusters are the redox-active centers found in ferredoxins, one of the largest classes of electron shuttles in biology, and they are the major components of the photosynthetic and respiratory electron transfer chains as electron wires, defining the electron transfer pathways in many soluble redox enzymes and membrane-bound complexes.[7] Besides this major function, iron-sulfur proteins have a wider role in nature, which includes catalysis of gases, non-redox catalysis (making use of its strong Lewis acid properties to polarize substrate bonds), radical chemistry (in radical-SAM dependent enzymes), regulation of transcription, and nucleic acid metabolism.[3,8,9]

Examples of iron-sulfur proteins involved in direct catalysis, regulation, and DNA processing will be described in Section 2.06.3, 2.06.4 and 2.06.5 of this Chapter, while Section 2.06.2 will focus mainly on the structure and properties of the basic iron-sulfur clusters, unique iron-sulfur clusters and of the organometallic and mixed-metal clusters. These examples show that the field of the iron-sulfur clusters has increased with clusters coordinated by different atoms, from the canonic ligands provided by the sulfur atoms of cysteines, such as nitrogen or oxygen atoms from residue sidechains. In this section is also described the structure of clusters with a higher number of iron atoms (up to 8), that are involved in the catalysis of gases (nitric oxide, nitrogen, hydrogen, and carbon monoxide), as well as sulfite. Some of these complex clusters contain iron and sulfur and other metals, and/or organic molecules.

The authors would like to make a remark that this chapter is a revised and updated version of one published in 2013, but the biosynthesis of iron-sulfur clusters and complex clusters will not be addressed, since in 2020–2021 a series of comprehensive reviews have been published (on their maturation in plants,[10] prokaryotes and eukaryotes, including mammals[11–17]). The main changes in this chapter are related with the recent discoveries on nitrogenase active site, hydrogenases, other catalytic activities, and enzymes involved in nucleic acid metabolism, including transcription regulators.

2.06.2 Type of centers and variability of coordination

2.06.2.1 Basic structures and cluster coordination modes

Iron-sulfur clusters were first detected as electron paramagnetic resonance signatures in mitochondrial membrane proteins,[18] and afterwards in small proteins, such as ferredoxins.[19,20] In few years, many other small iron-sulfur proteins were found and characterized.[21]

During the last decades, several studies implementing X-ray crystallography, mass-spectrometry, chemical synthesis of structural analogs, and several spectroscopic techniques revealed the structural components and the chemical and magnetic properties of the different iron-sulfur clusters.[22–25] The four basic or canonical structures of iron-sulfur clusters can be distinguished by the number of iron and inorganic sulfur atoms as: [1Fe], [2Fe-2S], [3Fe-4S] and [4Fe-4S], which are represented in Fig. 1. In addition, there are larger and complex clusters containing up to eight iron atoms[26,27] or containing other metals (e.g., nickel and molybdenum) besides iron, that will be discussed in Section 2.06.2.2.[26,28]

Relative to the atoms (and residues) that coordinate the iron-sulfur clusters, there is a clear preference for thiolate ligation, with cysteinyl sulfhydryl side chains being the most frequently observed ligands.[23] However, different coordination has been identified and it is in many cases related with the role played by the iron-sulfur cluster in the protein function. The imidazole of histidine and, to a lesser extent, oxygen from aspartate, glutamate, glutamine, or nitrogen from arginine have been observed as ligands (Table 1). The oxygen atom from serine side-chains can also coordinate iron-sulfur cluster in variant proteins, and coordinating cysteines have been substituted by other residues as a mean to study the spectroscopic properties of the iron-sulfur cluster, though in many cases resulted in apo-proteins.[52] In most cases there is two different type of ligands (Table 1), but there is already one report of three different types of ligands coordinating a [2Fe-2S] cluster in RsrR, a redox-sensitive response regulator (see Fig. 4C and Section 2.06.4.2.1.4 and Fi). Thus, it is plausible to hypothesize that different coordination will be identified in the future. This fact increases the difficulty for searching novel iron-sulfur clusters in the genome: (i) diverse and non-canonical coordination motifs are being described, and (ii) other conserved residues, besides cysteines (distantly located in the polypeptide or in different subunits) can coordinate these clusters.

As it will be discussed in the following sections, iron-sulfur clusters can also be coordinated by non-protein ligands, such as water molecules, substrates (e.g., aconitase) or S-adenosylmethionine (in radical SAM enzymes).

As mentioned, iron-sulfur proteins are widespread in the three kingdoms of life and are essential for life. Their prevalence is higher in anaerobic prokaryotic organisms, and in the majority of these organisms they account for around 5% of the genome.[53] Their occurrence decreases to around 2.5% in facultative-anaerobic prokaryotes, and to around 2% in aerobic prokaryotes. In prokaryotes, the most common iron-sulfur clusters bound to proteins are [2Fe-2S] and [4Fe-4S] clusters, with a higher prevalence of [4Fe-4S] clusters. However, the relative abundance of each is dependents on the organism.[53,54]

The genome of eukaryotes encodes a much lower number of iron-sulfur proteins (around 0.4%), with most of these having a universal common ancestor. Another difference is the relative fraction of each type of iron-sulfur cluster, as in these organisms the number of [4Fe-4S] and [2Fe-2S] clusters is similar and they are mainly bound to proteins located in the mitochondria, cytosol, and nucleus.[53]

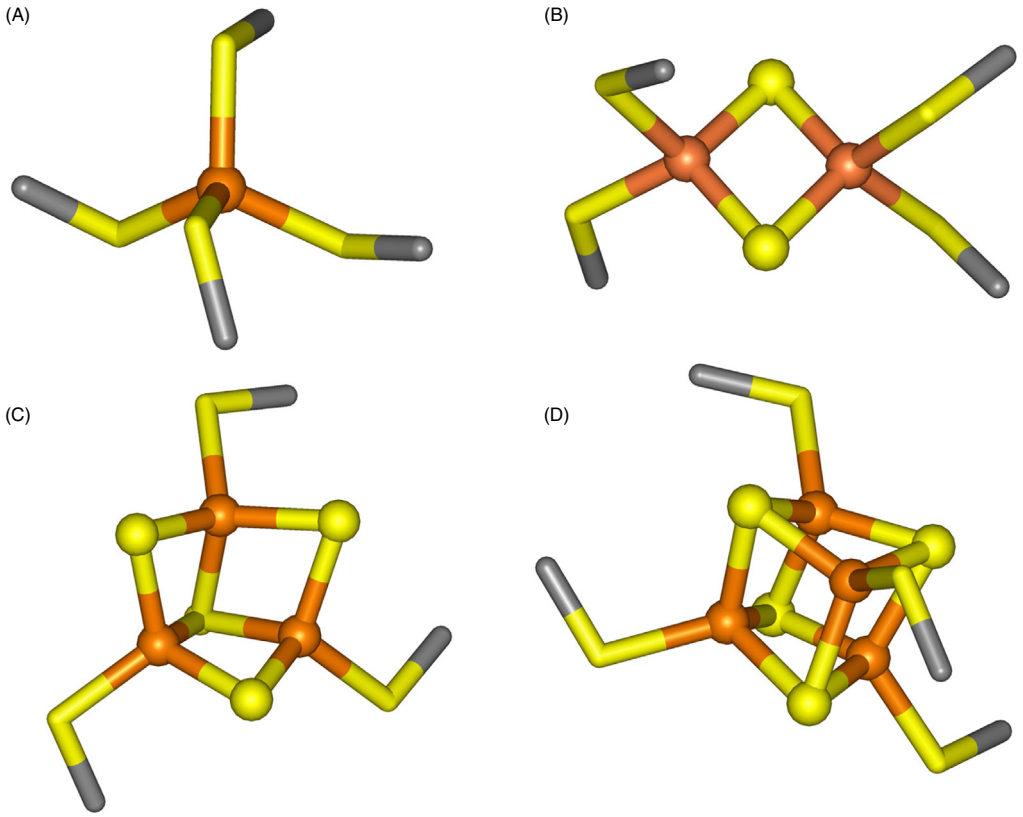

Fig. 1 Structure of the basic iron-sulfur clusters. (A) [1Fe] rubredoxin (PDB ID 7RXN), (B) [2Fe-2S] cluster (PDB ID 1M2A), (C) [3Fe-4S] cluster (PDB ID 6FD1) and (D) [4Fe-4S] cluster (PDB ID 1E2U). The carbon, iron and sulfur atoms are represented as gray, orange, and yellow spheres, respectively. The image was created in Discovery Studio Visualizer (BIOVIA).

2.06.2.1.1 [1Fe] cluster

The [1Fe] cluster can be found in small proteins, named rubredoxins (with approximately 55 residues). This center is unique among iron-sulfur clusters, as it does not bind inorganic sulfur. Rubredoxins have a single iron atom tetrahedrally coordinated by four thiolate ligands (Fig. 1A) provided by two Cys-X_2-Cys segments located in two symmetrically related loops. The reduction potential of the $[1Fe]^{3+/2+}$ couple in rubredoxins is within the -100 to $+200$ mV range (Fig. 2),[55–58] and its spectroscopic properties showed that the metal center in the native state is a high-spin Fe^{3+} ($S = 5/2$) and in the reduced state is a high-spin Fe^{2+} with an integer spin state ($S=2$).[59,60] The absorption spectrum of oxidized rubredoxin is characterized by two absorption bands with a maximum absorbance at 350 nm, 380 nm, and 490 nm, with a shoulder at 570 nm, corresponding to a ligand to metal charge transfer (LMCT) of the sigma orbital. The electron paramagnetic resonance (EPR) spectrum, typical of a high-spin Fe^{3+} center with a large zero-field splitting and high rhombic distortion ($E/D \approx 1/3$, $D > 0$), has a resonance at $g \sim 9.5$ (from the lowest Kramers doublet) and a narrow intense signal at 4.3 (from the middle Kramers doublet).[61]

These proteins are electron shuttles in several metabolic pathways, such as hydrocarbon oxidation, and protection against reactive oxygen species (superoxide and hydrogen peroxide, as electron donors of superoxide reductase and rubrerythrin).[55-57,62,63] These proteins have also been identified in plastids and play a role in electron transfer under certain environmental conditions.

Another small protein that also contains a rubredoxin-type center is the *Desulfovibrio gigas* desulforedoxin.[30,63–66] This protein is a homodimer with each monomer presenting a shortened rubredoxin-like fold with one Cys-X_2-Cys and one Cys-Cys ligand loop. However, this protein is spectroscopically different from rubredoxin, which has been attributed to the distorted tetrahedral geometry of its iron-center due to the presence of two adjacent cysteines.[67]

An interesting property of these small proteins containing the simple [1Fe] center is the possibility of replacing the iron atom by other metals. In the case of rubredoxin its iron atom has been substituted by cobalt, copper, nickel, molybdenum and zinc,[61,68–74] while desulforedoxin iron atom has been replaced by In^{3+}, Ga^{3+}, Cd^{2+} and Hg^{2+}.[75] The metal-substituted rubredoxins and desulforedoxins have been investigated by visible, EPR and NMR spectroscopy.[64,65,76]

A longer rubredoxin has been identified in the aerobe *Pseudomonas oleovorans* and in *Pseudomonas putida*. These 170 residue-long proteins contain two rubredoxin-like domains connected by a linker of 70 residues.[77,78]

The rubredoxin-like center (either the "canonical" or the distorted-type center) has been identified in other proteins, that also bind other metal or non-metal co-factors. Superoxide reductase (named desulfoferrodoxin when was first isolated[79]) contains

Table 1 Examples of proteins containing [1Fe], [2Fe-2S], [3Fe-4S] or [4Fe-4S] clusters and their coordinating residues, with the unusual ligands highlighted in bold.

Protein	*Iron-sulfur coordinating residues*[a]	*References*
[1Fe]		
Rubredoxin	Cys6 Cys9 Cys39 Cys42	29
Desulforedoxin	Cys9 Cys12 Cys28 Cys29	30
Desulfoferrodoxin	Cys9 Cys12 Cys28 Cys29	31
NarE	**His46 His57** Cys67 Cys128	32
[2Fe-2S]		
Plant-and vertebrate-type ferredoxin	Cys41 Cys46 Cys49 Cys79	33
Aldehyde oxidoreductase	Cys40 Cys45 Cys48 Cys60 Cys100 Cys103 Cys137 Cys139	34
Ferrochelatase[b]	Cys196 Cys403Cys406 Cys411	35
Biotin synthase	Cys97 Cys128 Cys188 **Arg290(N$^{\eta}$)**	36
Rieske-type protein	Cys140 **His142(N$^{\delta}$)** Cys170 **His173(N$^{\delta}$)**	37
mitoNEET[b]	Cys72 Cys74 Cys83 **His87(N$^{\delta}$)**	38
RsrR	**Glu8(O$^{\varepsilon}$) His12(Nε)** Cys90 Cys110	39
[3Fe-4S]		
3Fe Ferredoxin	Cys8 Cys14 Cys50	40
7Fe Ferredoxin	Cys8 Cys16 Cys49	41
Aconitase	Cys358 Cys421 Cys424	42
[NiFe]-Hydrogenase[c]	Cys228 Cys246 Cys249	43
[4Fe-4S]		
4Fe Ferredoxin	Cys8 Cys11 Cys14 Cys50	44
4Fe Ferredoxin (*Pyrococcus furiosus*)	Cys12 **Asp15(O$^{\delta}$)** Cys18 Cys57	45
8Fe Ferredoxin (2 × [4Fe-4S])	Cys8 Cys11 Cys14 Cys47 Cys18 Cys37 Cys40 Cys43	46
HiPIP	Cys41 Cys46 Cys61 Cys75	47
Hybrid cluster protein[d]	Cys3 Cys6 Cys15 Cys21	48
[NiFe]-Hydrogenase[e]	**His185(N$^{\delta}$)** Cys188 Cys213 Cys219	43
[FeFe]-Hydrogenase[e]	**His94(N$^{\varepsilon}$)** Cys98 Cys101 Cys107	49
Dihydropyrimidine dehydrogenase[b]	Cys91 Cys130 Cys136 **Gln156(O$^{\varepsilon}$)**	50
IspG	Cys265 Cys 268 Cys 300 **Glu307(O$^{\varepsilon}$)**	51

[a]The residue numbering in the ligation mode is related with the protein in the reference. Proteins from other sources can present different coordination motifs.
[b]These proteins have only been identified in eukaryotes.
[c]This protein contains two additional [4Fe-4S] clusters, one of them is represent in this table and presents an unusual coordination motif.
[d]This protein also contains an unusual iron-sulfur cluster.
[e]These proteins contain more than one [4Fe-4S] cluster, but in here it is only represented the one with the unusual coordination mode. HiPIP - high potential iron protein.

a distorted rubredoxin-type center (as the one found in desulforedoxin).[31] In addition to this center, it contains a single non-heme iron center, the active center, that is coordinated by four histidine residues and one cysteine ligand in a square pyramidal geometry.[31,80]

Rubrerythrin, similarly to superoxide reductase, is a non-heme iron enzyme, involved in reduction of hydrogen peroxide. This enzyme is a dimer with each monomer being a four-helix bundle, with a diiron-oxo center in the middle, and a rubredoxin-like center in the C-terminus.[81]

A rubredoxin-type center has also been identified as an additional domain in some classes of flavodiiron proteins.[82] These enzymes, constituted by a two-domain core harboring a diiron center and a FMN (flavodoxin domain), are proposed to have oxygen, nitric oxide, and hydrogen peroxide reductase activities.[83,84]

2.06.2.1.2 [2Fe-2S] cluster

The proteins belonging to this class constitute a large family with several subgroups.[85] The plant-type ferredoxins, that coordinate a [2Fe-2S] cluster (Fig. 1B), are electron carriers between photosystem I and several enzymes. The vertebrate (e.g., adrenodoxin) and

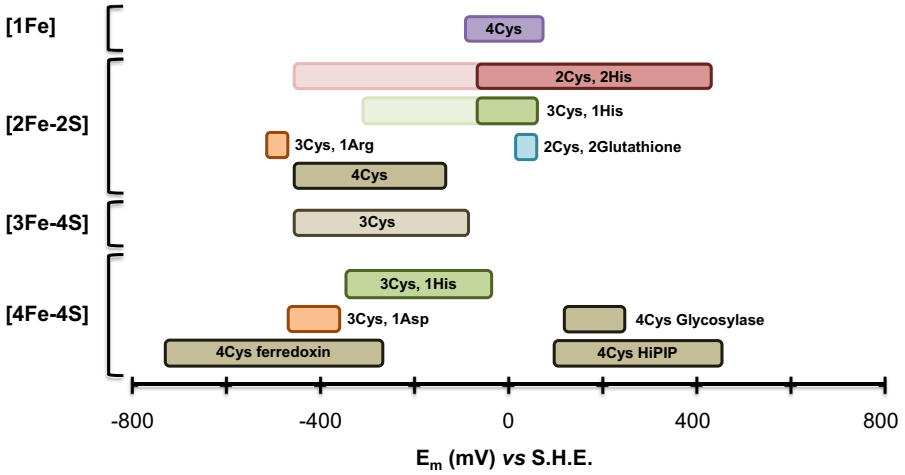

Fig. 2 Reduction potentials observed for the different type of iron-sulfur clusters. The shaded region indicates the potential range observed for those clusters in pH dependence experiments. Adapted from Bak, D. W.; Elliott, S. J., Alternative FeS Cluster Ligands: Tuning Redox Potentials and Chemistry. *Curr. Opin. Chem. Biol.* **2014**, *19*, 50–58.

bacterial (e.g., putidaredoxin) ferredoxins transfer electrons to hydroxylating enzymes, which are usually P450 cytochromes.[86] Another group include the [2Fe-2S] ferredoxins involved in the biosynthesis of iron-sulfur clusters (ISC machinery),[3,87] and the XylT-type [2Fe-2S] ferredoxin implicated in the activation of some oxygenases.[88] Other [2Fe-2S] ferredoxins have been isolated from hyperthermophile *Aquifex aeolicus*[89] and halobacteria.[90]

The biotin synthase (SAM enzyme) also contains a [2Fe-2S] cluster that is involved in sulfur donation for the conversion of dethiobiotin to biotin during a single catalytic turnover (this enzyme and the role of the iron-sulfur cluster will be further discussed in Section 2.06.3.1.1.2). In this protein the binding motif of the [2Fe-2S] cluster is atypical, as it includes a nitrogen atom from an arginine side chain (Table 1 and Fig. 4D).[36,91,92]

Another curious example of [2Fe-2S] proteins is the mammalian ferrochelatase,[35] the terminal enzyme of heme biosynthesis. The observation that the cluster is vital for activity and it is readily degraded by NO but it is not present in most of the equivalent bacterial enzymes, has led to the suggestion that it is part of a defense mechanism that prevents the infecting organism from using the heme synthesized by the host.[93]

The plant and vertebrate [2Fe-2S] ferredoxins are globular proteins (of approximately 100 residues), with the cluster located near the surface, but protected by a long loop that has three of the four coordinating cysteine residues.[33,86,88,90,94] The opposite side of the protein consists of a four-stranded β-sheet covered by an α-helix, that together form a ubiquitin-like fold known as the β-grasp.[95]

The [2Fe-2S] cluster can exist in two oxidation states that differ by a single electron, $[2Fe\text{-}2S]^{2+}$ and $[2Fe\text{-}2S]^{1+}$. The reduction potential of this redox pair ranges from - 420 to - 250 mV (Fig. 2), revealing the high reducing nature of these clusters.[1] In the two oxidation states of the [2Fe-2S] cluster, the formal oxidation state of the two iron atoms are localized, being Fe^{3+}-Fe^{3+} and Fe^{3+}-Fe^{2+}, as represented in Fig. 3A.

In the all-ferric state, $[2Fe\text{-}2S]^{2+}$, the two Fe^{3+} are antiferromagnetically coupled, since the spins of the five *d* electrons on the two iron atoms are oppositely aligned, so that their pairing produces an effective $S = 0$, diamagnetic ground state (EPR silent). In the reduced form, $[2Fe\text{-}2S]^{1+}$, the iron atoms have localized valences ($S = 5/2$ (Fe^{3+}) and $S = 2$ (Fe^{2+})) and are antiferromagnetically coupled, leaving one net unpaired spin (with a $S = 1/2$ ground state). The EPR signal has *g* values around 1.88, 1.94 and 2.04.

These proteins have a characteristic dark-brown color and an absorption spectrum with maxima at around 330 nm, 420 nm, 460 nm, with a shoulder at 560 nm, corresponding to metal to ligand charge transfer bands.[96] The circular dichroism (CD) spectrum of the oxidized state of [2Fe-2S] proteins presents positive bands at 420 nm and 460 nm, while in the reduced state there are negative bands at 440 nm and 510 nm.[96,97] The resonance Raman spectra of these proteins have a few vibration modes in the low frequency region (in both oxidized and reduced state).[97,98]

2.06.2.1.2.1 Rieske proteins

The Rieske proteins are considered a subclass of the [2Fe-2S] proteins. The Rieske clusters were first discovered and characterized as subunits of respiratory and photosynthetic complexes, as well as in small electron transfer proteins, such as ferredoxins.[99,100] These proteins contain a [2Fe-2S] center that is coordinated by nitrogen atoms from the imidazole moiety of two histidine sidechains (Fig. 4A), instead of the usual four cysteinyl sulfhydryl.

The basic structural framework of Rieske proteins (with approximately 120 residues) consists of three stacked β-sheets, of which the upper one includes the two ligand loops holding the [2Fe–2S] cluster.[99,101] These two loops contain one cysteine and one histidine ligand each and are interconnected by a disulfide bond, which contributes significantly to the stability of the protein. The iron

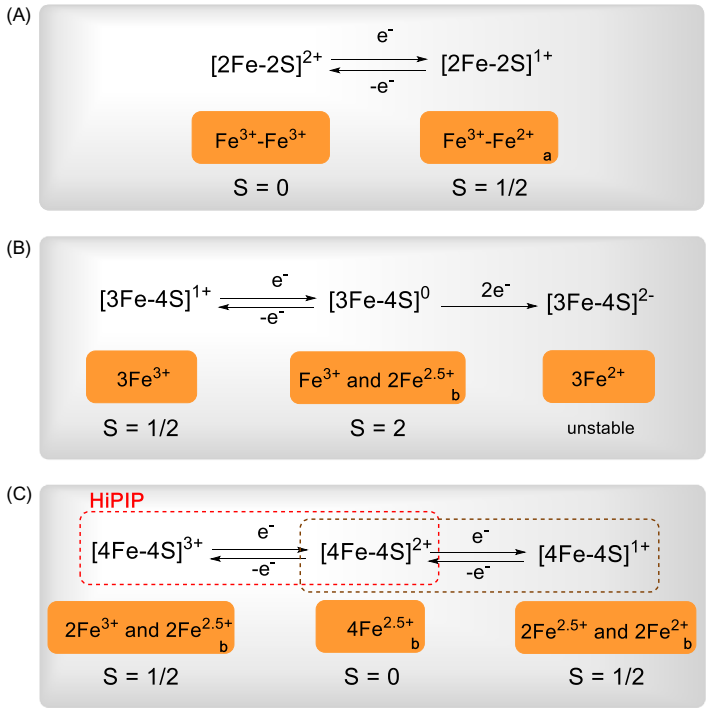

Fig. 3 The most usual oxidation states and respective spin states of the canonical iron-sulfur clusters: (A) [2Fe-2S] cluster, (B) [3Fe-4S] cluster, and (C) [4Fe-4S] cluster. In (C) the usual redox pair is highlighted by a dotted brown line and the redox pair of HiPIP is highlighted by a dotted red line. Legend: a – iron atoms with localized valences and b – iron atoms with delocalized valences with a formal charge of 2.5+.

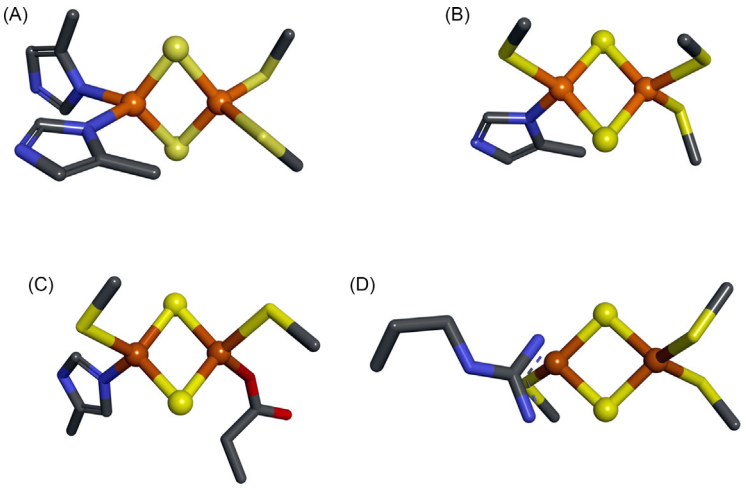

Fig. 4 Structure of the [2Fe-2S] clusters with non-canonical coordination. (A) Rieske center (PDB ID 3h1J), (B) mitoNEET center (PDB ID 3EW0), (C) [2Fe-2S] cluster in RsrR (PDB ID 6HSE) and (D) [2Fe-2S] cluster in biotin synthase (PDB ID 1R30). The carbon, iron, nitrogen, oxygen, and sulfur atoms are represented as gray, orange, blue, red, and yellow, respectively. The image was created in Discovery Studio Visualizer (BIOVIA).

atom closer to the surface has two solvent-exposed histidine ligands and the other iron is bound to two buried cysteine residues.[99,101]

The oxidation states of [2Fe–2S]-Rieske cluster are the same as the ones of [2Fe–2S] plant-type ferredoxins, $[2Fe–2S]^{2+/1+}$ (Fig. 3A), but the histidine coordination causes an increase in the reduction potential. Therefore, many Rieske proteins present positive reduction potentials (−100 to +400 mV)[102] (Fig. 2). Moreover, as this cluster is coordinated by histidine sidechains, the reduction potential is pH dependent above pH 8. The pH profile has a slope of −120 mV/pH and is explained by two pKa values in the oxidized state (at 7.8 and 9.6) and one in the reduced state (at 12.5).[103,104] This pH dependence was also observed in the visible and CD spectra.[103]

The visible spectrum of Rieske proteins has absorption maxima at 325 nm and 460 nm with a shoulder at 560–580 nm. The CD spectra is quite unique, with two positive bands (310 nm and 350 nm) and a negative band at 375–380 nm, in the oxidized state, whist in the reduced state it has a positive band at 314 nm and a negative band at 385 nm and 500 nm.[105] The EPR spectrum has a rhombic signal, but it varies significantly between proteins with g_x of 1.72–1.834, g_y of 1.888–1.92 and g_z of 2.008–2.042.[105] Electron nuclear double resonance (ENDOR), electron spin echo envelope modulation and hyperfine sublevel correlation (HYSCORE) experiments have also been used to characterize this cluster and to confirm the histidine coordination.[105,106]

Both oxidation states of Rieske proteins have been characterized by resonance Raman. The spectra show only small differences with shifts in the vibration modes, and when compared with the resonance Raman spectra of other [2Fe-2S] proteins, the spectra presents additional vibration modes corresponding to the histidine ligands (260–261 cm^{-1} Fe-His bending mode, weak peak at 266–270 cm^{-1} Fe^{3+}-His stretching mode).[107,108] These spectra have also more bands in the 250–450 cm^{-1} regions as these clusters are less symmetric then the [2Fe-2S] clusters. The resonance Raman spectra also show a pH dependence but only at values above the pKa of the second histidine, which warrants a rapid proton-coupled electron transfer at physiological pH.[108]

2.06.2.1.2.2 NEET proteins

The mitoNEET (*cisd1*), NAF-1/Miner1 (*cisd2*) and MiNT/Miner2 (*cisd3*) belong to the NEET family of iron-sulfur cluster binding proteins that are involved in iron homeostasis and response to reactive oxygen species (ROS) in eukaryotes.[109–111] In humans, these proteins have also been associated with the proliferation of cancer cells.[111] These proteins have in common a CDGSH domain, and a C-terminal sequence Asn-Glu-Glu-Thr (that gave their name NEET) and bind a [2Fe-2S] cluster coordinated by 3 cysteines and a histidine residue (**Table 1** and **Fig. 4**B), that is redox active and labile.

MitoNEET and NAF-1 are homodimers found in the outer membrane of the mitochondria, and NAF-1 has also been found in the endoplasmic reticulum, while MiNT is co-localized with the mitochondria. MitoNEET and NAF-1 are bound to the membrane by one N-terminal transmembrane helix and have a common fold.[112]

The CDGSH domain was also found in both bacteria and archaea, but in this case the proteins are monomeric and present two of these domains. The plant homolog (At-NEET) has also a N-terminal transmembrane domain and a single CDGSH domain. The NEET-fold is composed by a cluster binding domain and β-cap domain. The CDGSH domain comprises the cluster binding domain that harbors the [2Fe-2S] cluster. The coordinating histidine is solvent accessible, which has been proposed to confer lability to this iron-sulfur cluster.

These proteins present an absorption spectrum with absorption bands with maxima at 340 nm (8.5 mM^{-1} cm^{-1}), 460 nm (5 mM^{-1} cm^{-1}) and a less intense band at 530 nm (4 mM^{-1} cm^{-1}),[109,113] in the oxidized state, while in the dithionite-reduced spectrum these bands lose intensity. This cluster was shown to be redox active as upon exposure to molecular oxygen, the absorption bands recover the initial intensity. MitoNEET [2Fe-2S] cluster is EPR silent in the oxidized state, while in the reduced state its EPR spectrum, acquired in Ka-band at a microwave frequency of 31 GHz, has a rhombic signal with *g* values of 2.007, 2.937 and 1.897.[114] The X-band EPR spectrum showed splitting in g_y and g_z, which was explained by a magnetic-dipolar interaction between the two iron-sulfur clusters in the homodimer.[114] This interaction was not observed in the first preparations and EPR studies of this protein because the samples were not fully reduced.[109]

The resonance Raman spectrum shows a pH dependence between 6.2 and 8.0, consistent with protonation of the coordinating histidine, and it is characterized by intense vibrational modes at 330 cm^{-1}, 347 cm^{-1}, 394 cm^{-1}, and less intense modes at 267 cm^{-1}, 284 cm^{-1}, and 293 cm^{-1} (associated with the coordinating histidine), that are sensitive to pH and phosphate binding.[115]

The reduction potential of mitoNEET was estimated to be 0 mV, at pH 7.0[116,117] (**Fig. 2**) and has a pH dependence with a slope of −40 mV/pH. Different models were used to adjust the data, but in all these models the pKa of the coordinating histidine was determined to be around 7.[117,118]

Proteins involved in iron metabolism and biogenesis of iron-sulfur clusters (cluster transfer and repair) have iron-sulfur clusters coordinated by histidine residues.[13] One of these is the heterodimeric complex Grx3/4-Bol2, that binds a [2Fe-2S] cluster. The Grx homodimer coordinate a bridging [2Fe-2S] cluster through a cysteine residue in each monomer (found in the conserved CGFS sequence motif) and two glutathione molecules. Upon formation of the heterocomplex Grx3/4-Bol2, the [2Fe-2S] cluster locates in the interface between the two proteins and is coordinated by one histidine and one cysteine from Bol2 (previously known as Fra2) and two cysteines from Grx.[119]

2.06.2.1.3 [3Fe-4S] cluster

The existence of a [3Fe-4S] cluster (**Fig. 1**C) was first recognized in ferredoxin I from the anaerobic nitrogen fixing bacterium *Azotobacter vinelandii*, which is a seven iron (7Fe) ferredoxin that contains, besides the [3Fe-4S] cluster, a [4Fe-4S] cluster.[120] In parallel with this discovery, two other proteins played an important role in the identification and understanding of the nature of the [3Fe-4S] cluster: *D. gigas* ferredoxin II and aconitase (see **Section 2.06.3.2.1**). Several spectroscopic studies on these proteins clearly showed that they should contain a cubic [3Fe-4S] cluster[121–126] (**Fig. 1**C).

However, the first structure determined for *A. vinelandii* ferredoxin I erroneously modeled this center as being an almost planar cyclic [3Fe-3S] core.[127] The controversy around the existence of a [3Fe-4S] cluster was later resolved with the reevaluation of *A. vinelandii* ferredoxin I crystal structure[128] and the determination of the crystal structure of *D. gigas* ferredoxin II at 1.7 Å resolution.[129]

The presence of a [3Fe-4S] cluster was later identified in other ferredoxins and in several enzymes, such as succinate dehydrogenase,[130] fumarate reductase,[131] nitrate reductase,[132] glutamate synthase,[133] and [NiFe] hydrogenases.[134]

The magnetic and electronic properties of the [3Fe-4S] cluster, in the +1 and 0 oxidation states, have been extensively explored by several spectroscopic (e.g., EPR and Mössbauer,[121,124] magnetic circular dichroism (MCD),[125] extended X-ray absorption fine structure (EXAFS),[135] resonance Raman[98]) and electrochemical[136] techniques. In the oxidized state, $[3Fe\text{-}4S]^{1+}$, the cluster presents three high-spin ferric atoms (Fig. 3B), which are spin coupled to form an $S = 1/2$ state and exhibits an almost isotropic EPR signal centered around $g = 2.02$. Reduction of the cluster by one electron yields a $[3Fe\text{-}4S]^{0}$ with an integer spin ($S=2$), but the Mössbauer spectrum revealed the presence of two quadrupole doublets with an intensity ratio of 2:1. This suggested that the reduced state involved a coupled, delocalized Fe^{2+}-Fe^{3+} unit responsible for the outer doublet, with a single Fe^{3+} unit responsible for the inner doublet with half the intensity. In the couple Fe^{2+}-Fe^{3+}, the two iron atoms are formally in a $Fe^{2.5+}$ oxidation state (Fig. 2B).

The reduction potential of the redox pair $[3Fe\text{-}4S]^{1+}/[3Fe\text{-}4S]^{0}$ depends on the protein, varying between −460 and − 70 mV[137] (Fig. 2). Using electrochemical techniques, it was observed that the $[3Fe\text{-}4S]^{0}$ cluster of *D. gigas* ferredoxin II can accept two additional electrons attaining a $[3Fe\text{-}4S]^{2-}$ oxidation state (Fig. 3B). This state is only possible to attain at very low reduction potentials (*ca.* -690 mV), at an electrode surface, and it was proposed that the three iron atoms are unusually in the ferrous state.[136] This all-ferrous state was also observed for the *Pyrococcus furiosus* ferredoxin[138] and for the [3Fe-4S] cluster of the *Desulfovibrio africanus* 7Fe ferredoxin III.[139]

The [3Fe-4S] cluster is coordinated by two cysteines in a Cys-X_2-Y-X_2-Cys motif with a more remote -CysPro- providing the third cysteine ligand[137] (Table 1). In *P. furiosus* ferredoxin, Y is an aspartate, which coordinates the fourth iron atom.[45,140,141] In fact, this ferredoxin is isolated with a [4Fe-4S] cluster that can be converted to a [3Fe-4S] cluster. On the contrary, *Desulfovibrio alaskensis* G20 7Fe ferredoxin is isolated with a [3Fe-4S] that can be converted to a [4Fe-4S] center.[142]

Another [3Fe-4S] cluster protein that has been extensively characterized is *D. gigas* ferredoxin II,[129,143] which has a cysteine as the Y residue, coordinating the labile Fe atom in the [4Fe-4S] cluster of these ferredoxins.[141,144] *D. gigas* ferredoxin II can also be isolated with a [4Fe-4S] cluster, and it was designated as ferredoxin I.[136,145] The two ferredoxins differ in their reduction potentials and appear to have different metabolic functions in this bacterium.[145] Moreover, the two clusters proved to be interconvertible, as when ferredoxin I is oxidized it leads to ferredoxin II, and the treatment of ferredoxin II with iron salts in a reducing environment leads to ferredoxin I (see Section 2.06.2.1.5).

Although [3Fe-4S] clusters have been identified in some proteins, these clusters are rare when compared with the ubiquitous [2Fe-2S] and [4Fe-4S] clusters that are present in the three kingdoms of life.[137] However, in contrast with the [2Fe-2S] and [4Fe-4S] clusters, all the available evidence indicates that biologically relevant [3Fe-4S] clusters are coordinated exclusively by cysteine residues (Table 1).

2.06.2.1.4 [4Fe-4S] cluster

Historically, within this group a strong distinction has been made between ferredoxins with a negative reduction potential (−700 to −150 mV),[24] and the ones with a positive reduction potential (+100 to +450 mV) (Fig. 2), which are named *H*igh *P*otential *I*ron *P*roteins (HiPIPs).[146] The HiPIPs have been isolated mostly, but not exclusively from photosynthetic bacteria,[114] although their physiological role has only been well-established in photosynthetic pathways.[147,148]

The [4Fe-4S] clusters are found in numerous microbial, plant, and mammalian redox enzymes, including nitrate reductase,[132] sulfite reductase,[149] trimethylamine dehydrogenase[150] and hydrogenases.[151]

The first suggestion for the presence of a [4Fe-4S] cluster (Fig. 1D) in a protein occurred in 1968, when a 4 Å resolution crystallographic study indicated the presence of a potentially tetrahedral [4Fe-4S] cluster in the HiPIP from *Allochromatium vinosum* (formely *Chromatium vinosum*).[152] This fact was only clearly established in 1972, with the high-resolution structure of both *A. vinosum* HiPIPs.[153] Moreover, the structures of both oxidized and reduced HiPIP have been determined, revealing that the [4Fe-4S] cluster remained intact during the redox interconversion.[154] Later, other [4Fe-4S] clusters were identified in several crystallographic studies, such as in *A. vinelandii* ferredoxin I (that also harbors a [3Fe-4S] cluster[155]), and in the active form of aconitase.[42]

The [4Fe-4S] clusters are usually bound to the polypeptide chain by four cysteine residues, as shown in Table 1. The protein ligands of these clusters are arranged in a particular motif, since three of the iron atoms are bound to almost adjacent cysteines (Cys-X_2-Cys-X_2-Cys), while the fourth iron atom is bound to a cysteine from a distant portion of the polypeptide chain.[4] The binding of a given cluster by cysteine residues from different segments of the polypeptide chain apparently helps stabilizing the tertiary structure of the protein.[156] Besides cysteines, the [4Fe-4S] cluster can be coordinated by other residues, as shown in Table 1 (e.g., [NiFe][43] and [FeFe] hydrogenases,[49] dihydropyrimidine dehydrogenase,[50] only found in eukaryotes, and IspG[51]).

The thiocubane unit can exist in at least three stable oxidation states (Fig. 2C). This so-called three-state model[1,153,157] contrasts significantly with the previously described clusters, in which only two stable oxidation states are observed. It is important to point out that, in strong contrast with the [2Fe-2S] clusters, and similarly to $[3Fe\text{-}4S]^{0}$, the valence electrons are delocalized in the [4Fe-4S] clusters (Fig. 3C). The three oxidation states that can be attained are: $[4Fe\text{-}4S]^{3+}$, $[4Fe\text{-}4S]^{2+}$ and $[4Fe\text{-}4S]^{1+}$, corresponding to $[2Fe^{3+}\text{-}2Fe^{2.5+}]$, $[4Fe^{2.5+}]$ and $[2Fe^{2.5+}\text{-}2Fe^{2+}]$ valence-state combinations, respectively.

The $[4Fe\text{-}4S]^{3+}/[4Fe\text{-}4S]^{2+}$ pair is the high-potential redox couple characteristic of HiPIPs, while the $[4Fe\text{-}4S]^{2+}/[4Fe\text{-}4S]^{1+}$ pair is responsible for the low-potential process characteristic of the classic ferredoxins. Under physiological conditions, only one of these redox couples appears to be accessible and functional.[1,153]

The absorption spectrum of [4Fe-4S]-ferredoxin type proteins has a characteristic broad absorption band with a maximum at around 400 nm in the oxidized state, while the HiPIP absorption spectrum has a broad band centered at 388 nm. Both the $[4Fe\text{-}4S]^{3+}$ and the $[4Fe\text{-}4S]^{1+}$ oxidation states of the cluster are paramagnetic and display characteristic EPR spectra. The $[4Fe\text{-}4S]^{1+}$ cluster in reduced ferredoxins displays a rhombic EPR signal with g values of 1.88, 1.92, and 2.06. The oxidized form

($[4Fe\text{-}4S]^{2+}$ state) of low-potential ferredoxins is EPR-silent and attempts to achieve a higher oxidation state, $[4Fe\text{-}4S]^{+3}$, led to irreversible cluster decomposition, probably through a [3Fe-4S] intermediate. The $[4Fe\text{-}4S]^{+3}$ signal is usually referred to as the HiPIP signal and shows distinct *g* values at 2.00–2.04 ($g_{\perp}$) and 2.08–2.14 ($g_{||}$). This signal is present in oxidized HiPIP but absent in reduced HiPIP.[158–161] Reduction of HiPIP to the $[4Fe\text{-}4S]^{1+}$ oxidation state, occurs in aqueous/DMSO solution but under partially denaturing conditions.[157]

EPR can also be used to distinguish a [2Fe-2S] cluster from a [4Fe-4S] cluster by performing a temperature dependence of the signal, as they differ in the relaxation time, which usually follows the order $[2Fe\text{-}2S] < [3Fe4S] < [4Fe\text{-}4S]^{3+} < [4Fe\text{-}4S]^{1+}$.[162] Nevertheless, enhanced relaxation times can occur due to spin-spin interactions between clusters.

The resonance Raman of [4Fe-4S]-ferredoxin type proteins have a predominant feature at 336 cm^{-1} assigned to vibration modes of the $Fe\text{-}S_{bridging}$, due to the total symmetry of the cubane structure.[98] The CD spectra of HiPIP in the reduced and oxidized state are similar with a positive peak at 450 nm and two negative peaks at 350 nm and 390 nm. Nevertheless, some HiPIPs present quite distinct features.[163]

2.06.2.1.5 Linear clusters and cluster interconversions

Proteins containing [3Fe-4S] clusters proved to be particularly useful to study cluster conversions and to understand and identify the iron-sulfur cluster present in aconitase (see **Section 2.06.3.2.1**). The interconversion of [3Fe-4S] into [4Fe-4S] was shown to occur when the coordinating ligand of the fourth iron atom is not a cysteinyl ligand,[122,139,140] as is the case of *D. desulfuricans* 7Fe ferredoxin and *P. furiosus* ferredoxin (being an oxygen from an aspartate,[45,140–142] as mentioned before). Cluster interconversion have also been observed in transcription regulators upon reaction with molecular oxygen (see **Section 2.06.4**).

The pathways of cluster interconversions were extensively probed and enabled the specific isotopic labeling of iron-sulfur clusters[124] (**Fig. 5**). The *in vitro* interconversions studies were performed under non-physiological and near physiological conditions using *D. gigas* cell extracts.[164]

Further insights into the electronic, magnetic, and redox properties of the iron-sulfur clusters, as well as information on the site-specific properties of the cubane clusters, was achieved based on the preparation of the so-called heterometallic cubane clusters $[MFe_3S_4]$ by incorporation of a heterometal, M, in the vacant coordination site of a [3Fe-4S] cluster. This pioneer work of Munck, Moura, and co-workers led to the synthesis of heterometallic $[CoFe_3S_4]$, $[ZnFe_3S_4]$, $[CdFe_3S_4]$, $[NiFe_3S_4]$, $[CuFe_3S_4]$, and $[CrFe_3S_4]$ clusters, using *D. gigas* and *P. furiosus* ferredoxins as templates.[44,165–168] These interconversion studies gathered important information on spin states, localized and delocalized valences, as well as reduction potentials. This same experimental procedure continues

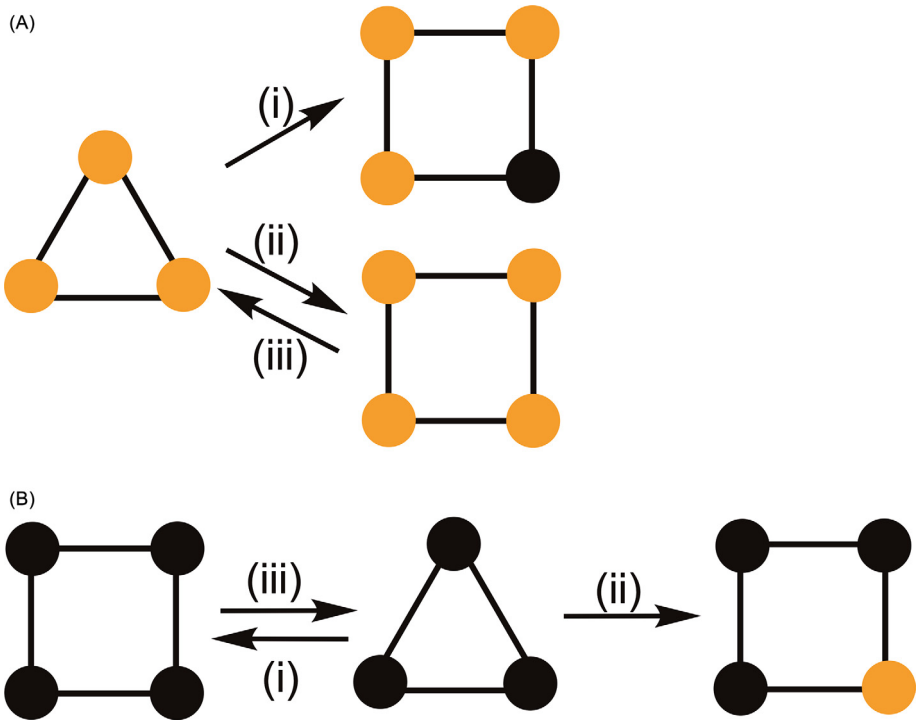

Fig. 5 Iron-sulfur cluster interconversion pathways and isotopic labelling. In panel (A) is shown the possible interconversions starting with ferredoxin II, and in panel (B) the possible interconversions starting with apo ferredoxin II reconstituted with ^{57}Fe. Interconversion pathway after incubation with (i) $^{57}Fe^{2+}$ or (ii) $^{56}Fe^{2+}$, in the presence of sodium dithionite, dithiothreitol and sulfide (S^{2-}), or (iii) upon oxidation with ferricyanide. ^{56}Fe and ^{57}Fe are represented by orange and black circles, respectively.

to be used to study more complex systems, either introducing other metals or ^{57}Fe for Mössbauer experiments (see Section 2.06.3 and 2.06.4).[169,170]

The [3Fe-3S] intermediate cluster with a planar hexagonal structure has been proposed to be the intermediate in cluster interconversion and degradation mechanism of the transcription regulator RirA (an iron sensor) and in FNR (an oxygen sensor) upon exposure to molecular oxygen (see Section 2.06.4).

A "linear" [3Fe-4S] cluster has been identified in the first spectroscopic studies of aconitase[155,171] (Fig. 6). Although its physiological relevance is unclear, this cluster will be mentioned here due to its importance in cluster interconversion, protein-cluster interactions, and synthesis of heterometallic clusters. The [3Fe-4S] linear cluster was observed after subjecting aconitase to alkaline conditions, and its structure was confirmed by comparing the visible, EPR, Mössbauer and MCD data with the one obtained for a mimetic [3Fe-4S] linear cluster.[172–174] Besides its linear structure, this cluster differs from the native one as it is coordinated by four cysteines, instead of three: Cys421 and Cys424 that also coordinate the native cluster, and two adjacent cysteine residues, Cys250 and Cys257, in substitution of Cys358[155] (Fig. 6).

The presence of similar linear clusters have been proposed to occur as intermediate species during the unfolding of ferredoxins,[175,176] although there are some evidences that in this case there is formation of iron sulfide species rather than a stable linear cluster.[177]

A biologic linear $[Fe\text{-}2S]_n$ has been observed in IssA, an iron-sulfur storage protein from *P. furiosus*. This protein forms nanoparticles (~300 nm, comprised of 20 nm spheres) inside the cell when this bacterium is grown in the presence of S^0. The thioferrate-type linear structure of this cluster has been assigned through Fe and S and K-edge X-ray absorption spectroscopy (XAS) and EXAFS, and EPR. *P. furiosus* IssA has 179 amino acids, with a N-terminal globular domain of 109 residues (IPR003731) and a cationic glycine-rich tail region in the C-terminus.[178] The globular domain binds iron and sulfur spontaneously forming the linear cluster, and oligomerizes, while the tail is proposed to stabilize the structure through electrostatic interactions. *In vitro* studies showed that holo-IssA can reconstitute the [4Fe-4S] cluster of *P. furiosus* apo-ferredoxin.[178] Although IssA physiological function remains unknown it is phylogenetically distant from NIF-related families (involved in the biosynthesis of nitrogenase cluster).[178]

Moreover, linear clusters with a similar structure but containing no iron (*D. gigas* Orange protein with Mo-Cu-Mo coordinated by sulfide[179]) or containing other metals in addition to iron (Mo or Cu, in the Blue protein from *D. alaskensis* or *Desulfovibrio aminophilus*, respectively[180,181]) have been identified as being non-covalently bound to the polypeptide chain. In fact, the visible spectra of these Blue proteins have a similar signature to the one of aconitase at high pH,[172] indicating the presence of a [Fe-S] moiety.

2.06.2.2 Complex iron-sulfur clusters

Besides the classic iron-sulfur clusters already discussed, unique, larger, and more complex iron-sulfur clusters are present in a few proteins and enzymes. Among these are the hybrid cluster of hybrid cluster protein, the active site of sulfite reductases, the [8Fe-7S] (P-clusters) and [Mo-7Fe-9S] (FeMo-cofactor) clusters of nitrogenase, the unique organometallic site (H-cluster) of [FeFe] hydrogenases and the mixed-metal clusters of [NiFe] hydrogenase and carbon monoxide dehydrogenase/acetylCo-A synthase.

Two other complex iron-sulfur clusters have been identified: a [8Fe–9S] cluster in the active site of a ATP-dependent reductase from *Carboxydothermus hydrogenoformans*[182]and a noncubane [4Fe-4S] cluster in the heterodisulfide reductase from methanogenic archaea.[183]

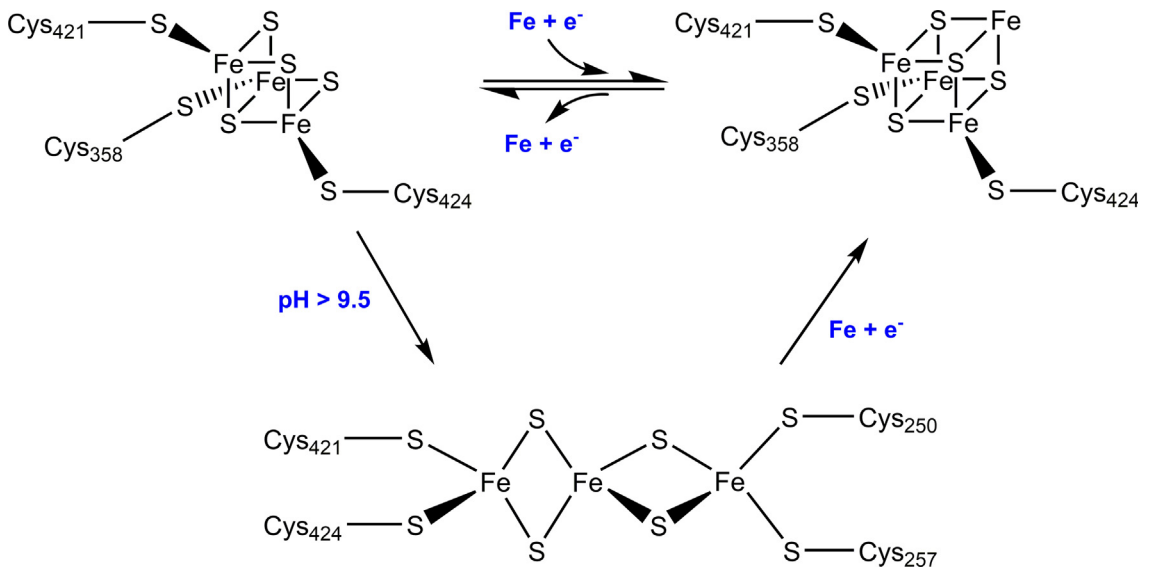

Fig. 6 Proposed mechanism for the interconversion of the cubane cluster into a "linear" cluster in aconitase.

2.06.2.2.1 Unique clusters

The relevant features of unique iron-sulfur clusters will be discussed in this section. The structures of these clusters are shown in Fig. 7.

2.06.2.2.1.1 Hybrid cluster protein

In 1989, an unusual iron-sulfur protein was isolated from *Desulfovibrio vulgaris* Hildenborough.[184] The preliminary characterization of this protein showed that it was constituted by six iron atoms and six inorganic sulfur atoms per protein. Upon reduction with sodium dithionite, the protein showed an EPR signal ($S = 1/2$) distinct from the canonical [2Fe-2S] and [4Fe-4S] clusters, but similar to synthetic compounds containing a $[6Fe\text{-}6S]^{3+}$ cluster and known as the prismane center.[184] Based on these observations, this unusual iron-sulfur protein was considered to contain a [6Fe-6S] cluster and was named as prismane protein. Not very long after this first discovery, in 1992, another iron-sulfur protein with similar features was isolated from *Desulfovibrio desulfuricans* ATCC 27774.[185] A detailed spectroscopic study of this protein, which included EPR and Mössbauer spectroscopies, led to the conclusion that the protein contained not one [6Fe-6S] prismane cluster, but two distinct multinuclear iron-sulfur clusters.

In 1998, the three-dimensional structure of the *D. vulgaris* Hildenborough protein was determined at 1.72 Å resolution[186] and it was undoubtedly proven that the protein contains two distinct clusters, as previously predicted from the Mössbauer studies on the *D. desulfuricans* 27774 protein. However, the nuclearity of the clusters was incorrect and the protein was not constituted by [6Fe-6S]

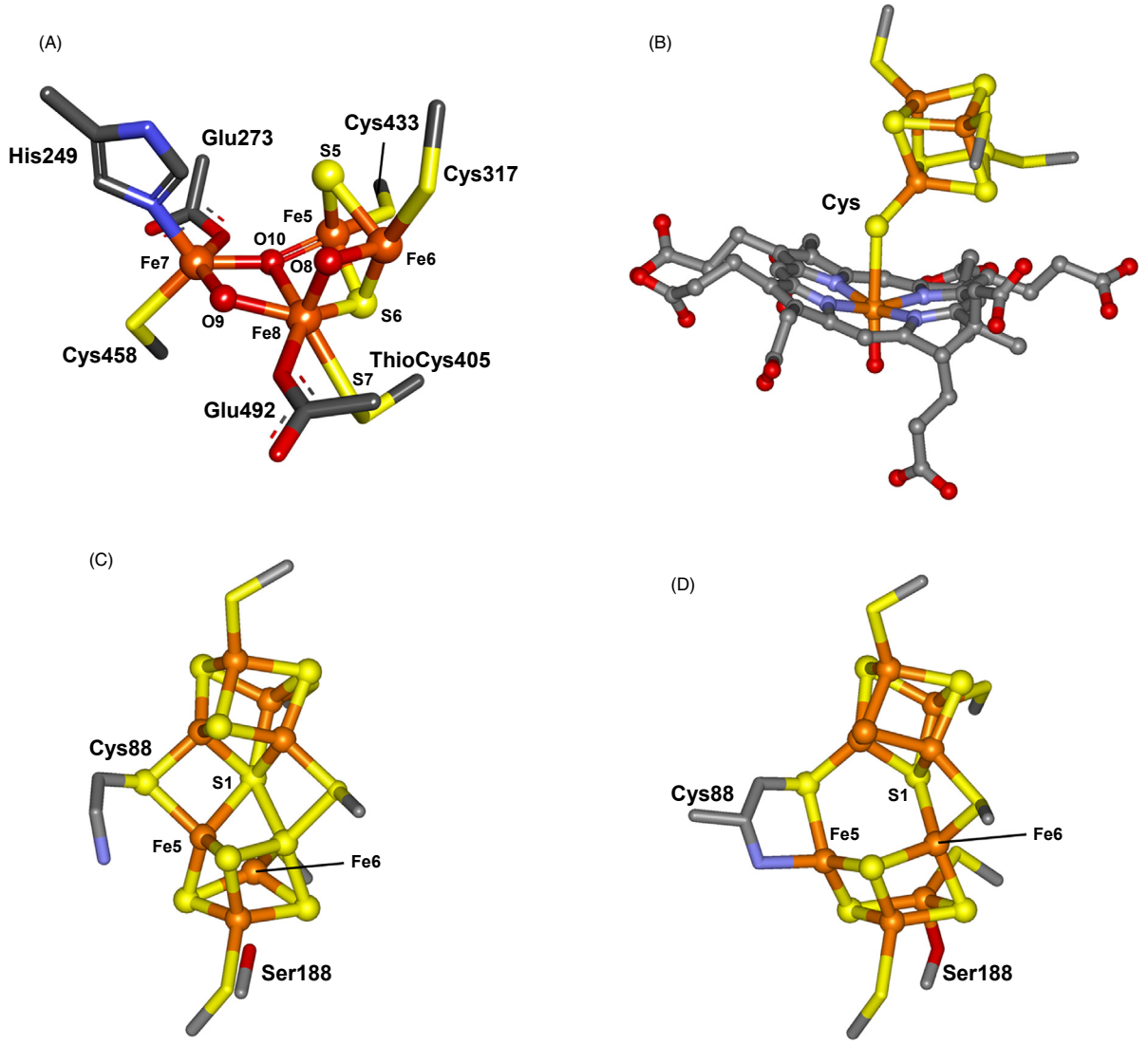

Fig. 7 Structures of the unique iron-sulfur clusters described in this chapter. (A) Hybrid cluster (PDB ID 7DE4), (B) sulfite reductase active site (PDB ID 1AOP), (C) P-cluster (P^N) in the reduced state (PDB ID 3MIN) and (D) P-cluster (P^{OX}) in the oxidized state (PDB ID 2MIN) of nitrogenase. The carbon, iron, molybdenum, nitrogen, oxygen, and sulfur are represented in gray, orange, purple, blue, red, and yellow, respectively. The images were created in Discovery Studio Visualizer (BIOVIA).

cluster but by two tetranuclear clusters, a cubane-type [4Fe-4S] cluster (cluster 1) and a cluster with a novel and unique structure (hybrid cluster), [4Fe-2S-3O]. The name prismane protein was abandoned since it became clear that the protein does not contain the initially postulated [6Fe-6S] cluster. The name fuscoredoxin was given to the protein by Moura et al.[187] due to its brown color and because the protein could stabilize the iron-sulfur cluster in various oxidation states. Nevertheless, it was afterwards decided to name this protein as hybrid cluster protein (Hcp).[187,188]

Phylogenetic analysis of these proteins revealed three different families that differ in the sequence motif that binds the cubane cluster located in the N-terminus. Family 1 and 3, found in *D. vulgaris* Hildenborough and *D. desulfuricans* 27774, in methanogens and in (hyper)thermophilic bacteria and archaea, has the sequence motif Cys-X_2-Cys-X_{7-8}-Cys-X_5-Cys. Family 2, found in facultative anaerobic Gram-negative bacteria (e.g., *Escherichia coli* and *Salmonella enterica*), has the sequence motif Cys-X_2-Cys-X_{11}-Cys-X_6-Cys. Family 3 differs from Family 1 due to 100-residues deletion between the N- and C-terminal domains.

In Family 1 and 3, the cubane cluster is a conventional [4Fe-4S] cluster bound to the protein by the unusual sequence motif of the four cysteine residues.[188] In Family 2, this sequence motif was initially proposed to bind a [2Fe-2S] cluster,[189] but was then shown to also bind a [4Fe-4S] cluster.[190]

The hybrid cluster, [4Fe-2S-3O], is unique among the iron-sulfur clusters for which structures are available, in that it has both sulfur and oxygen bridges (**Fig. 7**A).[188,190,191] The local environments of the metal atoms can be described as tetrahedral for Fe5 and Fe6, and trigonal bipyramidal for Fe7 and Fe8. Fe5 is coordinated by one protein ligand Cys433, two bridging S atoms (S5 and S6) and an oxygen, O10. Fe6 is also coordinated by one protein ligand, Cys317, which adopts a cis-peptide conformation, and two bridging S atoms (S5 and S6). Thus, this part of the cluster resembles either a [2Fe-2S] moiety or one face of a cubane cluster. However, Fe6 is also coordinated by an oxygen atom (O8), which bridges F6 and Fe8 to give a tetrahedral environment to Fe6. Fe7 is bound to three protein ligands, His249, Glu273 and Cys458, and to two oxygen atoms, O9 and O10, which bridges Fe8 and Fe5, respectively. Fe8 is coordinated by one protein ligand, Glu492, two bridging oxygen atoms (O8 and O9), a bridging sulfur, S6 (bridges Fe5 and Fe6) and a sulfur atom S7. S7 forms a persulfide with S_γ of Cys405, producing a thiocysteine moiety. Thus, Fe8 has a distorted trigonal bipyramidal geometry[188] (the residue numbering used are according with *E. coli* Hcp). The thiocysteine is a distinctive iron ligand that has also been observed in catalytic intermediates in sulfur transfer reactions.[192]

In 2002, Macedo et al. determined the X-ray structure of *D. desulfuricans* 27774 and *D. vulgaris* Hildenborough Hcp at 1.25 Å,[191] showing that the structures of both proteins are essentially the same, comprising three domains and two iron-sulfur clusters. In that work, it was demonstrated that although the two Hcps were purified under different conditions, *D. desulfuricans* 27774 Hcp in the absence of oxygen and *D. vulgaris* Hildenborough Hcp in the presence of oxygen, the nature and the oxidation state of the hybrid cluster remained the same, thus being independent of the presence of oxygen. In the following year, these two Hcps were crystallized in the reduced state.[48] The overall structure of the backbone did not differ from the as-isolated form (either under oxic or anoxic conditions), but structural changes in the hybrid cluster were observed, especially in the iron atom bonded to the persulfide. These changes were proposed to reflect the function of this protein, possibly as a reductase, though the nature of the substrate was unknown.[48]

In fact, to support this hypothesis there is a putative electron transfer pathway, composed by aromatic residues that bridge the hybrid cluster, the [4Fe-4S] cluster 1 and the protein surface. The distance between the two clusters is around 11 Å, which is amenable for electron transfer.[48] A similar hypothesis has been proposed based on the *E. coli* Hcp structure,[190] though in this case the redox partner is Hcr (*vide infra*).

[4Fe-4S] cluster 1 is a one-electron accepting $[4Fe\text{-}4S]^{2+}$ cubane that in the reduced state $[4Fe\text{-}4S]^{1+}$ presents an unusual magnetism of a spin-admixed system ($S = 3/2$). The hybrid cluster can be stabilized in four distinct oxidation states, ranging from the most oxidized state (+6), containing four Fe^{3+}, to the fully reduced state (+3), with three Fe^{2+} and one Fe^{3+}. Upon successive one-electron reduction and starting from the fully oxidized protein, four oxidation states were observed with spins states of $S = 0$ (+6), $S = 9/2$ and 1/2 (+5), $S = 0$ and 4 (+4) and finally a spin state of $S = 1/2$ for the fully reduced state (+3).[185,187,193]

For three decades the physiological function of Hcp remained unknown, and initially it was wrongly proposed to be a hydroxylamine oxidoreductase, converting hydroxylamine to ammonia.[194,195] However, as mentioned, Hcps are present in several anaerobic and facultative bacteria, as well as in anaerobic archaea. In *E. coli* and *Morganella morganii*, *hcp* was shown to be expressed mainly under anaerobic conditions in the presence of either nitrate or nitrite.[189] In fact, *hcp* is under the transcription regulation of NsrR.[196] Moreover, in *D. gigas* a mutant strain that cannot produce Hcp was shown to be sensitive to nitrosative stress.[197] In *E. coli*, Hcp is encoded by the operon, *hcp-hcr*, with the second gene coding for a NADH-dependent reductase (Hcr). These two proteins form a complex and together can reduce NO. This led to the hypothesis that Hcp is a high affinity NO reductase, being able to detoxify low concentrations of NO that accumulates in the bacterial cytoplasm during anaerobic growth.[198] *D. vulgaris* Hildenborough Hcp was also shown to be a NO reductase and its catalytic mechanism was studied by EPR, showing the presence of a dinitrosyl Fe intermediate and that N_2O binds Hcp in the reduced state.[199]

2.06.2.2.1.2 Sulfite reductase

The reduction of sulfite is a vital reaction both in assimilatory pathways, which leads to the incorporation of sulfur into amino acids and other metabolites, or in dissimilatory pathways that are used by anaerobic microorganisms that respire sulfur compounds.[200] Both assimilatory and dissimilatory sulfite reductases (SiRs) contain in the active site a unique combination of co-factors that includes a reduced porphyrin, designated by siroheme, which is coupled through a thiolate to a [4Fe-4S] cluster (see **Fig. 7**B).[201,202]

The assimilatory sulfite reductases (aSiRs) have been extensively investigated and served as a model for this family of proteins since they are structurally well characterized.[201] These proteins are monomeric and share low sequence similarity to dissimilatory sulfite reductases (dSiRs). One of the most extensively studied dSiRs is the protein also known as desulfoviridin from *Desulfovibrio* genus.[203–205] dSiRs are large oligomeric proteins with a molecular weight in the order of 200 kDa and composed by two different types of subunits in a $\alpha_2\beta_2$ arrangement. This protein, DsrAB, forms a stable complex with DsrC, which is also essential for its activity. It is proposed that DsrAB catalyzes, not the 6-electron but the 4-electron reduction of sulfite, forming a S^0 intermediate. DrsC is the acceptor of this intermediate, forming a persulfide in one of its cysteine residues. After dissociation from DsrAB, DrsC is reduced by a membrane-bound protein complex (DsrMKJOP).[206,207]

The SiRs enzymes present unusual magnetic and electronic properties, which result from the close association of the paramagnetic siroheme and nominally diamagnetic [4Fe-4S] cluster. Most probably, this direct association of an iron-sulfur cluster to a siroheme has been conserved to provide efficient delivery of multiple electrons to a substrate bound to the other side of the siroheme in a controlled and specific manner.[202,208–210]

The isolated SiRs have a high-spin ferric ($S = 5/2$) siroheme and a diamagnetic [4Fe-4S] cluster with a + 2 charge, with exception of the so-called low molecular weight SiRs (alSiR), which are found in *D. vulgaris* Hildenborough, *Methanosarcina barkeri* and *Desulfuromonas acetoxidans*, that have a low-spin ferric ($S = 1/2$) siroheme.[204,211]

For the *E. coli* SiR each co-factor can be reduced by one electron: the siroheme to a ferrous state ($S=2$), and the iron-sulfur cluster to a + 1 state ($S = 1/2$). These two co-factors can undergo electron-exchange interactions conferring paramagnetic properties to all the irons in the assembly, even when the [4Fe-4S] cluster is oxidized and nominally diamagnetic.[210,212,213] The electron coupling between the two prosthetic groups was extensively characterized for this enzyme using several spectroscopic techniques (e.g. Mössbauer,[209] EPR,[202] ^{57}Fe ENDOR[214]), leading to the hypothesis that a ligand should be shared between the two cofactors. This assumption was confirmed when the structure of the enzyme was solved by X-ray crystallography, which proved that a cysteine residue bridges the two redox centers.[201]

The electron-coupling was also observed in the dSiRs and alSiRs, although the electronic and structural properties of the coupled siroheme-[4Fe-4S] unit are not identical and differ from the ones of *E. coli* SiR. It seems that the different spectral and redox properties of this class of enzymes are induced by variations in the protein environment surrounding each coupled center.[204,211,215,216] Novel structural insights have been given for dSiRs with the studies on *D. vulgaris* Hildenborough dSiR, *Desulfomicrobium norvegicum* SiR,[206,217,218] *D. gigas* SiR in two active forms[219] and *A. vinosum* SiR.[220]

2.06.2.2.1.3 Nitrogenase (FeMo-cofactor and P-cluster)

Nitrogenase is a two metalloprotein component system that catalyzes the reduction of dinitrogen to ammonia coupled to the hydrolysis of ATP.[221–224] The two protein components are the Fe-protein, a homodimer containing a [4Fe-4S] cluster and the MFe protein, an heterotetramer that contains the P-cluster and the active site, the FeM cofactor (FeMco). The active site can be heterometallic (M = Mo, V) or be homometallic (M = Fe) as in the iron-only nitrogenase.[225,226] Even though several mechanistic aspects of the catalysis need to be clarified it is a consensus that the process involves association and dissociation between the Fe-protein and the MFe protein and four electrons resulting from four bridging hydrides are essential for reductive hydrogen elimination with concomitant activation and reduction of the N≡N triple bond.[225,227,228]

The MoFe protein is the most extensively studied nitrogenase containing the catalytic FeMoco, a [1Mo-7Fe-9S-1C]-homocitrate cluster.[229] However, several diazotrophs under Mo scarcity conditions can activate a different set of genes encoding a vanadium-containing protein with a similar FeV cofactor (FeVco) that has important structural and functional differences.[230] So far, there are no X-ray structural data for the iron-only nitrogenases, but the FeFe cofactor is thought to be a [8Fe-9S-1C] cluster.[231,232]

The Fe-protein has two identical subunits that symmetrically coordinates a single [4Fe-4S] cluster. The dimer has a α/β fold that is common in nucleotide binding proteins. The residues Cys97 and Cys132 (in *Azotobacter vinelandii* residue numbering) from both subunits coordinate the [4Fe-4S] cluster, and in the interface between the subunits are located several nucleotide binding motifs.[233,234] Near the N-terminal of the Fe-protein is located a Walker A motif where the ATP or ADP binds, as this protein is a P-loop containing ATPase. The [4Fe-4S] cluster can have three oxidation states of +2 (oxidized state), +1 (reduced with dithionite) or 0 (reduced with Ti(III)).[235,236] In nitrogenase the Fe-protein functions as a reductase that receives electrons, binds, and hydrolyses ATP, transferring an electron to the catalytic protein namely to the P-cluster. The P-cluster is an [8Fe-7S] cluster in the MFe protein that subsequently transfers this electron to the active site of the enzyme, the FeMco where the substrate is reduced. The catalytic versatility associated with nitrogenase that allows the reduction of different substrates (such as, C_2H_2, CN^- or CO), and not only N_2 or H_2 is associated with the ability to shuttle electrons throughout the enzyme cofactors.[221,237,238] The MoFe protein is a $\alpha_2\beta_2$ heterotetramer, where the α and β subunits exhibit a similar polypeptide fold consisting of three domains of the α/β-type, with some extra helices.[239,240] This protein contains two copies of two different types of unique metalloclusters: the FeMco and the P-cluster.

The P-clusters are [8Fe-7S] clusters (**Figs. 7**C and D) that are proposed to be involved in electron transfer between the Fe-protein and the substrate reduction site of the FeMoco.[241,242] The P-cluster has a unique overall architecture, constructed from two linked [4Fe-4S] subclusters that share a μ_6-sulfide at one corner, and it is the only known naturally occurring iron-sulfur cluster that contains serinate-O (β-Ser188) and amide-N (α-Cys88) ligands coordinating an iron atom, in addition to the typical cysteinyl-S ligands.[243,244] The P-cluster is obtained after the purification process of the MFe protein in all ferrous state, as determined by Mössbauer spectroscopy[245,246] with the 8 irons in the +2 oxidation state (dithionite is used in the purification) and this form of P-cluster, a $[8Fe\text{-}7S]^{2+}$, is called the P^N-state. X-ray crystallographic data of two different oxidation states of the MoFe protein, the P^N-state and

the two electrons oxidized P^{OX}-state, revealed that the P-cluster can undergo structural rearrangements.[240,247] The P-cluster in the P^{N}-state is highly symmetric and can be described as two [4Fe-4S] linked by a sulfur that is hexacoordinated, whereas in the P^{OX}-state the symmetry is lost. In the P^{OX}-state (see Fig. 7D), the [4Fe-4S] moieties are distorted, become more open and the Fe5 and Fe6 move away from the central sulfur and coordinate a backbone amide-N (α-Cys88) and a serinate-O (β-Ser188), respectively. In some nitrogenases, like the one isolated from *Gluconacetobacter diazotrophicus*, instead of Fe6 is Fe8 that is moved and becomes coordinated by a O from a tyrosine (Tyr 98).[248] The coordinating Cys88 and Ser188 become deprotonated, and this may stabilize the P^{OX}-cluster lowering the reduction potential of the P-cluster and enabling conformational changes that could facilitate the electron transfer to the FeMco.[249]

The conformational changes observed in the P-cluster in different oxidation states are observed for either Mo or V nitrogenases.[230,250] Going from the P^{N}- to the P^{OX}-states, two electrons are transferred, though the catalytic mechanism involving N_2 reduction is usually identified by a one-electron transfer steps. It is known that the treatment of the MoFe protein with small electron transfer molecules can induce different oxidation states in the P-cluster. In the P^{N}-state, all the Fe atoms are in the ferrous oxidation state.[245,246] Using mediators,[246,251,252] the P^{N}-state can be sequentially oxidized by three electrons, attaining the P^{1+}, P^{2+} (P^{OX}), and P^{3+} oxidation states. The $P^{3+/2+}$ redox couple is not reversible *in vitro*, and thus, it is concluded that this couple does not function *in vivo*. This suggests a model where the $P^{1+/N}$ and $P^{2+/1+}$ couples could be involved in P-cluster electron transfer, presenting the possibility of transferring one or two electrons from the P-cluster to the FeMoco during catalysis. The reduction potential of the couple $P^{2+/1+}$ is associated with aproton transfer and changes from - 224 mV vs. SHE at pH 6 to - 340 mV *vs*. SHE at pH=8.5, whereas the reduction potential of the couple $P^{1+/N}$ is - 290 mV *vs*. SHE and is pH independent. – [253] These reduction potentials are similar to the reduction potential of the [4Fe-4S] cluster in the Fe protein (−420 mV *vs.* SHE, when MgATP is bound to the Fe-protein).[254]

The P^{N}-state of the P-cluster is EPR silent, while the P^{1+} and P^{2+} states are paramagnetic; the P^{1+} state is a mixed spin system with a spin sate of $S = 1/2$ and $S = 5/2$, and the P^{2+} state is an $S > 3$ system with a EPR signal in the perpendicular mode.[255] Although being EPR active, the P^{1+} and P^{2+} states have been difficult to detect during nitrogenase turnover, and there is little information about the oxidation states that the P-cluster attains during turnover.[256]

In the P^{1+} state, the Fe5 remains in the same position as in P^{N}-state but the Fe6 is coordinated by Ser188, this implies P^{1+} can be an intermediate and the P-cluster can accept or donate one or two electrons, as the Fe protein [4Fe-4S] cluster. The transfer of two electrons could represent a 50% ATP saving for the enzyme.

The active site of nitrogenases, the FeMco cluster, is a bridged double [4Fe-4S] cubane cluster with a metal M at an apical position. The metal can be Mo, V or Fe and so far, X-ray crystallographic data is available only for the heterometallic nitrogenases, as mentioned. Mo^{3+} and the V^{3+} are coordinated by 3 sulfide ligands from one of the cubane clusters.[229,230] The FeMco cluster is bound to the polypeptide chain by a histidine residue that also coordinates the metal and a Cys residue that coordinates the Fe1 in the opposite side of the FeMco cluster (Fig. 8A). An homocitrate molecule coordinates bidently the Mo/V atom that are octahedrally coordinated. In both nitrogenases a central ligand (a C^{4-}) from a S-adenosyl methionine binds the two cubane clusters and it is hexacoordinated by 6 iron atoms (Fe2, Fe3 and F4 from one cubane cluster and Fe6, Fe7 and Fe5 from the other cubane).[240] The main difference observed between the active site of both Mo and V nitrogenases besides the replacement of Mo by V is the nature of an additional ligand bridging the two cubane clusters, between the Fe5 and the Fe4 (Fig. 8B). The FeMoco cluster has a sulfide binding these two irons, whereas in the FeVco cluster this ligand is a carbonate (CO_3^{2+}).[230] The difference in size between these two ligands is responsible for higher distances between the two irons in the FeV protein and a general distortion observed in all different metal-metal bonds between the two cofactors.[230,240] The different metals in the active site have a major impact in the reduction of N_2 to ammonia.

The catalytic efficiency of the three types of nitrogenases is associated with differences observed for the rate constant concerning the ratio N_2 reduction/H_2 formation being the Mo nitrogenase the most efficient and the Fe nitrogenase the least.[257] The binding of the substrate in still a matter of discussion. The FeMco cluster has no available coordination sites but the sulfide S2B that coordinates the Fe2 and Fe6, have a His and a Gln residues in the vicinity, and can be replaced by CO in both the VFe protein and the MoFe protein (Fig. 8C).[250,258,259] The His residue can form a hydrogen bond with 2B sulfide, connecting the active site with the protein surface by accessing to a hydrogen-bonding pathway that is probably involved in proton transfer during catalysis. In the resting state the side chain of the conserved Gln in the vicinity of the FeMco is directed away from the cluster. However, for the VFe protein in a turnover state Gln176 can rotate toward the cluster with the amide oxygen from this residue forming two hydrogen bonds, one with His180 at a 2.84 Å and a second hydrogen bond with a bridging ligand (N/O).

Recently a crystal structure of a Mo-nitrogenase obtained in the presence of N_2 (turnover conditions) suggested a displacement of the belt-sulfur sites corresponding to S2B, S3A and S5B by N_2,[260] however this is still a matter of controversy.[261,262]

2.06.2.2.2 Organometallic and mixed-metal clusters

In this section, the properties of the fascinating and unusual organometallic and mixed-metal clusters will be described. The structure of these clusters is presented in Fig. 9.

2.06.2.2.2.1 Hydrogenases

Hydrogenases are a family of enzymes that catalyze the reversible two electron oxidation of hydrogen: $H_2 \leftrightarrow 2H^+ + 2\,e^-$, and many microorganisms use hydrogenase to metabolize H_2. They are a heterogeneous group of enzymes that differ in size, subunit composition, metal content and cellular location. However, based on their metal content, two main groups can be distinguished: the [FeFe]

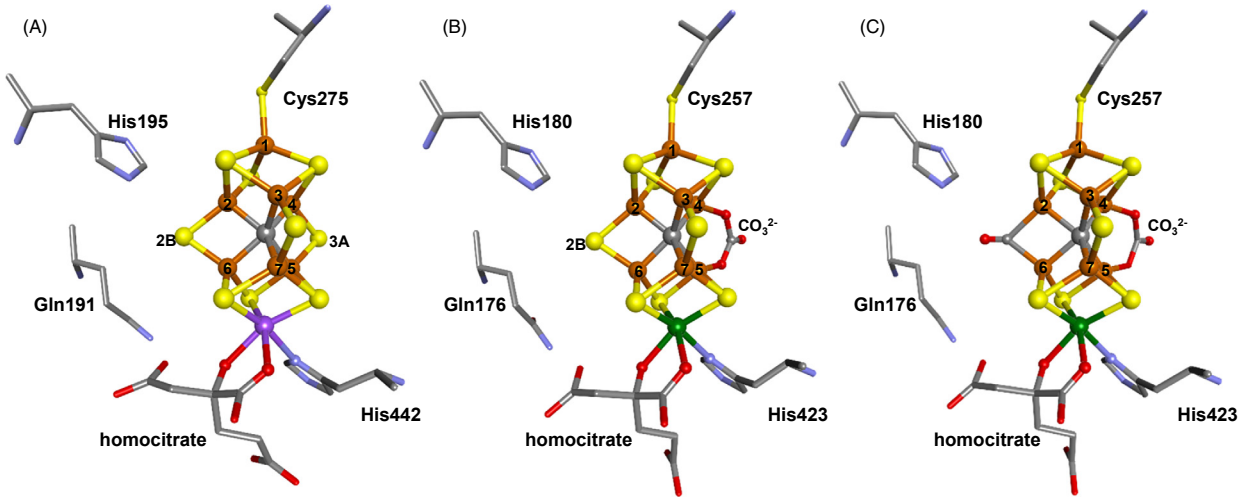

Fig. 8 The catalytic FeMco of nitrogenase [M:7Fe:9/8S:C] is a complex iron-sulfur cluster bound to an apical metal (M = Mo, V, Fe) coordinated to a homocitrate molecule. In panel (A) is shown the FeMoco (PDB ID 3U7Q), in panel (B) the FeVco (PDB ID 5N6Y) and in panel (C) the FeVco with bound CO in the position of S2B (PDB ID 7ADR). The iron, sulfur, molybdenum, and vanadium atoms are represented in orange, yellow, purple, and green, respectively. The carbon, oxygen and nitrogen atoms are represented in gray, red and blue, respectively. Images were created with the program Discovery Studio Visualizer (BIOVIA).

hydrogenases, which contain only Fe, and the [NiFe] hydrogenases, which contain both Ni and Fe in the active site. The [FeFe] hydrogenases catalyze the reduction of proton as terminal electron acceptor to yield H_2 and thus mainly function in H_2 production, while the [NiFe] hydrogenases most often catalyze the forward reaction in which H_2 is consumed.[151,263–266] Hydrogenases have been the subject of great attention and research, which is mainly related with the potential application of these enzymes in green hydrogen production, a future important alternative energy source.[267] However, one of the major drawbacks is their sensitivity toward oxygen. All hydrogenases are oxygen sensitive but the [FeFe] hydrogenases are more sensitive toward oxygen than the [NiFe] hydrogenases that can be aerobically purified because the oxygen inhibition is reversible.[268,269] Some membrane-bound [NiFe] hydrogenases found in aerobic bacteria can even oxidize H_2 and promote hydrogen cycling in the presence of oxygen. The majority of the [FeFe] hydrogenases are irreversibly inactivated by oxygen and even though some exceptions are found in nature, so far only a particular type of [NiFe] hydrogenase can oxidize hydrogen.[270–273]

2.06.2.2.2.1.1 [FeFe] hydrogenases

Several [FeFe] hydrogenases isolated from anaerobic bacteria, such as *D. vulgaris* and *D. desulfuricans*, *Megasphaera elsdenii* and *Clostridium pasteurianum* (which contains two different hydrogenases, CpI and CpII) have been well characterized using several spectroscopic techniques.[151,274–282] Despite some similarities among the various [FeFe] hydrogenases, variations in the metal content exist that translate into differences in their iron-sulfur cluster content. However, all of them have in common the presence of iron-sulfur clusters (termed F clusters), the H-cluster (the catalytic site), and carbon monoxide (CO) as a potent inhibitor. The F clusters usually are [4Fe-4S] cubane-type clusters with exception of *C. pasteurianum* CpI that also contains a [2Fe-2S] cluster.

The structures of two [FeFe] hydrogenases have been solved by X-ray crystallography: the periplasmic [FeFe] hydrogenase from *D. desulfuricans*[283] and the cytoplasmic [FeFe] hydrogenase from *C. pasteurianum* (CpI).[49,283,284] The structures of these enzymes clearly revealed the presence of an unusual active site, the so-called H-cluster, which is constituted by a $[2Fe]_H$ subcluster linked to the [4Fe-4S] subcluster via a cysteine thiol group (see **Fig. 9**A). The binuclear cluster is formed by two iron atoms, the proximal Fe (Fe_p), which is the one near the [4Fe-4S] cluster, and the distal Fe (Fe_d) (**Fig. 9**A), each coordinated by two diatomic, non-protein ligands, CO and CN^-. This site also carries a bridging CO and an azapropane-1,3-dithiolate (ADT) bridge between the two Fe atoms. In result, the Fe_p is hexacoordinated whereas the Fe_d is pentacoordinated and therefore the Fe_d was identified as the substrate binding site where the catalysis occurs. This was later corroborated by a structure obtained with a CO coordinated to the Fe_d.[285–287] The distal Fe can either bind CO inhibiting hydrogenase activity or a hydride or a hydrogen, as part of the catalytic cycle. The conjugation between the ADT nitrogen, acting as a base, and the low valent Fe_d provides the conditions for heterolytic splitting of hydrogen.[288,289] Furthermore, the CN^- ligands can provide H-bonding with a serine and a lysine present in the cluster surroundings that helps stabilizing the $[2Fe]_H$ cluster that is bound to the $[4Fe4S]_H$ cluster by a thiol group from a cysteine residue.

Several oxidation states of the H-cluster have already been identified and characterized spectroscopically. The active oxidized state (H_{ox}) is characterized by a mixed valence (Fe^{1+}-Fe^{2+}) configuration of the bi-nuclear cluster. These iron atoms are in a low spin state and present an $S = 1/2$ EPR signal. Reduction of the H-cluster in the H_{ox} state leads to the active reduced state (H_{red}), which is EPR silent and has both iron atoms of the [2Fe] subcluster most probably in the Fe^{1+}-Fe^{1+} formal oxidation state.[151] The CO-inhibited state is EPR active due to a Fe^{1+}-Fe^{2+} mixed valence state of the bi-nuclear cluster, similar to $H_{ox.}$[290–294] According to Mössbauer studies, large ^{57}Fe hyperfine coupling are observed between $[4Fe4S]_H$ and $[2Fe]_H$ clusters, suggesting a strong

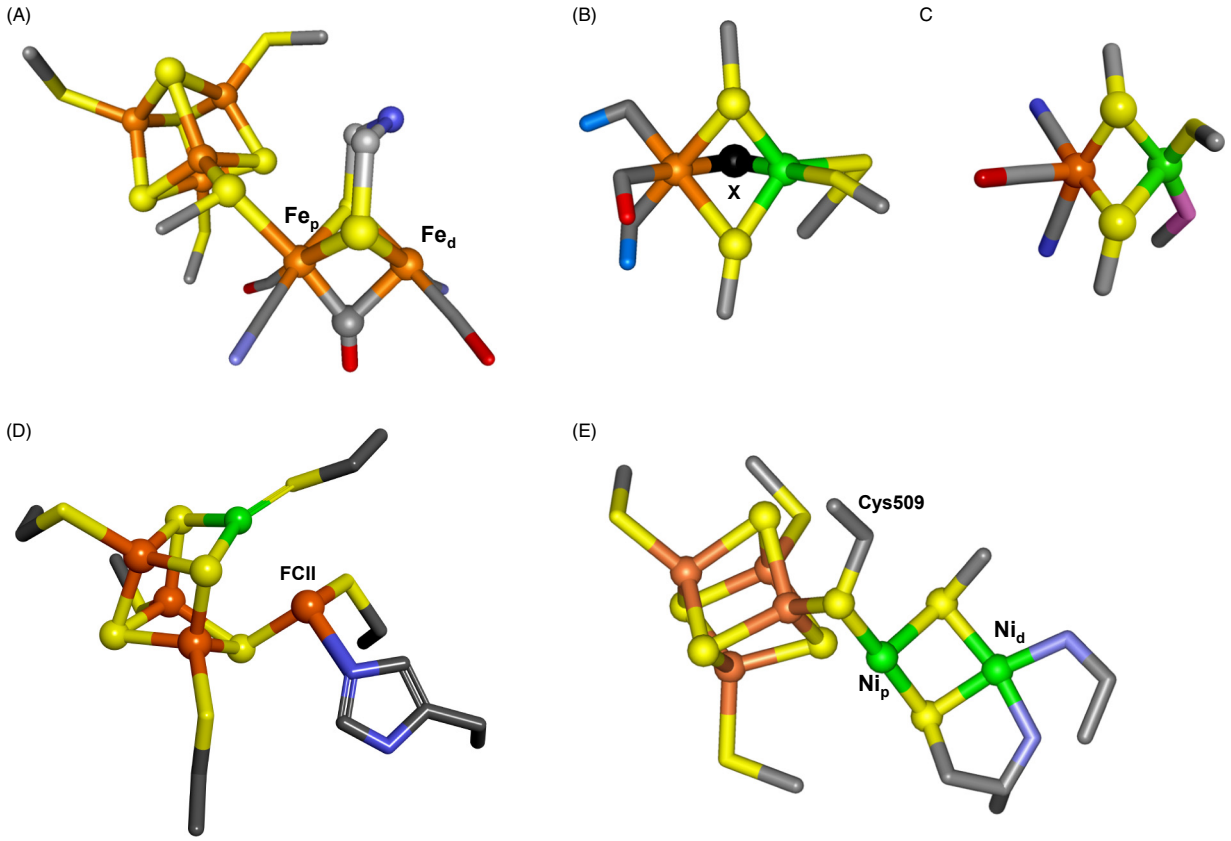

Fig. 9 Structures of the organometallic and mixed-metal clusters described in this chapter. (A) H-cluster of [FeFe] hydrogenase (PDB ID 1HFE), (B) NiFe active site of [NiFe] hydrogenase in the oxidized form (PDB ID 1FRV), (C) NiFe active site of [NiFeSe] hydrogenase (PDB ID 5JT1), (D) C-cluster (PDB ID 6B6X) and (E) A-cluster (PDB ID 1OAO) of CO dehydrogenase/acetyl Co-A synthase. The iron, sulfur, selenium, and nickel atoms are represented in orange, yellow, pink and green, respectively. The carbon, oxygen and nitrogen atoms are represented in gray, red and blue, respectively. The X identifies the position of a third bridging ligand that can be an oxygenated species in inactive states of the enzyme (Ni-A or Ni-B) or a hydride in active forms (Ni-C and Ni-R). Images were created with the program Discovery Studio Visualizer (BIOVIA).

exchange coupling between them.[281] ^{1}H NMR spectroscopy was used to identify paramagnetically shifted ^{1}H resonances from *Chlamydomonas reinhardtii* hydrogenase.[295] A signal similar to bacterial ferredoxins was observed for the unmaturated enzyme containing only the $[4Fe\text{-}4S]_H$. In the maturated protein in the H_{ox} and H_{ox}-CO states, shifted ^{1}H resonances were identified originated from the methylene protons of the ADT bridging ligand of the $[2Fe]_H$ subsite.[295]

Furthermore, in the H_{ox} state the spin density is shifted toward de distal Fe whereas for H_{ox}-CO states the spin density is more evenly distributed between the two Fe atoms indicating that upon the substrate binding electron density can be modulated between the two subsites.[294,296]

In the H-cluster the single reduced state can occur with or without protonation of the nitrogen of the ADT ligand depending on the pH. At low pH values, the protonation occurs, and the CO bridging ligand is absent whereas at high pH values the protonation is not observed and the CO bridge is kept.

The protonation converts NH into NH_2 causing electronic rearrangement moving the reducing equivalent from the $[4Fe4S]_H$ to the $[2Fe]_H$ subsite and this step is extremely important in catalysis. The reduction potentials associated with the first and second reduction steps are similar to the H^+/H_2 potential and the transition between the H_{red} state and the $H_{red}H^+$ state has a pKa close to 7.[297] The two electrons and the one proton can probably combine and generate a hydride in the Fe_d and further protonation will generate H_2. However, states like $H_{hyd}H+$ and Hox-H_2 were not yet observed maybe due to its highly transient nature.

2.06.2.2.2.1.2 [NiFe] hydrogenases

[NiFe] hydrogenases can be divided into two major groups according to its sensitivity toward oxygen, the standard O_2-sensitive and the O_2-tolerant [NiFe] hydrogenases. X-ray crystallographic structures of [NiFe] hydrogenases belonging to the O_2-sensitive group are available from *D. gigas*,[43,298] *Desulfovibrio vulgaris* Miyazaki F,[299–301] *D. desulfuricans*,[302] *Desulfovibrio fructosovorans*[303] and *Desulfomicrobium baculatum*,[304] closely related sulfate reducing bacteria. All these hydrogenases have a small ($\approx$ 30 kDa) and a large subunit ($\approx$ 60 kDa). The small subunit contains the three iron-sulfur clusters (two [4Fe-4S] clusters and one [3Fe-4S] cluster) that are involved in the electron transport to/from the active site ([NiFe] cluster). In the catalytically active hydrogenases, a proximal

$[4Fe\text{-}4S]_p^{2+/+}$ cluster is located near the [NiFe] cluster, flanked by a medial $[3Fe\text{-}4S]_m^{+1/0}$ cluster. Near the protein surface, a distal $[4Fe\text{-}4S]_d^{+2/+}$ completes the biological electron transfer pathway in these type of enzymes.[305] The reduction potential estimated for these clusters in *D. gigas* hydrogenase was - 315 mV for the $[4Fe\text{-}4S]_p$, −80 mV for the $[3Fe\text{-}4S]_m$ and −445 mV for the $[4Fe\text{-}4S]_d$.[306] Upon reduction, the $[4Fe\text{-}4S]_p^{+}$ magnetically interacts with the [NiFe] active site[151] and the $[4Fe\text{-}4S]_p^{2+/+}$ controls the electron flow from the buried [NiFe] active site present in the large subunit to the hydrogenase surface in the small subunit, controlling the electrons flow with the redox partner in the enzyme surface.[307]

The large subunit contains the [NiFe] active site (see Fig. 9B), and the geometry of this site is highly conserved throughout all [NiFe] hydrogenases.[308] The nickel and iron atoms are separated by a distance of about 2.5–2.9 Å[264] and are bridged by the thiol groups of two cysteines. The nickel atom is coordinated by two additional thiol groups from cysteines bound in a terminal position. The iron atom carries three inorganic diatomic ligands that have been identified by infrared (IR) spectroscopy as two CN^- and one CO.[309–311] The oxidized inactive state in general is a mixture of the so-called "unready" or Ni-A and "ready"-Ni-B states that correspond to a slow or fast catalytic activation state respectively. In these states additional electron density is detectable between nickel and iron, which seems to arise from a third oxygenated bridging ligand.[299,312] Both oxidized states, are paramagnetic and characterized by different *g* values. The bridging ligand in the Ni-B state is an OH^- and probably the same bridging ligand is present in the Ni-A state. The differences observed in the hyperfine coupling constants between the two states may be due to rotation of Cys549 about C_α–C_β–S_γ–Ni dihedral angle. Cys546 rotation can also account for differences observed in the intermediate *g* value.[301,313–315] In the active state of the enzyme (Ni-C/Ni-R) the bridging ligand is a hydride (H^-).[316] In all states of standard hydrogenases, the nickel atom has an open coordination site, which defines an axial direction, and it is therefore believed that the Ni represents the primary hydrogen binding site. This is supported by the fact that the inhibitor CO binds at this position and that the H_2 transfer channel ends near the Ni.[300,303] It has been shown by X-ray crystallography of single crystals treated with CO,[300] that the CO binds at the sixth free-coordination site of the nickel atom (see Fig. 9B). The Ni-CO state is paramagnetic and photosensitive. Upon illumination at low temperatures, the CO molecule photodissociates, resulting in the Ni-L state, the same state formed from Ni-C.[317] The H_2 molecule can access the buried [NiFe] active site through four hydrophobic tunnels that combine into one, leading to the Ni atom.

In the process of enzyme "activation" and during the catalytic cycle, the [NiFe] hydrogenase passes through several intermediate states (Fig. 10) observed and characterized by EPR spectroscopy, which showed that the enzyme cycles between EPR silent and EPR-detectable (paramagnetic) nickel-centered states. The oxidized inactive states Ni-A, Ni-B, mentioned above, and the active Ni-C state are all paramagnetic and EPR active, Ni-L is *l*ight-induced and EPR active, Ni-SI is EPR *si*lent, and Ni-R is *r*educed, and EPR-silent.[318] A full characterization has become possible by Fourier-transform infrared (FTIR) spectroscopy by which the IR vibrations of the CN^- and CO ligands at the iron are monitored. In the IR experiments, both the paramagnetic and EPR-silent states are detected.[310]

Upon one-electron reduction of Ni-A and Ni-B, the EPR-silent states Ni-SU (*si*lent *u*nready) and Ni-SIr (*si*lent *r*eady) are formed. The Ni^{3+} is reduced to Ni^{2+} in both EPR silent states and the oxygenated species is still present as a bridging ligand. Under reducing conditions at temperatures ≥30 °C, the Ni-SIr is converted into another EPR-silent state, Ni-SIa (silent active). This step leads to removal of the OH^- binding ligand and the Ni^{2+} is then tetracoordinated leaving a vacant coordination position. The Ni-Sia can be further hydrogen reduced and generate the fully reduced state Ni-R. In this state a hydride is present between Ni^{2+} (Ni-H^- −1.58 Å) and Fe^{2+} (Fe-H^- −1.78 Å), and the Cys546 that coordinates the Ni atom becomes protonated. Alternatively, the conserved Arg479 in *D. vulgaris* Miyazaki F [NiFe] hydrogenase was proposed as proton acceptor. One-electron oxidation of

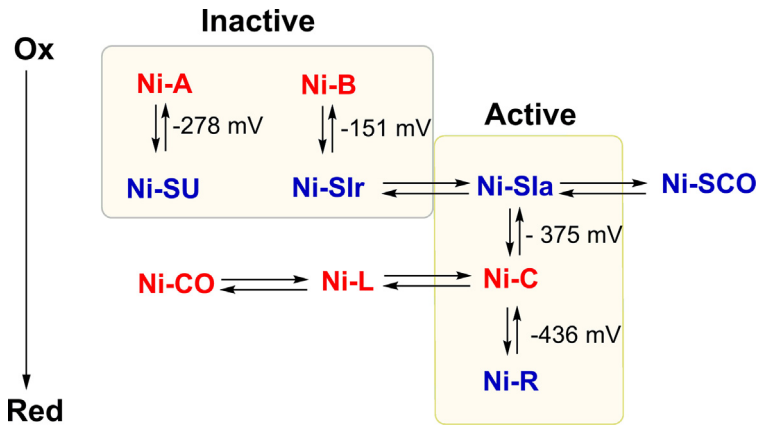

Fig. 10 Scheme of the oxidation states of [Ni-Fe] hydrogenase. The EPR-detectable states and the EPR-silent states are shown in red and blue, respectively. The states involved in the catalytic cycle of the enzyme are represented in the yellow box. The nomenclature of the states is the following Ni-A (unready state), Ni-B (ready state), Ni-SU (EPR-*si*lent *u*nready state), Ni-SIr (EPR-*si*lent *r*eady state), Ni-SIa (EPR-*si*lent *a*ctive state), Ni-SCO (EPR-*si*lent *CO* inhibited state), Ni-C (EPR-detectable reduced state), Ni-L (*L*ight induced state), Ni-CO (EPR-detectable *CO* inhibited state), and Ni-R (EPR-silent *r*educed state). The reduction potential of the redox couples is given for pH 7.4, except for the Ni-A/Ni-SU pair, that is given for pH 8.2. Adapted from Pandelia, M. E.; Ogata, H.; Currell, L. J.; Flores, M.; Lubitz, W. Inhibition of the [NiFe] Hydrogenase from Desulfovibrio vulgaris Miyazaki F by Carbon Monoxide: An FTIR and EPR Spectroscopic Study. *Biochim. Biophys. Acta* **2010,** *1797*(2), 304–313.

Ni-R leading to the oxidation of Ni^{2+} to Ni^{3+} generates the Ni-C EPR active state. In this state the hydride remains a bridging ligand between the Ni and Fe atoms and the terminal Cys546 coordinating the Ni is no longer protonated (Cys546-S^-).

The Ni-C state is light-sensitive. Upon illumination with white light, the characteristic EPR signal disappears, and a new signal named Ni-L emerge. In Ni-L, the light irradiation reduces Ni^{+3} to Ni^{1+} and the hydride is transformed in H^+. The proton formed is transferred to Cys546. Ni-L can be oxidized and generates Ni-Sia oxidizing the Ni^{1+} to Ni^{2+} and releasing a H^+. The [4Fe-4S]p cluster needs to be oxidized and ready to receive an electron to enable the conversion of Ni-L state in Ni-Sia. At least two subforms have been identified with different *g* values, Ni-L1 and Ni-L2, depending on the temperature and the duration of light exposure and pH conditions.

Throughout the catalytic cycle the Fe^{2+} does not change its oxidation state and maintains the coordination to two CN^- and one CO ligands keeping the organometallic nature of the [NiFe] active site of hydrogenases.

The different EPR active and EPR-silent oxidation states of *D. vulgaris* Miyazaki F [NiFe] hydrogenase are depicted in **Fig. 10**, as well as the reduction potentials determined through spectroelectrochemical titrations for the various steps.[311,319] Similar titrations have been performed for *D. gigas*,[320] *D. fructosovorans*[321] and also for [310] [NiFe] hydrogenases. Each electron transfer is accompanied by a proton-transfer step. The two EPR-silent states Ni-SIr and Ni-SIa are in an acid-base equilibrium.[311,320]

Biohydrogen has gain importance in the discussion of future alternative energy sources to fossil fuel due to the harmless final product, water.[322] An effort has been made to produce H_2/O_2 biofuel cells and artificial hybrid solar fuels combining hydrogenase and dot-in-rod components.[266,323–326] One major drawback to further developments in this field is the O_2-sensitivity of the standard hydrogenases. Special attention is being given now to hydrogenases that are O_2-tolerant and can retain catalytic activity (hydrogen oxidation) for considerable periods of time in oxygenic environments. O_2-tolerant hydrogenases have been purified from different microorganisms. Some examples are the membrane-bound hydrogenases form *Hydrogenovibrio marinus*, *E. coli* (EcHyd-1), *A. aeolicus* and *Ralstonia eutropha*.[271-273,327] These O_2-tollerant hydrogenases upon reaction with oxygen form only the Ni-B inactive "ready" state.[272] X-Ray crystallographic structures revealed that the [4Fe-3S]p cluster is quite unique since it is coordinated by 6 cysteine residues instead of the 4 cysteine residues that coordinate the [4Fe-4S]p cluster of the O_2-sensitive enzymes (**Fig. 11**).[327] The structure of the proximal [4Fe-3S]$p^{+5/+4/+3}$ cluster enables two consecutive electron transfers with close reduction potentials, being the second electron transfer associated with a proton coupled reaction (+230 mV and +30 mV for EcHyd-1[328]). The [3Fe-4S]$m^{1+/0}$ and the proximal [4Fe-3S]p exhibit higher reduction potentials compared with the ones from the O_2-sensitive hydrogenases. The [3Fe-4S]m can transfer one electron (+190 mV for EcHyd-1[328]) and the [NiFe] active site can oxidize Ni^{2+} to Ni^{3+} supplying another electron. In the O_2-tolerant hydrogenases redox structural changes occur at the [4Fe-3S]p. For *R. eutropha* hydrogenase upon oxidation, the Fe4 position is shifted toward the amide of Cys20 in a similar manner to the Fe6 of the P-cluster of nitrogenase (**Fig. 11**).[270]

The Fe4 forms a covalent bond with the deprotonated amide nitrogen from Cys20 stabilizing the super oxidized state (**Fig. 11**). These results were also observed for super oxidized *H. marinus* and EcHyd-1 hydrogenases.[271,327] Resonance Raman and pulsed EPR spectroscopy detected a OH^- ligand at Fe1.[270]

[NiFeSe] hydrogenases are enzymes that belong to the group of [NiFe] hydrogenases but whereas a selenocysteine replaces one cysteine that coordinates the Ni in the NiFe active site. In this type of enzymes, the Ni is coordinated by three sulfur atoms from three cysteine residues and one Se atom from a selenocysteine[329,330] (**Fig. 9**C). The [NiFe] and [NiFeSe] enzymes are structurally similar with identical subunits, with the active site buried in the large subunit. The electron transfer in [NiFeSe] enzymes is also performed by a set of three iron-sulfur clusters present in the small subunit connecting the active site to the surface, however, the medial cluster is a [4Fe4S] cluster instead of the [3Fe4S] cluster present in [NiFe] hydrogenases.[304,329–332]

The [NiFeSe] hydrogenases have high catalytic activity directed toward H_2 production[333–336] and is less sensitive to oxygen showing lower reactivation times after oxygen exposure.[336] As-purified [NiFeSe] hydrogenases are EPR silent.[337–339] The aerobically purified enzymes do not form the inactive states Ni-A and Ni-B observed in [NiFe] hydrogenases characterized by the presence of a bridging oxygenated species between Ni and Fe (**Fig. 9**B). The oxygen inhibition occurs through different pathways. Computational studies suggest that the oxygen permeation pathways in [NiFe] and [NiFeSe] hydrogenases are different even though

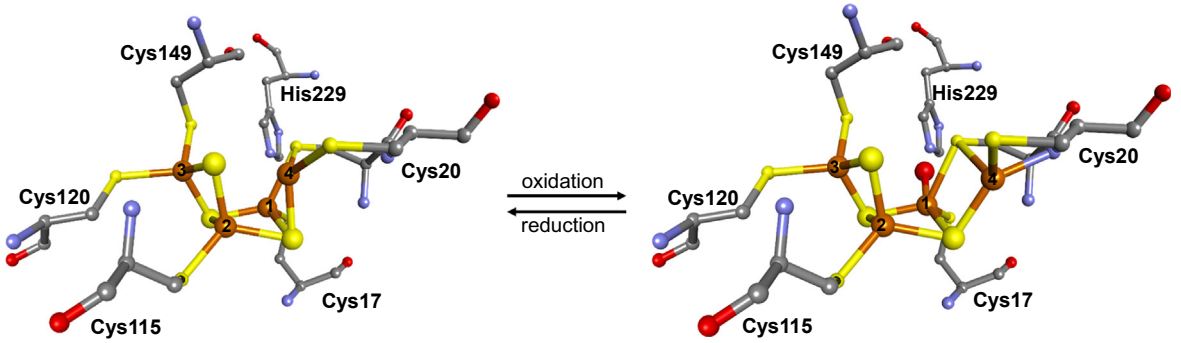

Fig. 11 The redox dependent conformational changes occurring at the [4Fe-3S]p cluster of *R. eutropha* O_2-tolerant [NiFe] hydrogenase (PDB ID 4IUD). The iron and sulfur atoms are represented in orange, yellow and green, respectively. The carbon, oxygen and nitrogen atoms are represented in gray, red, and blue, respectively. Images were created with the program Discovery Studio Visualizer (BIOVIA).

some of the resides are conserved, with the latter having a lower oxygen permeation efficiency.[340] The lower oxygen permeation along with the selenocysteine properties in the active site, different structural features like the "cage effect" surrounding the active site corroborated by the high H^+/D^+ exchange activity[341] or differences in proton transfer,[342] contributes to the unique catalytic properties of [NiFeSe] hydrogenases and their associated oxygen tolerance.

2.06.2.2.2.2 Carbon monoxide dehydrogenases/acetyl-CoA synthases

Carbon monoxide dehydrogenases/acetyl-CoA synthases (CODH/ACSs) are believed to be ancient enzymes, perhaps responsible for the ability of early organisms to live in the CO_2-rich atmospheres that existed at the origin of life.[343] These enzymes can be divided in two major groups: (i) the monofunctional enzymes, carbon monoxide dehydrogenases (CODHs), which catalyze the reversible oxidation of CO to CO_2 and (ii) the bifunctional enzymes, which in the direction of CO_2 reduction couple the synthesis of acetyl-CoA. This second group of enzymes is known as the carbon monoxide dehydrogenases/acetyl-CoA synthases, CODH/ACS complex, found in anaerobic bacteria, or as the acetyl-CoA decarbonylases/synthases, ACDS, a multienzyme complex found in archaea.[344–347] Nevertheless, based on subunit composition Lindahl et al. have grouped these enzymes into five classes.[348]

These enzymes participate in one of the known six carbon fixation pathways, the Wood-Ljungdahl pathway, which is used for energy conservation and carbon fixation in bacteria and archaea. The first produce acetate as the end-product, while the second produce methane.[347]

The monofunctional CODH enzymes have been isolated from anaerobic CO-utilizing bacteria, such as *C. hydrogenoformans and Rhodospirillum rubrum*. These enzymes are homodimers, and its X-ray structure shows the presence of three domains (a helical domain at the N-terminus, and two α/β Rossmann-like domains). The homodimer binds five metal clusters: each monomer binds one [4Fe-4S] cluster (named B-cluster) and one highly unusual [Ni-4Fe-4S] cluster (named C-cluster), which is the catalytic site (**Fig. 9**D), and there is another [4Fe-4S] cluster bound between the subunits (named D-cluster).[349,350] In the *D. vulgaris* CODH, the D-cluster is a [2Fe-2S] cluster, which is proposed to be responsible for the enzyme tolerance to oxidative damage by oxygen.[351,352]

The C-cluster is a [Ni-3Fe-4S] cubane bound to a mononuclear iron atom through one of the sulfur atoms of the cubane, (named the FCII) (**Fig. 9**D). Each metal of the [Ni-3Fe-4S] is coordinated by a cysteine residue (**Fig. 9**D), while the iron atom, FCII, is coordinated by a histidine and a cysteine residue, plus an inorganic sulfur in an approximately trigonal planar geometry.[348,352–354]

The B-cluster has reduction potentials between −390 and −440 mV, and *g* values of 2.04, 1.94 and 1.90,[355] and together with the D-cluster form an electron transfer pathway, connecting the C-cluster to the protein surface. The D-cluster, located near the protein surface, has a very negative reduction potential (below −530 mV). This cluster might play a role in holding the two subunits together,[356] and in exchanging electrons with a redox partner, such as ferredoxin.[357] As mentioned, the D-cluster is usually a [4Fe-4S] cluster bound to the polypeptide chain through the sequence motif Cys-X_7-Cys in each subunit, with exception of the *D. vulgaris* CODH, in which the [2Fe-2S] D-cluster is bound to a Cys-X_2-Cys motif.[352]

The bifunctional CODH/ACS enzymes have been identified in acetogenic bacteria and methanogenic archaea, such as *Moorella thermoacetica* (previously known as *Clostridium thermoaceticum*) and *M. barkeri*. These enzymes are tetramers with the subunits arranged as $\alpha_2\beta_2$. The X-ray structures of *M. thermoacetica* CODH/ACS complex[358] and of *C. hydrogenoformans* ACS subunit[359] revealed that the ACS α-subunits are located toward the outside, while the CODH β-subunits form a central core. The ACS subunit has three structural domains: (i) the N-terminal domain that interacts with the CODH subunit, (ii) the middle domain, and (iii) the C-terminal domain that binds the catalytic site (named A-cluster) (**Fig. 9**E). The CODH subunit binds similar metal clusters to the ones described above for the monofunctional CODH. The three-domain ACS subunit can adopt different conformations, depending on the reaction catalyzed: (i) for the carbonylation, the CO reduced from CO_2 in the C-cluster of CODH travels through the hydrophobic channels, in a diffusion controlled manner, to the A-cluster in ACS, to be assembled with coenzyme (CoA) and a methyl group to form acetyl-CoA, while (ii) for the methylation, the ACS is in an open state, so that a corrinoid iron-sulfur protein can bind, delivering the methyl group.[360]

The A-cluster, [2Ni-4Fe-4S], is constituted by a [4Fe-4S] cluster bridged by a cysteine side chain to a proximal nickel atom (Ni_p), and this proximal metal site is in turn bridged by two cysteine side chains to the distal nickel atom (Ni_d), which is in a square-planar thiolato- and carboxamido-type N_2S_2 coordination environment.[348,353] The overall architecture of the A-cluster is similar to the H-cluster of the [FeFe]-hydrogenases, since both contain a [4Fe-4S] cluster bridged to a binuclear site.[361] Thus, the A-cluster is also a unique and one of the most complex cofactors found in biological systems. The proximal nickel atom (Ni_p) in the A-cluster can be substituted by Cu or Zn, and thus this binuclear part of the A-cluster can be found as Cu-Ni or as Zn-Ni, besides the physiologically relevant Ni-Ni.[358,359,362,363] X-ray structures are available for these different clusters, but as the physiologically relevant form of the A-cluster is the one containing Ni-Ni, only this cluster is depicted in **Fig. 9**E. The structure of A-cluster with bound CO has been solved, which provided further insights into the catalytic mechanism of this enzyme.[360]

Similarly to iron-sulfur clusters, hydrogenase and nitrogenase, the unique C- and A-clusters have specific biosynthetic pathways that involve dedicated chaperones and proteins. A description of this molecular systems is outside of the scope of this chapter, but more information can be found in.[364,365]

2.06.2.2.2.2.1 Redox and spectroscopic properties of the C-cluster

The C-cluster can be in four oxidation states, named C_{ox}, C_{red1}, C_{red2} and C_{int}. The inactive C_{ox} state is diamagnetic, but at potentials below −200 mV, it is reduced by one electron to the C_{red1} state, with a $S = 1/2$, exhibiting an EPR signal with a g_{av} of 1.82 (*g* values

of 2.01, 1.81 and 1.65).[366,367] Mössbauer studies revealed that C_{red1} contains four iron atoms, two of which are designated FCII and FCIII (the other two iron atoms could not be individually characterized). FCIII is a high-spin Fe^{2+} that, along with the uncharacterized iron atoms, probably constitutes the [3Fe-4S] subsite. FCII is a high-spin five- or six-coordinated Fe^{2+} and it is almost certainly the iron of the [Ni-S-Fe] subsite. ENDOR studies by Hoffman and co-workers indicated that a histidine residue coordinates the FCII site,[368] and that cyanide, a potent tight-binding inhibitor of CO/CO_2 catalysis, binds to FCII in the C_{red1} state and displaces a strongly coupled OH^- group.[357,368,369]

The C-cluster exhibits two additional oxidation states named C_{red2} and $C_{int.}$[366,370–372] The two-electron reduced C_{int} is EPR silent, while C_{red2} is a three-electron reduced form, that binds CO (C_{red1}/C_{red2} has a reduction potential of approximately −530 mV). C_{red2} has a $S = 1/2$ spin state and exhibits an EPR signal similarly to that of C_{red1} but with a g_{av} around 1.86 (g values of 1.97, 1.87 and 1.75). The C_{red1}-to-C_{red2} conversion is substrate-dependent and occurs under argon atmosphere, presenting a reduction potential close to the CO/CO_2 couple (−558 mV).

The spectroscopic properties of C_{red2} have been difficult to study since B-clusters (and probably D-clusters) are paramagnetic under conditions where C_{red2} is produced.[369] However, it is clear, that FCII is present in C_{red2} spectra, and that the strongly coupled OH^-, evident in the ENDOR studies of C_{red1} is absent.[368,369] Although the electronic structure of C_{red1} and C_{red2} is not known, the unpaired electron spin density is proposed to be localized on the iron atom, to account for the large ^{57}Fe and small ^{61}Ni hyperfine coupling.[366,373]

The catalytic mechanism at the C-cluster has been the subject of several studies,[28,368,374,375] with one of the most difficult aspects of the cycle, being the location of the two electrons in the most reduced state of the cluster (C_{red2}). Three hypotheses are currently accepted: (i) dative Ni-Fe bond, (ii) Ni^0 atom, and (iii) hydride-bond Ni^{2+}.[348,376,377]

Further insights into the structure and catalytic mechanism of the C-cluster have been obtained through inhibition studies, using cyanide and molecular oxygen.[378–380] These studies revealed that these enzymes have different susceptibilities to oxygen, and that the C-cluster can adopt different conformations.[351,352,378,381] The structure of the oxidized form of *D. vulgaris* CODH C-cluster showed that the FCII and the Ni atom, as well as some of the residue sidechains in the cluster binding site are shifted from the canonical position. This rearrangement, in which those two metal exchange positions,[352] can confer plasticity to the cluster to avoid oxygen damage, and be critical for cluster assembly (Ni incorporation) and show that the metals in these complex clusters are mobile.

2.06.2.2.2.2.2 Redox and spectroscopic properties of the A-cluster

The A-cluster can be stabilized in two oxidation states, the A_{ox} state with a $S = 0$ spin state and the $A_{red\text{-}CO}$ state with a $S = 1/2$. Conversion of the A_{ox} to $A_{red\text{-}CO}$ involves one-electron reduction and CO binding. The $A_{red\text{-}CO}$ state exhibits the so-called NiFeC EPR signal, (with g values of 2.074 and 2.028) since the incorporation of ^{61}Ni ($I = 3/2$), ^{57}Fe ($I = 1/2$), and ^{13}CO ($I = 1/2$) in the cluster, the hyperfine-lines broadens the signal. These studies conducted by Ragsdale, Wood, and Ljungdahl provided the first evidence for a [NiFeS] cluster in Biology.[345,382]

The basic structure of the A-cluster was determined using EPR, ENDOR and Mössbauer spectroscopies, model compounds and XAS,[345,373,382–384] with the strongest evidence being revealed when methods were developed to isolate the α-subunits from *M. thermoacetica* CODH/ACS.[385,386] This procedure enabled the evaluation of the spectroscopic properties of the A-cluster without interference from the other clusters in the β-subunit. The Mössbauer and UV–visible spectroscopic studies demonstrated that the nickel atom in the A_{ox} state presents a +2 oxidation state, while in the $A_{red\text{-}CO}$ state it is in the reduced +1 oxidation state. Thus, A_{ox} corresponds to $[4Fe\text{-}4S]^{2+}$-X-Ni^{2+}, and $A_{red\text{-}CO}$ corresponds to $[4Fe\text{-}4S]^{2+}$-X-Ni^{1+}-CO.[385,386]

The intensity of the NiFeC signal was also determined and only ≈ 0.3 spin/α-subunit was obtained, which is significantly lower than the expected value of 1. This was explained based on the lability of the nickel atom at the Ni_p site, which can be removed using 1,10-phenanthroline.[387] This procedure eliminates acetyl-CoA synthase activity and the ability to generate the $A_{red\text{-}CO}$ state and the NiFeC signal. The Ni reincorporation reactivates the enzyme and restores its ability to generate this state and signal. The amount of nickel removed and replaced (≈ 0.3 Ni/αβ) suggested that only ≈ 30% of the A-cluster has labile nickel atoms and are catalytically active, exhibiting the NiFeC EPR signal.[385,387] The remaining A-cluster has nonlabile Ni atoms and do not exhibit the NiFeC signal, thus being inactive.

2.06.3 Direct catalysis at iron-sulfur clusters

The focus of this chapter will be the catalysis mediated by iron-sulfur clusters, which include the expanding group of iron-sulfur cluster-mediated radical catalysis, new and old dehydratases, and isomerase activities, and ADP-ribosyltransferases.

Most of these enzymes have a [4Fe-4S] cluster in its active site, which is usually bound by three cysteinyl ligands, in opposition to the cubane-type [4Fe-4S] cluster involved in electron transfer that is coordinated by four cysteine residues. The unique fourth iron atom, with an empty or weak coordination, found in catalytic iron-sulfur clusters, is usually the binding site for different substrates and/or involved in the binding of intermediate species.[388] A similar feature is also observed in copper or heme binding enzymes.[389]

Moreover, the catalytic properties of the iron-sulfur clusters are related to their capacity to shift electrons within the cluster and its ligands, leading to the polarization of attached or nearby groups or molecules.

2.06.3.1 Radical-SAM enzymes

The first enzyme shown to be S-adenosylmethionine-dependent was the pyruvate formate-lyase activating enzyme, in 1965 by Knappe and co-workers.[390] Five years later, Barker and co-workers reported the isolation and characterization of 2,3-aminomutase from *Clostridium subterminale* SB4.[391] These researchers found that the activity of these enzymes was dependent on S-adenosylmethionine (SAM) and Fe^{2+}. In recent years, the number of enzymes belonging to this family has increased from 650, in the years 2000's identified by primary sequence alignments in all kingdoms of life,[392,393] to over 100,000 using metagenomic data.[394] More than 50 different reactions have been recognized to be catalyzed by these enzymes,[394,395] which usually involve difficult chemistries. Some examples are sulfur insertion, glycyl radical formation, the cleavage of non-activated C—H and C—C bonds, dehydration of 2-hydroxyacyl-CoA, the reduction of aromatic compounds, unusual methylation, methylthiolation, isomerization and ring formation. Thus, these enzymes catalyze different steps in several pathways,[393] such as nucleic acid modification,[396,397] antibiotic and herbicide biosynthesis,[398,399] synthesis of organic cofactors (e.g., biotin[400] and menaquinone (vitamin K)[397]), and the biosynthesis of the complex iron-sulfur clusters of nitrogenase (FeMoco),[401–403] and [FeFe] hydrogenase (H-cluster).[404] Some of these enzymes are listed in **Table 2** and some of the most studied SAM-dependent enzymes will be briefly described here. A comprehensive list of these enzymes and the reaction they catalyze can be found in.[394,395,426]

The radical-SAM superfamily of proteins has a conserved cysteine motif, usually at the N-terminus with a consensus Cys-X_3-Cys-X_2-Cys motif[393] that coordinates the [4Fe-4S] cluster, leaving one iron atom with an incomplete coordination, and the possibility to be coordinated by the amino and carboxylate groups of S-adenosylmethionine. This bidentate ligation of this unique iron was first proposed based on spectroscopic studies[427–432] and confirmed afterwards when the X-ray structure of biotin synthase was solved.[36] This bidentate ligation is proposed to be pivotal for proper positioning for radical generation.[431,433] The mentioned consensus sequence motif is present in 90% of the primary sequences, but variations in the spacing between cysteine 1 and 2 or 2 and 3 have been observed, with the number of residues varying between 3 and 22.

Adjacent to the third cysteine, there is also a conserved aromatic residue (His, Phe, Tyr or Trp), which protects the iron-sulfur cluster from the solvent and thus lowers its reduction potential.[393,434] Sequence alignments also revealed the presence of a "glycine-rich region" or a "GGE motif" (Gly-X-Ile-X-Gly-X_2-Glu) that binds the amino group of adenosylmethionine through H-bonds,[393,435] and positions it in the correct orientation to coordinate the unique iron of the iron-sulfur cluster.

The active site [4Fe-4S] cluster is oxygen sensitive and can rapidly degrade to a [3Fe-4S] cluster (or be destroyed) during isolation and characterization when oxic conditions are used, which made the initial studies on these enzymes difficult. Nevertheless, the structure of several radical-SAM enzymes has been determined. These structures share a common core fold composed by eight or six β,α-pair motifs arranged in a triose phosphate isomerase (TIM) barrel-fold, that is not completely closed in most of the known structures.[36,433,436,437] This TIM-fold has also been found in domains of multidomain proteins, such as viperin.[396]

The exposed face of the β-sheet harbors the active site residues that bind the essential oxygen-sensitive [4Fe-4S] cluster and the adenosylmethionine. In most of the radical-SAM enzymes, the active site [4Fe-4S] cluster is buried at 7–10 Å from the surface,[433] but being somewhat solvent accessible and in an amenable distance to receive electrons from redox partners. Some of these enzymes have other redox active centers, mainly [4Fe-4S] and [2Fe-2S] clusters,[438] but cobalamin has also been observed in other structural domains.[439]

The catalytic mechanism of most of these enzymes shares a common step in which SAM is reductively cleaved by a reduced $[4Fe\text{-}4S]^{1+}$ cluster (**Fig. 12**), giving rise to methionine and to a highly oxidizing and unstable radical, the 5′-deoxyadenosyl radical, which is then used to initiate each specific reaction.

The detailed mechanism for the formation of this radical has been a matter of debate for many years, with several spectroscopic and computational studies performed on both enzymes and model compounds. In one of the proposed mechanisms, it is the unique iron of the $[4Fe\text{-}4S]^{1+}$ cluster that mediates the electron transfer to the sulfonium of adenosylmethionine[421,428,440] and the formation of the iron-sulfur bond reduces the activation energy for the homolytic cleavage of C-S bond (**Fig. 12**A). This proposal is based on the binding geometry of the S-adenosylmethionine, which positions its sulfur in a closer distance to the Fe (3.4 Å) than the sulfur (3.8 Å) of the iron-sulfur cluster.

Based on ENDOR and Mössbauer experiments another mechanism has been proposed, in which the $[4Fe\text{-}4S]^{1+}$ will function as an electron donor, with an electron being transferred from a sulfide (from the iron-sulfur cluster) to the sulfonium (**Fig. 12**B).[429,431,432,441] Recent quantum mechanical/molecular mechanical (QM/MM) computations on the mechanisms of biotin synthase supports this later proposal, which is now considered to be the accepted mechanism for radical SAM cleavage.[421,442]

The first step of this mechanism is the one-electron reduction of the $[4Fe\text{-}4S]^{2+}$ cluster to $[4Fe\text{-}4S]^{1+}$, by a reducing agent. For some of the enzymes their physiological reducing agent has been identified to be single electron donors, such as NADPH,[443] flavodoxin[443,444] or flavodoxin reductase.[445] However, for many enzymes the reductant has still not been established, though in *in vitro* assays, sodium dithionite or photoreduced 5-deazariboflavin are the electron donors usually used.[446] Protein film voltammetry has also been applied to the characterization of some of these enzymes, which avoids the use of electron donors, and enables the determination of the reduction potential of the active site and of the additional redox centers, as well as its pH dependence under turnover and non-turnover conditions.[447]

Most of the studied radical-SAM dependent enzymes have in common the formation of a radical, 5′-deoxyadenosyl radical, that is used for stereospecific hydrogen abstraction and formation of a carbon radical (**Fig. 13**A), as mentioned before. However, these enzymes differ on how the radical is used in the reaction cycle. Another group of SAM-dependent enzymes catalyze the adenosylation of substrates by adding the generated 5′-deoxyadenosyl radical to a sp2 carbon (**Fig. 13**B). These enzymes are involved in natural product biosynthetic pathways and are attracting attention due to its potential in biocatalysis and bioengineering applications.[448] Examples of these enzymes are adenosylhopane synthase (HpnH) and aminofutalosine synthase (MqnE). Adenosylhopane synthase is an enzyme involved in the biosynthesis of a bacteriohopanepolyol, aminobacteriohopanetriol, by *Streptomyces*

Table 2 Some examples of radical SAM-dependent enzymes.

			References
Radical SAM Mutases			
LAM	Lysine 2,3-aminomutase	β-Lysine antibiotics, lysine metabolism	405
PylB	Lysine Mutase	Pyrrolysine Biosynthesis	406
Radical SAM Chemistry to Cleave C-X (X= C,N,P) Bonds			
SplB	Spore photoproduct lyase	initiates DNA repair	407
Sulfur Insertion			
LipA	Lipoyl synthase	Sulfur Insertion/Lipoic acid biosynthesis	408
BioB	Biotin synthase	Sulfur Insertion/Biotin biosynthesis	36
Modified Tetrapyrroles Synthesis			
HemN	Coproporphyrinogen III oxidase	Heme biosynthesis	409
Glycyl Radical Enzyme Activation			
PFL-AE	Pyruvate formate-lyase activating enzyme	Glycyl radicalization in pyruvate metabolism	410
ARN-AE	Anaerobic ribonucleotide reductase activating enzyme	Glycyl radicalization in dNTP synthesis	411
GD-AE	Glycerol dehydratase activating enzyme	Glycyl radicalization of glycerol dehydratase	412
BSS-AE	Benzylsuccinate synthase activating enzyme	Glycyl radicalization in toluene metabolism	413
HPD-AE	4-Hydroxyphenylacetate decarboxylase activating enzyme	Formation of *p*-cresol	414
FGS	Formyl glycine synthase		415
Methylation and Methylthiolation			
MiaB	Methylthiolation of tRNA	Sulfur Insertion/Thiomethylation of isopentenyl adenosine in tRNA	416
RimO	Methylthiolation of ribosomal protein S12	Methylthiolation of residue D88 of S12	417
RlmN	rRNR methyltransferase	Methylation of position 2 of adenosine2503 in 23S ribosomal RNA	418
Cfr	rRNR methyltransferase	Methylation of position 8 of adenosine2503 in 23S ribosomal RNA	418
Complex Rearrangements and Cyclizations			
ThiC	Hydroxymethylpyrimidine phosphate synthase	Thiamine pyrimidine biosynthesis	419
MoaA	Molybdopterin biosynthesis protein A	Molybdenum cofactor (Moco) biosynthesis	420
Complex Metal Cluster Biosynthesis			
HydE	[FeFe] Hydrogenase maturase protein	[FeFe] hydrogenase cluster biosynthesis	421
NifB	FeMoco maturase protein	Biosynthesis of the FeMoco of nitrogenase	403,422
Dehydration			
BtrN	Biosynthesis of 2-deoxystreptamine	Conversion of 2-deoxy-scyllo-inosamine into 3-amino-2,3-dideoxy- scyllo-inosose	423
Viperin	Viperin - antiviral activity – 3'-deoxy-3',4'-didehydro-CTP (ddhCTP) synthase	Conversion of cytidine triphosphate (CTP) to 3′-deoxy-3′,4′-didehydro-CTP (ddhCTP)	424
Other chemistries outside SAM superfamily			
Dph2	Diphthamide biosynthesis protein 2	diphthamide biosynthesis	425

coelicolor, while aminofutalosine synthase is involved in an alternative pathway of menaquinone biosynthesis, which has been identified in some human pathogens, such as *Campylobacter jejuni* and *Helicobacter pylori*.

2.06.3.1.1 Examples of radical-SAM enzymes

2.06.3.1.1.1 Radical SAM mutases - lysine 2,3-aminomutase

In some enzymes that catalyze isomerizations, such as lysine 2,3-aminomutase (LAM),[405] spore photoproduct lyase,[407] SAM is used as a reversible source of the 5′-deoxyadenosyl radical, and thus it functions as a coenzyme. Then the 5′-deoxyadenosyl radical mediates hydrogen transfer from the substrate and is regenerated to SAM after each catalytic cycle.

LAM isolated from *C. subterminale* SB4, catalyzes the interconversion of L-lysine and L-β-lysine (**Fig. 14**) and was the first enzyme to be characterized as a radical-SAM dependent enzyme.[391] It was shown that LAM binds an iron-sulfur cluster and requires pyridoxal-5′-phosphate and SAM for full activity.[449,450]

Several spectroscopic and kinetic studies were used to elucidate LAM kinetic mechanism.[451] This mechanism is initiated by the formation of the 5′-deoxyadenosyl radical, which is then used to cleave the C-H bond at C-3 of the lysine bound to the pyridoxal-5′-phosphate through an imine linkage, by abstracting a hydrogen atom. The intermediate that is formed, with a carbon radical, undertakes two rearrangement steps with migration of the nitrogen to C-3, and in the last step the 5′-deoxyadenosyl radical is regenerated.[452–454] ENDOR has been used to elucidate the mechanism of this enzyme, in which the 5′-deoxyadenosyl radical is never in the free state.[455]

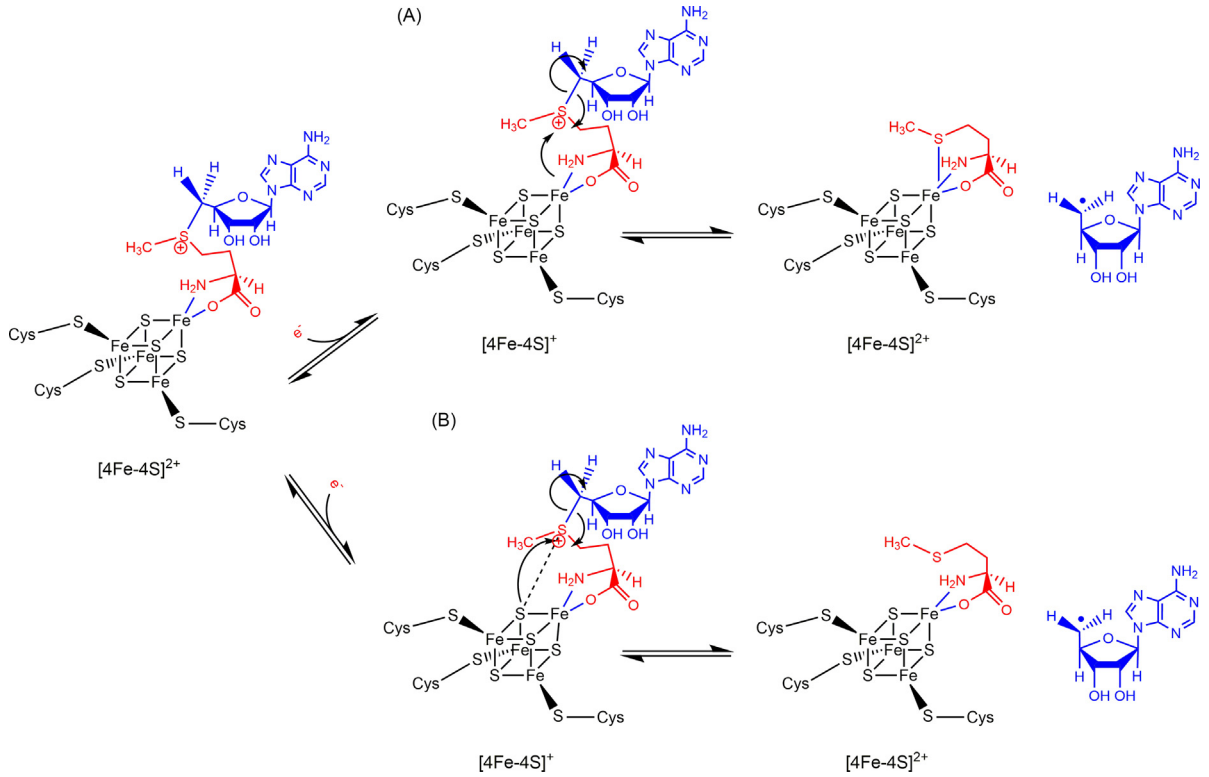

Fig. 12 The binding mode of S-adenosyl-L-methionine to the iron-sulfur cluster and the two proposed mechanisms for the formation of the 5′-deoxyadenosyl radical through the homolytic cleavage to the C5'-S bond of adenosylmethionine. In (A) the formation of the radical is driven by the formation of the bond between the sulfonium ion and the unique iron, while in (B) there is an electron transfer mediated by the interaction of the sulfide of the iron-sulfur cluster with the sulfonium of adenosylmethionine. This is the accepted mechanism.

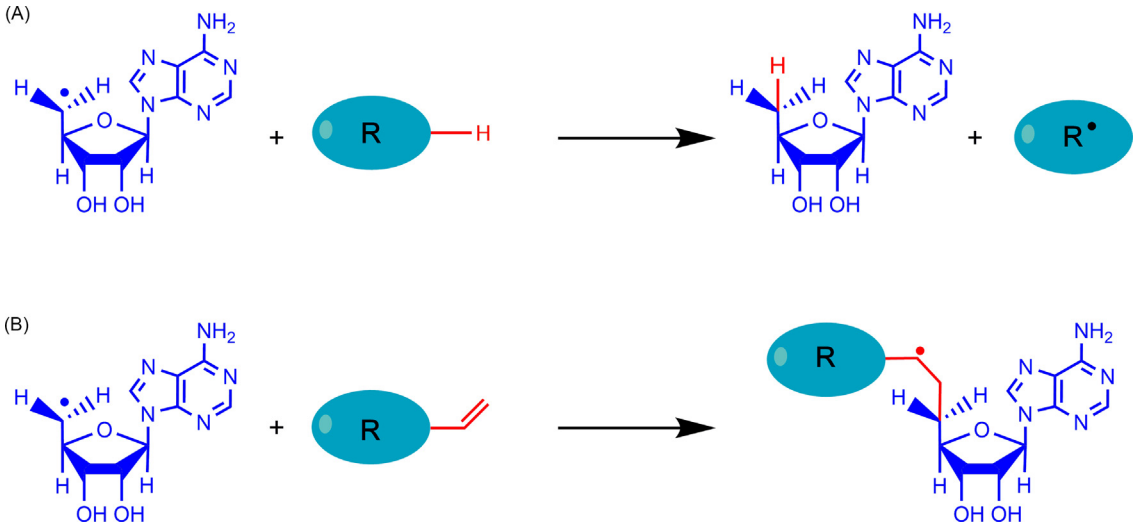

Fig. 13 Generic reactions catalyzed by radical SAM-dependent enzymes. In panel (A) is shown the hydrogen abstraction mediated by 5′-deoxyadenosyl radical (the canonical reaction). In panel (B) is shown the 5′-deoxyadenosyl radical addition that results in the adenosylation of a substrate.

2.06.3.1.1.2 Catalysis of sulfur insertion - biotin synthase

Biotin synthase catalyzes the sulfur insertion in dethiobiotin to form biotin, through the formation of two C-S bonds in non-activated carbons (C6 and C9). In each catalytic cycle, the enzyme requires two molecules of SAM[36,400,456] (Fig. 15).

This enzyme, like lysine aminomutase, has also been extensively studied, but some questions remain. For many years, it had been debated what was the source for the sulfur, though now it is generally accepted that it is the [2Fe-2S] center present in the

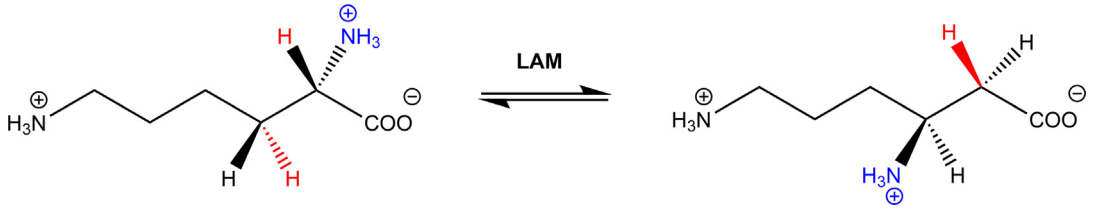

Fig. 14 Reaction catalyzed by lysine 2,3-aminomutase.

enzyme. The clarification of the mechanism of biotin synthase was based on experiments that used ^{33}S isotopic labeling,[457] the observation that the [2Fe-2S] cluster disassembles at each turnover of the enzyme,[92,456,458] and that this cluster and dethiobiotin are in close proximity.[36] However, the mechanism and intermediates that are formed are still a matter of debate and of extensive study, as it is proven by the several publications on the subject.[442,459,460]

Since the [2Fe-2S] cluster is destroyed after each turnover cycle, it has been questioned whether this enzyme could be a suicidal enzyme. However, it was later shown that *in vivo* the enzyme can perform several turnovers, and thus the [2Fe-2S] cluster must be regenerated after each catalytic cycle.[461]

Lipoyl synthase, like biotin synthase, also requires two equivalents of the 5′-deoxyadenosyl radical (thus two SAM molecules) to activate chemically unreactive C-H bonds of octanoyl group and inserts one mole of sulfur.[36,408,456,462]

2.06.3.1.1.3 Glycyl radical enzyme activation - pyruvate formate-lyase activating enzyme

In this family of SAM-dependent enzymes the substrate is another enzyme, that requires the generation of an active site radical.[410,411,413] In this case, stoichiometric SAM is used as an oxidizing substrate to stereospecificaly abstract a proton from a conserved active site-glycine residue, forming a stable glycyl radical, and releasing methionine and 5′-deoxyadenosyl radical, as by-products. This glycyl radical is transferred to a cysteine and the cysteinyl radical is then used to activate the enzyme substrate (**Fig. 16**). The rational for using a cysteinyl radical in the catalysis is the formation of a weak S-H bond that will then donate H• to the product.

Pyruvate formate-lyase activating enzyme has been highly studied, and several spectroscopic techniques have been applied to clarify its catalytic mechanism.[431,432,463–465] This enzyme catalyzes the formation of a glycyl radical in the partner protein, the pyruvate formate-lyase, through the abstraction of the pro-S hydrogen from Gly734 in a SAM dependent reaction,[466] which also requires the presence of reduced flavodoxin (or other artificial one-electron donors)[467] (**Fig. 17**).

The pyruvate formate-lyase activating enzyme presents an oxygen sensitive [4Fe-4S] cluster per monomer, that is active in the reduced $[4Fe\text{-}4S]^{1+}$ form in the presence of SAM.[468–470] However, even when the enzyme was purified under anaerobic conditions, which increased the content in [4Fe-4S] cluster, Mössbauer data revealed the presence of iron mainly as $[3Fe\text{-}4S]^{1+}$, with minor amounts of $[2Fe\text{-}2S]^{2+}$ and $[4Fe\text{-}4S]^{2+}$ clusters, in the as-isolated form, which converted to $[4Fe\text{-}4S]^{2+/1+}$, when reduced with sodium dithionite.[469,471] Further *in vivo* Mössbauer studies of this enzyme showed the presence of a cluster interconversion process in response to higher oxygen levels, which has been proposed to be a process to control the pyruvate formate-lyase activity.[472] Although, a similar activity control by cluster interconversion has been observed in aconitase/IRP1 (*vide infra*), in the case of pyruvate formate-lyase activating enzyme, the cluster is proposed to interconvert between $[2Fe\text{-}2S]^{2+}$ and $[4Fe\text{-}4S]^{2+}$.[472] These *in vivo* studies also established that this $[4Fe\text{-}4S]^{2+}$ was valence-localized, an unusual feature, while the one in the as-isolated enzyme is valence delocalized, possibly indicating the loss of a ligand during protein purification.[472] The identity of this small molecule is still unknown, but Broderick and co-workers showed that addition of adenosyl-based molecules causes valence localization of $[4Fe\text{-}4S]^{2+}$.[472]

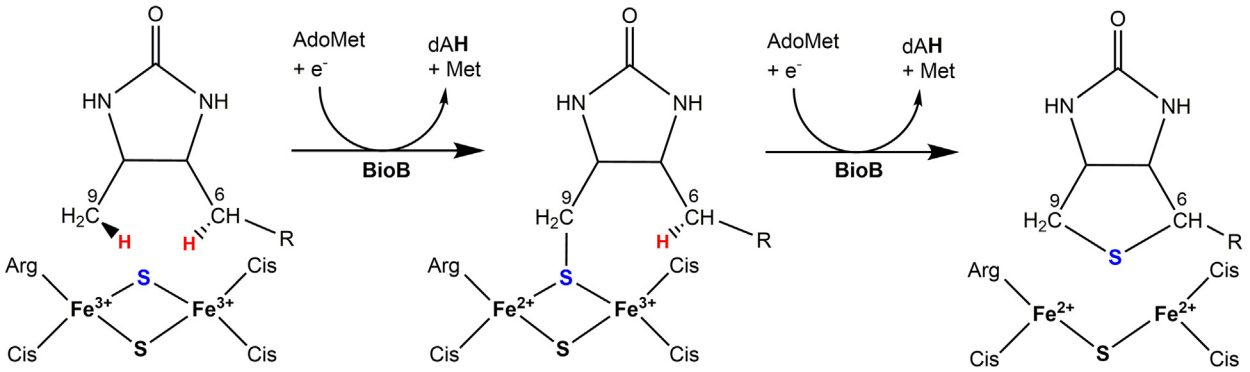

Fig. 15 Reaction catalyzed by biotin synthase. Adapted from Taylor, A. M.; Stoll, S.; Britt, R. D.; Jarrett, J. T., Reduction of the [2Fe-2S] Cluster Accompanies Formation of the Intermediate 9-Mercaptodethiobiotin in Escherichia coli Biotin Synthase. *Biochemistry* **2011,** *50*(37), 7953–7963.

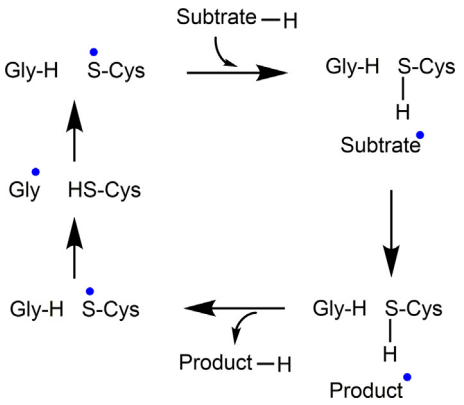

Fig. 16 Generic mechanism of the catalytic cycle of glycyl radical enzymes. Adapted from Selmer, T.; Pierik, A. J.; Heider, J., New Glycyl Radical Enzymes Catalysing Key Metabolic Steps in Anaerobic Bacteria. *Biol. Chem.* **2005,** *386*(10), 981–988.

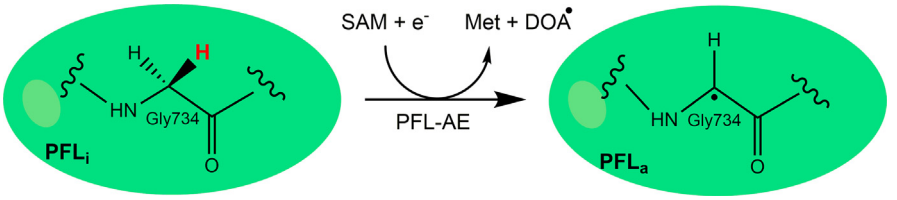

Fig. 17 Reaction catalyzed by pyruvate formate-lyase activating enzyme (PFL-AE), that through the formation of 5′-deoxyadenosyl radical (DOA) produces the glycyl radical at Gly734 activating PFL. a – active, i – inactive.

Moreover, an important question remains to be answered relative to the mechanism and conformational changes that are required in the complex of the two proteins for the direct and stereospecific abstraction of the hydrogen from the specific glycyl residue. Nevertheless, some insights have been obtained through structural studies on the pyruvate formate-lyase activating enzyme complexed with a 7-mer peptide with the sequence surrounding Gly734,[473] which pointed out for the occurrence of a conformational change in the structure of the protein. In fact, other structural studies indicated that Gly734, buried at 8 Å from the surface in the active pyruvate formate-lyase, is more solvent exposed in an open conformation of the inactive enzyme, probably to enable hydrogen abstraction by the activating enzyme.[474]

A monovalent cation was identified in the X-ray structure of the protein, being coordinated by a backbone carbonyl, the side-chain of two conserved aspartate residues, and an oxygen of SAM's carboxylate. The role and identity of this cation is still under investigation, though an increase in enzymatic activity of the pyruvate formate-lyase activating enzyme was attained in the presence of K^{1+}.[475]

2.06.3.1.1.4 Catalysis of methylations by RlmN and Cfr

RlmN and Cfr are methyltransferases (recently proposed to be methyl synthases) involved in the methylation of a specific adenosine nucleotide (adenosine2503) in the peptidyl transferase center of the ribosome.[476,477] This methylation is a post-transcriptional modification of 23S rRNA nucleotides and functions as a mechanism to modulate the ribosome's function and confer bacterial resistance to ribosome-targeting antibiotics.[477,478]

These enzymes are radical SAM enzymes containing an iron-sulfur cluster bound to the usual motif Cys-X_3-Cys-X_2-Cys,[479] and use S-adenosylmethionine as the source of 5′-deoxyadenosyl radical and methyl donor to the aromatic carbon atoms to form the 2,8-dimethylated product.[480] The proposed mechanism includes the formation of a 5′-deoxyadenosyl radical that abstracts hydrogen from a second S-adenosylmethionine molecule to form a SAM-derived radical cation, which is then added to the substrate.[481] The reactions catalyzed by these enzymes proceed through a ping-pong mechanism that involves the transient methylation of a conserved cysteine residue that is then transferred to a electrophilic *sp2*-hybridized carbon of adenosine (**Fig. 18**), and provide evidences for these enzymes to be renamed as methyl synthases.[418,482] Thus, these enzymes use SAM to methylate an electrophilic rather than the usual nucleophilic carbon center.[482]

2.06.3.1.1.5 Dehydration – synthesis of ribonucleotide - viperin

Viperin is a protein discovered, in 1997, to respond to viral infections via the immune response pathway.[483] This 42 kDa protein has three domains: a N-terminal amphipathic alfa-helix domain, a radical SAM central domain (homologous to MoaA/NifB) and a C-terminal domain of still undefined function, with the N- and C-terminus being essential for antiviral activity.[396,484] The radical SAM containing domain was identified by the presence of conserved motifs common to other radical SAM enzymes: the Cys-X_3-Cys-X_2-Cys sequence motif that binds the [4Fe-4S] cluster and the "GGE motif", that it is responsible for the enzymatic activity.

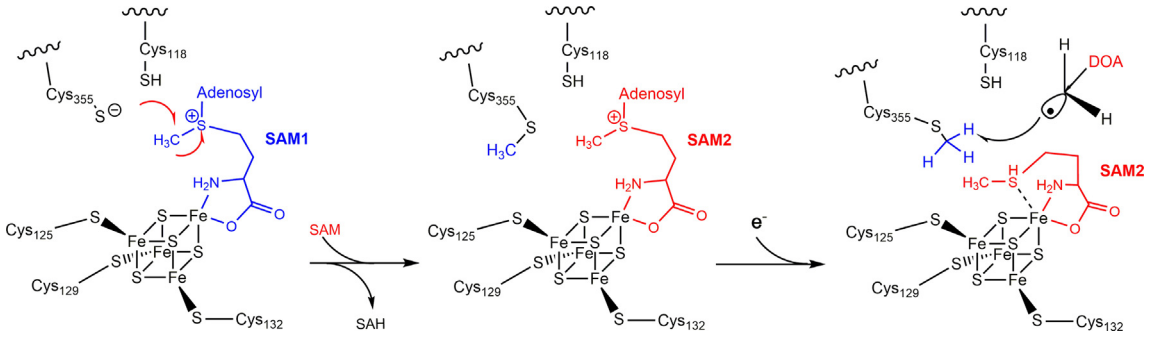

Fig. 18 Proposed mechanism of the S-adenosylmethionine activation by Cfr and RlmN. SAM – S-adenosylmethionine, SAH – S-adenosylhomocysteine, DOA – 5′-deoxyadenosyl radical. Adapted from Grove, T. L.; Radle, M. I.; Krebs, C.; Booker, S. J., Cfr and RlmN Contain a Single [4Fe-4S] cluster, which Directs Two Distinct Reactivities for S-Adenosylmethionine: Methyl Transfer by SN2 Displacement and Radical Generation. *J. Am. Chem. Soc.* **2011,** *133*(49), 19586–19589.

Viperin is encoded in the genome of both vertebrates and invertebrates, and the crystal structure of the mouse viperin has been solved by X-ray crystallography, showing to adopt a TIM-barrel fold and to bind an iron-sulfur cluster, a SAM, and a CTP molecule.[396,485–487] The enzymatic activity of viperin was demonstrated to be the conversion of cytidine triphosphate to 3′deoxy-3′,4′-didehydro-CTP (**Fig. 19**).[424,486,488] This ribonucleotide when incorporated by RNA-dependent RNA polymerase of some virus leads to premature termination of the RNA synthesis.[489]

2.06.3.1.1.6 Atypical SAM-dependent enzymes

- Noncanonical radical SAM enzyme - Diphthamide biosynthesis protein 2

A different mechanism of SAM cleavage was observed in diphthamide biosynthesis protein 2 (Dph2), which instead of the 5′-deoxyadenosyl radical generates a 3-amino-3-carboxypropyl radical.[425] In addition, this radical also undergoes a different chemistry, an addition and not the classical hydrogen abstraction.

Dph2 is responsible for the catalysis of the first step of diphthamide biosynthesis, a rare amino acid.[490,491] Diphthamide modification is a post-translational modification of a histidine residue in the translation elongation factor 2 (EF-2) of eukaryotes and archaea, which is essential for ribosomal protein synthesis.[492,493] This modified histidine is the target of a toxin secreted by *Corynebacterium diphtheriae*, the diphtheria toxin, which catalysis the ADP-ribosylation of that histidine.[494]

Biophysical and structural studies on this enzyme have shown that it is a homodimer in archaea (e.g., *Pyrococcus horikoshii* Dph2), with the [4Fe-4S] cluster being coordinated by three cysteines Cys59-X_n-Cys163-X_n-Cys287, which are located in the three different domains and not arranged in the conserved motif found in most radical SAM-dependent enzymes.[425] In eukaryotes, the enzyme that catalyzes the same reaction is heterodimeric formed by Dph1 and Dph2.[495]

As mentioned, the catalytic mechanism of Dph2 does not involve the formation of the canonical 5′-deoxyadenosyl radical. Instead, it was observed the formation of a 3-amino-3carboxipropyl radical due to the reductive cleavage of the $C_{\gamma,Met}$-S bond of SAM.[425,496] This radical also undergoes a different chemistry, instead of hydrogen abstraction in the case of the 5′-deoxyadenosyl radical, the radical generated in Dph2 carries out an addition: the generated 3-amino-3-carboxipropyl (ACP) radical is proposed to be added to the imidazole ring of histidine for the formation of the diphthamide modification.[496] This C-C coupling forms an ACP-histidine radical intermediate (an organic radical), that can be protonated, releasing the modified EF2[497] (**Fig. 20**).

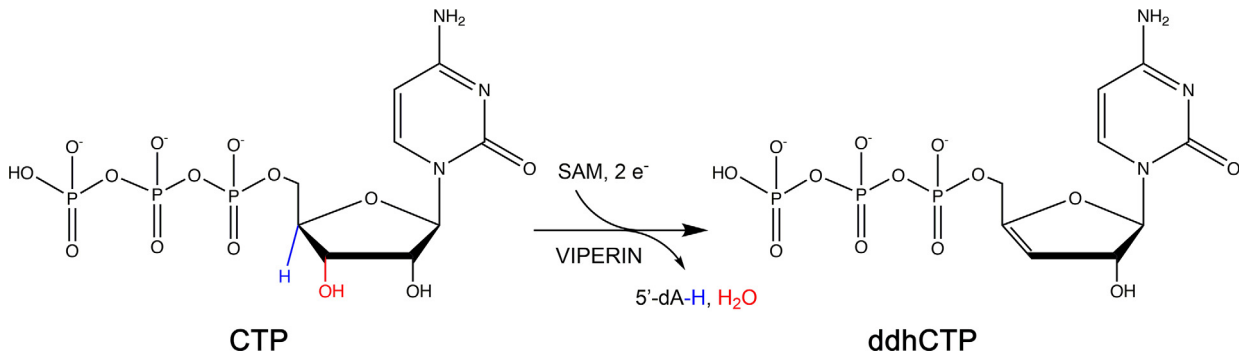

Fig. 19 Reaction catalyzed by viperin, as an antiviral ribonucleoside synthase. Adapted from Gizzi, A. S.; Grove, T. L.; Arnold, J. J.; Jose, J.; Jangra, R. K.; Garforth, S. J.; Du, Q.; Cahill, S. M.; Dulyaninova, N. G.; Love, J. D.; Chandran, K.; Bresnick, A. R.; Cameron, C. E.; Almo, S. C., A Naturally Occurring Antiviral Ribonucleotide Encoded by the Human Genome. *Nature* **2018,** *558*(7711), 610–614.

This complex catalytic mechanism has been elucidated by combining rapid-freezing EPR and ENDOR with crystallographic studies using isotopically labelled SAM. This approach enabled the captured of an organometallic intermediate formed between ACP radical and the [4Fe-4S] cluster, with an iron-carbon bond, as depicted in Fig. 20.

The electronic structure of the [4Fe-4S] cluster was shown by classical molecular dynamics and quantum mechanics/molecular mechanics to control the reductive cleavage of SAM's $C_{\gamma,Met}$-S bond, through a spin-regulated electron transfer mechanism.[498]

- Adenosylation

There is a group of enzymes that catalyze the radical SAM-dependent adenosylation (Fig. 13B) in biosynthetic pathways of natural products.[448] These enzymes have also been exploited to catalyze unnatural transformation using synthetic substrates, opening their applications to biotechnology and bioengineering. These applications include the production of nucleoside-containing compounds by modifying different olefins. Examples of these enzymes are adenosylhopane synthase and aminofutalosine synthase.[499–501]

o Aminofutalosine synthase MqnE

The synthesis of menaquinone (vitamin K2) in some pathogenic microorganisms follows an alternative pathway with aminofutalosine as an intermediate. The enzyme responsible for its synthesis, aminofutalosine synthase (MqnE), was reported to bind an iron-

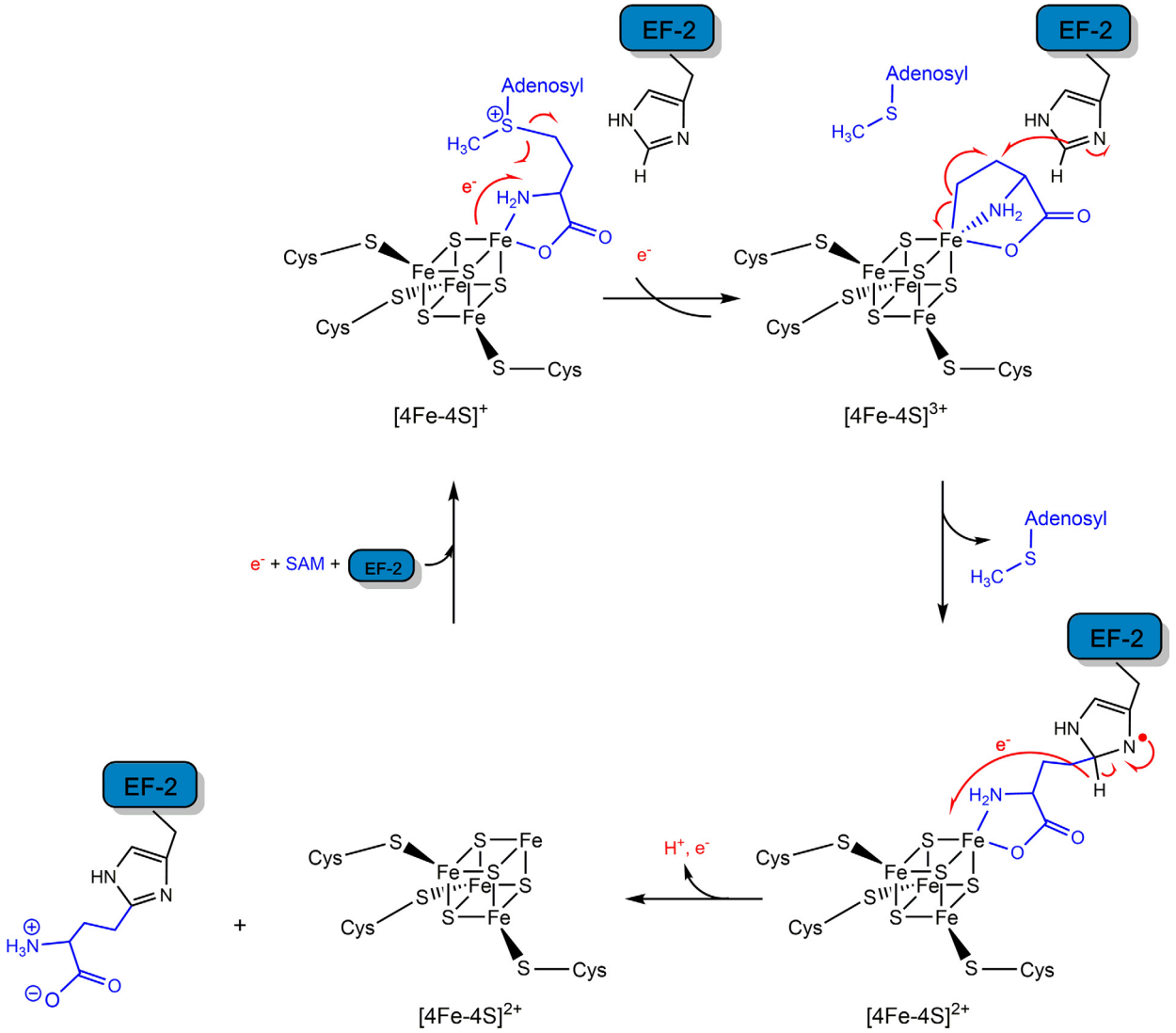

Fig. 20 Proposed catalytic mechanism of Dph2 with the formation of the 3-amino-3-carboxypropyl radical intermediate, followed by the formation of a 3-amino-3-carboxypropyl-histidine radical intermediate in the second step. Adapted from Zhu, X.; Dzikovski, B.; Su, X.; Torelli, A. T.; Zhang, Y.; Ealick, S. E.; Freed, J. H.; Lin, H. Mechanistic Understanding of *Pyrococcus horikoshii Dph2, a [4Fe-4S] Enzyme Required for Diphthamide Biosynthesis. Mol. Biosyst.* **2011,** *7*(1), 74–81; Feng, J.; Shaik, S.; Wang, B., Spin-Regulated Electron Transfer and Exchange-Enhanced Reactivity in $Fe_{4S}4$-Mediated Redox Reaction of the Dph2 Enzyme During the Biosynthesis of Diphthamide. Angew. Chem. *Int. Ed. Engl.* **2021,** *60*(37), 20430–20436.

sulfur cluster in 2013.[502] In the following years, the intermediates have been identified,[503–505] and as this enzyme is essential for some pathogenic bacteria it has been considered to be a target for the development of antibiotics.[506] In 2019, a compound, in which the bridging oxygen of 3-[(1-carboxyvinyl)oxy]-benzoic acid was substituted by a methylene group, was identified to be a potent inhibitor of *H. pylori* MqnE and also to present antimicrobial activity similar to amoxicillin and clarithromycin. This proved that this pathway and in particular this enzyme are promising targets for the development of new antibiotics against certain pathogenic bacteria, such as *H. pylori*, *Chlamydia* strains, *C. jejuni*, and Spirochaetes.

2.06.3.2 Iron-sulfur (de)hydratases

Iron-sulfur (de)hydratases are another group of non-redox enzymes that contain an iron-sulfur cluster in the active site and catalyze the removal of a water molecule from a carbon-carbon bond by converting an alcohol into a vinyl group.

These enzymes can be divided into two families that differ in the type of iron-sulfur cluster present in the active site. In one family there is a [4Fe-4S] cluster with a unique iron that is not coordinated by a cysteine side chain and define the substrate binding site. Examples of enzymes that belong to this family are L-serine dehydratase,[507] fumarase,[508,509] aconitase, a family of enzymes involved in the prokaryotic biosynthetic pathway of non-mevalonate isoprenoid (IspG and IspH), and others, such as quinolate synthase.[510–514] For most of these enzymes there has been extensive studies to elucidate their structure,[515,516] spectroscopic features (EPR, HYSCORE, Mössbauer), catalytic mechanism, and to identify intermediate species[515,517–519] and inhibitors (some with potential antibacterial properties).[520,521]

In the other family of enzymes, their active site has a [2Fe-2S] cluster, though they share the feature of having one of the iron atoms with an empty coordination site that is involved in the catalytic cycle, and transiently binds a hydroxyl group during catalysis.[522] These enzymes have been identified as belonging to a different class of aconitase enzymes and are involved in the metabolism and biosynthetic pathway of carbohydrates,[523,524] such as pentonate dehydratases.

2.06.3.2.1 Aconitase

Aconitase is an isomerase that catalysis the reversible and stereospecific dehydration/rehydration of citrate to isocitrate via cis-aconitate in the Krebs cycle.[172,525] This is a non-redox process, and for some time it was thought that this enzyme contained a simple iron center (with one Fe^{2+}), proposed to be involved in the Lewis-acid function of facilitating the hydrolytic reaction.[78]

Aconitase was the first enzyme[526,527] for which a catalytic function of an iron-sulfur cluster was identified. In addition, it has been a model system to study the role of the iron-sulfur cluster in non-redox reactions,[527] and the subject of extensive studies using different spectroscopic and biophysical methods, to elucidate its structure and catalytic cycle.

The aconitase family is composed by the true aconitases, which catalyze the isomerization of citrate to isocitrate, while there are three other groups that are involved in the isomerization of isopropylmalate in the leucine biosynthetic pathway, homocitrate in the lysine and coenzyme B biosynthetic pathways,[528–531] and methylcitrate dehydratase in the catabolism of propionate.[532,533]

In multicellular eukaryotes there are two aconitases, one in the cytoplasm (c_aconitase) and another in the mitochondria (m_aconitase), that share 30% sequence identity, but the iron-sulfur cluster sequence binding motif and other important residues in the active site are conserved.[172,534,535] The m_aconitase is one of the enzymes of the Krebs cycle, while c_aconitase is a bifunctional enzyme as in its apo-form it is the iron responsive protein1 (IRP1), a post-transcriptional regulator of the iron metabolism[536,537] (see **Section 2.06.4.1**).

The [4Fe-4S] cluster of aconitase active site shares, with the iron-sulfur enzymes described so far, the feature of having one of the iron atoms (Fe_a or the so-called unique iron) not coordinated by a cysteine residue but interacting with the carboxyl and hydroxyl oxygen atoms of the substrate and solvent species (**Fig. 19**). In the first studies on aconitase it was reported the isolation of the enzyme in an inactive form, binding a [3Fe-4S] cluster, that could be activated by restoring the [4Fe-4S] cluster by addition of a reducing agent and Fe^{2+} (see **Section 2.06.2.1.5** and **Fig. 6**).[42,172,526,538–540] This has been named the "iron-sulfur cluster switch" (**Fig. 21**), a cluster assembly/disassembly mechanism that is also responsible for the regulation of the bifunctional activity of c_aconitase/IRP1.

The active site of aconitase encompasses 21 residues with different roles: coordination of the iron-sulfur cluster (cysteines), H-bonding the substrate carbonyl moieties, the cysteine, inorganic sulfur atoms, and bound water molecules (that are also involved in the reaction).[42,540] These residues are also responsible for the stabilization of intermediates and are involved in the steps of dehydration (the nucleophilic attack performed by Ser642 is represented as: B in **Fig. 22**) and rehydration.[535] In addition, these residues dictate the global positive charge of aconitase active site and contribute to its ability to bind anionic substrates. This positive charge is attributed to the presence of four arginine residues and due to the three-active site histidine residues being paired with aspartate or glutamate residues.[172]

The fourth iron (Fe_a), occupying the empty corner of the inactive [3Fe-4S] cluster (**Fig. 21**A), has a tetrahedral geometry, and is proposed to bind a hydroxyl group. This oxygen ligand has been observed in the X-ray structure of reconstituted aconitase[42,540] (**Fig. 21**B) and identified by ENDOR experiments.[541]

The [4Fe-4S] cluster of aconitase has been characterized in different oxidation states and bound to the substrate and inhibitors by X-ray crystallography (**Fig. 21**C) and spectroscopic techniques, such as EPR, ENDOR, MCD and Mössbauer,[42,540–545] which in combination with kinetic studies and isotopic labeling experiments[546,547] enabled the proposal of the catalytic mechanism presented in **Fig. 22**.

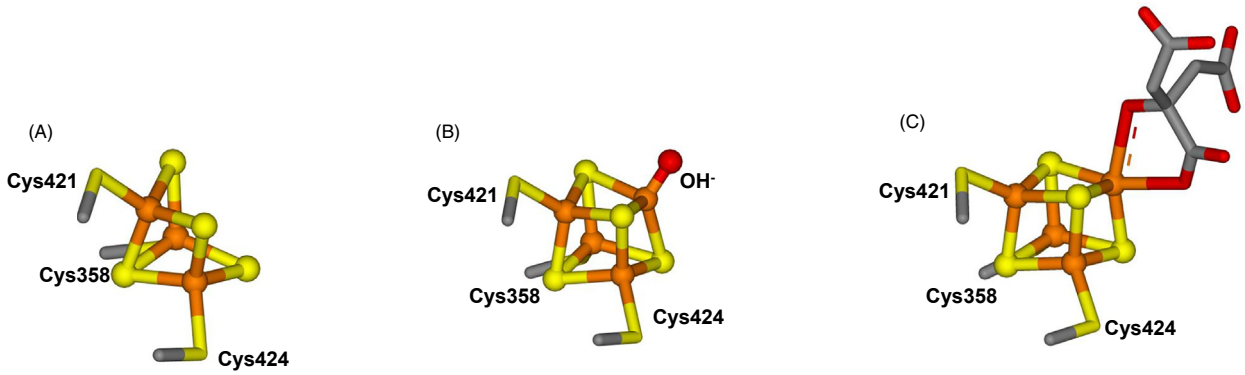

Fig. 21 Active site of aconitase in the inactive (A) and active (B) and bound to its substrate citrate (C). The atoms are colored according to element: carbon in gray, iron in orange, oxygen in red and sulfur in yellow. Figures A, B and C were prepared in Discovery Studio Visualizer (BIOVIA) using the coordinates from PDB ID 5ACN, 6ACN and 1C96, respectively.

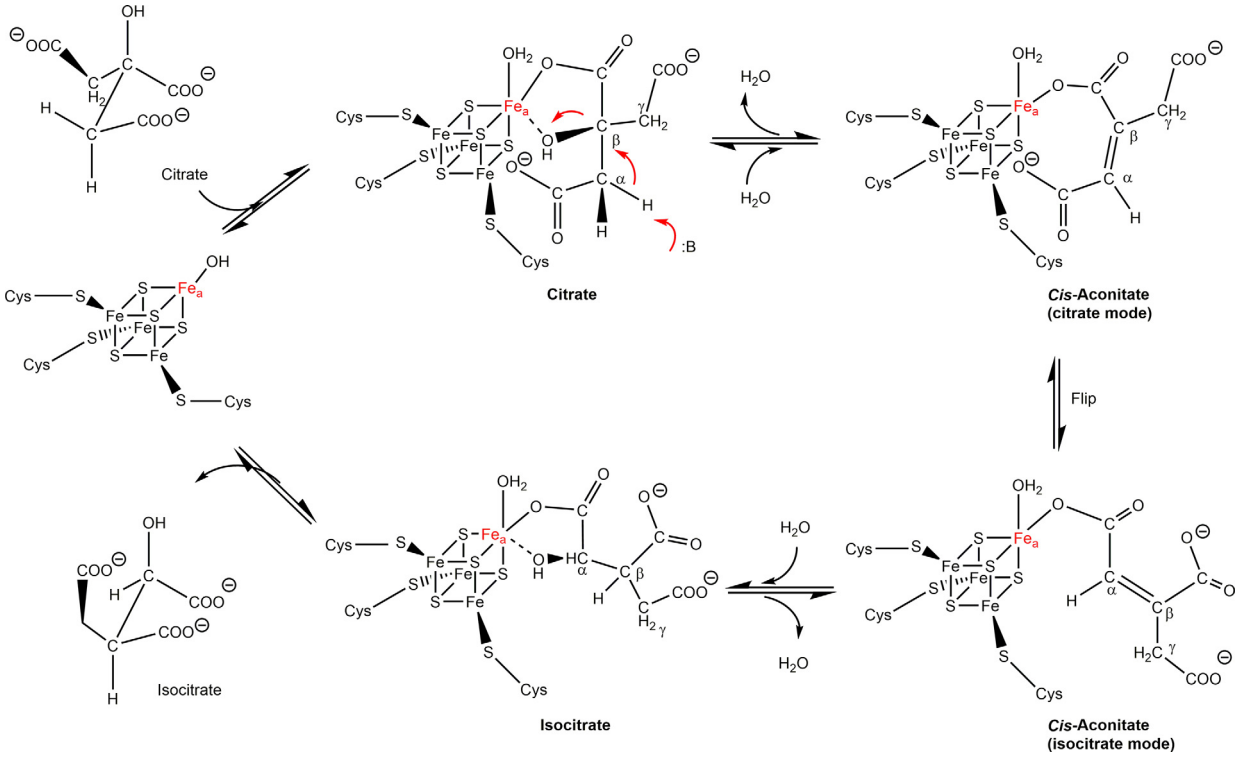

Fig. 22 Proposed catalytic mechanism of aconitase. In the "flip" step the *cis*-aconitate is released (displaced), and re-binds to the iron-sulfur cluster in an alternate mode. Adapted from Lauble, H.; Kennedy, M. C.; Beinert, H.; Stout, C. D., Crystal Structures of Aconitase with Trans-Aconitate and Nitrocitrate Bound. *J. Mol. Biol.* **1994,** *237*(4), 437–451.

This mechanism explains the stereospecificity of the reactions and the requirements for the *trans* eliminations/addition of a hydroxyl group and a proton at the first and third steps after the binding of citrate. During the catalytic cycle, the unique iron (Fe_a) is penta-coordinated after the release of and prior to the re-binding of a water molecule, that originates from and is incorporated into the substrate hydroxyl group, respectively (step two and four).[172]

2.06.3.2.2 IspG and IspH involved in isoprenoid biosynthesis

IspG (4-hydroxy-3-methylbut-2-enyl diphosphate synthase also designated as GcpE) and IspH (4-hydroxy-3-methylbut-2-enyl diphosphate reductase also designated as LytB) are iron-sulfur enzymes that catalyze the reaction of reductive dehydration in non-mevalonate isoprenoid prokaryotic biosynthetic pathway, also named methylerythritol phosphate pathway.[548] IspG catalyzes the reductive dehydroxylation opening of the eight-member ring of methylerythritol cyclic diphosphate, yielding 4-hydroxy-3-methylbut-2-enyl diphosphate, then the hydroxy group of this compound is reductively removed by IspH, to form isopentenyl

diphosphate and dimethylallyl diphosphate[548] (Fig. 23). This biosynthetic pathway plays an important role in pathogenic bacteria and parasites, and since it is absent in humans, it is an excellent target for drug design.[549–551]

IspG is a functional homodimer with the two subunits arranged in a "head-to-tail configuration. Each subunit has two domains: the N-terminal domain is a $(\beta\alpha)_8$ TIM barrel, while the C-terminal domain is a five-stranded β-sheet flanked by helices on both sides, which harbors the iron-sulfur cluster[51,551] (Fig. 24A). This [4Fe-4S] cluster is located in between the two subunits, in an interface with the C-terminal domain of the other subunit. It is coordinated by three cysteine residues found in the consensus sequence motif Cys-X-Cys-Cys-X_5-Gly-Glu, and in the absence of substrate it is also coordinated by a glutamate (Fig. 24B). This glutamate (Glu307 in *A. aeolicus*) does not directly participate in the activation of the substrate (neither as proton donor nor nucleophile), but it has been suggested to have three important roles: (i) stabilization of the [4Fe-4S] cluster against loss of the fourth unique iron atom, (ii) binding of the substrate and, (iii) tuning the reduction potential of the [4Fe-4S] cluster.[552,553] In addition, the active site cavity has several positively charged residues (four arginine residues and one lysine) that interacts with the diphosphate moiety.[554]

The unique iron atom of the [4Fe-4S] cluster participate in the catalysis by forming an iron-oxo intermediate complex, which implies an induced-fit mechanism with structural rearrangements between the N- and C-terminal domains.[51,553,555] The X-ray structure of IspG solved in the presence of substrate revealed that for substrate binding and product release, a conformational change must occur from the "closed form" to an "open form", corresponding to a 64° rotation of the C-terminal domain. The "closed form" of IspG corresponds to the catalytically competent conformation of the active site.[51,554,556]

The catalytic mechanism of IspG has been studied for several years,[551,553,555,557–559] combining isotope labeling experiments, modeling studies, structural and spectroscopic data from EPR, ENDOR, and HYSCORE. Although there is still some debate about the identity and lifetime of the intermediate species identified so far.[555,560] The first step is the replacement of Glu307 carboxylate group coordinating the fourth iron atom by the substrate. This leads to the conformational change mentioned above that brings another glutamate sidechain close to the substrate C3 hydroxyl group to abstract a proton.[51,556,560,561] Thus, the ionized substrate interacts with the [4Fe-4S] cluster forming an alkoxide complex. Then, there is the formation of a series of intermediates,[555] in which the C2 alternates between a carbocation and a radical state assisted by electron transfer from the $[4Fe\text{-}4S]^{2+/3+}$ cluster. In the next step, there is another electron transfer event to form a stable intermediate, a monocarbanionic species bound to $[4Fe\text{-}4S]^{2+}$. The last two steps include two proton transfer, and release of a water molecule. The residue Glu232 is proposed to donate the proton, facilitating the release of the Fe-bound oxygen, and in connecting the active site to a proton channel that is involved in the delivery of the second proton, necessary for the release of the water molecule.[555]

As mentioned, IspH catalyzes the reductive dehydration of 4-hydroxy-3-methylbut-2-enyl diphosphate (HMBPP) to form a 5:1 mixture of isopentenyl diphosphate and dimethylallyl diphosphate (Fig. 23), isoprenoid building blocks.[562] IspH is a monomeric enzyme composed of three domains with similar fold, that are related between each other by a pseudo-C_3 symmetry in a trefoil-like protein structure[563–565] (Fig. 25A).

The iron-sulfur cluster is in a hydrophobic pocket in the center of the three domains and is coordinated by three cysteine residues[564,565] (Fig. 25B). The iron-sulfur cluster present in the first crystallographic structures was a [3Fe-4S] cluster, which was later proven to be an artifact caused by iron loss during crystallization. The active site is in fact a [4Fe-4S] cluster, as observed in the X-ray structure analysis of the enzyme with bound substrate[563] (Fig. 24B), corroborating the kinetic, spectroscopic (Mössbauer and EPR) and other biochemical studies.[563,566–568]

Similarly to IspG, the catalytic mechanism of IspH has been a matter of discussion,[551] but spectroscopic data on the wild-type and key mutants, along with crystallographic data and QM/MM studies elucidated the catalytic mechanism of this enzyme, as a bio-organometallic mechanism,[562,563,569,570] as there was no evidence for the involvement of a radical species.[571] The active oxidation state is the $[4Fe\text{-}4S]^{1+}$, which facilitates the rotation of the 4-OH group of HMBPP away from the iron-sulfur cluster, giving rise to a π-complex intermediate with the C2=C3 double bond. The 4-OH group interacts with Glu126, which is then protonated, mediated by a conserved water molecule, to remove the 4-OH as a water molecule, and forming a η^1-allyl complex (with C2-C3 atoms).

Next, the iron-sulfur cluster is reduced by a second electron and there is the formation of another intermediate species containing a metal-carbon bond, with similar structure to nitrogenase bound to allyl alcohol complex, a η^3-allyl complex.[571] The following step comprises another protonation, which occurs at C2 or C3, giving rise to isopentenyl diphosphate and dimethylallyl diphosphate, respectively. The residues His124 and Glu126 are proposed to be involved in this last protonation step.[562,563]

2.06.3.2.3 Pentonate dehydratases

Pentonate dehydratases are a family of enzymes with biotechnology value for the bioconversion of biomass into different organic compounds (e.g., D-pantothenic acid), and production of biofuels (e.g., ethanol and isobutanol).[572–575] These enzymes are involved in the non-phosphorylative oxidation pathways of pentose sugars, such as the catalysis of dehydration of D-xylonate, by D-xylonate dehydratase, and L-arabinonate, by L-arabinonate dehydratase.[576,577]

These enzymes contrary to the ones described before have a [2Fe-2S] cluster in its active site,[523,578] that is stable under oxic conditions. Similarly to the other iron-sulfur enzymes, visible and EPR spectroscopies have been employed in their characterization. Moreover, X-ray structure of several enzymes show the presence of a [2Fe-2S] cluster,[524,579,580] with a unique iron atom that is coordinated by one cysteine sidechain, instead of two, and having a close by Mg^{2+}. The unique iron atom has a vacant coordination position to which the intermediate hydroxyl can bind (Fig. 26) and will also function as strong Lewis' acid facilitating the loss of the substrate hydroxyl group. The Mg^{2+} is proposed to be important in the stabilization of the carbanion that is transiently formed, and in reducing the electronegativity of the C2 oxygen, which weakens the C—O bond at C3.[580]

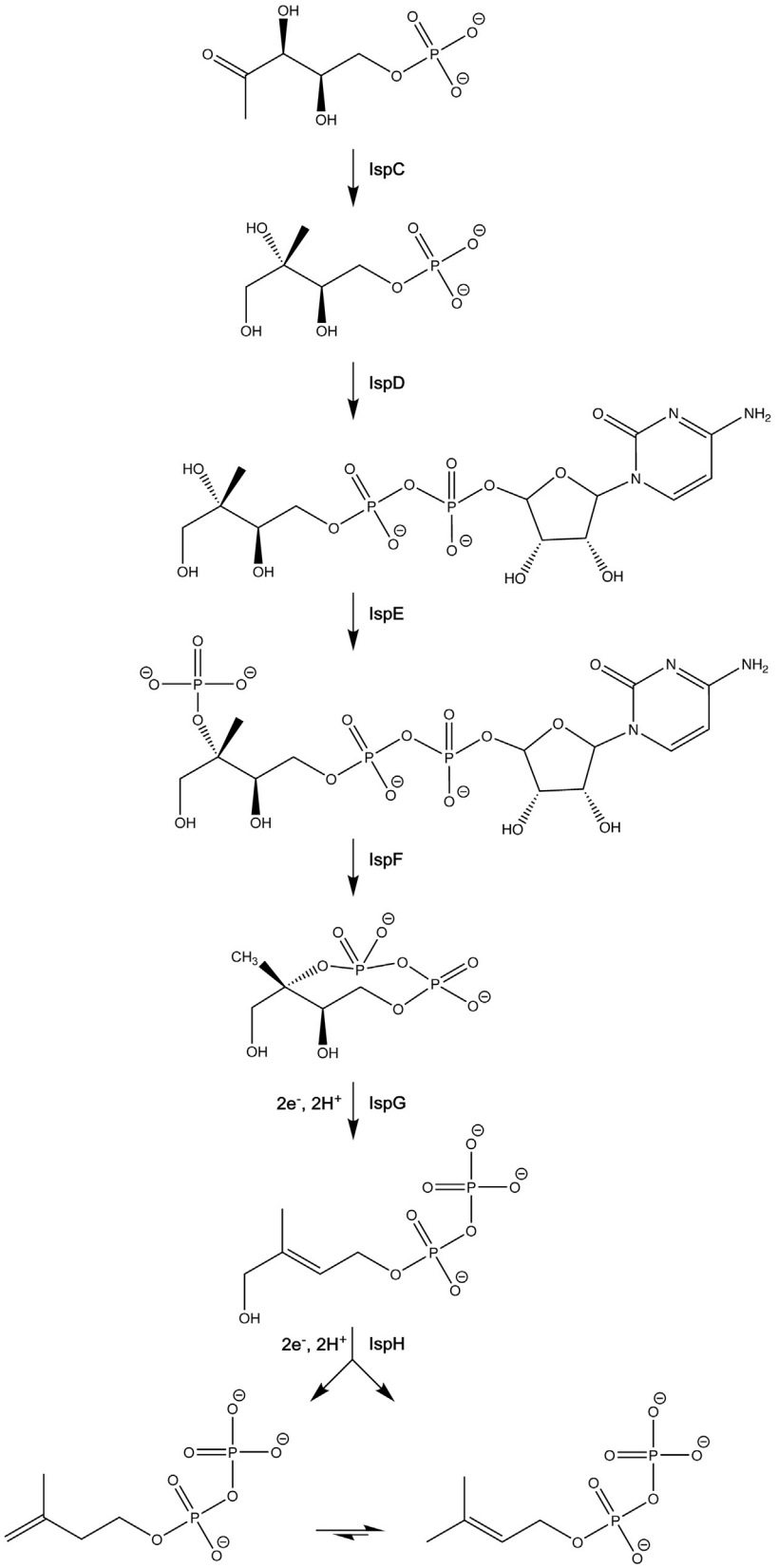

Fig. 23 The canonical non-mevalonate isoprenoid prokaryotic biosynthetic pathway. Adapted from Grawert, T.; Groll, M.; Rohdich, F.; Bacher, A.; Eisenreich, W. Biochemistry of the Non-Mevalonate Isoprenoid Pathway. *Cell. Mol. Life Sci.* **2011,** *68*(23), 3797–3814; Perez-Gil, J.; Rodriguez-Concepcion, M. Metabolic Plasticity for Isoprenoid Biosynthesis in Bacteria. *Biochem. J.* **2013**, *452*(1), 19–25; Rohdich, F.; Zepeck, F.; Adam, P.; Hecht, S.; *Kaiser, J.; Laupitz, R.; Grawert, T.; Amslinger, S.; Eisenreich, W.; Bacher, A.; Arigoni, D. The Deoxyxylulose Phosphate Pathway of Isoprenoid Biosynthesis: Studies on the Mechanisms of the Reactions Catalyzed by IspG and IspH Protein. Proc. Natl. Acad. Sci. USA* **2003**, *100*(4), 1586–1591.

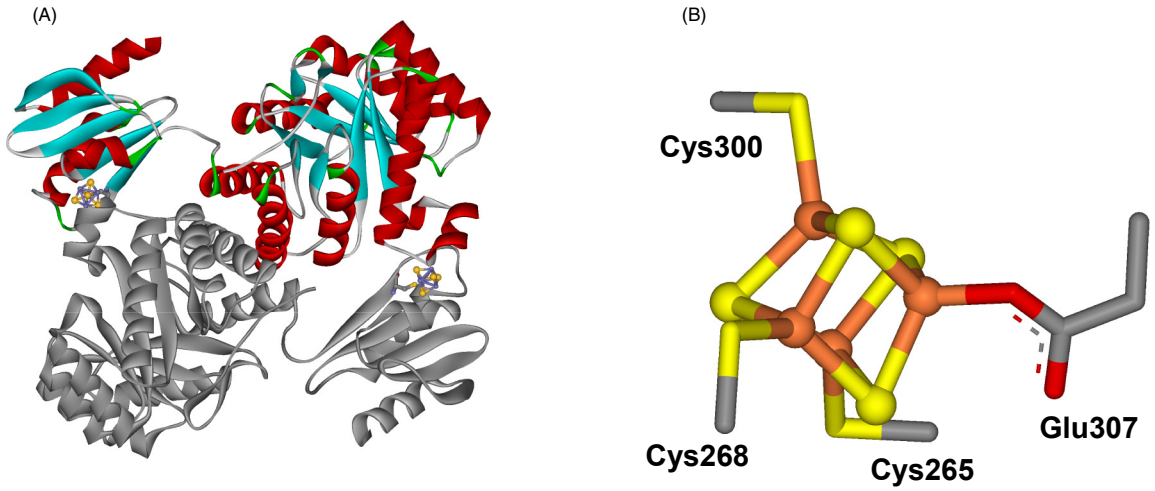

Fig. 24 (A) Structure of IspG dimer, with one monomer colored by secondary structure and the other gray. (B) Structure of the iron-sulfur cluster of IspG. In Panel B the atoms are colored according to element: carbon, iron, oxygen, and sulfur in gray, orange, red and yellow, respectively. Panel A and B were prepared in Discovery Studio Visualizer (BIOVIA) using the coordinates from PDB ID 3NOY.

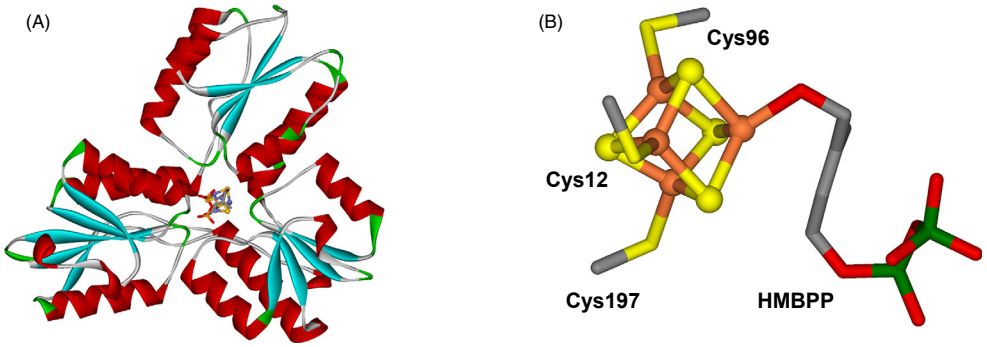

Fig. 25 The active site of IspH. (A) Structure of IspH monomer colored by secondary structure, and (B) structure of the iron-sulfur cluster of IspH bound to substrate HMBPP. The atoms are colored according to element: carbon, iron, oxygen, phosphorus, and sulfur in gray, orange, red, green, and yellow, respectively. Panel A and B were generated with the program Discovery Studio Visualizer (BIOVIA), using the coordinates from PDB ID 3KE8.

These enzymes are tetramers (dimer of dimers) in solution, with each subunit having two domains with a unique complex fold: the N-terminal domain has a α/β structure, and the C-terminal domain a central mixed eight-stranded β-barrel. The cysteine residues that coordinate the [2Fe-2S] cluster are in the N-terminal domain, with the cluster located in a pocket between the two domains, and partially in the interface between the monomers.[524,580] The Mg^{2+} binding site is also located in the N-terminal domain.

2.06.3.3 ADP-ribosyltransferases (unusual iron-sulfur cluster)

The ADP-ribosyltransferases catalyze the ADP-ribosylation, in which an ADP-ribose moiety is transferred from β-nicotinamide adenine nucleotide (NAD^+) to an arginine in the target proteins, releasing nicotinamide.[581,582] These enzymes constitute a group of exotoxins produced by several bacterial pathogens and viruses that are responsible for diseases, such as gonorrhea, meningitis, whooping cough, cholera, and diphtheria.[583]

It is known that this type of exotoxins interferes with signal transduction, protein synthesis or modify cytoskeleton functions, by ADP-ribosylation of host proteins, such as GDP-binding proteins, elongation factor-2, or actin, respectively,[582] as well as antimicrobial peptides.[584] Other targets besides proteins have been identified, such as DNA and antibiotics.[583,585,586]

NarE from *Neisseria meningitidis* is a dual enzyme as it has ADP-ribosyl transferase and NAD^+-glycohydrolase activities,[587] modulated by the presence of its substrate, which include actin and other cytoskeleton-related proteins.[588,589] NarE toxin binds an iron center,[587,590] with the iron atom coordinated by two cysteine and two histidine side-chains (Cys67, Cys128, His46 and His57), in an atypical rubredoxin-type center.[32] The EPR spectrum of this protein has the features of a high-spin ferric iron (with *g* values of 4.4, 4.3 and 4.2) and a maximum absorption band at 420 nm in the visible spectrum.[32,590]

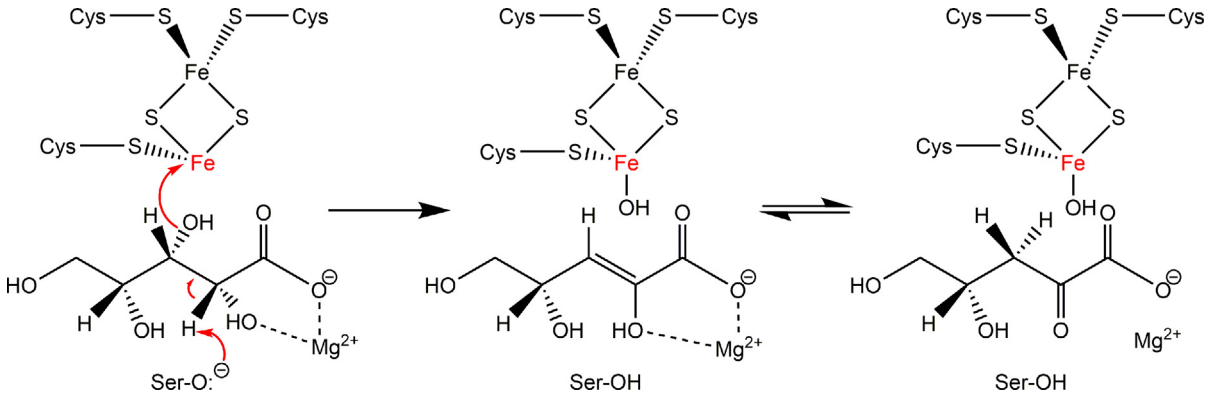

Fig. 26 Reaction mechanism of D-xylonate dehydrogenase. In the last step, the enol intermediate is tautomerized to the ceto form. Adapted from Rahman, M. M.; Andberg, M.; Koivula, A.; Rouvinen, J.; Hakulinen, N. The Crystal Structure of D-Xylonate Dehydratase Reveals Functional Features of Enzymes from the Ilv/ED Dehydratase Family. *Sci. Rep.* **2018**, *8*(1), 865; Rahman, M. M.; Andberg, M.; Thangaraj, S. K.; Parkkinen, T.; Penttila, M.; Janis, J.; Koivula, A.; Rouvinen, J.; Hakulinen, N. The crystal structure of a bacterial l-arabinonate dehydratase contains a [2Fe-2S] cluster. *ACS Chem. Biol.* **2017**, *12*(7), 1919–1927.

The NarE structure in the apo-form, determined by solution state biomolecular NMR, is similar to other enzymes of this family. The NAD^+ binding site was modeled using chemical shift perturbation data and a docking software HADDOCK.[32,591] The atypical iron-sulfur cluster was shown initially to be essential for the catalytic activity of the enzyme as ADP-ribosyltransferase but not for its glycohydrolase activity.[590] The oxidation state of the iron atom modulates the activity of the enzyme: ADP-ribosyl transferase is stimulated by the ferric state, while NAD-glycohydrolase activity is activated by the ferrous state.[592]

The catalytic mechanism of NarE has not yet been proposed, though NMR data supports the hypothesis that iron coordination is required for the recognition and binding of the target protein.[32] However, the coordination of this center, with two cysteine and two histidine sidechains, is more characteristic of a zinc-binding site and therefore, the *in vitro* role of zinc, iron and of Mg^{2+} ions (the latest required to activate other bacterial enzymes of this family) in the activity of this enzyme has been assessed, but no effect was observed.[592]

2.06.3.4 Other enzymatic activities

Besides the catalytic activities reported before, iron-sulfur cluster can also catalyze other reactions, such as the reductive cleavage of a disulfide substrate, by disulfide reductases,[593–595] or the α,β-elimination reaction adjacent to a carboxylate group, by the L-cysteine desulfidase.[596]

The membrane bound elemental sulfur reducing reductase, MBS, is an early ancestor of complex I. The cryo-EM structure of MBS shows the presence of 26 protein subunits, with the monomer consisting of a peripheral cytoplasmic arm anchored (MbsJ, K, L and N) to the membrane by MbsM. There are three [4Fe-4S] clusters (two in MbsN and one in MbsJ), that form an electron transfer pathway from ferredoxin to polysulfide. The proximal iron-sulfur cluster located in MbsJ is coordinated by only 3 cysteines, instead of the usual four, creating a catalytic site,[595] where polysulfide reduction can occur. In fact, the role of the unique iron in catalysis was provided using cluster interconversion to generate a [3Fe-4S] cluster[140] (**Section 2.06.2.1.5**), that lost catalytic activity. EPR spectroscopy was also employed to show the involvement of this center in catalysis,[595] and a novel mechanism for sulfur reduction was proposed without the formation of H_2S since tri- and disulfides are kept stable in the hydrophobic pocket.

The L-cysteine desulfidase catalyzes the decomposition of L-cysteine to hydrogen sulfide, ammonia, and pyruvate, and up-to-now has only been isolated from *Methanocaldococcus jannaschii*,[596] and its gene expression and organization has been characterized in *Yersinia ruckeri*,[597] *S. enterica* and *E. coli*.[598] In common with other enzymes containing an iron-sulfur cluster in the active site, these enzymes present a [4Fe-4S] cluster that can exist in an active and inactive form, due the loss of the unique iron atom that is not coordinated by any residue and is the substrate binding site.

Contrary to the disulfidase, disulfide reductases have been more extensively characterized using spectroscopic and other biophysical techniques. This family of enzymes comprise the ferredoxin:thioredoxin reductase (FTR) and the heterodisulfide reductase (HTR) isolated from methanogenic archaea. The former catalyzes the reaction of an active site disulfide, while the second subfamily catalyzes the reduction of the heterodisulfide of the methanogenic thiol-coenzyme and coenzyme B. These enzymes differ from all the other presented here since each of the iron atoms of its active site [4Fe-4S] cluster is coordinated by a cysteine residue. However, the iron-sulfur cluster interacts directly with either the substrate (HTR) or with an active site disulfide (FTR), delivering one of the two electrons required to complete the reaction.[593,594] For this reason, these enzymes are not further discussed, though further information can be found from the cited literature.

2.06.4 Iron-sulfur clusters involved in metabolic regulation

Iron-sulfur proteins with a role as sensors and regulators are widespread in both prokaryotic and eukaryotic organisms. Their function includes iron sensing and homeostasis (e.g., IRP1, IscR, RirA), sensing gases, such as oxygen (FNR) and nitric oxide (e.g., WhiB, NsrR), or responding to oxidative stress conditions (e.g., SoxR).

The environmental stimulus is sensed by these proteins through disassembly and assembly of their iron-sulfur cluster, modification of the cluster or change in its oxidation state, with most of the proteins studied up-to-now falling into the first categories.

Moreover, these proteins differ in the way they transmit the information, some are simultaneously transcription regulators that bind to regulatory DNA sequences, activating the transcription, while in others the information is transmitted to an effector protein through phosphorylation, and it is this protein that either binds to DNA or activates a cascade.

Here, these regulatory proteins are divided according to their action as post-transcriptional or transcriptional regulators.

2.06.4.1 Post-transcriptional regulation of iron homeostasis

All living organisms present molecular systems that are involved in different metal homeostasis,[599] and are responsible for maintaining a tight control of the intracellular levels of metals, their storage, and their distribution between tissue (in the case of eukaryotes). In the case of iron, the presence of these homeostasis systems is essential since in one hand there are many different enzymes and proteins that require iron or iron-containing cofactors for their function (e.g., hemoglobin, cytochrome *c*, cytochrome *c* oxidase) and, on the other hand, free iron can originate, through Fenton chemistry, reactive oxygen species that can lead to cell damage and death.[600]

In mammalian, iron homeostasis is controlled at the post-transcriptional level by IRP1 and IRP2, *i*ron *r*egulatory *p*roteins. IRP1 and IRP2 bind to iron responsive elements (IRE) in the UTRs (untranslated regions) of mRNA encoding proteins involved in iron use, storage, export, and uptake.[601,602] These two proteins sense not only the intracellular iron levels, but also respond to nitric oxide and reactive oxygen species,[603,604] providing a link between the iron metabolism and oxidative stress.[605]

IRP1 is also known as cytoplasmic apo-aconitase (or apo c-aconitase)[172,536] and is an example of a bifunctional protein (also known as moonlighting protein[606]) as mentioned before (**Section 2.06.3.2.1**). In fact, IRP1 can catalyze the conversion of citrate to isocitrate when an [4Fe-4S] cluster is bound to its polypeptide chain (see **Section 2.06.3.2.1**). However, when there is a change in the intracellular level of iron, and there is the need for iron uptake, the iron-sulfur cluster present in IRP1 disassembles (**Fig. 27**A), and this protein is then able to bind to IREs in the 5′UTR of mRNAs of heavy- and light-ferritin polypeptide, and ferroportin, inhibiting ribosome binding and the translation of these mRNAs (**Fig. 27**B). At the same time, IRP1 inhibits nucleolytic degradation of mRNA coding for the transferrin receptor 1 by stabilizing this mRNA through the binding to its IRE in the 3′UTR[607] (**Fig. 27**B).

The regulation of c_aconitase/IRP1 dual function is a complex mechanism that is still not completely understood but seems to be related with the level of iron and synthesis of iron-sulfur clusters in the mitochondria.[608,609] For activity, IRP1 requires not just the complete removal of iron-sulfur cluster, but also the concomitant reduction of coordinating cysteine residues.[537] However, the disassembly of the [4Fe-4S] cluster is not kinetically favorable, simply as a response to low intracellular levels of iron[172] and it has been shown that it can be triggered by reactive oxygen species[610,611] and reactive nitrogen species.[605,612] In the presence of reactive oxygen species, it was observed the release of the unique iron, Fe_a, and formation of an intermediate $[3Fe\text{-}4S]^{1+}$ cluster,[613,614] while in the presence of NO/peroxynitrite the complete disassembly of the cluster is observed with no stable intermediate species being detected.[612,615] The Fe_a atom is the most solvent exposed iron atom and the one that is not coordinated by any cysteinyl residue (named also unique iron atom) (see **Section 2.06.3.2.1**).

The interconversion of [4Fe-4S] cluster in aconitase to [3Fe-4S] was observed *in vivo* by whole cell EPR, and it was also demonstrated that phosphorylation can control the response of IRP1 to iron levels by affecting the iron-sulfur cluster stability and turnover of the conversion.[614] Moreover, phosphorylation of Ser138 allows the $[4Fe\text{-}4S]^{2+}$ cluster to cycle to $[3Fe\text{-}4S]^{0}$ and thus it seems that regulation of the cluster disassembling can be initiated solely due to iron availability.[616,617]

The structure of IRP1 bound to the IRE of ferritin has been determined.[618] The comparison between this structure and the one of aconitase elucidated the extensive conformational changes that need to occur for IRE recognition and binding (**Fig. 28**). These conformational changes occur mainly in domain 3 and 4, with its rotation and translation relative to the core domains (domain 1 and 2). These motions separate these two domains, creating a space where the IRE-stem loop will be accommodated. Moreover, the shifts that occur in domain 3 are also accompanied by a conformational change of two other regions in the interface of domains 2 and 3, residues 436 to 442 and 534 to 544, that play an important dual structural-functional role as forming the ligand-binding environment for the [4Fe-4S] cluster (**Fig. 28**A) or being involved in the interaction with A^{15} and G^{16} bases of the IRE-stem loop[618] (**Fig. 28**B). Therefore, as shown in **Fig. 28**, IRP1 adopts an extended L-shaped conformation that embraces the IRE stem-loop.

Contrary to IRP1, IRP2 does not assemble an iron-sulfur cluster and thus it is not a bifunctional protein, but its activity is also dependent on the presence of an iron-sulfur cluster (*vide infra*). In addition, IRP2 shares 65% of sequence identity with IRP1,[619,620] and like IRP1 also functions as a post-transcriptional regulator of genes involved in iron metabolism (**Fig. 27**B). The activity of IRP2 is dependent on another protein, FBXL5,[621,622] that binds an [2Fe-2S] cluster in its C-terminal domain,[623] and has a N-terminal hemerythrin-like domain.[624–626] The UV–visible spectrum of this protein has absorption bands with maxima at 330 nm and 425 nm, and it is EPR silent in the as-isolated and oxidized state, while in the reduced state presents a signal with *g* values of 2.042, 1.918 and 1.889 (with an average *g*-value of 1.950), which are consistent with the presence of a $[2Fe\text{-}2S]^{1+}$ cluster coordinated by 4-cysteine residues.[623]

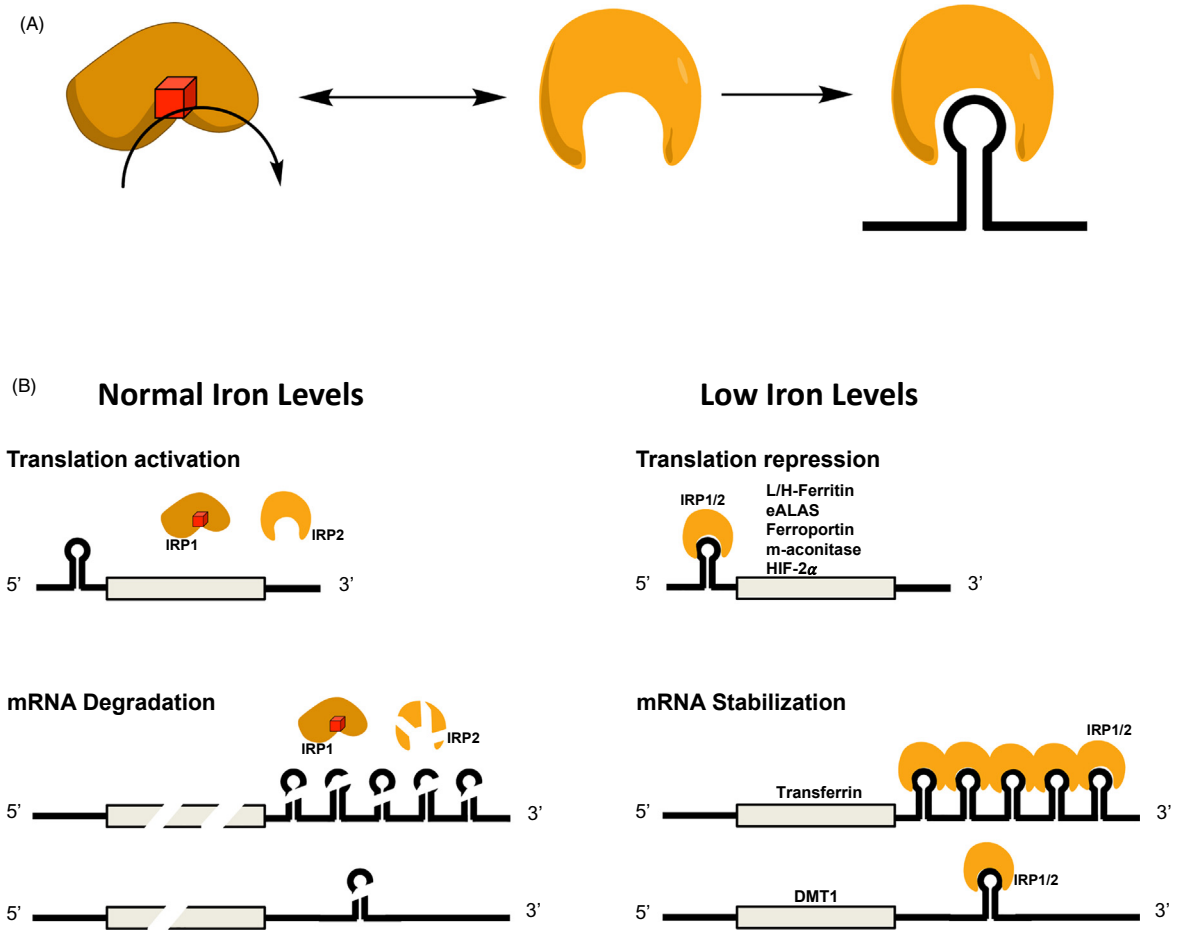

Fig. 27 Schematic representation of the mode of action of IRP1 and IRP2 as post-transcriptional regulators. In panel A is represented the interconversion of aconitase-IRP1 that occurs depending on the cellular iron level, due to oxidative disruption by superoxide anion, peroxynitrite and carbonate radical. In panel B is represented the function of IRP1 and IRP2 in translation activation and repression during normal and low iron levels, respectively.

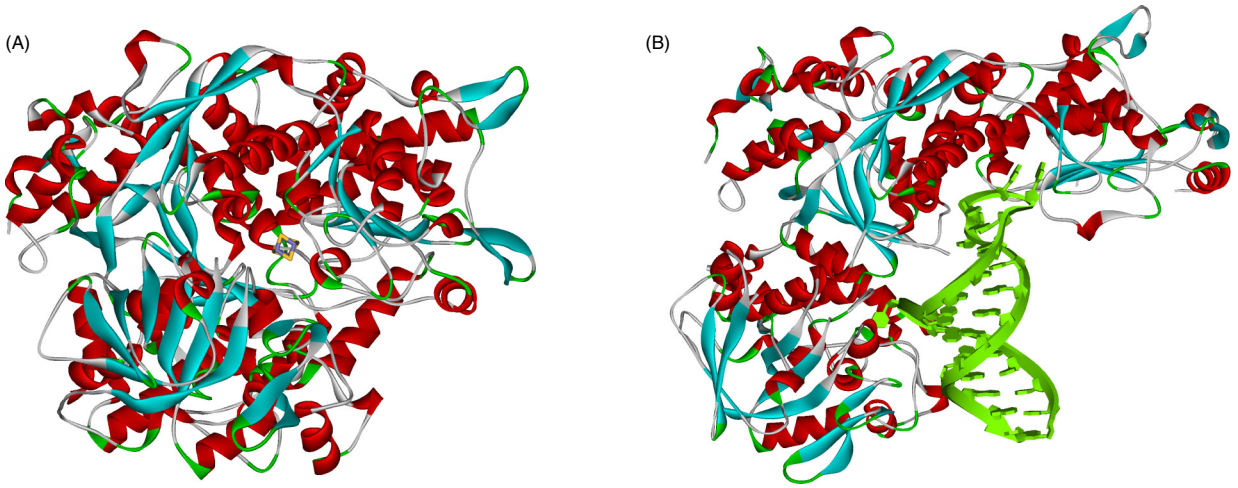

Fig. 28 Conformational changes observed in cytosolic IRP1 (or holo c_aconitase) upon iron-sulfur cluster disassembly. In panel A is represented the structure of the inactive human holo-cytosolic IRP1, and in panel B the structure of IRP1 (apo c_aconitase) bound to ferritin IRE mRNA. Panel A and B were prepared using the coordinates 2B3Y and 3SNP, respectively. Protein structure is colored according to secondary structure, iron-sulfur cluster is represented as sticks and RNA is colored green. Images in Panel A and B were created with the program Discovery Studio Visualizer (BIOVIA).

The cryoelectron microscopy structure of IRP2 in complex with FBXL5 was determined and shows that IRP2 adopts a L-shape open conformation, like apo-IRP1, and FBXL5 binds in the middle through its C-terminal domain,[623] with the iron-sulfur cluster being close but not in the immediate interface. The binding of FBXL5 with its iron-sulfur cluster in the oxidized state, $[2Fe\text{-}2S]^{2+}$, is required to displace IRP2 from the IRE-stem loop, and it is also critical for ubiquitin ligase binding.[623] Therefore, the presence of this cluster explains how IRP2 activity is dependent on iron (through its N-terminal hemerythrin-like domain that binds a diiron center, changing its structure[621,624–626]) and oxygen, as in the presence of high levels of iron and oxygen there is formation of an oxidized $[2Fe\text{-}2S]^{2+}$ cluster in FBXL5, that then binds to IRP2, displacing it from its IRE. In the following steps, FBXL5 recruits IRP2 for poly-ubiquitination and degradation (**Fig. 27**B).

The biological relevance of having two IRP proteins is still not completely understood, but it might be related with cell specificity[627] and the signals that are sensed, since they are active under different conditions. In fact, these two proteins were shown to be reductant as mice without both alleles of *Irp1* and *Irp2* are not viable,[628] while mice lacking either *Irp1* or *Irp2* are viable and fertile.[629] Moreover, IRP2 has been associated with erythropoietic homeostasis and nervous system, while IPR1 is essential for controlling the equilibrium between iron homeostasis and erythropoiesis, with an important role in the cardiovascular and pulmonary systems.[630,631]

Therefore, further studies are required to completely understand the role of the IRP1/IRP2 system in human health and disease.

2.06.4.2 Transcription regulators

Several transcription regulators have been shown to bind iron-sulfur clusters, either [2Fe-2S] or [4Fe-4S] type clusters. These transcription regulators are usually composed of two domains, one that is the regulatory domain and usually contains the iron-sulfur cluster and the other that binds to specific DNA sequences (**Fig. 29**). Primary sequence alignment enabled the grouping of these transcription regulators into two main families, the Rrf2 family and the CRP-family.

A third family includes different transcription regulators that have a domain that also binds an iron-sulfur cluster, but either their domain organization or mode of action differs from the ones in the other two families. In this latter family are also included PAS domains of sensor kinases of two-component systems (NreB) and of a σ^{54}-dependent activator (OrpR), that bind an iron-sulfur cluster.

GAF domains have also been shown to bind [2Fe-2S] cluster, as in the case of *Staphylococcus aureus* AirS-AirR, a two-component system involved in sensing O_2 and oxidative stress (similarly to the NreBC system).[632] Moreover, like RirA, Aft1 and Aft2 are involved in the regulation of iron uptake through its [2Fe-2S] cluster in *Saccharomyces cerevisiae*.[633,634] For a more complete list of iron-sulfur protein involved in the regulation of gene expression see Mettert & Kiley.[635]

These transcription regulators make use of the versatile properties of their iron-sulfur clusters, such as the ability to delocalize electrons over the Fe and S atoms of the cluster, to change oxidation state (by reacting with oxygen, reactive oxygen species and redox-cycling compounds), and to be vulnerable to modification by molecular oxygen and NO. In addition, the presence or absence of the iron-sulfur cluster can be used to sense the iron or even the iron-sulfur cluster cellular level. The sensing mode involves, in many cases, cluster interconversion that leads to conformational changes in the protein and modulates its DNA affinity. This enables these transcription regulators to respond to different stimuli, such as reactive oxygen species, cellular redox potential, nitric oxide, and iron availability, and control transcription of different metabolic pathways.

2.06.4.2.1 Rrf2 family

The Rrf2 family of transcription factors is widespread but still poorly characterized. Four members of this family that bind an iron-sulfur cluster will be described here: IscR, RirA, NsrR and RsrR. IscR senses the iron-sulfur cluster level in the cell and regulates the biogenesis of iron-sulfur clusters, while RirA responds to the level of iron and controls iron uptake and storage systems (**Fig. 30**). NsrR senses a gas, nitric oxide, and regulates the nitric oxide stress response or reactive nitrogen species stress in many prokaryotes, while RsrR senses the cellular redox status.

The analysis of the primary sequence of Rrf2 family of transcription regulators shows that there is a winged helix-turn-helix (wHTH) at the N-terminus domain, and a cysteine rich region at the C-terminus located in an insertion segment absent in the proteins that do not bind an iron-sulfur cluster, as in CymR[636] (**Fig. 31**).

The analysis of the structures of apo-IscR, holo-NsrR and holo-RsrR, and that of CymR (a non-iron-sulfur cluster binding protein) show that they share a common fold composed mainly by α-helixes and two anti-parallel β-strands, organized in two domains. The wHTH DNA-binding domain, and the dimerization helix are connected through a loop that contains the two/three conserved cysteines.

The location of these cysteine residues places the iron-sulfur cluster close to the wHTH motif of an opposing monomer, and thus its presence/absence can modulate the DNA binding properties of the transcription factor.

The fourth ligand of the iron-sulfur cluster in these proteins has been confirmed with the characterization of variants of conserved residues or by the comparative analysis of their holo-structures (see **Section 2.06.4.2.1.1 to 2.06.4.2.1.4**). The nature of the fourth ligand varies between the Rrf2 family members, which can determine the properties of the iron-sulfur cluster and play a role in regulating its function.

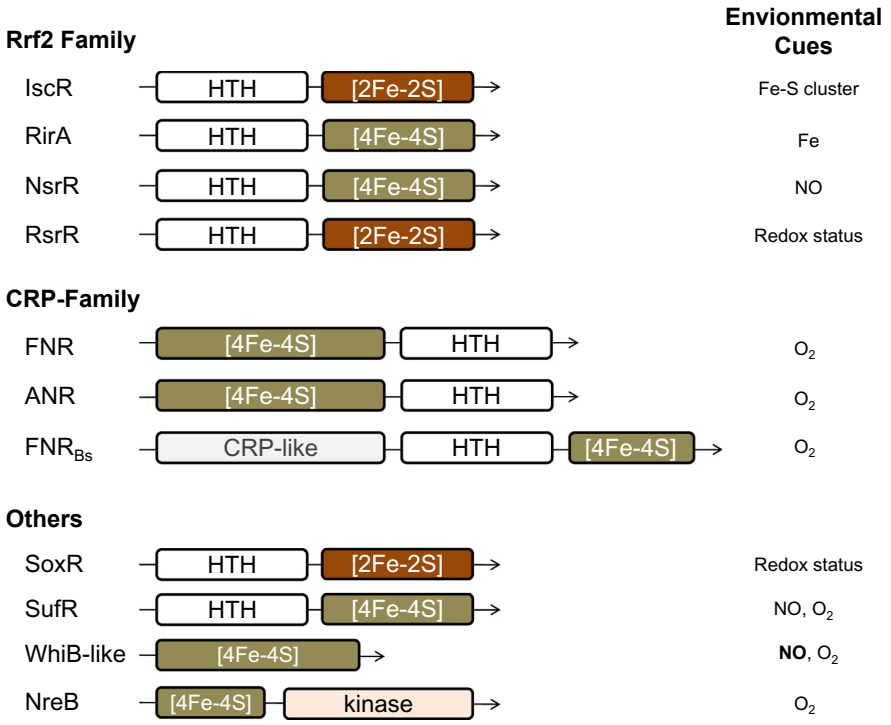

Fig. 29 Schematic representation of the different families of transcription regulators that contain an iron-sulfur cluster. HTH – helix turn helix domain. AAA^+ – ATPase associated activity. The domains are not represented to scale. FNR_{BS} is the FNR homolog found in *Bacillus subtilis*.

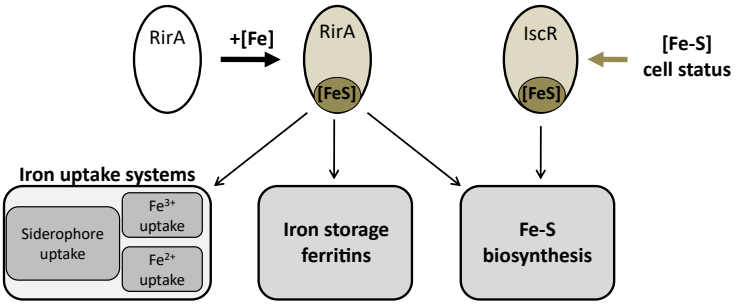

Fig. 30 Schematic representation of the role of iron-sulfur cluster containing transcription regulators in iron homeostasis.

2.06.4.2.1.1 IscR, *iron-sulfur cluster biogenesis regulator*

The gene encoding IscR is located immediately upstream of the iron-sulfur cluster biosynthesis system (Isc), *isc* operon, *iscRSUA-hscBA-fdx*.[637] The expression of this operon and of *sufABCDSE*, also involved in iron-sulfur cluster biosynthesis, is induced by oxidants. In fact, under oxidative stress conditions the cell has an increased demand for the maintenance and assembly of iron-sulfur clusters,[638] which are in many cases oxygen-sensitive.

Under anaerobic conditions, IscR is a feedback repressor of the *iscRSUA* operon as a $[2Fe\text{-}2S]^{1+}$ cluster containing protein,[637] while under oxidative stress conditions and iron limitation, apo-IscR is a transcriptional activator of the *suf* operon and de-represses the *isc* operon.[638] This mechanism enables IscR to regulate the function of Isc and Suf systems and coordinate the consumption of iron and cysteine between these two systems.[639]

IscR binds an [2Fe-2S] cluster and its presence changes IscR DNA binding specificity. The holo-IscR binds a type I sequence motif with high affinity,[640] while both the apo and holo-IscR bind to a type II sequence motif. As mentioned, the regulatory mechanism of IscR depends on the presence of a [2Fe-2S] cluster, as it is proposed that the conformational change that occurs upon loss of the [2Fe-2S] cluster, induces unfavorable interactions of the protein with the type-I motif.[641] The position of these motifs in relation to the promoter dictates whether IscR will function as an activator or a repressor.

The anaerobically isolated *E. coli* IscR binds a [2Fe-2S] cluster. The EPR signal of the $[2Fe\text{-}2S]^{1+}$ state has *g* values at 1.99, 1.94 and 1.88,[637] which suggested a full cysteinyl coordination of the cluster. This iron-sulfur cluster has a low relaxation rate and can be reversibly oxidized to $[2Fe\text{-}2S]^{2+}$, without significant loss of the cluster.[637] In the case of IscR from *Acidithiobacillus ferrooxidans*, its visible spectrum presents maximum absorption bands at 315 nm and 410 nm, and an EPR signal with a g_{av} value at 2.013.[642]

```
                        1       10         20         30         40         50         60
                        |       |          |          |          |          |          |
IscR Ecoli              MRLTSKGRYA VTAMLDVALN SEAGPVPLAD ISERQGISLS YLEQLFSRLR KNGLVSSVRG
IscR Psa                MRLTTKGRYA VTAMLDLALH AQQGPVSLAD ISERQGISLS YLEQLFAKLR RGNLVTSVRG
IscR Ac                 MKLTTKGRYA VTAMLDLALN QRGGVVTVAD ISQRQQISVA YLEQLFGRLR RFGLVESVRG
RsrR Sv                 MKLSGGVEWA LHCCVVLTA- -ASRPVPAAR LAELHDVSPS YLAKQMQALS RAGLVRSVQG
RsrR Mc                 MKMSGGVEWA LHCCVVLTV- -SSRPVPAAR LAELHDVSSS YLAKQLQSLA RAGLIHSVQG
RirA Sinor              MRLTKQTNYA VRMLMYCAA- NGEKLSRIPE IARAYGVSEL FLFKILQPLT RAGLVETVRG
RirA Rhiz               MRLTKQTNYA VRMLMYCAA- NDGHLSRIPE IARAYGVSEL FLFKILQPLN KAGLVETVRG
NsrR Ecoli              MQLTSFTDYG LRALIYMASL PEGRMTSISE VTDVYGVSRN HMVKIINQLS RAGYVTAVRG
NsrR Nm                 MYLTQHTDYG LRVLIYTAI- NDDALVNIST IAVTYGISKS HLMKVVTALV KGGFLHSVRG
                        * ::    :. :   :  :               ::    :*   .: : .  *  : . : :*:*

IscR Ecoli              PGGGYLLGKD ASSIAVGEVI SAVDESVDAT RCQGKGG--- -----C-QGG DKCLTHALWR
IscR Psa                PGGGYQLSRH MSGIHVAQVI DAVNESVDAT RCQGQGD--- -----C-HSG DTCLTHHLWC
IscR Ac                 PGGGYRLAMP DSEIPLTRIV EAVNESISTT QCGGDPH--- ---LCCKGDG QQCLTHDLWE
RsrR Sv                 KTGGYVLTRP AVEITLLDVV QAVDGPDPAF VCTEIRQRGP LATPPEKCTK -ACPIARAMG
RsrR Mc                 KSGGYALTRA PESITLLDVV RAVDGPGPAF VCTEIRQRGP LATPANACTR -ACPVARAMW
RirA Sinor              RNGGVRLPRP ASEITLFDVV KVTEDSFAMA ECFEA-G--E ---IDCPLVD -SCGLNAALR
RirA Rhiz               RNGGVRLGKP AADITLFDVV RVTEDSFAMA ECFEDDG--V ---VECPLVD -SCGLNSALR
NsrR Ecoli              KNGGIRLGKP ASAIRIGDVV RELEP-LSLV NCSSE----- ----FCHITP -ACRLKQALS
NsrR Nm                 KGGGLRLAAP PDRINIGSVV RHLEP-MQLV ECMGE----N ---NECLITP -SCRLTGILG
                          **  *       * :  ::    :         *                      * :   :

IscR Ecoli              DLSDRLTGFL NNITLGELVN NQEVLDVSGR QHTHDA---- PRTRTQDAID VKLRA
IscR Psa                DLSLQIHEFL SGISLADLVS RQEVQEVALR QDERRCSGKT PRLDKIEASA ID---
IscR Ac                 ELGNRIAEFL GGITLGQLVQ KQLHKELMQA AP-IAMTDKT PLRETHDTA- -----
RsrR Sv                 AAEAAWRASL ASTTIADLVA TVDDES---- ---GPDALPG VGAWLIEGLG -----
RsrR Mc                 TAEEAWREAL AAVTIADLAR DVGTDS---- ---GPEALPA VRTWLTGASD H----
RirA Sinor              KALNAFFEVL QGYTIDDLVK AR-PQINFLL GLEEPVRPQT SAA------- -----
RirA Rhiz               KALNAFFAVL SEYSIDDLVK AR-PQINFLL GITGEQPYRK PAIVAPAA-- -----
NsrR Ecoli              KAVQSFLTEL DNYTLADLVE ENQPLYKLLL VE-------- ---------- -----
NsrR Nm                 GAMKSFFTYL DGFTLQDLLN --KPTYDLLY EPRIPIAVQ- ---------- -----
                                 *    :: :*
```

Fig. 31 Primary sequence alignment of the transcription regulators belonging to the Rrf2 family that bind an iron-sulfur cluster, IscR, NsrR and RirA. Legend: *Ecoli – E. coli*, *Psa – Pseudomonas aeruginosa*, *Ac - Acidothiobacillus ferrooxidans*, *Sv – Streptomyces venezuelae*, *Mc – Micromonospora coriariae*, *Sinor – Sinorhizobium*, *Rhiz – Rhizobium*, *Nm – Neisseria meningitidis*. Asterisks, colons or stops below the sequence indicate identity, high conservation, or conservation of the amino acids, respectively. Conserved cysteines are highlighted in yellow, the third and/or fourth ligand is in pink, and putative fourth ligand of [4Fe-4S] RirA is in gray.

The primary sequence analysis of IscR revealed the presence of only 3 conserved cysteine residues (Fig. 31), indicating that the [2Fe-2S] cluster could not have only cysteinyl coordination. The fourth ligand of the iron-sulfur cluster was then identified by site-directed mutagenesis as being His107,[643] also a conserved residue (Fig. 31).

The mechanism of assembly and disassembly of the [2Fe-2S] cluster into IscR has not been deeply investigated, though is it proposed that the cluster is sensitive to oxygen, enabling IscR to oscillate between the holo and apo-forms.[639] Moreover, while the Mössbauer analysis showed that in whole cells over-expressing IscR its iron-sulfur cluster is in the $[2Fe\text{-}2S]^{1+}$ oxidation state,[643] this does not influence its DNA binding affinity.[643]

The structure of apo-IscR shows that it binds to DNA as a dimer with a long helix forming the dimer interface and the two wHTH are in two opposite sides of the dimer.[641] The position of two wHTH enables this transcription regulator to bind 23–27 DNA consensus motifs.

The position of the proposed fourth ligand is located at the surface of the monomer, an indication that IscR iron-sulfur cluster can be solvent-exposed, and thus prone to the action of reactive oxygen or nitrogen species. As mentioned, the conformational changes that occur in the iron-sulfur cluster bound form, even if small and local, modulate the DNA consensus motifs that IscR recognizes.

2.06.4.2.1.2 Rhizobial iron regulator A (RirA)

Another transcription regulator that binds an iron-sulfur cluster is RirA, a *r*hizobial *i*ron *r*egulator *A*, that was initially just identified to be an iron-responsive regulator in *Rhizobium leguminosarum*.[644]

RirA and its homologs have been found in all members of the α-proteobacteria of the genus *Rhizobiaceae*. Similarly to the well-studied *E. coli* Fur (*f*erric *u*ptake *r*egulator), RirA is proposed to be a global iron-responsive transcription regulator involved in the regulation of iron uptake and metabolism in *Rhizobium*[644] and *Sinorhizobium*.[645] Proteomic and transcriptomic studies have shown that, in Fe-replete growth conditions, RirA represses the expression of several genes involved in the synthesis and uptake of

siderophores, uptake of heme, synthesis of iron-sulfur clusters and of genes that code for proteins that probably participate in Fe^{3+} transport[646] (Fig. 30).

RirA is proposed to bind an iron-sulfur cluster in analogy to another Rrf2-type proteins (see Sections 2.06.4.2.1.1 to 2.06.4.2.1.4),[647] and due to the presence of a triad of conserved cysteines in its C-terminal region,[644] which are essential for its function[646] (Fig. 29).

In fact, bioinformatic analysis of several genomes of α-proteobacteria, identified a palindromic motif with the consensus 5′-TGA-(N_9)-TCA-3′, as being the RirA-box (IRO-box).[648]

The heterologously produced RirA after *in vitro* cluster reconstitution was shown to bind an [4Fe-4S] cluster, having a visible spectrum with a broad absorption band with a maximum below 400 nm.[649] The presence of an [4Fe-4S] cluster was supported by its CD spectrum and by its mass spectrum.[649] RirA is a dimer in solution and binds DNA with a high affinity in the holoform. In the presence of low concentrations of iron (mimicked by the presence of EDTA), it is observed a red shift in the absorption bands of [4Fe-4S] RirA, consistent with the formation of a [2Fe-2S] cluster, and then there is a decay in intensity of these bands corresponding to the loss of cluster and formation of apo-RirA. These forms of RirA have decreased DNA binding affinity[649] when compared with [4Fe-4S] RirA.

The mechanism of decomposition of the [4Fe-4S] cluster to a [2Fe-2S] cluster has been studied by CD, EPR and time-resolved mass spectrometry, and two intermediate species were identified: a $[3Fe\text{-}4S]^0$ and a [3Fe-3S] cluster.[649,650] The first step of this process is the loss of iron with a dissociation constant of around 3 μM, while the following steps in cluster conversion are O_2-dependent, with formation of a $[3Fe\text{-}4S]^{1+}$ cluster.[650] The dissociation constant for the release of the first Fe atom is within the physiological range, which is consistent with this protein being an iron-dependent transcription regulator.[651]

The coordinating residues of the intermediate [2Fe-2S] cluster are proposed to be the ones that coordinate the [4Fe-4S] cluster, with one of the coordinating residues not yet identified (in either case). The analysis of the sequence alignment shown in Fig. 31 indicates that Gln6, Asn8, Arg12 (opposing subunit) and Asn109 are conserved and in proximity of the iron-sulfur cluster in the model structure generated using SwissModel (Fig. 32). However, it is also possible that the fourth ligand is a oxygen fom a non-protein molecule (N. E. LeBrun personnal communication).

2.06.4.2.1.3 Nitrite-sensitive transcription repressor (NsrR)

NsrR, a *n*itrite-*s*ensitive transcription *r*epressor, is also part of the Rrf2 family. NsrR regulates several genes,[196,652] and it has been suggested to be a global transcriptional regulator of the bacterial NO stress response.[653] One of these genes encodes the hybrid cluster protein, Hcp, indicating that this protein might be part of a defense mechanism against reactive nitrogen species,[196] as it is a NO reductase[198] (see Section 2.06.2.2.1.1). Another gene that is under the control of NsrR is *hmp*, which encodes a flavohemoglobin that converts NO to nitrous oxide (N_2O) or to nitrate (NO_3^-).[654–656]

NsrR has been isolated from either Gram-positive (such as, *Bacillus subtilis*,[657] and *S. coelicolor* [658]) or Gram-negative (such as, *E. coli*,[659] *S. enterica*,[660] *Neisseria meningitides*,[661] *Neisseria gonorrhoeae*,[662] and *Nitrosomonas* spp.[663]) bacteria.

Like other members of the Rrf2 family of transcription regulators, NsrR presents three conserved cysteines (Fig. 31), that are proposed to coordinate an iron-sulfur cluster,[658] that is NO-sensitive and essential for its DNA binding properties.

The iron-sulfur cluster present in *S. coelicolor* NsrR was initially identified to be a [2Fe-2S] cluster by different spectroscopic techniques, such as CD, UV–visible and EPR.[658] The CD spectrum of NsrR is similar to the one of other proteins containing a $[2Fe\text{-}2S]^{2+}$-Rieske type cluster, such as BphF[664] (with three positive features, with λ_{max} at 324 nm, 445 nm and 490 nm, and two negative features, with λ_{max} at 375 nm and 550 nm).[658] The visible spectrum has absorption bands with maxima at 325 nm and 420 nm and shoulders at 460 nm and 550 nm, while being EPR silent is consistent with the presence of an oxidized $[2Fe\text{-}2S]^{2+}$ cluster.[658]

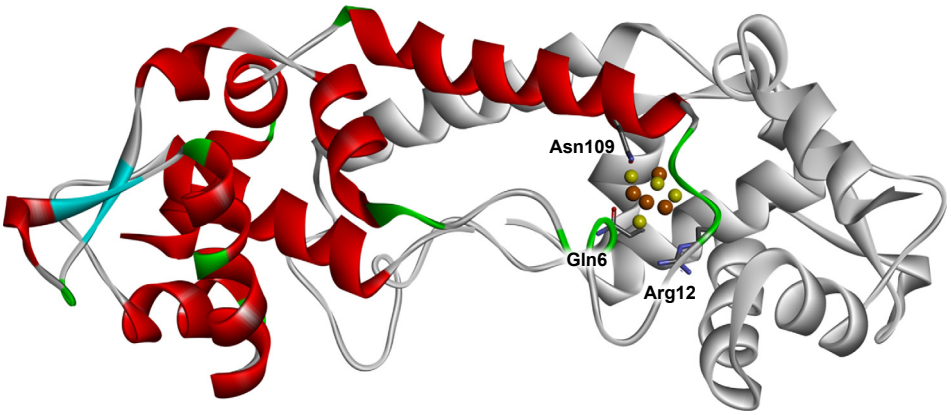

Fig. 32 Model structure of *Sinorhizobium meliloti* SM11 RirA obtained with SwissModel and the coordinates of NsrR (PDB ID 5N07), which has 37% primary sequence identity with RirA. The iron and sulfur atoms are represented by orange and yellow spheres, respectively. The putative fourth coordinating residues are represented as sticks colored by element. One of the monomers of RirA is colored in gray and the other by secondary structure. The model was generated in SwissModel, and image prepared in Discovery Studio Visualizer (BIOVIA).

A similar cluster was proposed to be present in *N. gonorrhoeae* NsrR, though the evidence was only the 145 Da difference between the expected mass of the apo-NsrR and the isolated NsrR.[662]

However, the iron-sulfur center present in *B. subtilis* NsrR was proposed to be a [4Fe-4S] cluster, based on its UV–visible (maximum absorption band at 412 nm) and resonance Raman spectra.[657] As in other NsrR proteins, *B. subtilis* NsrR [4Fe-4S] cluster is NO-sensitive and required to bind the specific DNA sequence.[665]

The initial discrepancy in the type of iron-sulfur cluster bound to NsrR was clarified by the isolation of *S. coelicolor* NsrR under anaerobic conditions in the absence of low molecular weight thiols and lead to the identification of a bound [4Fe-4S] cluster.[666] In fact, it was shown that these compounds (such as DTT, usually added to the purification and storage buffers of oxygen sensitive proteins) modified the NsrR iron-sulfur cluster,[657,666] that decomposes to a [2Fe-2S] cluster. On the contrary, physiological thiols, such as cysteine and mycothiol did not induce this decomposition.[666]

The [4Fe-4S] cluster is coordinated by three conserved cysteine residues (**Fig. 31**) and by an oxygen ligand, as suggested by its resonance Raman,[666] and later confirmed by its X-ray structure.[667] The structure of holo-NsrR identified Asp8, of the opposite monomer, as the fourth coordinating residue. This was the first report of such asymmetrically coordinated iron-sulfur cluster.[667]

The active form of NsrR is a dimer containing a $[4Fe\text{-}4S]^{2+}$ cluster and its nitrosylated form loses the ability to bind the DNA consensus regions. The mechanism by which NsrR is proposed to sense nitric oxide encompasses the nitrosylation of the iron-sulfur cluster, with formation of cysteine thiolate-bound dinitrosyl iron complex species, that loses the ability to bind to DNA.[656,668] Earlier studies detected the formation of tetrahedral $[Fe^{I}(NO)_2(SR)_2]^{-}$, with SR^{-} being cysteinate ligands provided by the protein,[658] using EPR spectroscopy, as this cluster has a distinctive signal at $g = 2.03$.[658] Afterwards, with the improvement in protein production and sample handling, as well as novel techniques developed for iron proteins, such as nuclear resonance vibrational spectroscopy, complemented by liquid chromatography electrospray ionization mass spectrometry, enabled the identification of the nitrosylation products that are formed during this complex process.[656] In the case of NsrR there is formation of Roussin's Red Ester, $[Fe_2(NO)_4(SR)_2]$, and a persulfide form $[Fe_2(NO)_4(S\text{-}Cys)(Cys)]$.[669–671]

2.06.4.2.1.4 Redox-sensitive response regulator (RsrR)

Streptomyces venezuelae genome encodes a Rrf2 family transcription regulator that responds to the redox status of the cell and was named *r*edox-*s*ensitive *r*esponse *r*egulator (RsrR). RsrR regulates the cellular concentrations of NADH and NAD(*P*)H by controlling the expression of the gene *sven6562* (a putative $NAD(P)^{+}$ binding repressor belonging to the NmrA family (nitrogen metabolite repression)), and genes evolved in glutamine and glutamate metabolism. RsrR binds to a binding motif organized in a 11–3-11 base pairs inverted repeated sequence.[672]

This dimeric protein binds a [2Fe-2S] cluster that can oscillate between the $[2Fe\text{-}2S]^{2+}$ and $[2Fe\text{-}2S]^{1+}$ oxidation state. This redox process controls RsrR DNA binding activity, with the RsrR-$[2Fe\text{-}2S]^{2+}$ oxidation state having higher affinity than the RsrR-$[2Fe\text{-}2S]^{1+}$ oxidation state.[672]

The visible and CD spectra of RsrR have the features of a [2Fe-2S] cluster with absorbance bands with a maximum at 460 nm, in the oxidized state, and at 540 nm in the reduced state, with this form being EPR active with *g* values of 1.997, 1.919 and 1.867.[672]

The structure of [2Fe-2S] RsrR was determined in different oxidation states.[39] The protein backbone adopts the already described conserved fold of Rrf2 family but revealed that the iron-sulfur cluster has a unique coordination being bound by two cysteines, Cys90 and Cys110, located in the C-terminal domain and two other residues in the N-terminal domain of the other subunit, Glu8 and His12 (**Fig. 4**C). This was the first report of an iron-sulfur cluster coordinated by a glutamate sidechain and having three different types of residues as ligands.[39]

Additionally, these structures revealed the role of Trp9 in the sensing process, in which a change in the oxidation state of the iron-sulfur cluster translates into a conformational change of the DNA binding domain, and alteration in the DNA binding affinity of this transcription regulator.[39]

The presence of the sequence motif EWXXH is observed in other proteins of the Rrf2 family, which could indicate that this type of cluster is more widely present in nature than initially though, and that the role of Trp9 is not unique to RsrR.

2.06.4.2.2 CRP-family

2.06.4.2.2.1 *F*umarate and *n*itrate *r*eductase (FNR)

FNR, a member of the CRP (cAMP receptor) family, is a global transcriptional regulator that senses O_2 levels via an iron-sulfur cluster bound to the N-terminal domain of the protein, and that binds to the DNA through its helix-turn-helix motif at the C-terminal domain[673,674] (**Fig. 33**).

The FNR isolated from *E. coli* has been extensively characterized both at the molecular and structural level. FNR is involved in the transcriptional regulation of more than 100 genes, activating genes encoding proteins involved in anaerobic metabolism, such as *nar* operon (nitrate reductase), *dms* operon (dimethyl sulfoxide reductase) and *frd* operon (fumarate reductase) and repressing the ones involved in aerobic metabolism.[675,676]

The primary sequence of FNR shows that there are four conserved cysteine residues in the motif Cys-X_2-Cys-X_5-Cys, with the fourth cysteine ligand located around 90 residues toward the C-terminus (Cys20, Cys23, Cys29, and Cys122).[677] These cysteine residues bind a $[4Fe\text{-}4S]^{2+}$ cluster per monomer, required for FNR to bind specific DNA consensus sequence, the FNR-box, TTGAT-N_4-ATCAA.[678]

The mechanism of regulation has been extensively characterized using spectroscopic techniques and time resolved electrospray ionization mass spectrometry enabling the identification of several intermediate species in what was thought to be a simple cluster

conversion from a [4Fe-4S] to [2Fe-2S] cluster.[679] Some of these studies employed a variant of *E. coli* FNR, FNR S24F, for which the initial reactions of the [4Fe-4S] to [2Fe-2S] cluster conversion was determined to be 4 times slower.[680] These experiments allowed not only the identification of intermediate species in the cluster conversion but also changes in the protein oligomerization state that occur during this process.

The FNR's $[4Fe\text{-}4S]^{2+}$ cluster ($S=0$), when exposed to oxygen, is converted to $[2Fe\text{-}2S]^{2+}$, with a $[3Fe\text{-}4S]^{1+}$ ($S = 1/2$),[673,681–683] and a [3Fe-3S] clusters as intermediate species,[684] and release of two Fe atoms. In fact, the primary target of O_2 has been proposed to be Cys23 or the Fe bound to this cysteine,[680] with the loss of one Fe^{2+}, but without formation of any oxygen adduct species,[668,684] as initially proposed. The exact mechanism for this initial step is still not completely understood and could include an $[3Fe\text{-}4S]^0$ cluster in equilibrium with free iron (Fe^{2+}), that is oxidized to $[3Fe\text{-}4S]^0$ by O_2.[668] Then, there is formation of the [3Fe-3S] intermediate species through the loss of sulfide.[684] The decay of this intermediate to the [2Fe-2S] cluster is slow and is the rate-limiting step of the [3Fe-4S] to the [2Fe-2S] conversion.[680,684] Single and double persulfide intermediate species have been identified by mass spectrometry and resonance Raman, with a [2Fe-3S] species proposed to be generated by the decomposition of the [3Fe-3S], and [2Fe-4S] from [3Fe-4S]. Thus, this process is not due to the incorporation of S^0 but an oxidative process with loss of an iron atom, that can then decay into a persulfide apo-form.[684,685] The formation of these persulfide species can be a way to easily revert the O_2-inactived FNR to an active form without the intervention of the iron-sulfur biogenesis system.[684]

Further exposure to oxygen leads to the complete disassembly of the [2Fe-2S] cluster or persulfide versions. This conversion of holo-FNR to apo-FNR has been confirmed to occur also *in vivo*, with all the cysteine residues in the apo-FNR kept in the thiol state,[686] which, as mentioned, facilitates the re-assembly of the $[4Fe\text{-}4S]^{2+}$ cluster upon decrease of O_2 availability.

Besides the modifications that occur at the level of the iron-sulfur cluster, it was also observed that FNR is only a dimer when binding the $[4Fe\text{-}4S]^{2+}$ cluster, and that the other FNR forms are monomeric and do not efficiently bind to the FNR-box[677,687,688] (**Fig. 33**). This change in the oligomerization state of FNR might be due to conformational changes that occur at the dimer interface, driven by alterations in the iron-sulfur cluster binding site.[689,690]

The dimerization interface is proposed to be mediated by the formation of a coiled-coil of an α-helix in between the DNA-binding and iron-sulfur domains, which contains mainly hydrophobic residues.[689] The analysis of the two FNR structures identified a negatively charged residue in this helix, Asp154, that is in a region that cannot stabilize this charged residue. These factors have been proposed to mediate the charge repulsion monomerization of the FNR under aerobic conditions.[690] In addition, Ile151 is involved in coiled-coil interactions that stabilize the dimer in the absence of O_2, and there is a salt bridge between Arg140 and Asp130 in opposing monomers that also contributes to this stabilization. The disruption of these interactions upon exposure to O_2 will lead to the opening of the coiled-coil and dislocation of the equilibrium toward the monomer.[691,692]

FNR plays a secondary role by sensing and responding to NO.[678,693] The iron-sulfur cluster present in FNR becomes nitrosylated upon exposure to NO, forming a dinitrosyl-iron-cysteine complex, which abolishes its capacity to recognize and bind to the specific DNA promoter sequences.[678] The physiological significance of the reaction of NO with FNR has been questioned. However, it has been shown that when *E. coli* cells are exposed to NO there are several FNR-repressed genes that become activated.[694,695]

Orthologs of FNR have been isolated from other organisms, such as *Aliivibrio fischeri*,[691] *Paracoccus denitrificans* (FnrP),[696] *N. meningitidis*,[697] *A. vinelandii* (CydR),[698,699] *B. subtilis* (FNR_{Bc}),[700] which also bind an oxygen-sensitive iron-sulfur cluster, but the mechanism of disassembly is still unknown. Furthermore, the type of iron-sulfur cluster that is bound to these proteins might be different, since the iron-sulfur cluster binding motif of *E. coli* FNR is not conserved in these organisms. In fact, in the case of

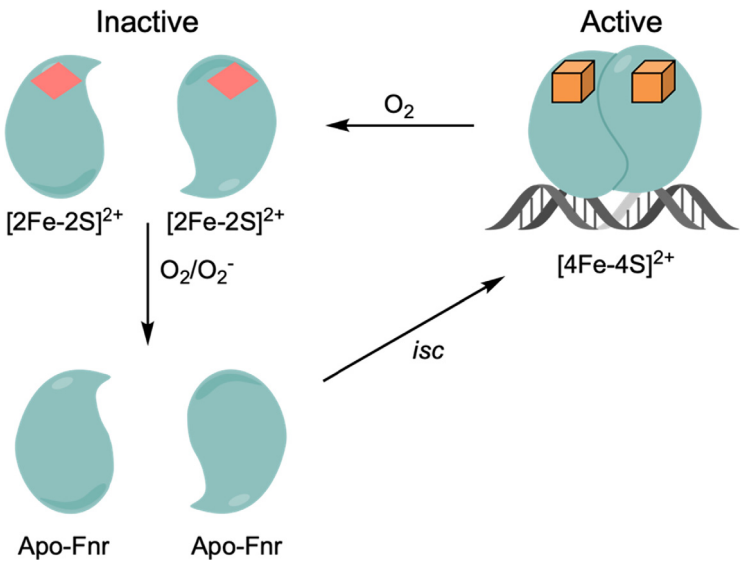

Fig. 33 Schematic representation of the mode of action of FNR transcription regulator. Adapted from Green, J.; Paget, M. S., Bacterial Redox Sensors. *Nat. Rev. Microbiol.* **2004**, *2*(12), 954–966.

B. subtilis FNR_{Bc}, it was identified that there are three conserved cysteines in the C-terminal and the fourth ligand of the $[4Fe\text{-}4S]^{2+}$ cluster is an aspartate residue, Asp141.[700] This cluster was characterized using UV–visible (λ_{max} at ~420 nm and a shoulder at 320 nm) and Mössbauer ($\Delta E_Q = 0.92$ mm/s and $\delta = 0.42$ mm/s) spectroscopies,[700,701] and its monomer dimer equilibrium was shown not to be dependent on the presence of the iron-sulfur cluster, in contrast to FNR.[701]

2.06.4.2.2.2 Anaerobic regulation of *a*rginine deiminase and *n*itrate reduction (ANR)

ANR (anaerobic regulation of arginine deiminase and nitrate reduction) is a FNR/CRP-like transcription activation homologous to FNR that has been identified in *Pseudomonas aeruginosa*.[702,703] In *Pseudomonas* spp., ANR, involved in the switch between the aerobic and anaerobic way of life, is an oxygen-sensing transcription regulator.[704,705] The initial studies showed that ANR regulates nitrate transport and reduction, $narK_1K_2GHJI$, and two other transcription regulators NarXL and Dnr.[706,707] However, a more global analysis indicates that ANR is a global anaerobic regulator, controlling the expression of around 250 genes, involved in central metabolism and aerobic electron transport chain.[708]

The primary sequence of ANR presents conservation of the four cysteine residues proposed to bind a $[4Fe\text{-}4S]^{2+}$ cluster and it has been shown that ANR can functionally complement an *E. coli fnr* knock-out variant.[703] ANR, akin to FNR, is composed of two domains, with the helix-turn-helix found at the C-terminus, and the iron-sulfur cluster in the consensus motif Cys-X_2-Cys-X_5-Cys in the N-terminus domain.

The type of iron-sulfur cluster was shown by Mössbauer spectroscopy ($\Delta E_Q = 1.2$ mm/s and $\delta = 0.43$ mm/s) and visible (λ_{max} at ~420 nm and a shoulder at 320 nm) spectroscopies[709] to be a $[4Fe\text{-}4S]^{2+}$ cluster, similarly to the one present in FNR.[709] This $[4Fe\text{-}4S]^{2+}$ cluster is converted to a $[2Fe\text{-}2S]^{2+}$ cluster upon exposure to oxygen or NO, and as a consequence ANR loses its ability to bind to its DNA binding consensus sequence,[709] in a mechanism akin to the one described in **Section 2.06.4.2.2.1** for FNR.

In *P. putida* there are two other proteins with high sequence homology to ANR, that also bind [4Fe-4S] clusters, judging by its UV–visible and CD spectra, but differ in their O_2-sensitivity.[710]

2.06.4.2.3 Other transcription regulators

2.06.4.2.3.1 Superoxide response regulator (SoxR)

In *E. coli* and other enteric bacteria, SoxRS are two separate transcription activators that participate in a two-step activation process in response to redox-cycling compounds. SoxR (*s*uper*ox*ide response *r*egulator) enhances to 100-times the transcription of the gene *soxS*,[711,712] and it is SoxS, a member of the AraC family, that will control the expression of around 100 genes, such as the ones encoding for aconitase, manganese-containing superoxide dismutase, endonuclease IV, and Fur, that are involved in repair or avoiding the oxidative stress damage.[713,714]

However, in other bacteria, such as *Pseudomonas* spp., SoxR is itself responsible for the transcriptional activation of genes, such as the ones encoding a putative flavin-dependent monooxygenase, and two multidrug efflux pumps, in response to the presence of phenazines, endogenous redox-active pigments, in a superoxide-independent manner.[715,716] These genes have been suggested to be involved in phenazine transport and detoxification.[716–718] Moreover, in *P. aeruginosa* and *S. coelicolor*, SoxR was shown to regulate genes that are involved in the production and transport of endogenously produced redox-active antibiotics.[719,720]

Although SoxR from different bacteria respond to different signals and is possibly involved in different regulatory networks, its mode of action is proposed to be similar. In fact, expression of *P. putida soxR* in *E. coli* complements a *soxR* deletion mutant.[721,722]

SoxR, a transcription regulator of the Mer-family, is a homodimer of 17 kDa that binds a $[2Fe\text{-}2S]^{1+}$ cluster per monomer in the consensus sequence Cys-X_2-Cys-X-Cys-X_5-Cys near the C-terminus.[723] The presence of this iron-sulfur cluster does not change the affinity of SoxR to the target promoter region, though its transcriptional activity is completely dependent on the oxidation state of the [2Fe-2S] cluster.[711,724,725] In fact, the iron-sulfur cluster present in SoxR needs to be oxidized to $[2Fe\text{-}2S]^{2+}$, for SoxR to function as a transcription activator,[711] and its affinity is 4-fold higher than when its iron-sulfur cluster is in the reduced state, $[2Fe\text{-}2S]^{1+}$.[726]

Although, an increase in almost 500 mV in the iron-sulfur cluster reduction potential upon DNA binding (from -285 ± 10 mV (pH 7.6)[711] to $+200$ mV[727]) was initially reported, latter a different result was obtained. In fact, using electron transfer mediators and a different experimental approach, it was shown that there is a much smaller impact on the reduction potential upon DNA binding, and that this change corresponds to a negative shift, from -293 mV to -320 mV (pH 7.6).[726] This smaller difference can be attributed to the small conformational change observed in the structure of the protein in the two oxidation states.[728]

Although, many advances of the SoxR activation mechanism have been made it is still poorly understood (**Fig. 34**). Previous studies pointed out that in *E. coli*, SoxR was activated in response to superoxide anion, that would be generated when the cells were exposed to redox-cycling agents, such as methyl viologen, quinone or phenazine.[729,730] However, the direct reaction of this anion with SoxR had not been shown. In 2011, Gu and Imlay[731] demonstrated that SoxR does not respond to superoxide anion, but that redox-cycling drugs trigger its activation, by directly oxidizing its $[2Fe\text{-}2S]^{1+}$ cluster. Therefore, SoxRS is proposed to be responsible for the response against these compounds, which are produced by several bacteria and plants to inhibit the growth of competitors.[732,733] However, *in vivo* SoxR is maintained in the reduced state by SoxR reductases (Rsx/Rse system)[734,735] that use NADPH as electron donor, thus SoxRS system could be triggered by an imbalance in the $NADPH/NADP^+$ cellular content, reflecting a change in the redox state of the cell.[736]

The promoter region under the control of SoxR has a long 19 or 20 bp spacer between the -35 and -10 operator elements that need to be untwisted for transcription activation. This process is accomplished by the conformational change that occurs in SoxR upon the one-electron oxidation of the $[2Fe\text{-}2S]^{1+}$ cluster to $[2Fe\text{-}2S]^{2+}$, conformational change that is also transmitted to the target promoter region.[728,737] The extent of the proposed conformational change was determined by comparing the free and DNA-bound

SoxR structures.[728] SoxR is composed by a DNA-binding domain, a dimerization helix, and an iron-sulfur cluster-binding domain at the C-terminus.[728] The dimerization helix forms an anti-parallel coiled-coil that stabilizes the dimer, and the [2Fe-2S] cluster is solvent exposed (with S2 and two Fe atoms being completely exposed) and located in an asymmetric environment that is stabilized by interactions with the other subunit.[728] It was proposed that the existence of a single glycine residue, Gly123, in between the two internal cysteine residues is required to induce the SoxR conformational changes coupled with the DNA distortion.[728,738] Other residues, such as lysines (namely Lys89 and Lys92) have been shown to be important in the reaction with superoxide anion *in vitro* and affect the transcription activity *in vivo*.[739]

However, how the oxidation state of the [2Fe-2S] cluster influences the conformation of SoxR remains unknown, though it has been proposed that a change in the oxidation state can change the hydrogen bonding network in the protein.[737]

The presence of the solvent exposed iron-sulfur cluster might facilitate its oxidation and can also explain its nitrosylation by NO.[740,741] The nitrosylation of the SoxR [2Fe-2S] cluster has been shown to form a dinitro iron complex by EPR both *in vitro* and *in vivo*.[740,742] Complementary studies using CD and pulse radiolysis enabled the identification of rate limiting steps and other intermediate species.[742,743] The dinitro iron complex-SoxR was shown to have a similar DNA affinity as SoxR $[2Fe\text{-}2S]^{2+}$, and thus to activate gene transcription.[740] However, since there are other transcription regulators that specifically respond to NO (with higher affinity for NO and activate several NO scavenging system) (such as NsrR, see **Section 2.06.4.2.1.3**), the question remains as whether NO reaction is physiologically relevant for the SoxR system.[744]

2.06.4.2.3.2 WhiB-family of transcription factors regulators

WhiB-like proteins, identified in several Actinomycetales, such as *Streptomyces* spp., *Corynebacterium glutamicum*, and pathogenic bacteria, such as *Mycobacterium tuberculosis* and *Corynebcterium diphtheria*, are proposed to play critical roles in the biology of these bacteria, including morphological differentiation, virulence, and antibiotic resistance.[745,746] WhiB-like proteins have also been identified in the genome of several mycobacteriophages, and these also bind an iron-sulfur cluster that regulates their DNA-binding activity.[747]

The WhiB-like family of proteins is involved in different functions in *Streptomyces*, such as slow-down of biomass accumulation and changes that precede sporulation (WhiA), multi-drug resistance (WhiC), septation during sporulation (WhiB), and in later stages of sporulation (WhiD).[748,749] Moreover, in *M. tuberculosis*, proteins of this family (WhiB1 to WhiB7) have been shown to be involved in diverse functions, such as antibiotic tolerance and enabling this bacterium to survive for longer periods within its host, maintaining redox homeostasis[750] and virulence.[750,751] For instance, WhiB1 was shown to be encoded by an essential gene, *whiB1*, and bind to specific DNA sequences[752] and WhiB3 is essential for optimal growth on tricarboxylic acid cycle intermediates during infection[753] (further information on WhiB-like protein classes can be found in[679,746]).

The analysis of the primary sequence of several members of the WhiB-family revealed that these proteins can be grouped into five classes, and the presence of (i) four conserved cysteine residues arranged in the motif Cys-X_n-Cys-X_2-Cys-X_5-Cys, (ii) a motif named β-turn, G[I/V/L]W[G/A]G, after the last conserved cysteine, and (iii) a patch of positively charged residues (with Lys/Arg) at the C-terminus.[746,754] The four cysteine residues are proposed to coordinate an iron-sulfur cluster,[754] essential for the function of these proteins, that can sense O_2 and NO. The β-turn has been proposed to be important for protein interactions, as these proteins do not present the usual DNA-binding domain. The exception is the class that includes Whib7/WblC, as these have a AT-hook that is known to bind AT-rich sequences in the minor groove,[755] though as mentioned all these proteins have a positively charged patch at the C-terminus. The mode of action of WhiB-like proteins is not completely known, and vary between the different classes, but it seems to involve the coordinated action of accessory proteins to provide DNA binding specificity.[746]

The type of iron-sulfur center bound to WhiB-like proteins was identified by its characteristic spectroscopic features: a broad absorption band with a maximum around 400 nm and positive features at 429 nm and 512 nm in its CD spectrum.[752,756–758]

WhiD from *S. coelicolor*, isolated under anoxic conditions, binds an oxygen-sensitive $[4Fe\text{-}4S]^{2+}$ cluster that has a very low reduction potential (< -460 mV at pH 8.0),[759] and is essential for its function as transcription regulator.[754]

In some of these proteins, the $[4Fe\text{-}4S]^{2+}$ cluster reacts with O_2 and completely disassembles from the protein in a slow process, with the conversion of $[4Fe\text{-}4S]^{2+}$ to a $[3Fe\text{-}4S]^{1+}$ intermediate, which then decays to the EPR silent $[2Fe\text{-}2S]^{2+}$ intermediate species before complete cluster disassembly.[753,754,758] On the contrary, the reaction with NO is more universal in these proteins and their

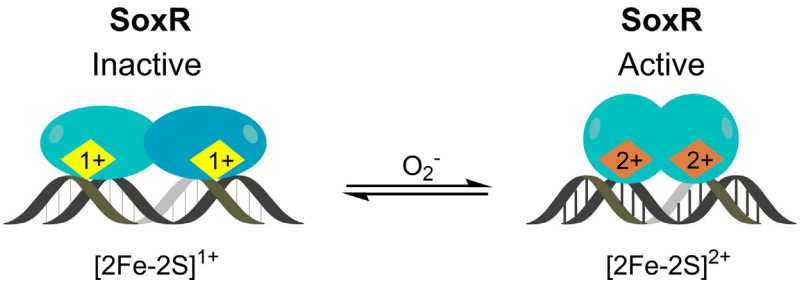

Fig. 34 Schematic representation of the mode of action of SoxR transcription regulator. Adapted from Green, J.; Paget, M. S., Bacterial Redox Sensors. *Nat. Rev. Microbiol.* **2004,** *2*(12), 954–966.

nitrosylation mechanism seems to be similar. The $[4Fe\text{-}4S]^{2+}$ cluster reacts very rapidly with NO in a multiphasic reaction, with stepwise formation of [4Fe-4S](NO), and $[4Fe\text{-}4S](NO)_2$. In the presence of higher concentrations of NO there is formation of $[4Fe\text{-}4S](NO)_4$ and of novel nitrosylated cluster $[Fe_3S_3(NO)_7]$.[756,757]

The nitrosylation of the iron-sulfur cluster activates the protein, enabling it to bind to specific DNA regulatory sequences.[752,755] This activation might involve a conformational change, driven by the rearrangement of the iron positions relative to the cysteine thiols due to the formation of the nitrosylated species.[756,757] The structure of WhiB1 and WhiB7 has been determined by solution NMR and X-ray crystallography,[755,756,760] showing that it is constituted by a 4-helix bundle, with the [4Fe-4S] cluster held by three α-helices. Their mechanism of interaction with sigma factor σ^A has been proposed based on these structures,[755,756,760] and it was also shown that nitrosylation of the iron-sulfur cluster abolish this interaction, allowing the protein to interact with the DNA. In the case of WhiB7, its AT-hook was also proposed to be important for the binding to the −35 element.

In conclusion, the WhiB-like proteins are proposed to be intracellular redox sensors that sense the physiological relevant host signaling molecules O_2 and NO, and integrate these signals with core intermediary metabolism, essential for survival.[761] Nevertheless, their mechanism of action still needs to be completely understood, as well as the role played by the iron-sulfur cluster in their diverse functions.

2.06.4.2.3.3 Sensing oxygen by NreBC two component system

NreB (*n*itrogen *re*gulation), isolated from *Staphylococcus carnosus* and found in other *Staphylococcus* species,[762] is encoded by the operon *nreABC*, a novel two-component system, which controls the dissimilatory nitrate/nitrite reduction and simultaneously responds to oxygen and nitrate.[762,763]

In the regulatory model, the oxygen-sensor NreB phosphorylates NreC that is the transcription regulator and binds to the promoter regions of the *narGHJI* and *nirRBD* operons to activate their expression. NreA is a nitrate-sensing protein[764,765] that controls the autophosphorylation activity of NreB, as in the absence of nitrate converts NreB from a kinase to a phosphatase.[766–768]

NreB is a sensory histidine kinase of 347 residues with a N-terminal PAS domain with four conserved cysteine residues arranged in the Cys-X_2-Cys-X_{11}-Cys-X_2-Cys motif,[765] that binds an iron-sulfur cluster identified as a $[4Fe\text{-}4S]^{2+}$ cluster, using spectroscopic techniques. This iron-sulfur cluster is oxygen-sensitive and completely disassembles when exposed to oxygen. A diamagnetic $[2Fe\text{-}2S]^{2+}$ cluster is proposed to be an intermediate species in this process.[769,770] The presence of the oxygen-sensitive iron-sulfur cluster is required for the kinase activity of NreB but does not seem to be essential for its dimerization.[769]

2.06.4.2.3.4 SufR transcription repressor

The Suf system is involved in the biosynthesis of iron-sulfur clusters in many organisms (prokaryotes and plastids), in response to iron starvation and oxidative stress. Some organisms have both Isc and Suf system while others only have the Suf system. The gene composition and organization of the Suf system differ between species.[771] In Actinobacteria and Cyanobacteria these genes are under the regulation of SufR.

SufR is a transcription regulator that belongs to the ArsR-family, with a HTH DNA binding domain at the N-terminus and binds a [4Fe-4S] cluster through three conserved cysteines located in the C-terminus (the fourth ligand has not yet been identified)[772] (**Fig. 29**). This protein is a repressor of the *suf* operon by binding to the palindromic sequence CAAC-N_6-GTTG present in the promoter region of *sufRBDCSU*, which is involved in the biosynthesis of iron-sulfur clusters in Gram-positive bacteria.[772,773]

In the presence of O_2, the absorption band with a maximum at 413 nm decreases rapidly in intensity, without passing through an intermediate species. This might be an indication that this protein is extremely sensitive to O_2, and its iron-sulfur cluster decomposes rapidly without formation of a [2Fe-2S] stable intermediate. The loss of [4Fe-4S] cluster abolishes DNA binding.[772]

The *M. tuberculosis* SufR is a dimer in solution. Its [4Fe-4S] cluster responds to NO, and upon nitrosylation, the *suf* operon transcription is activated. SufR [4Fe-4S] cluster was spectroscopically characterized by UV-visible (λ_{max} at 413 nm) and CD (positive peaks at 330 nm and 420 nm) spectroscopy,[773] while its reaction with O_2, H_2O_2 and NO was followed by UV-visible and EPR spectroscopies. The presence of NO was proposed to lead to the formation of a dinitrosyl-iron dithiol complex.[773]

2.06.4.2.3.5 OrpR σ^{54}-dependent activator

OrpR is a σ^{54}-dependent activator found in *D. vulgaris* Hildenborough and *D. alaskensis* G20.[774,775] The analysis of its primary sequence showed that it is composed by three domains: a N-terminus PAS domain, a central AAA+ domain (that can hydrolyze ATP) and a C-terminus DNA binding domain.

The PAS domain binds an oxygen-sensitive $[4Fe\text{-}4S]^{2+}$ cluster, that was identified by EPR and visible spectroscopy.[776] This iron-sulfur cluster is coordinated by three conserved cysteines present in a C-X_8-C-X_3-C motif, and the fourth ligand is proposed to be an aspartate. The mechanism of action has not yet been completely unraveled, but it is proposed to be a redox sensor. In fact, in the presence of O_2 the cluster completely disassembles, but in the presence of mild oxidative conditions it is converted to a $[3Fe\text{-}4S]^{1+}$ cluster, that has the same affinity to the specific palindromic DNA sequence as the $[4Fe\text{-}4S]^{2+}$ OrpR.[776]

OrpR activates the transcription of two divergent operons in *D. vulgaris* Hildenborough that encodes the Orange Protein (Orp) complex.[775] This protein complex was identified by pool-down assays and is composed by a core group of three proteins, Orp and two-ATPases proposed to bind iron-sulfur clusters.[775] Besides these, two other proteins encoded by these operons are proposed to be iron-sulfur proteins.[774,777] The Orp is a 12 kDa protein that has been isolated from *D. gigas* and *D. alaskensis* G20 and binds non-

covalently a Mo-Cu-Mo linear cluster bridged by sulfur atoms[778,779] (Section 2.06.2.1.5). The heterologously produced apo-Orp can be reconstituted *in vitro*.[778–781] However, the physiological function of this non-redox heterometallic cluster remains unknown, as well as what is the function of the Orp complex.

2.06.5 The role of iron-sulfur clusters in DNA processing enzymes

DNA is subjected to modifications due to oxidative stress, radiation, and chemical modification, such as alkylation, and to misincorporation of nucleotides. Therefore, the action of molecular repair systems is essential to correct these DNA damages and mismatches that would change the genomic code and lead to mutagenic effects that can be the cause of diseases, such as cancer.

Although, the presence of iron-sulfur clusters in DNA and RNA processing enzymes can be counterintuitive, as iron can generate hydroxyl radicals via Fenton reactions that damage DNA,[782] these clusters has been identified in several enzymes, such as Rad3 family helicases,[783–788] AddAB helicase-nuclease,[789] archaea RNA polymerases,[790–792] DNA polymerase,[793] DNA primase[794–796] and elongator domains.[797] In fact, iron-sulfur clusters are present in all replicative DNA polymerases and helicase-nuclease Dna2.[793,798]

In common, these enzymes bind a [4Fe-4S] cluster through four cysteine residues organized in a sequence motif, which is unique for each enzyme family and different from the canonical motifs described so far (see Table 1 in Ref. 799). The iron-sulfur cluster is a $[4Fe\text{-}4S]^{2+}$ identified by visible, EPR and Mössbauer spectroscopies, and in a few cases by CD, resonance Raman,[800,801] FTIR[802] and surface enhanced IR.[803]

Another peculiarity is that the presence of the iron-sulfur cluster is not restricted to prokaryotic DNA processing enzymes, but it is present in bacteria, archaea, and eukaryotic enzymes, and in some cases, it is present in novel iron-sulfur cluster domains.[796] In fact, there are several human diseases that are related with iron-sulfur proteins involved in DNA and RNA metabolism.[9]

As mentioned in Section 2.06.3 and 2.06.4, iron-sulfur clusters can be employed in radical SAM chemistry (methylthiolate tRNA, e.g., MiaB), or as sensors in transcription factors. Nevertheless, in other DNA/RNA processing enzymes the role of the iron-sulfur cluster is still unclear. One exception are glycosylases, in which iron-sulfur clusters have been proposed to be involved in DNA damage recognition (*vide infra*), via DNA-mediated charge transport. A similar mechanism might be important in other DNA-processing enzymes, thus the question "why this mechanism in not ubiquitous or conserved even in an enzyme family" remains to be answered.[804]

A detailed characterization of the iron-sulfur cluster in this group of proteins is required to determine its contribution to their function. In most cases, there is no detailed spectroscopic characterization, the reduction potential (in the presence and absence of nucleic acid) and the contribution of the iron-sulfur cluster to the protein function *in vivo* is unknown. However, the presence of this prosthetic group has been used as an endogenous quencher of fluorescence to study the protein-DNA interaction in Rad3 family helicases.[787]

Moreover, the location of the iron-sulfur cluster in the three-dimensional structure of these proteins has shed some light into their function, that can go beyond the simple structural role. In some of these proteins, as is the case of Dna2 helicase-nuclease and XPD helicase, the iron-sulfur cluster is in the catalytic domain, while in others, as glycosylases, the iron-sulfur cluster is in a distant domain.[805,806] Such locations might correspond to a difference in the role played by this cofactor: (i) sense double helix disruption, or (ii) modulate DNA affinity and processivity.

Here, only the DNA repair glycosylases will be described since the contribution of the iron-sulfur cluster for their function is better understood.

2.06.5.1 DNA repair glycosylases

Base excision repair (BER) glycosylases are responsible for identifying in the genome chemically modified bases and mismatches, and catalyze their removal, constituting one of the most common mechanisms of DNA repair.[807] In the first step, BER glycosylases need to locate the modified base and then flip it into their catalytic site and catalyze the break of the N-glycosidic bond between the damaged base and the sugar-phosphate backbone.[807]

These enzymes are divided into six superfamilies,[808,809] and up-to-now in two of these some were found to bind iron-sulfur clusters: (i) the helix-hairpin-helix superfamily, containing *E. coli* endonuclease III (EndoIII) and MutY (including the mammalian homologs hNTH1, MUTYH) and (ii) the uracil DNA glycosylase superfamily (Table 3).

In EndoIII and MutY the unique cysteine binding motif Cys-X_6-Cys-X_2-Cys-X_5-Cys coordinates the iron-sulfur cluster, that is located near the surface at the C-terminus domain, in a loop that has been named as the $[4Fe\text{-}4S]^{2+}$ cluster loop (FCL) domain.[815,816] The comparison between the structure of the free and DNA-bound EndoIII, shows that the overall structure is very similar, and that there is a loop projecting from the cluster with several positively charged residues, which directly interacts with the DNA phosphate backbone,[816–818] which led to the hypothesis that iron-sulfur cluster had a structural role important for DNA binding.

In the case of EndoIII the iron-sulfur cluster was identified to be a $[4Fe\text{-}4S]^{2+}$ by EPR and Mössbauer spectroscopies,[819] and it was shown that it could not be easily oxidized nor reduced. Further characterization by resonance Raman showed that the presence of oligonucleotides containing a reduced apyrimidinic site or thymine glycol (an inhibitor) resulted in small shifts in the stretching modes assigned to Fe-S(Cys), which also contributed to the assignment of a structural role to this cluster.[800] However, later it

was shown that in MutY, the presence of the iron-sulfur cluster was not required for protein folding and stability, though essential for DNA-binding and activity.[810,820]

The identification of a redox active iron-sulfur cluster and its importance in the function of these proteins was only demonstrated using electrochemistry. Different electrochemical methods were applied to EndoIII and MutY, showing that the reduction potential of the iron-sulfur cluster in the presence of DNA has a positive value (around 130 mV, depending on the electrode surface) (**Fig. 2**), consistent with the observation of a $[4Fe\text{-}4S]^{2+/3+}$ redox pair,[811,821,822,824] as observed in HiPIP iron-sulfur proteins (see **Section 2.06.2.1.4**). Binding of EndoIII to DNA has an impact of – 50 mV in its reduction potential.[824] This negative shift indicates that the enzyme binds more tightly to DNA when its [4Fe-4S] cluster is in the $[4Fe\text{-}4S]^{3+}$ state (K_D of 11 nM) than in the reduced $[4Fe\text{-}4S]^{2+}$ state (K_D of 6 μM),[825,826] as no conformational change was observed between the DNA free and bound forms.

A value of 80 mV has been determined for the reduction potential of other repair and replication proteins using DNA modified electrodes (either DNA films on gold surfaces or DNA duplexes on highly oriented pyrolytic graphite),[811,827–832] a value that falls within the physiological range. These studies also pointed toward a DNA-mediated charge transport between the electrode and the iron-sulfur cluster.

Micro-FTIR microscopy has been used to study the interaction between EndoIII and DNA. The change in the vibration modes, assigned to the iron-sulfur cluster, indicated an increase in the bond lengths, that makes the cluster more stable, and prepares it to a higher oxidation state, $[4Fe\text{-}4S]^{3+}$, without much energy change, which is required for the damage detection in the DNA[802] (*vide infra*).

In the family-4 uracil-DNA glycosylases (4 UDGs) from thermophilic organisms, the cysteine binding motif that coordinates the iron-sulfur cluster is Cys-X_2-Cys-X_n-Cys-$X_{(14-17)}$-Cys, in which *n* can range from 70 to 100 residues.[806]

The X-ray structure of *Thermus thermophilus* 4 UDG shows that the $[4Fe\text{-}4S]^{2+}$ has a distorted cuboidal structure, located 10 Å from its active site.[812] In the absence of further experimental data, a structural role was also initially attributed to this iron-sulfur cluster. However, it is clear from the available crystal structures that the distance between the iron-sulfur cluster and the DNA is comparable in all these glycosylases and thus its contribution to the enzyme function must be similar.[812] The impact of DNA binding in the reduction potential of these proteins is in the same range as the one reported for EndoIII.[811]

Therefore, the function of the iron-sulfur cluster in the glycosylases might not be structural, and it has been proposed that the $[4Fe\text{-}4S]^{2+}$ cluster is responsible for the detection of DNA lesions through DNA-mediated charge transport.[804] The base-pair π-stack of duplex DNA can mediate charge transport over 200 Å distances, which is disrupted when the DNA is damaged.[833,834] Thus, this could be the mechanism used by this type of glycosylases to sense these disruptions and repair the DNA damage.

The proposed mechanism for the action of the iron-sulfur glycosylases is the one in which in the DNA unbound form, the [4Fe-4S] cluster is in the 2+ oxidation state, and in the presence of DNA there is a shift in ~50 mV in the reduction potential that increases the glycosylase DNA binding affinity (**Fig. 35**A, (Step1)). The protein is activated toward oxidation, and this electron is going to reduce a distally bound protein in a DNA-mediated charge transport reaction (**Fig. 35**A, (Step2)). This protein loses affinity for the DNA and is released (**Fig. 35**A, (Step3)). However, in the presence of a lesion, this charge transport mechanism cannot occur, and the glycosylase stays bound to the DNA and repairs it[811,822,823] (**Fig. 35**B).

Moreover, since guanine radicals are the first products of oxidative DNA damage inside the cell, and it has been shown that they can also oxidize the iron-sulfur of MutY glycosylase, these base radicals may provide the *in vivo* driving force for iron-sulfur glycosylates to initiate DNA-mediated signaling.[835]

In the case of the 4UDGs family, it has been observed that the presence of the iron-sulfur cluster is not conserved in all the proteins but seems to be ubiquitous for the ones isolated from thermophilic bacteria.[806,812] Therefore, this cluster might provide a faster detection of the DNA damage since these organisms need to deal with a higher rate of temperature-induced DNA damage.[806]

This mechanism might be common to other DNA processing enzymes,[828,829] in which a change in the oxidation state of its [4Fe-4S] cluster increases the enzyme DNA binding affinity and modulates its activity.

Table 3 Some DNA glycosylases that bind [4Fe-4S] clusters.

Enzyme Name	*Substrate*	*References*
MutY/MUTYH	OG:**A**	810
Nth (EndoIII)/hNTH1	Oxidized pyrimidines; **T-T**	811
Thermophilic family-4 UDGs	**U**:A/G	812
Methanibacterium thermoautotrophicum TDG	**T**:G	813
rpS3 (UV-endonuclease)	**T-T**; C:**OG**	814

The excised base is highlighted in bold.
OG:A - 7,8-dihydro-8-oxo-2′-deoxyguanosine-2′-deoxyadenosine; TDG – thymine DNA glycosylase; rpS3 – human ribosomal protein S3.

2.06.6 Conclusions

Iron-sulfur clusters are ancient metal centers participating in a wide range of biological functions. The tetrahedral $Fe(S)_4$ unit, formed by iron and sulfur, is used as a basic and versatile building block of proteins' metal centers and enzymes' active sites. Iron-sulfur clusters are optimized devices for electron transfer due to the multiple oxidation and spin states attainable, the possibility of magnetic coupling, as well as the ability to stabilize localized and delocalized charges. In addition, the modulation of the cluster properties by varying the coordination (not exclusively made of sulfur atoms), inserting other metal atoms (such as, nickel and molybdenum) and having flexible coordination spheres, opens their biological relevance to non-redox catalysis and radical chemistry, gene regulation and nucleic acid metabolism.

The ability found in certain iron-sulfur proteins for sulfur transfer and ligand swapping has been exploited in the biosynthesis of iron-sulfur containing proteins. In fact, the complexity involved in iron-sulfur cluster assembly, not described in here, contrasts with the self-assembly chemistry most often observed when apo-forms are reconstituted by addition of iron and inorganic sulfur under reducing conditions.

It is worth mentioning that all the chemical and biochemical processes observed in this field were inspiring topics for the generation of biocatalysts mimicking enzyme active sites[23] and possible roles in biotechnological oriented processes. Medical aspects related with iron-sulfur cluster containing proteins are out of the scope of this review but represent an emergent and important field,[836–841] for which it will be necessary to develop appropriate strategies.

It is remarkable the speed of expansion of the field and the new directions to which our understanding of the role of iron-sulfur clusters is moving. In this review we intended to provide an update on our previous work on the same subject, highlighting the main discoveries in the field of iron-sulfur cluster containing proteins in the last 8 years, such as the identity of the X atom in the nitrogenase cofactor, the identification of Fe-hydrogenases that are oxygen-tolerant, the increasing number of radical SAM enzymes, the sensor mechanism in many transcription regulators, and the role played by iron-sulfur cluster in DNA processing enzymes.

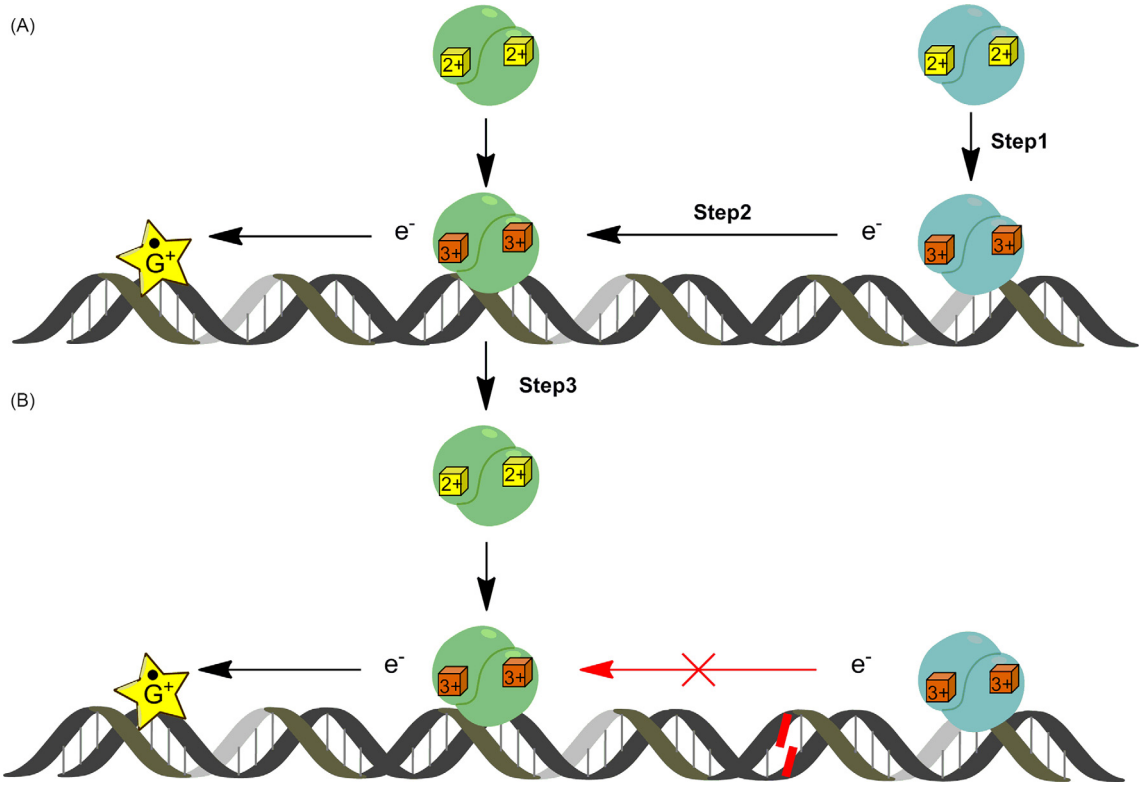

Fig. 35 Schematic representation of the mechanism of action of iron-sulfur glycosylases in the absence (A) and in the presence (B) of a DNA lesion. Adapted from Boal, A. K.; Yavin, E.; Barton, J. K., DNA Repair Glycosylases with a [4Fe-4S] Cluster: A Redox Cofactor for DNA-Mediated Charge Transport? *J. Inorg. Biochem.* **2007**, *101*(11–12), 1913–1921; Barton, J. K.; Silva, R. M. B.; O'Brien, E., Redox Chemistry in the Genome: Emergence of the [4Fe4S] Cofactor in Repair *and Replication. Annu. Rev. Biochem.* **2019**, *88*, 163–190.

Acknowledgments

This work is financed by national funds from FCT - Fundação para a Ciência e a Tecnologia, I.P., in the scope of the project UIDP/04378/2020 and UIDB/04378/2020 of the Research Unit on Applied Molecular Biosciences - UCIBIO and the project LA/P/0140/2020 of the Associate Laboratory Institute for Health and Bioeconomy - i4HB, and in the scope of the project UIDB/50006/2020, UIDP/50006/2020 and LA/P/0008/2020 of the Associate Laboratory for Green Chemistry-LAQV. FCT supported SRP through the projects FCT-ANR/BBB-MET/0023/2012 and PTDC/BIA-BQM/29442/2017, and JJGM through the project PTDC/BTA-BTA/0935/2020.

Author contributions: SRP and RG has planned the manuscript with contributions from JJGM and IM. SRP, RG and MSPC wrote the manuscript, which was critically revised by JJGM and IM.

References

1. Stiefel, E. I.; George, G. N. Ferredoxins, Hydrogenases and Nitrogenases: Metal-Sulfide Proteins. In *University Science Books California*; 1994, vol. 7; pp 365–453.
2. Bian, S. M.; Cowan, J. A. Protein-Bound Iron-Sulfur Centers. Form, Function, and Assembly. *Coord. Chem. Rev.* **1999,** *190,* 1049–1066.
3. Johnson, D. C.; Dean, D. R.; Smith, A. D.; Johnson, M. K. Structure, Function, and Formation of Biological Iron-Sulfur Clusters. *Annu. Rev. Biochem.* **2005,** *74,* 247–281.
4. Meyer, J. Iron-Sulfur Protein Folds, Iron-Sulfur Chemistry, and Evolution. *J. Biol. Inorg. Chem.* **2008,** *13* (2), 157–170.
5. Glaser, T.; Hedman, B.; Hodgson, K. O.; Solomon, E. I. Ligand K-Edge X-Ray Absorption Spectroscopy: A Direct Probe of Ligand-Metal Covalency. *Acc. Chem. Res.* **2000,** *33* (12), 859–868.
6. Noodleman, L.; Case, D. A. Density-Functional Theory of Spin Polarization and Spin Coupling in Iron-Sulfur Clusters. In *Advances in Inorganic Chemistry;* Richard, C., Ed.; vol. 38; Academic Press, 1992; pp 423–458, 458a, 458b, 459-470.
7. Johnson, M. K. Iron-Sulfur Proteins. In *Encyclopedia of Inorganic Chemistry;* King, R. B., Ed., Wiley: Chichester, 1994; pp 1896–1915.
8. Beinert, H. Iron-Sulfur Proteins: Ancient Structures, Still Full of Surprises. *J. Biol. Inorg. Chem.* **2000,** *5* (1), 2–15.
9. Khodour, Y.; Kaguni, L. S.; Stiban, J. Iron-Sulfur Clusters in Nucleic Acid Metabolism: Varying Roles of Ancient Cofactors. *Enzyme* **2019,** *45,* 225–256.
10. Przybyla-Toscano, J.; Christ, L.; Keech, O.; Rouhier, N. Iron-Sulfur Proteins in Plant Mitochondria: Roles and Maturation. *J. Exp. Bot.* **2021,** *72* (6), 2014–2044.
11. Braymer, J. J.; Freibert, S. A.; Rakwalska-Bange, M.; Lill, R. Mechanistic Concepts of Iron-Sulfur Protein Biogenesis in Biology. *Biochim. Biophys. Acta Mol. Cell Res.* **2021,** *1868* (1), 118863.
12. Baussier, C.; Fakroun, S.; Aubert, C.; Dubrac, S.; Mandin, P.; Py, B.; Barras, F. Making Iron-Sulfur Cluster: Structure, Regulation and Evolution of the Bacterial ISC System. *Adv. Microb. Physiol.* **2020,** *76,* 1–39.
13. Talib, E. A.; Outten, C. E. Iron-Sulfur Cluster Biogenesis, Trafficking, and Signaling: Roles for CGFS Glutaredoxins and BolA Proteins. *Biochim. Biophys. Acta* **2021,** *1868* (1), 118847.
14. Blahut, M.; Sanchez, E.; Fisher, C. E.; Outten, F. W. Fe-S Cluster Biogenesis by the Bacterial Suf Pathway. *Biochim. Biophys. Acta Mol. Cell Res.* **2020,** *1867* (11), 118829.
15. Maio, N.; Rouault, T. A. Outlining the Complex Pathway of Mammalian Fe-S Cluster Biogenesis. *Trends Biochem. Sci.* **2020,** *45* (5), 411–426.
16. Lill, R. From the Discovery to Molecular Understanding of Cellular Iron-Sulfur Protein Biogenesis. *Biol. Chem.* **2020,** *401* (6-7), 855–876.
17. Lill, R.; Freibert, S. A. Mechanisms of Mitochondrial Iron-Sulfur Protein Biogenesis. *Annu. Rev. Biochem.* **2020,** *89,* 471–499.
18. Beinert, H.; Sands, R. H. Studies on Succinic and DpnH Dehydrogenase Preparations by Paramagnetic Resonance (EPR) Spectroscopy. *Biochem. Bioph. Res. Co* **1960,** *3* (1), 41–46.
19. Mortenson, L. E.; Valentine, R. C.; Carnahan, J. E. An electron transport factor from *Clostridium pasteurianum. Biochem. Bioph. Res. Co* **1962,** *7,* 448–452.
20. Tagawa, K.; Arnon, D. I. Ferredoxins as Electron Carriers in Photosynthesis and in the Biological Production and Consumption of Hydrogen Gas. *Nature* **1962,** *195,* 537–543.
21. Malkin, R.; Rabinowitz, J. C. The Reconstitution of Clostridial Ferredoxin. *Biochem. Bioph. Res. Co* **1966,** *23* (6), 822–827.
22. Beinert, H.; Holm, R. H.; Munck, E. Iron-sulfur clusters: nature's modular, multipurpose structures. *Science* **1997,** *277* (5326), 653–659.
23. Venkateswara Rao, P.; Holm, R. H. Synthetic Analogues of the Active Sites of Iron-Sulfur Proteins. *Chem. Rev.* **2004,** *104* (2), 527–559.
24. Beinert, H.; Meyer, J.; Lill, R. Iron-Sulfur Proteins. In *Encyclopedia of Biological Chemistry;* Lennarz, W. J., Lane, M. D., Eds., Elsevier: Amsterdam, 2004; pp 482–489.
25. Liu, J.; Chakraborty, S.; Hosseinzadeh, P.; Yu, Y.; Tian, S.; Petrik, I.; Bhagi, A.; Lu, Y. Metalloproteins Containing Cytochrome, Iron-Sulfur, or Copper Redox Centers. *Chem. Rev.* **2014,** *114* (8), 4366–4469.
26. Rees, D. C. Great Metalloclusters in Enzymology. *Annu. Rev. Biochem.* **2002,** *71,* 221–246.
27. Jeoung, J. H.; Martins, B. M.; Dobbek, H. Double-Cubane [8Fe9S] Clusters: A Novel Nitrogenase-Related Cofactor in Biology. *ChemBioChem* **2020,** *21* (12), 1710–1716.
28. Volbeda, A.; Fontecilla-Camps, J. C. Structural Bases for the Catalytic Mechanism of Ni-Containing Carbon Monoxide Dehydrogenases. *Dalton Trans.* **2005,** *21,* 3443–3450.
29. Chen, C. J.; Lin, Y. H.; Huang, Y. C.; Liu, M. Y. Crystal Structure of Rubredoxin from *Desulfovibrio Gigas* to Ultra-High 0.68 Å Resolution. *Biochem. Bioph. Res. Co* **2006,** *349* (1), 79–90.
30. Archer, M.; Huber, R.; Tavares, P.; Moura, I.; Moura, J. J. G.; Carrondo, M. A.; Sieker, L. C.; LeGall, J.; Romão, M. J. Crystal Structure of Desulforedoxin from *Desulfovibrio Gigas* Determined at 1.8 Å Resolution: A Novel Non-heme Iron Protein Structure. *J. Mol. Biol.* **1995,** *251* (5), 690–702.
31. Coelho, A. V.; Matias, P.; Fülöp, V.; Thompson, A.; Gonzalez, A.; Carrondo, M. A. Desulfoferrodoxin Structure Determined by MAD Phasing and Refinement to 1.9-Å Resolution Reveals a Unique Combination of a Tetrahedral FeS4 Centre with a Square Pyramidal $FeSN_4$ Centre. *J. Biol. Inorg. Chem.* **1997,** *2* (6), 680–689.
32. Koehler, C.; Carlier, L.; Veggi, D.; Balducci, E.; Di Marcello, F.; Ferrer-Navarro, M.; Pizza, M.; Daura, X.; Soriani, M.; Boelens, R.; Bonvin, A. M. Structural and Biochemical Characterization of NarE, an Iron-Containing ADP-Ribosyltransferase from *Neisseria meningitidis. J. Biol. Chem.* **2011,** *286* (17), 14842–14851.
33. Fukuyama, K.; Ueki, N.; Nakamura, H.; Tsukihara, T.; Matsubara, H. Tertiary Structure of [2Fe-2S] Ferredoxin from *Spirulina Platensis* Refined at 2.5 Å Resolution: Structural Comparisons of Plant-Type Ferredoxins and an Electrostatic Potential Analysis. *J. Biochem.* **1995,** *117* (5), 1017–1023.
34. Rebelo, J.; Macieira, S.; Dias, J. M.; Huber, R.; Ascenso, C. S.; Rusnak, F.; Moura, J. J.; Moura, I.; Romao, M. J. Gene Sequence and Crystal Structure of the Aldehyde Oxidoreductase from *Desulfovibrio Desulfuricans* ATCC 27774. *J. Mol. Biol.* **2000,** *297* (1), 135–146.
35. Wu, C. K.; Dailey, H. A.; Rose, J. P.; Burden, A.; Sellers, V. M.; Wang, B. C. The 2.0 Å Structure of Human Ferrochelatase, the Terminal Enzyme of Heme Biosynthesis. *Nat. Struct. Biol.* **2001,** *8* (2), 156–160.
36. Berkovitch, F.; Nicolet, Y.; Wan, J. T.; Jarrett, J. T.; Drennan, C. L. Crystal Structure of Biotin Synthase, an S-Adenosylmethionine-Dependent Radical Enzyme. *Science* **2004,** *303* (5654), 76–79.
37. Bönisch, H.; Schmidt, C. L.; Schäfer, G.; Ladenstein, R. The Structure of the Soluble Domain of an Archaeal Rieske Iron-Sulfur Protein at 1.1 Å Resolution. *J. Mol. Biol.* **2002,** *319* (3), 791–805.
38. Paddock, M. L.; Wiley, S. E.; Axelrod, H. L.; Cohen, A. E.; Roy, M.; Abresch, E. C.; Capraro, D.; Murphy, A. N.; Nechushtai, R.; Dixon, J. E.; Jennings, P. A. MitoNEET Is a Uniquely Folded 2Fe 2S Outer Mitochondrial Membrane Protein Stabilized by Pioglitazone. *Proc. Natl. Acad. Sci. U. S. A.* **2007,** *104* (36), 14342–14347.
39. Volbeda, A.; Martinez, M. T. P.; Crack, J. C.; Amara, P.; Gigarel, O.; Munnoch, J. T.; Hutchings, M. I.; Darnault, C.; Le Brun, N. E.; Fontecilla-Camps, J. C. Crystal Structure of the Transcription Regulator RsrR Reveals a [2Fe-2S] Cluster Coordinated by Cys, Glu, and His Residues. *J. Am. Chem. Soc.* **2019,** *141* (6), 2367–2375.
40. Kissinger, C. R.; Sieker, L. C.; Adman, E. T.; Jensen, L. H. Refined Crystal-Structure of Ferredoxin-II from *Desulfovibrio gigas* at 1.7 Å. *J. Mol. Biol.* **1991,** *219* (4), 693–715.

41. Stout, C. D. Crystal Structures of Oxidized and Reduced *Azotobacter Vinelandii* Ferredoxin at pH 8 and 6. *J. Biol. Chem.* **1993,** *268* (34), 25920–25927.
42. Robbins, A. H.; Stout, C. D. Structure of Activated Aconitase: Formation of the [4Fe-4S] Cluster in the Crystal. *Proc. Natl. Acad. Sci. U. S. A.* **1989,** *86* (10), 3639–3643.
43. Volbeda, A.; Charon, M. H.; Piras, C.; Hatchikian, E. C.; Frey, M.; Fontecilla-Camps, J. C. Crystal Structure of the Nickel-Iron Hydrogenase from *Desulfovibrio gigas*. *Nature* **1995,** *373* (6515), 580–587.
44. Moura, J. J.; Macedo, A. L.; Palma, P. N. Ferredoxins. *Methods Enzymol.* **1994,** *243,* 165–188.
45. Zhou, Z. H.; Adams, M. W. Site-Directed Mutations of the 4Fe-Ferredoxin from the Hyperthermophilic Archaeon *Pyrococcus furiosus*: Role of the Cluster-Coordinating Aspartate in Physiological Electron Transfer Reactions. *Biochemistry* **1997,** *36* (36), 10892–10900.
46. Dauter, Z.; Wilson, K. S.; Sieker, L. C.; Meyer, J.; Moulis, J. M. Atomic Resolution (0.94 Å) Structure of *Clostridium acidurici* Ferredoxin. Detailed Geometry of [4Fe-4S] Clusters in a Protein. *Biochemistry* **1997,** *36* (51), 16065–16073.
47. Liu, L.; Nogi, T.; Kobayashi, M.; Nozawa, T.; Miki, K. Ultrahigh-Resolution Structure of High-Potential Iron-Sulfur Protein from *Thermochromatium tepidum*. *Acta Crystallogr. D Biol. Crystallogr.* **2002,** *58* (Pt 7), 1085–1091.
48. Aragão, D.; Macedo, S.; Mitchell, E. P.; Romão, C. V.; Liu, M. Y.; Frazão, C.; Saraiva, L. M.; Xavier, A. V.; LeGall, J.; van Dongen, W.; Hagen, W. R.; Teixeira, M.; Carrondo, M. A.; Lindley, P. Reduced Hybrid Cluster Proteins (HCP) from *Desulfovibrio desulfuricans* ATCC 27774 and *Desulfovibrio vulgaris* (Hildenborough): X-Ray Structures at High Resolution Using Synchrotron Radiation. *J. Biol. Inorg. Chem.* **2003,** *8* (5), 540–548.
49. Peters, J. W.; Lanzilotta, W. N.; Lemon, B. J.; Seefeldt, L. C. X-Ray Crystal Structure of the Fe-Only Hydrogenase (Cpl) from *Clostridium pasteurianum* to 1.8 Angstrom Resolution. *Science* **1998,** *282* (5395), 1853–1858.
50. Dobritzsch, D.; Schneider, G.; Schnackerz, K. D.; Lindqvist, Y. Crystal Structure of Dihydropyrimidine Dehydrogenase, a Major Determinant of the Pharmacokinetics of the Anti-Cancer Drug 5-Fluorouracil. *EMBO J.* **2001,** *20* (4), 650–660.
51. Lee, M.; Grawert, T.; Quitterer, F.; Rohdich, F.; Eppinger, J.; Eisenreich, W.; Bacher, A.; Groll, M. Biosynthesis of Isoprenoids: Crystal Structure of the [4Fe-4S] Cluster Protein IspG. *J. Mol. Biol.* **2010,** *404* (4), 600–610.
52. Moulis, J. M.; Davasse, V.; Golinelli, M. P.; Meyer, J.; Quinkal, I. The Coordination Sphere of Iron-Sulfur Clusters: Lessons from Site-Directed Mutagenesis Experiments. *J. Biol. Inorg. Chem.* **1996,** *1* (1), 2–14.
53. Sosa Torres, M. E.; Kroneck, P. M. H. Introduction: Transition Metals and Sulfur. *Met. Ions Life Sci.* **2020,** *20*.
54. Fontecave, M. Iron-Sulfur Clusters: Ever-Expanding Roles. *Nat. Chem. Biol.* **2006,** *2* (4), 171–174.
55. Herriott, J. R.; Sieker, L. C.; Jensen, L. H.; Lovenberg, W. Structure of Rubredoxin: An X-Ray Study to 2.5 Å Resolution. *J. Mol. Biol.* **1970,** *50* (2), 391–406.
56. Meyer, J.; Moulis, J.-M. Rubredoxin. In *Handbook of Metalloproteins;* Messerschmidt, A., Huber, R., Poulos, T., Wieghardt, K., Eds., Wiley: Chichester, 2006; pp 505–517.
57. Auchere, F.; Pauleta, S. R.; Tavares, P.; Moura, I.; Moura, J. J. Kinetics Studies of the Superoxide-Mediated Electron Transfer Reactions between Rubredoxin-Type Proteins and Superoxide Reductases. *J. Biol. Inorg. Chem.* **2006,** *11* (4), 433–444.
58. Bak, D. W.; Elliott, S. J. Alternative FeS Cluster Ligands: Tuning Redox Potentials and Chemistry. *Curr. Opin. Chem. Biol.* **2014,** *19,* 50–58.
59. Bachmayer, H.; Piette, L. H.; Yasunobu, K. T.; Whiteley, H. R. The Binding Sites of Iron in Rubredoxin from *Micrococcus aerogenes*. *Proc. Natl. Acad. Sci. U. S. A.* **1967,** *57* (1), 122–127.
60. Peisach, J.; Blumberg, W. E.; Lode, E. T.; Coon, M. J. An Analysis of the Electron Paramagnetic Resonance Spectrum of *Pseudomonas oleovorans* Rubredoxin. A Method for Determination of the Liganids of Ferric Iron in Completely Rhombic Sites. *J. Biol. Chem.* **1971,** *246* (19), 5877–5881.
61. Thapper, A.; Rizzi, A. C.; Brondino, C. D.; Wedd, A. G.; Pais, R. J.; Maiti, B. K.; Moura, I.; Pauleta, S. R.; Moura, J. J. Copper-Substituted Forms of the Wild Type and C42A Variant of Rubredoxin. *J. Inorg. Biochem.* **2013,** *127,* 232–237.
62. Sushko, T.; Kavaleuski, A.; Grabovec, I.; Kavaleuskaya, A.; Vakhrameev, D.; Bukhdruker, S.; Marin, E.; Kuzikov, A.; Masamrekh, R.; Shumyantseva, V.; Tsumoto, K.; Borshchevskiy, V.; Gilep, A.; Strushkevich, N. A New Twist of Rubredoxin Function in *M. tuberculosis*. *Bioorg. Chem.* **2021,** *109*, 104721.
63. Almeida, R. M.; Turano, P.; Moura, I.; Moura, J. J.; Pauleta, S. R. Superoxide Reductase: Different Interaction Modes with its Two Redox Partners. *ChemBioChem* **2013,** *14* (14), 1858–1866.
64. Goodfellow, B. J.; Nunes, S. G.; Rusnak, F.; Moura, I.; Ascenso, C.; Moura, J. J.; Volkman, B. F.; Markley, J. L. Zinc-Substituted *Desulfovibrio gigas* Desulforedoxins: Resolving Subunit Degeneracy with Nonsymmetric Pseudocontact Shifts. *Protein Sci.* **2002,** *11* (10), 2464–2470.
65. Goodfellow, B. J.; Rusnak, F.; Moura, I.; Domke, T.; Moura, J. J. NMR Determination of the Global Structure of the 113Cd Derivative of Desulforedoxin: Investigation of the Hydrogen Bonding Pattern at the Metal Center. *Protein Sci.* **1998,** *7* (4), 928–937.
66. Moura, I.; Bruschi, M.; Le Gall, J.; Moura, J. J.; Xavier, A. V. Isolation and Characterization of Desulforedoxin, a New Type of Non-heme Iron Protein from *Desulfovibrio gigas*. *Biochem. Bioph. Res. Co* **1977,** *75* (4), 1037–1044.
67. Yu, L.; Kennedy, M.; Czaja, C.; Tavares, P.; Moura, J. J. G.; Moura, I.; Rusnak, F. Conversion of Desulforedoxin into a Rubredoxin Center. *Biochem. Bioph. Res. Co* **1997,** *231* (3), 679–682.
68. Blake, P. R.; Park, J. B.; Zhou, Z. H.; Hare, D. R.; Adams, M. W.; Summers, M. F. Solution-State Structure by NMR of Zinc-Substituted Rubredoxin from the Marine Hyperthermophilic Archaebacterium *Pyrococcus furiosus*. *Protein Sci.* **1992,** *1* (11), 1508–1521.
69. Kowal, A. T.; Zambrano, I. C.; Moura, I.; Moura, J. J. G.; Legall, J.; Johnson, M. K. Electronic and Magnetic-Properties of Nickel-Substituted Rubredoxin - a Variable-Temperature Magnetic Circular-Dichroism Study. *Inorg. Chem.* **1988,** *27* (7), 1162–1166.
70. Dauter, Z.; Wilson, K. S.; Sieker, L. C.; Moulis, J. M.; Meyer, J. Zinc- and Iron-Rubredoxins from *Clostridium Pasteurianum* at Atomic Resolution: A High-Precision Model of a ZnS_4 Coordination Unit in a Protein. *Proc. Natl. Acad. Sci. U. S. A.* **1996,** *93* (17), 8836–8840.
71. Moura, I.; Teixeira, M.; LeGall, J.; Moura, J. J. Spectroscopic Studies of Cobalt and Nickel Substituted Rubredoxin and Desulforedoxin. *J. Inorg. Biochem.* **1991,** *44* (2), 127–139.
72. Slater, J. W.; Marguet, S. C.; Monaco, H. A.; Shafaat, H. S. Going beyond Structure: Nickel-Substituted Rubredoxin as a Mechanistic Model for the [NiFe] Hydrogenases. *J. Am. Chem. Soc.* **2018,** *140* (32), 10250–10262.
73. Prasad, P.; Selvan, D.; Chakraborty, S. Biosynthetic Approaches towards the Design of Artificial Hydrogen-Evolution Catalysts. *Chemistry* **2020,** *26* (55), 12494–12509.
74. Maiti, B. K.; Maia, L. B.; Silveira, C. M.; Todorovic, S.; Carreira, C.; Carepo, M. S.; Grazina, R.; Moura, I.; Pauleta, S. R.; Moura, J. J. Incorporation of Molybdenum in Rubredoxin: Models for Mononuclear Molybdenum Enzymes. *J. Biol. Inorg. Chem.* **2015,** *20* (5), 821–829.
75. Archer, M.; Carvalho, A. L.; Teixeira, S.; Moura, I.; Moura, J. J.; Rusnak, F.; Romão, M. J. Structural Studies by X-Ray Diffraction on Metal Substituted Desulforedoxin, a Rubredoxin-Type Protein. *Protein Sci.* **1999,** *8* (7), 1536–1545.
76. Goodfellow, B. J.; Duarte, I. C.; Macedo, A. L.; Volkman, B. F.; Nunes, S. G.; Moura, I.; Markley, J. L.; Moura, J. J. An NMR Structural Study of Nickel-Substituted Rubredoxin. *J. Biol. Inorg. Chem.* **2010,** *15* (3), 409–420.
77. Perry, A.; Lian, L. Y.; Scrutton, N. S. Two-Iron Rubredoxin of *Pseudomonas Oleovorans*: Production, Stability and Characterization of the Individual Iron-Binding Domains by Optical, CD and NMR spectroscopies. *Biochem. J.* **2001,** *354* (Pt 1), 89–98.
78. Galle, L. M.; Cutsail Iii, G. E.; Nischwitz, V.; DeBeer, S.; Span, I. Spectroscopic characterization of the Co-Substituted C-Terminal Domain of Rubredoxin-2. *Biol. Chem.* **2018,** *399* (7), 787–798.
79. Moura, I.; Tavares, P.; Moura, J. J.; Ravi, N.; Huynh, B. H.; Liu, M. Y.; LeGall, J. Purification and Characterization of Desulfoferrodoxin. A Novel Protein from *Desulfovibrio desulfuricans* (ATCC 27774) and from *Desulfovibrio vulgaris* (Strain Hildenborough) that Contains a Distorted Rubredoxin Center and a Mononuclear Ferrous Center. *J. Biol. Chem.* **1990,** *265* (35), 21596–21602.
80. Pinto, A. F.; Rodrigues, J. V.; Teixeira, M. Reductive Elimination of Superoxide: Structure and Mechanism of Superoxide Reductases. *Biochim. Biophys. Acta* **2010,** *1804* (2), 285–297.

81. Caldas Nogueira, M. L.; Pastore, A. J.; Davidson, V. L. Diversity of Structures and Functions of Oxo-Bridged Non-heme Diiron Proteins. *Arch. Biochem. Biophys.* **2021,** *705*, 108917.
82. Folgosa, F.; Martins, M. C.; Teixeira, M. Diversity and Complexity of Flavodiiron NO/O_2 Reductases. *FEMS Microbiol. Lett.* **2018,** *365* (3).
83. Folgosa, F.; Martins, M. C.; Teixeira, M. The Multidomain Flavodiiron Protein from *Clostridium Difficile* 630 Is an NADH:Oxygen Oxidoreductase. *Sci. Rep.* **2018,** *8* (1), 10164.
84. Kint, N.; Alves Feliciano, C.; Martins, M. C.; Morvan, C.; Fernandes, S. F.; Folgosa, F.; Dupuy, B.; Texeira, M.; Martin-Verstraete, I. How the Anaerobic Enteropathogen *Clostridioides difficile* Tolerates Low O_2 Tensions. *MBio* **2020,** *11* (5).
85. Bertini, I.; Luchinat, C.; Provenzani, A.; Rosato, A.; Vasos, P. R. Browsing Gene Banks for Fe2S2 Ferredoxins and Structural Modeling of 88 Plant-Type Sequences: An Analysis of Fold and Function. *Proteins* **2002,** *46* (1), 110–127.
86. Grinberg, A. V.; Hannemann, F.; Schiffler, B.; Muller, J.; Heinemann, U.; Bernhardt, R. Adrenodoxin: Structure, Stability, and Electron Transfer Properties. *Proteins* **2000,** *40* (4), 590–612.
87. Kakuta, Y.; Horio, T.; Takahashi, Y.; Fukuyama, K. Crystal Structure of *Escherichia coli* Fdx, an Adrenodoxin-Type Ferredoxin Involved in the Assembly of Iron-Sulfur Clusters. *Biochemistry* **2001,** *40* (37), 11007–11012.
88. Hugo, N.; Meyer, C.; Armengaud, J.; Gaillard, J.; Timmis, K. N.; Jouanneau, Y. Characterization of Three XylT-Like [2Fe-2S] Ferredoxins Associated with Catabolism of Cresols or Naphthalene: Evidence for their Involvement in Catechol Dioxygenase Reactivation. *J. Bacteriol.* **2000,** *182* (19), 5580–5585.
89. Mitou, G.; Higgins, C.; Wittung-Stafshede, P.; Conover, R. C.; Smith, A. D.; Johnson, M. K.; Gaillard, J.; Stubna, A.; Munck, E.; Meyer, J. An Isc-Type Extremely Thermostable [2Fe-2S] Ferredoxin from *Aquifex aeolicus*. Biochemical, Spectroscopic, and Unfolding Studies. *Biochemistry* **2003,** *42* (5), 1354–1364.
90. Frolow, F.; Harel, M.; Sussman, J. L.; Mevarech, M.; Shoham, M. Insights into Protein Adaptation to a Saturated Salt Environment from the Crystal Structure of a Halophilic 2Fe-2S Ferredoxin. *Nat. Struct. Biol.* **1996,** *3* (5), 452–458.
91. Ugulava, N. B.; Gibney, B. R.; Jarrett, J. T. Biotin Synthase Contains Two Distinct Iron-Sulfur Cluster Binding Sites: Chemical and Spectroelectrochemical Analysis of Iron-Sulfur Cluster Interconversions. *Biochemistry* **2001,** *40* (28), 8343–8351.
92. Jameson, G. N.; Cosper, M. M.; Hernandez, H. L.; Johnson, M. K.; Huynh, B. H. Role of the [2Fe-2S] Cluster in Recombinant *Escherichia coli* Biotin Synthase. *Biochemistry* **2004,** *43* (7), 2022–2031.
93. Sellers, V. M.; Johnson, M. K.; Dailey, H. A. Function of the [2Fe-2S] Cluster in Mammalian Ferrochelatase: A Possible Role as a Nitric Oxide Sensor. *Biochemistry* **1996,** *35* (8), 2699–2704.
94. Morales, R.; Charon, M. H.; Hudry-Clergeon, G.; Petillot, Y.; Norager, S.; Medina, M.; Frey, M. Refined X-Ray Structures of the Oxidized, at 1.3 A, and Reduced, at 1.17 Å, [2Fe-2S] Ferredoxin from the Cyanobacterium *Anabaena* PCC7119 Show Redox-Linked Conformational Changes. *Biochemistry* **1999,** *38* (48), 15764–15773.
95. Orengo, C. A.; Thornton, J. M. Protein Families and their Evolution-a Structural Perspective. *Annu. Rev. Biochem.* **2005,** *74,* 867–900.
96. Tsibris, J. C. M.; Woody, R. W. Structural Studies of Iron-Sulfur Proteins. *Coord. Chem. Rev.* **1970,** *5* (4), 417–458.
97. Fu, W.; Drozdzewski, P. M.; Davies, M. D.; Sligar, S. G.; Johnson, M. K. Resonance Raman and Magnetic Circular Dichroism Studies of Reduced [2Fe-2S] Proteins. *J. Biol. Chem.* **1992,** *267* (22), 15502–15510.
98. Todorovic, S.; Teixeira, M. Resonance Raman Spectroscopy of Fe-S Proteins and their Redox Properties. *J. Biol. Inorg. Chem.* **2018,** *23* (4), 647--661.
99. Link, T. A. Fe-S Rieske Center. In *Handbook of Metalloproteins;* Messerchmidt, A., Hubber, R., Poulos, T., Wieghardt, K., Eds., Wiley: Chichester, 2006; pp 518–531.
100. Lebrun, E.; Santini, J. M.; Brugna, M.; Ducluzeau, A. L.; Ouchane, S.; Schoepp-Cothenet, B.; Baymann, F.; Nitschke, W. The Rieske Protein: A Case Study on the Pitfalls of Multiple Sequence Alignments and Phylogenetic Reconstruction. *Mol. Biol. Evol.* **2006,** *23* (6), 1180–1191.
101. Iwata, S.; Saynovits, M.; Link, T. A.; Michel, H. Structure of a Water Soluble Fragment of The 'Rieske' Iron-Sulfur Protein of the Bovine Heart Mitochondrial Cytochrome bc_1 Complex Determined by MAD Phasing at 1.5 Å Resolution. *Structure* **1996,** *4* (5), 567–579.
102. Colbert, C. L.; Couture, M. M.; Eltis, L. D.; Bolin, J. T. A Cluster Exposed: Structure of the Rieske Ferredoxin from Biphenyl Dioxygenase and the Redox Properties of Rieske Fe-S Proteins. *Structure* **2000,** *8* (12), 1267–1278.
103. Konkle, M. E.; Muellner, S. K.; Schwander, A. L.; Dicus, M. M.; Pokhrel, R.; Britt, R. D.; Taylor, A. B.; Hunsicker-Wang, L. M. Effects of pH on the Rieske Protein from *Thermus thermophilus*: A Spectroscopic and Structural Analysis. *Biochemistry* **2009,** *48* (41), 9848–9857.
104. Anemuller, S.; Schmidt, C. L.; Schafer, G.; Bill, E.; Trautwein, A. X.; Teixeira, M. Evidence for a Two Proton Dependent Redox Equilibrium in an Archaeal Rieske Iron-Sulfur Cluster. *Biochem. Bioph. Res. Co* **1994,** *202* (1), 252–257.
105. Link, T. A. The structures of Rieske and Rieske-type proteins. In *Advances in Inorganic Chemistry;* Sykes, A. G., Ed.; vol. 47; Academic Press, 1999; pp 83–157.
106. Iwasaki, T.; Kounosu, A.; Samoilova, R. I.; Dikanov, S. A. ^{15}N HYSCORE Characterization of the Fully Deprotonated, Reduced Form of the Archaeal Rieske [2Fe-2S] Center. *J. Am. Chem. Soc.* **2006,** *128* (7), 2170–2171.
107. Kuila, D.; Schoonover, J. R.; Dyer, R. B.; Batie, C. J.; Ballou, D. P.; Fee, J. A.; Woodruff, W. H. Resonance Raman Studies of Rieske-Type Proteins. *Biochim. Biophys. Acta* **1992,** *1140* (2), 175–183.
108. Iwasaki, T.; Kounosu, A.; Kolling, D. R.; Crofts, A. R.; Dikanov, S. A.; Jin, A.; Imai, T.; Urushiyama, A. Characterization of the pH-Dependent Resonance Raman Transitions of Archaeal and Bacterial Rieske [2Fe-2S] Proteins. *J. Am. Chem. Soc.* **2004,** *126* (15), 4788–4789.
109. Wiley, S. E.; Paddock, M. L.; Abresch, E. C.; Gross, L.; van der Geer, P.; Nechushtai, R.; Murphy, A. N.; Jennings, P. A.; Dixon, J. E. The Outer Mitochondrial Membrane Protein mitoNEET Contains a Novel Redox-Active 2Fe-2S Cluster. *J. Biol. Chem.* **2007,** *282* (33), 23745–23749.
110. Zuris, J. A.; Harir, Y.; Conlan, A. R.; Shvartsman, M.; Michaeli, D.; Tamir, S.; Paddock, M. L.; Onuchic, J. N.; Mittler, R.; Cabantchik, Z. I.; Jennings, P. A.; Nechushtai, R. Facile Transfer of [2Fe-2S] Clusters from the Diabetes Drug Target mitoNEET to an Apo-Acceptor Protein. *Proc. Natl. Acad. Sci. U. S. A.* **2011,** *108* (32), 13047–13052.
111. Mittler, R.; Darash-Yahana, M.; Sohn, Y. S.; Bai, F.; Song, L.; Cabantchik, I. Z.; Jennings, P. A.; Onuchic, J. N.; Nechushtai, R. NEET Proteins: A New Link between Iron Metabolism, Reactive Oxygen Species, and Cancer. *Antioxid. Redox Signal.* **2019,** *30* (8), 1083–1095.
112. Karmi, O.; Marjault, H. B.; Pesce, L.; Carloni, P.; Onuchic, J. N.; Jennings, P. A.; Mittler, R.; Nechushtai, R. The Unique Fold and Lability of the [2Fe-2S] Clusters of NEET Proteins Mediate their Key Functions in Health and Disease. *J. Biol. Inorg. Chem.* **2018,** *23* (4), 599–612.
113. Tamir, S.; Paddock, M. L.; Darash-Yahana-Baram, M.; Holt, S. H.; Sohn, Y. S.; Agranat, L.; Michaeli, D.; Stofleth, J. T.; Lipper, C. H.; Morcos, F.; Cabantchik, I. Z.; Onuchic, J. N.; Jennings, P. A.; Mittler, R.; Nechushtai, R. Structure-Function Analysis of NEET Proteins Uncovers their Role as Key Regulators of Iron and ROS Homeostasis in Health and Disease. *Biochim. Biophys. Acta* **2015,** *1853* (6), 1294–1315.
114. Dicus, M. M.; Conlan, A.; Nechushtai, R.; Jennings, P. A.; Paddock, M. L.; Britt, R. D.; Stoll, S. Binding of Histidine in the (Cys)3(His)1-Coordinated [2Fe-2S] Cluster of Human mitoNEET. *J. Am. Chem. Soc.* **2010,** *132* (6), 2037–2049.
115. Tirrell, T. F.; Paddock, M. L.; Conlan, A. R.; Smoll, E. J., Jr.; Nechushtai, R.; Jennings, P. A.; Kim, J. E. Resonance Raman Studies of the (his)(Cys)3 2Fe-2S Cluster of MitoNEET: Comparison to the (Cys)4 Mutant and Implications of the Effects of pH on the Labile Metal Center. *Biochemistry* **2009,** *48* (22), 4747–4752.
116. Bak, D. W.; Zuris, J. A.; Paddock, M. L.; Jennings, P. A.; Elliott, S. J. Redox Characterization of the FeS Protein MitoNEET and Impact of Thiazolidinedione Drug Binding. *Biochemistry* **2009,** *48* (43), 10193–10195.
117. Bak, D. W.; Elliott, S. J. Conserved Hydrogen Bonding Networks of MitoNEET Tune Fe-S Cluster Binding and Structural Stability. *Biochemistry* **2013,** *52* (27), 4687–4696.
118. Zuris, J. A.; Halim, D. A.; Conlan, A. R.; Abresch, E. C.; Nechushtai, R.; Paddock, M. L.; Jennings, P. A. Engineering the Redox Potential over a Wide Range within a New Class of FeS Proteins. *J. Am. Chem. Soc.* **2010,** *132* (38), 13120–13122.
119. Li, H.; Mapolelo, D. T.; Dingra, N. N.; Naik, S. G.; Lees, N. S.; Hoffman, B. M.; Riggs-Gelasco, P. J.; Huynh, B. H.; Johnson, M. K.; Outten, C. E. The Yeast Iron Regulatory Proteins Grx3/4 and Fra2 Form Heterodimeric Complexes Containing a [2Fe-2S] Cluster with Cysteinyl and Histidyl Ligation. *Biochemistry* **2009,** *48* (40), 9569–9581.
120. Emptage, M. H.; Kent, T. A.; Huynh, B. H.; Rawlings, J.; Orme-Johnson, W. H.; Munck, E. On the Nature of the Iron-Sulfur Centers in a Ferredoxin from *Azotobacter Vinelandii*. Mossbauer Studies and Cluster Displacement Experiments. *J. Biol. Chem.* **1980,** *255* (5), 1793–1796.

121. Huynh, B. H.; Moura, J. J.; Moura, I.; Kent, T. A.; LeGall, J.; Xavier, A. V.; Munck, E. Evidence for a Three-Iron Center in a Ferredoxin from *Desulfovibrio gigas*. Mossbauer and EPR Studies. *J. Biol. Chem.* **1980,** *255* (8), 3242–3244.
122. Kent, T. A.; Dreyer, J. L.; Kennedy, M. C.; Huynh, B. H.; Emptage, M. H.; Beinert, H.; Munck, E. Mossbauer Studies of Beef Heart Aconitase: Evidence for Facile Interconversions of Iron-Sulfur Clusters. *Proc. Natl. Acad. Sci. U. S. A.* **1982,** *79* (4), 1096–1100.
123. Emptage, M. H.; Dreyers, J. L.; Kennedy, M. C.; Beinert, H. Optical and EPR Characterization of Different Species of Active and Inactive Aconitase. *J. Biol. Chem.* **1983,** *258* (18), 11106–11111.
124. Moura, J. J.; Moura, I.; Kent, T. A.; Lipscomb, J. D.; Huynh, B. H.; LeGall, J.; Xavier, A. V.; Munck, E. Interconversions of [3Fe-3S] and [4Fe-4S] Clusters. Mossbauer and Electron Paramagnetic Resonance Studies of *Desulfovibrio Gigas* Ferredoxin II. *J. Biol. Chem.* **1982,** *257* (11), 6259–6267.
125. Thomson, A. J.; Robinson, A. E.; Johnson, M. K.; Moura, J. J.; Moura, I.; Xavier, A. V.; Legall, J. The Three-Iron Cluster in a Ferredoxin from *Desulphovibrio Gigas*. A Low-Temperature Magnetic Circular Dichroism Study. *Biochim. Biophys. Acta* **1981,** *670* (1), 93–100.
126. Johnson, M. K.; Hare, J. W.; Spiro, T. G.; Moura, J. J.; Xavier, A. V.; LeGall, J. Resonance Raman Spectra of Three-Iron Centers in Ferredoxins from *Desulfovibrio gigas*. *J. Biol. Chem.* **1981,** *256* (19), 9806–9808.
127. Ghosh, D.; Furey, W., Jr.; O'Donnell, S.; Stout, C. D. Structure of a 7Fe Ferredoxin from *Azotobacter vinelandii*. *J. Biol. Chem.* **1981,** *256* (9), 4185–4192.
128. Stout, G. H.; Turley, S.; Sieker, L. C.; Jensen, L. H. Structure of Ferredoxin I from *Azotobacter vinelandii*. *Proc. Natl. Acad. Sci. U. S. A.* **1988,** *85* (4), 1020–1022.
129. Kissinger, C. R.; Adman, E. T.; Sieker, L. C.; Jensen, L. H. Structure of the 3Fe-4S Cluster in *Desulfovibrio gigas* Ferredoxin II. *J. Am. Chem. Soc.* **1988,** *110* (26), 8721–8723.
130. Johnson, M. K.; Morningstar, J. E.; Bennett, D. E.; Ackrell, B. A.; Kearney, E. B. Magnetic Circular Dichroism Studies of Succinate Dehydrogenase. Evidence for [2Fe-2S], [3Fe-xS], and [4Fe-4S] Centers in Reconstitutively Active Enzyme. *J. Biol. Chem.* **1985,** *260* (12), 7368–7378.
131. Morningstar, J. E.; Johnson, M. K.; Cecchini, G.; Ackrell, B. A.; Kearney, E. B. The High Potential Iron-Sulfur Center in *Escherichia Coli* Fumarate Reductase Is a Three-Iron Cluster. *J. Biol. Chem.* **1985,** *260* (25), 13631–13638.
132. Johnson, M. K.; Bennett, D. E.; Morningstar, J. E.; Adams, M. W.; Mortenson, L. E. The Iron-Sulfur Cluster Composition of *Escherichia coli* Nitrate Reductase. *J. Biol. Chem.* **1985,** *260* (9), 5456–5463.
133. Knaff, D. B.; Hirasawa, M.; Ameyibor, E.; Fu, W.; Johnson, M. K. Spectroscopic Evidence for a [3Fe-4S] Cluster in Spinach Glutamate Synthase. *J. Biol. Chem.* **1991,** *266* (23), 15080–15084.
134. Teixeira, M.; Moura, I.; Xavier, A. V.; Dervartanian, D. V.; Legall, J.; Peck, H. D., Jr.; Huynh, B. H.; Moura, J. J. *Desulfovibrio gigas* Hydrogenase: Redox Properties of the Nickel and Iron-Sulfur Centers. *Eur. J. Biochem.* **1983,** *130* (3), 481–484.
135. Antonio, M. R.; Averill, B. A.; Moura, I.; Moura, J. J.; Orme-Johnson, W. H.; Teo, B. K.; Xavier, A. V. Core Dimensions in the 3Fe Cluster of *Desulfovibrio gigas* Ferredoxin II by Extended X-Ray Absorption Fine Structure Spectroscopy. *J. Biol. Chem.* **1982,** *257* (12), 6646–6649.
136. Moreno, C.; Macedo, A. L.; Moura, I.; LeGall, J.; Moura, J. J. Redox Properties of *Desulfovibrio Gigas* [Fe_3S_4] and [Fe4S4] Ferredoxins and Heterometal Cubane-Type Clusters Formed within the [Fe3S4] Core. Square Wave Voltammetric Studies. *J. Inorg. Biochem.* **1994,** *53* (3), 219–234.
137. Johnson, M. K.; Duderstadt, R. E.; Duin, E. C. Biological and synthetic [Fe3S4] clusters. In *Adv Inorg Chem;* Sykes, A. G., Ed.; vol. 47; Academic Press, 1999; pp 1–82.
138. Fawcett, S. E.; Davis, D.; Breton, J. L.; Thomson, A. J.; Armstrong, F. A. Voltammetric Studies of the Reactions of Iron-Sulphur Clusters ([3Fe-4S] or [M3Fe-4S]) Formed in *Pyrococcus furiosus* Ferredoxin. *Biochem. J.* **1998,** *335* (Pt 2), 357–368.
139. George, S. J.; Armstrong, F. A.; Hatchikian, E. C.; Thomson, A. J. Electrochemical and Spectroscopic Characterization of the Conversion of the 7Fe into the 8Fe Form of Ferredoxin III from *Desulfovibrio Africanus*. Identification of a [4Fe-4S] Cluster with One Non-cysteine Ligand. *Biochem. J.* **1989,** *264* (1), 275–284.
140. Conover, R. C.; Kowal, A. T.; Fu, W. G.; Park, J. B.; Aono, S.; Adams, M. W.; Johnson, M. K. Spectroscopic Characterization of the Novel Iron-Sulfur Cluster in *Pyrococcus furiosus* Ferredoxin. *J. Biol. Chem.* **1990,** *265* (15), 8533–8541.
141. Calzolai, L.; Gorst, C. M.; Zhao, Z. H.; Teng, Q.; Adams, M. W.; La Mar, G. N. ^{1}H NMR Investigation of the Electronic and Molecular Structure of the Four-Iron Cluster Ferredoxin from the Hyperthermophile *Pyrococcus furiosus*. Identification of Asp14 as a Cluster Ligand in each of the Four Redox States. *Biochemistry* **1995,** *34* (36), 11373–11384.
142. Grazina, R.; de Sousa, P. M.; Brondino, C. D.; Carepo, M. S.; Moura, I.; Moura, J. J. Structural Redox Control in a 7Fe Ferredoxin Isolated from *Desulfovibrio alaskensis*. *Bioelectrochemistry* **2011,** *82* (1), 22–28.
143. Goodfellow, B. J.; Macedo, A. L.; Rodrigues, P.; Moura, I.; Wray, V.; Moura, J. J. The Solution Structure of a [3Fe-4S] Ferredoxin: Oxidised Ferredoxin II from *Desulfovibrio gigas*. *J. Biol. Inorg. Chem.* **1999,** *4* (4), 421–430.
144. Macedo, A. L.; Moura, I.; Moura, J. J. G.; Legall, J.; Huynh, B. H. Temperature-Dependent Proton NMR Investigation of the Electronic-Structure of the Trinuclear Iron Cluster of the Oxidized *Desulfovibrio Gigas* Ferredoxin-II. *Inorg. Chem.* **1993,** *32* (7), 1101–1105.
145. Bruschi, M.; Guerlesquin, F. Structure, Function and Evolution of Bacterial Ferredoxins. *FEMS Microbiol. Rev.* **1988,** *4* (2), 155–175.
146. Carter, C. W. High potential iron sulfur proteins. In *Handbook of Metalloproteins;* Messerchmidt, A., Huber, R., Poulos, T., Wieghardt, K., Eds., Wyley: Chichester, 2006; pp 602–609.
147. Bartsch, R. G. Purification of (4Fe-4S)1-2-Ferredoxins (High-Potential Iron-Sulfur Proteins) from Bacteria. *Methods Enzymol.* **1978,** *53,* 329–340.
148. Ciurli, S.; Musiani, F. High Potential Iron-Sulfur Proteins and their Role as Soluble Electron Carriers in Bacterial Photosynthesis: Tale of a Discovery. *Photosynth. Res.* **2005,** *85* (1), 115–131.
149. McRee, D. E.; Richardson, D. C.; Richardson, J. S.; Siegel, L. M. The Heme and Fe4S4 Cluster in the Crystallographic Structure of *Escherichia coli* Sulfite Reductase. *J. Biol. Chem.* **1986,** *261* (22), 10277–10281.
150. Lim, L. W.; Shamala, N.; Mathews, F. S.; Steenkamp, D. J.; Hamlin, R.; Xuong, N. H. Three-Dimensional Structure of the Iron-Sulfur Flavoprotein Trimethylamine Dehydrogenase at 2.4-Å Resolution. *J. Biol. Chem.* **1986,** *261* (32), 15140–15146.
151. Lubitz, W.; Reijerse, E.; van Gastel, M. [NiFe] and [FeFe] Hydrogenases Studied by Advanced Magnetic Resonance Techniques. *Chem. Rev.* **2007,** *107* (10), 4331–4365.
152. Strahs, G.; Kraut, J. Low-Resolution Electron-Density and Anomalous-Scattering-Density Maps of *Chromatium* High-Potential Iron Protein. *J. Mol. Biol.* **1968,** *35* (3), 503–512.
153. Carter, C. W., Jr.; Kraut, J.; Freer, S. T.; Alden, R. A.; Sieker, L. C.; Adman, E.; Jensen, L. H. A Comparison of Fe4S4 Clusters in High-Potential Iron Protein and in Ferredoxin. *Proc. Natl. Acad. Sci. U. S. A.* **1972,** *69* (12), 3526–3529.
154. Carter, C. W., Jr.; Kraut, J.; Freer, S. T.; Nguyen Huu, X.; Alden, R. A.; Bartsch, R. G. Two-Angstrom Crystal Structure of Oxidized *Chromatium* High Potential Iron Protein. *J. Biol. Chem.* **1974,** *249* (13), 4212–4225.
155. Plank, D. W.; Kennedy, M. C.; Beinert, H.; Howard, J. B. Cysteine Labeling Studies of Beef Heart Aconitase Containing a 4Fe, a Cubane 3Fe, or a Linear 3Fe Cluster. *J. Biol. Chem.* **1989,** *264* (34), 20385–20393.
156. Adman, E. T.; Sieker, L. C.; Jensen, L. H. Structure of a Bacterial Ferredoxin. *J. Biol. Chem.* **1973,** *248* (11), 3987–3996.
157. Cammack, R. "Super-Reduction" of Chromatium High-Potential Iron-Sulphur Protein in the Presence of Dimethyl Sulphoxide. *Biochem. Bioph. Res. Co* **1973,** *54* (2), 548–554.
158. Palmer, G. The Electron Paramagnetic Resonance of Metalloproteins. *Biochem. Soc. Trans.* **1985,** *13* (3), 548–560.
159. Cammack, R.; Patil, D. S.; Fernandez, V. M. Electron-Spin-Resonance/Electron-Paramagnetic-Resonance Spectroscopy of Iron-Sulphur Enzymes. *Biochem. Soc. Trans.* **1985,** *13* (3), 572–578.
160. Beinert, H. Electron-Paramagnetic-Resonance Spectroscopy in Biochemistry: Past, Present and Future. *Biochem. Soc. Trans.* **1985,** *13* (3), 542–547.

161. Guigliarelli, B.; Bertrand, P. Application of EPR spectroscopy to the structural and functional study of iron-sulfur proteins. In *Advances in Inorganic Chemistry;* Sykes, A. G., Ed.; vol. 47; Academic Press, 1999; pp 421–497.
162. Sweeney, W. V.; Rabinowitz, J. C. Proteins Containing 4Fe-4S Clusters: An Overview. *Annu. Rev. Biochem.* **1980,** *49,* 139–161.
163. Przysiecki, C. T.; Meyer, T. E.; Cusanovich, M. A. Circular Dichroism and Redox Properties of High Redox Potential Ferredoxins. *Biochemistry* **1985,** *24* (10), 2542–2549.
164. Moura, J. J.; LeGall, J.; Xavier, A. V. Interconversion from 3Fe into 4Fe Clusters in the Presence of *Desulfovibrio Gigas* Cell Extracts. *Eur. J. Biochem.* **1984,** *141* (2), 319–322.
165. Moura, I.; Moura, J. J. G.; Munck, E.; Papaefthymiou, V.; LeGall, J. Evidence for the Formation of a Cobalt-Iron-Sulfur (CoFe3S4) Cluster in *Desulfovibrio gigas* Ferredoxin II. *J. Am. Chem. Soc.* **1986,** *108* (2), 349–351.
166. Surerus, K. K.; Munck, E.; Moura, I.; Moura, J. J. G.; Legall, J. Evidence for the Formation of a ZnFe3S4 Cluster in *Desulfovibrio Gigas* Ferredoxin-II. *J. Am. Chem. Soc.* **1987,** *109* (12), 3805–3807.
167. Staples, C. R.; Dhawan, I. K.; Finnegan, M. G.; Dwinell, D. A.; Zhou, Z. H.; Huang, H.; Verhagen, M. F.; Adams, M. W.; Johnson, M. K. Electronic, Magnetic, and Redox Properties of [MFe(3)S(4)] Clusters (M = cd, cu, Cr) in *Pyrococcus furiosus* Ferredoxin. *Inorg. Chem.* **1997,** *36* (25), 5740–5749.
168. Conover, R. C.; Park, J. B.; Adams, M. W. W.; Johnson, M. K. Formation and Properties of an Iron-Nickel Sulfide ($NiFe_3S_4$) Cluster in *Pyrococcus furiosus* Ferredoxin. *J. Am. Chem. Soc.* **1990,** *112* (11), 4562–4564.
169. Rao, G.; Alwan, K. B.; Blackburn, N. J.; Britt, R. D. Incorporation of Ni(2+), Co(2+), and Selenocysteine into the Auxiliary Fe-S Cluster of the Radical SAM Enzyme HydG. *Inorg. Chem.* **2019,** *58* (19), 12601–12608.
170. Honarmand Ebrahimi, K.; Silveira, C.; Todorovic, S. Evidence for the Synthesis of an Unusual High Spin (S = 7/2) [Cu-3Fe-4S] Cluster in the Radical-SAM Enzyme RSAD2 (Viperin). *Chem. Commun. (Camb.)* **2018,** *54* (62), 8614–8617.
171. Kennedy, M. C.; Kent, T. A.; Emptage, M.; Merkle, H.; Beinert, H.; Munck, E. Evidence for the Formation of a Linear [3Fe-4S] Cluster in Partially Unfolded Aconitase. *J. Biol. Chem.* **1984,** *259* (23), 14463–14471.
172. Beinert, H.; Kennedy, M. C.; Stout, C. D. Aconitase as Iron-Sulfur Protein, Enzyme, and Iron-Regulatory Protein. *Chem. Rev.* **1996,** *96* (7), 2335–2374.
173. Holm, R. H. Trinuclear Cuboidal and Heterometallic Cubane-Type Iron-Sulfur Clusters - New Structural and Reactivity Themes in Chemistry and Biology. *Adv. Inorg. Chem.* **1992,** *38,* 1–71.
174. Richards, A. J. M.; Thomson, A. J.; Holm, R. H.; Hagen, K. S. The Magnetic Circular Dichroism Spectra of the Linear Trinuclear Clusters [Fe3S4(SR)4]3 − in Purple Aconitase and in a Synthetic Model. *Spectrochim. Acta A* **1990,** *46* (6), 987–993.
175. Jones, K.; Gomes, C. M.; Huber, H.; Teixeira, M.; Wittung-Stafshede, P. Formation of a Linear [3Fe-4S] Cluster in a Seven-Iron Ferredoxin Triggered by Polypeptide Unfolding. *J. Biol. Inorg. Chem.* **2002,** *7* (4-5), 357–362.
176. Higgins, C. L.; Wittung-Stafshede, P. Formation of Linear Three-Iron Clusters in *Aquifex Aeolicus* Two-Iron Ferredoxins: Effect of Protein-Unfolding Speed. *Arch. Biochem. Biophys.* **2004,** *427* (2), 154–163.
177. Leal, S. S.; Teixeira, M.; Gomes, C. M. Studies on the Degradation Pathway of Iron-Sulfur Centers during Unfolding of a Hyperstable Ferredoxin: Cluster Dissociation, Iron Release and Protein Stability. *J. Biol. Inorg. Chem.* **2004,** *9* (8), 987–996.
178. Vaccaro, B. J.; Clarkson, S. M.; Holden, J. F.; Lee, D. W.; Wu, C. H.; Poole Ii, F. L.; Cotelesage, J. J. H.; Hackett, M. J.; Mohebbi, S.; Sun, J.; Li, H.; Johnson, M. K.; George, G. N.; Adams, M. W. W. Biological Iron-Sulfur Storage in a Thioferrate-Protein Nanoparticle. *Nat. Commun.* **2017,** *8,* 16110.
179. George, G. N.; Pickering, I. J.; Yu, E. Y.; Prince, R. C.; Bursakov, S. A.; Gavel, O. Y.; Moura, I.; Moura, J. J. G. A Novel Protein-Bound Copper - Molybdenum Cluster. *J. Am. Chem. Soc.* **2000,** *122* (34), 8321–8322.
180. Rivas, M. G.; Carepo, M. S.; Mota, C. S.; Korbas, M.; Durand, M. C.; Lopes, A. T.; Brondino, C. D.; Pereira, A. S.; George, G. N.; Dolla, A.; Moura, J. J.; Moura, I. Molybdenum Induces the Expression of a Protein Containing a New Heterometallic Mo-Fe Cluster in *Desulfovibrio alaskensis*. *Biochemistry* **2009,** *48* (5), 873–882.
181. Rivas, M. G.; Mota, C. S.; Pauleta, S. R.; Carepo, M. S.; Folgosa, F.; Andrade, S. L.; Fauque, G.; Pereira, A. S.; Tavares, P.; Calvete, J. J.; Moura, I.; Moura, J. J. Isolation and Characterization of a New Cu-Fe Protein from *Desulfovibrio aminophilus* DSM12254. *J. Inorg. Biochem.* **2009,** *103* (10), 1314–1322.
182. Jeoung, J. H.; Dobbek, H. ATP-Dependent Substrate Reduction at an [Fe8S9] Double-Cubane Cluster. *Proc. Natl. Acad. Sci. U. S. A.* **2018,** *115* (12), 2994–2999.
183. Wagner, T.; Koch, J.; Ermler, U.; Shima, S. Methanogenic Heterodisulfide Reductase (HdrABC-MvhAGD) Uses Two Noncubane [4Fe-4S] Clusters for Reduction. *Science* **2017,** *357* (6352), 699–703.
184. Hagen, W. R.; Pierik, A. J.; Veeger, C. Novel Electron Paramagnetic Resonance Signals from an Fe/S Protein Containing Six Iron Atoms. *J. Chem. Soc., Faraday Trans. 1* **1989,** *85* (12), 4083–4090.
185. Moura, I.; Tavares, P.; Moura, J. J.; Ravi, N.; Huynh, B. H.; Liu, M. Y.; LeGall, J. Direct Spectroscopic Evidence for the Presence of a 6Fe Cluster in an Iron-Sulfur Protein Isolated from *Desulfovibrio desulfuricans* (ATCC 27774). *J. Biol. Chem.* **1992,** *267* (7), 4489–4496.
186. Arendsen, A. F.; Hadden, J.; Card, G.; McAlpine, A. S.; Bailey, S.; Zaitsev, V.; Duke, E. H. M.; Lindley, P. F.; Kröckel, M.; Trautwein, A. X.; Feiters, M. C.; Charnock, J. M.; Garner, C. D.; Marritt, S. J.; Thomson, A. J.; Kooter, I. M.; Johnson, M. K.; van den Berg, W. A. M.; van Dongen, W. M. A. M.; Hagen, W. R. The "Prismane" Protein Resolved: X-Ray Structure at 1.7 Å and Multiple Spectroscopy of Two Novel 4Fe Clusters. *J. Biol. Inorg. Chem.* **1998,** *3* (1), 81–95.
187. Tavares, P.; Pereira, A. S.; Krebs, C.; Ravi, N.; Moura, J. J.; Moura, I.; Huynh, B. H. Spectroscopic Characterization of a Novel Tetranuclear Fe Cluster in an Iron-Sulfur Protein Isolated from *Desulfovibrio desulfuricans*. *Biochemistry* **1998,** *37* (9), 2830–2842.
188. Cooper, S. J.; Garner, C. D.; Hagen, W. R.; Lindley, P. F.; Bailey, S. Hybrid-Cluster Protein (HCP) from *Desulfovibrio Vulgaris* (Hildenborough) at 1.6 Å Resolution. *Biochemistry* **2000,** *39* (49), 15044–15054.
189. van den Berg, W. A.; Hagen, W. R.; van Dongen, W. M. The Hybrid-Cluster Protein ('prismane protein') from *Escherichia coli*. Characterization of the Hybrid-Cluster Protein, Redox Properties of the [2Fe-2S] and [4Fe-2S-2O] Clusters and Identification of an Associated NADH Oxidoreductase Containing FAD and [2Fe-2S]. *Eur. J. Biochem.* **2000,** *267* (3), 666–676.
190. Fujishiro, T.; Ooi, M.; Takaoka, K. Crystal Structure of *Escherichia coli* Class II Hybrid Cluster Protein, HCP, Reveals a [4Fe-4S] Cluster at the N-Terminal Protrusion. *FEBS J.* **2021**.
191. Macedo, S.; Mitchell, E. P.; Romão, C. V.; Cooper, S. J.; Coelho, R.; Liu, M. Y.; Xavier, A. V.; LeGall, J.; Bailey, S.; Garner, D. C.; Hagen, W. R.; Teixeira, M.; Carrondo, M. A.; Lindley, P. Hybrid Cluster Proteins (HCPs) from *Desulfovibrio Desulfuricans* ATCC 27774 and *Desulfovibrio Vulgaris* (Hildenborough): X-Ray Structures at 1.25 A Resolution Using Synchrotron Radiation. *J. Biol. Inorg. Chem.* **2002,** *7* (4-5), 514–525.
192. Zheng, L.; White, R. H.; Cash, V. L.; Dean, D. R. Mechanism for the Desulfurization of L-Cysteine Catalyzed by the *nifS* Gene Product. *Biochemistry* **1994,** *33* (15), 4714–4720.
193. Pierik, A. J.; Hagen, W. R.; Dunham, W. R.; Sands, R. H. Multi-Frequency EPR and High-Resolution Mossbauer Spectroscopy of a Putative [6Fe-6S] Prismane-Cluster-Containing Protein from *Desulfovibrio Vulgaris* (Hildenborough). Characterization of a Supercluster and Superspin Model Protein. *Eur. J. Biochem.* **1992,** *206* (3), 705–719.
194. Overeijnder, M. L.; Hagen, W. R.; Hagedoorn, P. L. A Thermostable Hybrid Cluster Protein from *Pyrococcus Furiosus*: Effects of the Loss of a Three Helix Bundle Subdomain. *J. Biol. Inorg. Chem.* **2009,** *14* (5), 703–710.
195. Wolfe, M. T.; Heo, J.; Garavelli, J. S.; Ludden, P. W. Hydroxylamine Reductase Activity of the Hybrid Cluster Protein from *Escherichia Coli*. *J. Bacteriol.* **2002,** *184* (21), 5898–5902.
196. Filenko, N.; Spiro, S.; Browning, D. F.; Squire, D.; Overton, T. W.; Cole, J.; Constantinidou, C. The NsrR Regulon of *Escherichia Coli* K-12 Includes Genes Encoding the Hybrid Cluster Protein and the Periplasmic, Respiratory Nitrite Reductase. *J. Bacteriol.* **2007,** *189* (12), 4410–4417.
197. da Silva, S. M.; Amaral, C.; Neves, S. S.; Santos, C.; Pimentel, C.; Rodrigues-Pousada, C. An HcpR Paralog of *Desulfovibrio Gigas* Provides Protection against Nitrosative Stress. *FEBS Open Bio.* **2015,** *5,* 594–604.

198. Wang, J.; Vine, C. E.; Balasiny, B. K.; Rizk, J.; Bradley, C. L.; Tinajero-Trejo, M.; Poole, R. K.; Bergaust, L. L.; Bakken, L. R.; Cole, J. A. The Roles of the Hybrid Cluster Protein, hcp and its Reductase, Hcr, in High Affinity Nitric Oxide Reduction that Protects Anaerobic Cultures of *Escherichia coli* against Nitrosative Stress. *Mol. Microbiol.* **2016,** *100* (5), 877–892.
199. Hagen, W. R. EPR Spectroscopy of Putative Enzyme Intermediates in the NO Reductase and the Auto-Nitrosylation Reaction of *Desulfovibrio Vulgaris* Hybrid Cluster Protein. *FEBS Lett.* **2019,** *593* (21), 3075–3083.
200. Crane, B. R.; Getzoff, E. D. The Relationship between Structure and Function for the Sulfite Reductases. *Curr. Opin. Struct. Biol.* **1996,** *6* (6), 744–756.
201. Crane, B. R.; Siegel, L. M.; Getzoff, E. D. Sulfite Reductase Structure at 1.6 Å: Evolution and Catalysis for Reduction of Inorganic Anions. *Science* **1995,** *270* (5233), 59–67.
202. Janick, P. A.; Siegel, L. M. Electron Paramagnetic Resonance and Optical Spectroscopic Evidence for Interaction between Siroheme and Fe4S4 Prosthetic Groups in *Escherichia coli* Sulfite Reductase Hemoprotein Subunit. *Biochemistry* **1982,** *21* (15), 3538–3547.
203. Lee, J. P.; LeGall, J.; Peck, H. D., Jr. Isolation of Assimilatroy- and Dissimilatory-Type Sulfite Reductases from *Desulfovibrio vulgaris*. *J. Bacteriol.* **1973,** *115* (2), 529–542.
204. Moura, I.; LeGall, J.; Lino, A. R.; Peck, H. D.; Fauque, G.; Xavier, A. V.; DerVartanian, D. V.; Moura, J. J. G.; Huynh, B. H. Characterization of Two Dissimilatory Sulfite Reductases (Desulforubidin and Desulfoviridin) from the Sulfate-Reducing Bacteria. Moessbauer and EPR Studies. *J. Am. Chem. Soc.* **1988,** *110* (4), 1075–1082.
205. Pierik, A. J.; Hagen, W. R. S = 9/2 EPR Signals Are Evidence against Coupling between the Siroheme and the Fe/S Cluster Prosthetic Groups in *Desulfovibrio vulgaris* (Hildenborough) Dissimilatory Sulfite Reductase. *Eur. J. Biochem.* **1991,** *195* (2), 505–516.
206. Oliveira, T. F.; Vonrhein, C.; Matias, P. M.; Venceslau, S. S.; Pereira, I. A.; Archer, M. The Crystal Structure of *Desulfovibrio vulgaris* Dissimilatory Sulfite Reductase Bound to DsrC Provides Novel Insights into the Mechanism of Sulfate Respiration. *J. Biol. Chem.* **2008,** *283* (49), 34141–34149.
207. Venceslau, S. S.; Stockdreher, Y.; Dahl, C.; Pereira, I. A. The "Bacterial Heterodisulfide" DsrC Is a Key Protein in Dissimilatory Sulfur Metabolism. *Biochim. Biophys. Acta* **2014,** *1837* (7), 1148–1164.
208. Moura, I.; Lino, A. R.; Moura, J. J.; Xavier, A. V.; Fauque, G.; Peck, H. D., Jr.; LeGall, J. Low-Spin Sulfite Reductases: A New Homologous Group of Non-heme Iron-Siroheme Proteins in Anaerobic Bacteria. *Biochem. Bioph. Res. Co* **1986,** *141* (3), 1032–1041.
209. Christner, J. A.; Munck, E.; Janick, P. A.; Siegel, L. M. Mossbauer Evidence for Exchange-Coupled Siroheme and [4Fe-4S] Prosthetic Groups in *Escherichia coli* Sulfite Reductase. Studies of the Reduced States and of a Nitrite Turnover Complex. *J. Biol. Chem.* **1983,** *258* (18), 11147–11156.
210. Christner, J. A.; Muenck, E.; Kent, T. A.; Janick, P. A.; Salerno, J. C.; Siegel, L. M. Exchange Coupling between Siroheme and Iron-Sulfur ([4Fe-4S]) Cluster in *E. coli* Sulfite Reductase. Moessbauer Studies and Coupling Models for a 2-Electron Reduced Enzyme State and Complexes with Sulfide. *J. Am. Chem. Soc.* **1984,** *106* (22), 6786–6794.
211. Huynh, B. H.; Kang, L.; DerVartanian, D. V.; Peck, H. D., Jr.; LeGall, J. Characterization of a Sulfite Reductase from *Desulfovibrio vulgaris*. Evidence for the Presence of a Low-Spin Siroheme and an Exchange-Coupled Siroheme-[4Fe-4S] Unit. *J. Biol. Chem.* **1984,** *259* (24), 15373–15376.
212. Bominaar, E. L.; Hu, Z.; Muenck, E.; Girerd, J.-J.; Borshch, S. A. Double Exchange and Vibronic Coupling in Mixed-Valence Systems. Electronic Structure of Exchange-Coupled Siroheme-$[Fe_4S_4]^{2+}$ Chromophore in Oxidized *E. coli* Sulfite Reductase. *J. Am. Chem. Soc.* **1995,** *117* (26), 6976–6989.
213. Belinsky, M. I. Exchange Model of the {$[Fe_4S_4]$-Fe} Active Site of Sulfite Reductase. *Chem. Phys.* **1995,** *201* (2-3), 343–356.
214. Cline, J. F.; Janick, P. A.; Siegel, L. M.; Hoffman, B. M. Electron-Nuclear Double Resonance Studies of Oxidized *Escherichia coli* Sulfite Reductase: 1H, 14N, and 57Fe Measurements. *Biochemistry* **1985,** *24* (27), 7942–7947.
215. Tan, J.; Soriano, A.; Lui, S. M.; Cowan, J. A. Functional Expression and Characterization of the Assimilatory-Type Sulfite Reductase from *Desulfovibrio vulgaris* (Hildenborough). *Arch. Biochem. Biophys.* **1994,** *312* (2), 516–523.
216. Lui, S. M.; Soriano, A.; Cowan, J. A. Electronic Properties of the Dissimilatory Sulphite Reductase from *Desulfovibrio vulgaris* (Hildenborough): Comparative Studies of Optical Spectra and Relative Reduction Potentials for the [Fe4S4]-Sirohaem Prosthetic Centres. *Biochem. J.* **1994,** *304* (Pt 2), 441–447.
217. Oliveira, T. F.; Vonrhein, C.; Matias, P. M.; Venceslau, S. S.; Pereira, I. A.; Archer, M. Purification, Crystallization and Preliminary Crystallographic Analysis of a Dissimilatory DsrAB Sulfite Reductase in Complex with DsrC. *J. Struct. Biol.* **2008,** *164* (2), 236–239.
218. Oliveira, T. F.; Franklin, E.; Afonso, J. P.; Khan, A. R.; Oldham, N. J.; Pereira, I. A.; Archer, M. Structural Insights into Dissimilatory Sulfite Reductases: Structure of Desulforubidin from *Desulfomicrobium norvegicum*. *Front. Microbiol.* **2011,** *2,* 71.
219. Hsieh, Y. C.; Liu, M. Y.; Wang, V. C.; Chiang, Y. L.; Liu, E. H.; Wu, W. G.; Chan, S. I.; Chen, C. J. Structural Insights into the Enzyme Catalysis from Comparison of Three Forms of Dissimilatory Sulphite Reductase from *Desulfovibrio gigas*. *Mol. Microbiol.* **2010,** *78* (5), 1101–1116.
220. Ghosh, S.; Bagchi, A. Insight into the Molecular Mechanism of the Sulfur Oxidation Process by Reverse Sulfite Reductase (rSiR) from Sulfur Oxidizer *Allochromatium vinosum*. *J. Mol. Model.* **2018,** *24* (5), 117.
221. Burgess, B. K.; Lowe, D. J. Mechanism of Molybdenum Nitrogenase. *Chem. Rev.* **1996,** *96* (7), 2983–3012.
222. Howard, J. B.; Rees, D. C. Nitrogenase: A Nucleotide-Dependent Molecular Switch. *Annu. Rev. Biochem.* **1994,** *63* (1), 235–264.
223. Seefeldt, L. C.; Dean, D. R. Role of Nucleotides in Nitrogenase Catalysis. *Acc. Chem. Res.* **1997,** *30* (6), 260–266.
224. Smith, B. E. Structure, Function, and Biosynthesis of the Metallosulfur Clusters in Nitrogenases. In *Advances in Inorganic Chemistry;* Sykes, A. G., Ed.; vol. 47; Academic Press, 1999; pp 159–218.
225. Einsle, O.; Rees, D. C. Structural Enzymology of Nitrogenase Enzymes. *Chem. Rev.* **2020,** *120* (12), 4969–5004.
226. Hu, Y.; Ribbe, M. W. Historic Overview of Nitrogenase Research. *Methods Mol. Biol.* **2011,** *766,* 3–7.
227. Seefeldt, L. C.; Yang, Z. Y.; Lukoyanov, D. A.; Harris, D. F.; Dean, D. R.; Raugei, S.; Hoffman, B. M. Reduction of Substrates by Nitrogenases. *Chem. Rev.* **2020,** *120* (12), 5082–5106.
228. Hoffman, B. M.; Lukoyanov, D.; Dean, D. R.; Seefeldt, L. C. Nitrogenase: A Draft Mechanism. *Acc. Chem. Res.* **2013,** *46* (2), 587–595.
229. Einsle, O. Nitrogenase FeMo Cofactor: An Atomic Structure in Three Simple Steps. *J. Biol. Inorg. Chem.* **2014,** *19* (6), 737–745.
230. Sippel, D.; Einsle, O. The Structure of Vanadium Nitrogenase Reveals an Unusual Bridging Ligand. *Nat. Chem. Biol.* **2017,** *13* (9), 956–960.
231. Eady, R. R. Structure-Function Relationships of Alternative Nitrogenases. *Chem. Rev.* **1996,** *96* (7), 3013–3030.
232. Harris, D. F.; Lukoyanov, D. A.; Shaw, S.; Compton, P.; Tokmina-Lukaszewska, M.; Bothner, B.; Kelleher, N.; Dean, D. R.; Hoffman, B. M.; Seefeldt, L. C. Mechanism of N_2 Reduction Catalyzed by Fe-Nitrogenase Involves Reductive Elimination of H_2. *Biochemistry* **2018,** *57* (5), 701–710.
233. Hausinger, R. P.; Howard, J. B. Thiol Reactivity of the Nitrogenase Fe-Protein from *Azotobacter vinelandii*. *J. Biol. Chem.* **1983,** *258* (22), 13486–13492.
234. Howard, J. B.; Davis, R.; Moldenhauer, B.; Cash, V. L.; Dean, D. Fe:S cluster ligands are the only cysteines required for nitrogenase Fe-protein activities. *J. Biol. Chem.* **1989,** *264* (19), 11270–11274.
235. Tan, M. L.; Perrin, B. S., Jr.; Niu, S.; Huang, Q.; Ichiye, T. Protein Dynamics and the all-Ferrous [Fe4S4] Cluster in the Nitrogenase Iron Protein. *Protein Sci.* **2016,** *25* (1), 12–18.
236. Angove, H. C.; Yoo, S. J.; Munck, E.; Burgess, B. K. An all-Ferrous State of the Fe Protein of Nitrogenase. Interaction with Nucleotides and Electron Transfer to the MoFe Protein. *J. Biol. Chem.* **1998,** *273* (41), 26330–26337.
237. Hu, Y.; Lee, C. C.; Ribbe, M. W. Extending the Carbon Chain: Hydrocarbon Formation Catalyzed by Vanadium/Molybdenum Nitrogenases. *Science* **2011,** *333* (6043), 753–755.
238. Lee, C. C.; Hu, Y.; Ribbe, M. W. Vanadium Nitrogenase Reduces CO. *Science* **2010,** *329* (5992), 642.
239. Wiig, J. A.; Hu, Y.; Chung Lee, C.; Ribbe, M. W. Radical SAM-Dependent Carbon Insertion into the Nitrogenase M-Cluster. *Science* **2012,** *337* (6102), 1672–1675.
240. Spatzal, T.; Aksoyoglu, M.; Zhang, L.; Andrade, S. L.; Schleicher, E.; Weber, S.; Rees, D. C.; Einsle, O. Evidence for Interstitial Carbon in Nitrogenase FeMo Cofactor. *Science* **2011,** *334* (6058), 940.
241. Jimenez-Vicente, E.; Yang, Z. Y.; Ray, W. K.; Echavarri-Erasun, C.; Cash, V. L.; Rubio, L. M.; Seefeldt, L. C.; Dean, D. R. Sequential and Differential Interaction of Assembly Factors during Nitrogenase MoFe Protein Maturation. *J. Biol. Chem.* **2018,** *293* (25), 9812–9823.

242. Rupnik, K.; Lee, C. C.; Hu, Y.; Ribbe, M. W.; Hales, B. J. A VTVH MCD and EPR Spectroscopic Study of the Maturation of the "Second" Nitrogenase P-Cluster. *Inorg. Chem.* **2018,** *57* (8), 4719–4725.
243. Kim, J.; Rees, D. C. Structural Models for the Metal Centers in the Nitrogenase Molybdenum-Iron Protein. *Science* **1992,** *257* (5077), 1677–1682.
244. Peters, J. W.; Stowell, M. H.; Soltis, S. M.; Finnegan, M. G.; Johnson, M. K.; Rees, D. C. Redox-Dependent Structural Changes in the Nitrogenase P-Cluster. *Biochemistry* **1997,** *36* (6), 1181–1187.
245. Yoo, S. J.; Angove, H. C.; Papaefthymiou, V.; Burgess, B. K.; Münck, E. Mössbauer Study of the MoFe Protein of Nitrogenase from *Azotobacter vinelandii* Using Selective ^{57}Fe Enrichment of the M-Centers. *J. Am. Chem. Soc.* **2000,** *122* (20), 4926–4936.
246. Lindahl, P. A.; Papaefthymiou, V.; Orme-Johnson, W. H.; Munck, E. Mossbauer Studies of Solid Thionin-Oxidized MoFe Protein of Nitrogenase. *J. Biol. Chem.* **1988,** *263* (36), 19412–19418.
247. Einsle, O.; Tezcan, F. A.; Andrade, S. L.; Schmid, B.; Yoshida, M.; Howard, J. B.; Rees, D. C. Nitrogenase MoFe-Protein at 1.16 Å Resolution: A Central Ligand in the FeMo-Cofactor. *Science* **2002,** *297* (5587), 1696–1700.
248. Owens, C. P.; Katz, F. E.; Carter, C. H.; Oswald, V. F.; Tezcan, F. A. Tyrosine-Coordinated P-Cluster in *G. Diazotrophicus* Nitrogenase: Evidence for the Importance of O-Based Ligands in Conformationally Gated Electron Transfer. *J. Am. Chem. Soc.* **2016,** *138* (32), 10124–10127.
249. Cao, L.; Borner, M. C.; Bergmann, J.; Caldararu, O.; Ryde, U. Geometry and Electronic Structure of the P-Cluster in Nitrogenase Studied by Combined Quantum Mechanical and Molecular Mechanical Calculations and Quantum Refinement. *Inorg. Chem.* **2019,** *58* (15), 9672–9690.
250. Sippel, D.; Rohde, M.; Netzer, J.; Trncik, C.; Gies, J.; Grunau, K.; Djurdjevic, I.; Decamps, L.; Andrade, S. L. A.; Einsle, O. A Bound Reaction Intermediate Sheds Light on the Mechanism of Nitrogenase. *Science* **2018,** *359* (6383), 1484–1489.
251. Hagen, W. R.; Wassink, H.; Eady, R. R.; Smith, B. E.; Haaker, H. Quantitative EPR of an S = 7/2 System in Thionine-Oxidized MoFe Proteins of Nitrogenase. A Redefinition of the P-Cluster Concept. *Eur. J. Biochem.* **1987,** *169* (3), 457–465.
252. Pierik, A. J.; Wassink, H.; Haaker, H.; Hagen, W. R. Redox Properties and EPR Spectroscopy of the P-Clusters of *Azotobacter vinelandii* MoFe Protein. *Eur. J. Biochem.* **1993,** *212* (1), 51–61.
253. Lanzilotta, W. N.; Christiansen, J.; Dean, D. R.; Seefeldt, L. C. Evidence for Coupled Electron and Proton Transfer in the [8Fe-7S] Cluster of Nitrogenase. *Biochemistry* **1998,** *37* (32), 11376–11384.
254. Lanzilotta, W. N.; Seefeldt, L. C. Changes in the Midpoint Potentials of the Nitrogenase Metal Centers as a Result of Iron Protein-Molybdenum-Iron Protein Complex Formation. *Biochemistry* **1997,** *36* (42), 12976–12983.
255. Tittsworth, R. C.; Hales, B. J. Detection of EPR Signals Assigned to the 1-Equiv-Oxidized P-Clusters of the Nitrogenase MoFe-Protein from *Azotobacter vinelandii*. *J. Am. Chem. Soc.* **1993,** *115* (21), 9763–9767.
256. Lowe, D. J.; Fisher, K.; Thorneley, R. N. *Klebsiella Pneumoniae* Nitrogenase: Pre-Steady-State Absorbance Changes Show that Redox Changes Occur in the MoFe Protein that Depend on Substrate and Component Protein Ratio; a Role for P-Centres in Reducing Dinitrogen? *Biochem. J.* **1993,** *292* (Pt 1), 93–98.
257. Harris, D. F.; Lukoyanov, D. A.; Kallas, H.; Trncik, C.; Yang, Z. Y.; Compton, P.; Kelleher, N.; Einsle, O.; Dean, D. R.; Hoffman, B. M.; Seefeldt, L. C. Mo-, V-, and Fe-Nitrogenases Use a Universal Eight-Electron Reductive-Elimination Mechanism to Achieve N_2 Reduction. *Biochemistry* **2019,** *58* (30), 3293–3301.
258. Spatzal, T.; Perez, K. A.; Einsle, O.; Howard, J. B.; Rees, D. C. Ligand Binding to the FeMo-Cofactor: Structures of CO-Bound and Reactivated Nitrogenase. *Science* **2014,** *345* (6204), 1620–1623.
259. Rohde, M.; Grunau, K.; Einsle, O. CO Binding to the FeV Cofactor of CO-Reducing Vanadium Nitrogenase at Atomic Resolution. *Angew. Chem. Int. Ed. Engl.* **2020,** *59* (52), 23626–23630.
260. Kang, W.; Lee, C. C.; Jasniewski, A. J.; Ribbe, M. W.; Hu, Y. Structural Evidence for a Dynamic Metallocofactor during N_2 Reduction by Mo-Nitrogenase. *Science* **2020,** *368* (6497), 1381–1385.
261. Bergmann, J.; Oksanen, E.; Ryde, U. Critical Evaluation of a Crystal Structure of Nitrogenase with Bound N_2 Ligands. *J. Biol. Inorg. Chem.* **2021,** *26* (2-3), 341–353.
262. Peters, J. W.; Einsle, O.; Dean, D. R.; DeBeer, S.; Hoffman, B. M.; Holland, P. L.; Seefeldt, L. C. Comment on "Structural Evidence for a Dynamic Metallocofactor during N_2 Reduction by Mo-Nitrogenase". *Science* **2021,** *371* (6530).
263. Lemon, B. J.; Peters, J. W. Iron-Only Hydrogenases. In *Handbook of Metalloproteins;* Messerschmidt, A., Huber, R., Poulos, T., Wieghardt, K., Eds., Wiley Sons, Ltd: Weinheim, Germany, 2001; p 738.
264. Frey, M.; Fontecilla-Camps, J. C.; Volbeda, A. Nickel–Iron Hydrogenases. In *Handbook of Metalloproteins;* Messerschmidt, A., Huber, R., Poulos, T., Wieghardt, K., Eds., John Wiley & Sons, Ltd: Chichester, UK, 2001; p 880.
265. Fontecilla-Camps, J. C.; Volbeda, A.; Cavazza, C.; Nicolet, Y. Structure/Function Relationships of [NiFe]- and [FeFe]-Hydrogenases. *Chem. Rev.* **2007,** *107* (10), 4273–4303.
266. Tai, H.; Hirota, S. Mechanism and Application of the Catalytic Reaction of [NiFe] Hydrogenase: Recent Developments. *ChemBioChem* **2020,** *21* (11), 1573–1581.
267. Mertens, R.; Liese, A. Biotechnological Applications of Hydrogenases. *Curr. Opin. Biotechnol.* **2004,** *15* (4), 343–348.
268. Vincent, K. A.; Cracknell, J. A.; Lenz, O.; Zebger, I.; Friedrich, B.; Armstrong, F. A. Electrocatalytic Hydrogen Oxidation by an Enzyme at High Carbon Monoxide or Oxygen Levels. *Proc. Natl. Acad. Sci. U. S. A.* **2005,** *102* (47), 16951–16954.
269. Luo, X.; Brugna, M.; Tron-Infossi, P.; Giudici-Orticoni, M.; Lojou, É. Immobilization of the hyperthermophilic hydrogenase from *Aquifex aeolicus* bacterium onto gold and carbon nanotube electrodes for efficient H_2 oxidation. *J. Biol. Inorg. Chem.* **2009,** *14* (8), 1275–1288.
270. Frielingsdorf, S.; Fritsch, J.; Schmidt, A.; Hammer, M.; Lowenstein, J.; Siebert, E.; Pelmenschikov, V.; Jaenicke, T.; Kalms, J.; Rippers, Y.; Lendzian, F.; Zebger, I.; Teutloff, C.; Kaupp, M.; Bittl, R.; Hildebrandt, P.; Friedrich, B.; Lenz, O.; Scheerer, P. Reversible [4Fe-3S] Cluster Morphing in an O(2)-Tolerant [NiFe] Hydrogenase. *Nat. Chem. Biol.* **2014,** *10* (5), 378–385.
271. Volbeda, A.; Darnault, C.; Parkin, A.; Sargent, F.; Armstrong, F. A.; Fontecilla-Camps, J. C. Crystal Structure of the O(2)-Tolerant Membrane-Bound Hydrogenase 1 from *Escherichia coli* in Complex with its Cognate Cytochrome *b*. *Structure* **2013,** *21* (1), 184–190.
272. Radu, V.; Frielingsdorf, S.; Evans, S. D.; Lenz, O.; Jeuken, L. J. Enhanced Oxygen-Tolerance of the Full Heterotrimeric Membrane-Bound [NiFe]-Hydrogenase of *Ralstonia eutropha*. *J. Am. Chem. Soc.* **2014,** *136* (24), 8512–8515.
273. Lenz, O.; Ludwig, M.; Schubert, T.; Burstel, I.; Ganskow, S.; Goris, T.; Schwarze, A.; Friedrich, B. H_2 Conversion in the Presence of O_2 as Performed by the Membrane-Bound [NiFe]-Hydrogenase of *Ralstonia eutropha*. *Chemphyschem* **2010,** *11* (6), 1107–1119.
274. Hatchikian, E. C.; Forget, N.; Fernandez, V. M.; Williams, R.; Cammack, R. Further Characterization of the [Fe]-Hydrogenase from *Desulfovibrio desulfuricans* ATCC 7757. *Eur. J. Biochem.* **1992,** *209* (1), 357–365.
275. van der Westen, H. M.; Mayhew, S. G.; Veeger, C. Separation of Hydrogenase from Intact Cells of *Desulfovibrio vulgaris*. Purification and properties. *FEBS Lett.* **1978,** *86* (1), 122–126.
276. Chen, J. S.; Blanchard, D. K. Isolation and Properties of a Unidirectional H_2-Oxidizing Hydrogenase from the Strictly Anaerobic N_2-Fixing Bacterium *Clostridium Pasteurianum* W5. *Biochem. Bioph. Res. Co* **1978,** *84* (4), 1144–1150.
277. Chen, J. S.; Blanchard, D. K. Purification and Properties of the H_2-Oxidizing (Uptake) Hydrogenase of the N_2-Fixing Anaerobe *Clostridium Pasteurianum* W5. *Biochem. Bioph. Res. Co* **1984,** *122* (1), 9–16.
278. Filipiak, M.; Hagen, W. R.; Veeger, C. Hydrodynamic, Structural and Magnetic Properties of *Megasphaera elsdenii* Fe Hydrogenase Reinvestigated. *Eur. J. Biochem.* **1989,** *185* (3), 547–553.
279. Adams, M. W.; Eccleston, E.; Howard, J. B. Iron-Sulfur Clusters of Hydrogenase I and Hydrogenase II of *Clostridium pasteurianum*. *Proc. Natl. Acad. Sci. U. S. A.* **1989,** *86* (13), 4932–4936.

280. Patil, D. S.; Moura, J. J.; He, S. H.; Teixeira, M.; Prickril, B. C.; DerVartanian, D. V.; Peck, H. D., Jr.; LeGall, J.; Huynh, B. H. EPR-Detectable Redox Centers of the Periplasmic Hydrogenase from *Desulfovibrio vulgaris*. *J. Biol. Chem.* **1988,** *263* (35), 18732–18738.
281. Pereira, A. S.; Tavares, P.; Moura, I.; Moura, J. J.; Huynh, B. H. Mossbauer Characterization of the Iron-Sulfur Clusters in *Desulfovibrio vulgaris* Hydrogenase. *J. Am. Chem. Soc.* **2001,** *123* (12), 2771–2782.
282. Hagen, W. R.; van Berkel-Arts, A.; Kruse-Wolters, K. M.; Dunham, W. R.; Veeger, C. EPR of a Novel High-Spin Component in Activated Hydrogenase from *Desulfovibrio vulgaris* (Hildenborough). *FEBS Lett.* **1986,** *201* (1), 158–162.
283. Nicolet, Y.; Piras, C.; Legrand, P.; Hatchikian, C. E.; Fontecilla-Camps, J. C. *Desulfovibrio desulfuricans* Iron Hydrogenase: The Structure Shows Unusual Coordination to an Active Site Fe Binuclear Center. *Structure* **1999,** *7* (1), 13–23.
284. Pandey, A. S.; Harris, T. V.; Giles, L. J.; Peters, J. W.; Szilagyi, R. K. Dithiomethylether as a Ligand in the Hydrogenase H-Cluster. *J. Am. Chem. Soc.* **2008,** *130* (13), 4533–4540.
285. Lemon, B. J.; Peters, J. W. Binding of Exogenously Added Carbon Monoxide at the Active Site of the Iron-Only Hydrogenase (Cpl) from *Clostridium pasteurianum*. *Biochemistry* **1999,** *38* (40), 12969–12973.
286. Lemon, B. J.; Peters, J. W. Photochemistry at the Active Site of the Carbon Monoxide Inhibited Form of the Iron-Only Hydrogenase (Cpl). *J. Am. Chem. Soc.* **2000,** *122* (15), 3793–3794.
287. Bennett, B.; Lemon, B. J.; Peters, J. W. Reversible Carbon Monoxide Binding and Inhibition at the Active Site of the Fe-Only Hydrogenase. *Biochemistry* **2000,** *39* (25), 7455–7460.
288. Fan, H. J.; Hall, M. B. A Capable Bridging Ligand for Fe-Only Hydrogenase: Density Functional Calculations of a Low-Energy Route for Heterolytic Cleavage and Formation of Dihydrogen. *J. Am. Chem. Soc.* **2001,** *123* (16), 3828–3829.
289. Stephan, D. W.; Erker, G. Frustrated Lewis Pair Chemistry: Development and Perspectives. *Angew. Chem. Int. Ed. Engl.* **2015,** *54* (22), 6400–6441.
290. Albracht, S. P.; Roseboom, W.; Hatchikian, E. C. The Active Site of the [FeFe]-Hydrogenase from *Desulfovibrio desulfuricans*. I. Light Sensitivity and Magnetic Hyperfine Interactions as Observed by Electron Paramagnetic Resonance. *J. Biol. Inorg. Chem.* **2006,** *11* (1), 88–101.
291. Roseboom, W.; De Lacey, A. L.; Fernandez, V. M.; Hatchikian, E. C.; Albracht, S. P. The Active Site of the [FeFe]-Hydrogenase from *Desulfovibrio desulfuricans*. II. Redox Properties, Light Sensitivity and CO-Ligand Exchange as Observed by Infrared Spectroscopy. *J. Biol. Inorg. Chem.* **2006,** *11* (1), 102–118.
292. Chen, Z.; Lemon, B. J.; Huang, S.; Swartz, D. J.; Peters, J. W.; Bagley, K. A. Infrared Studies of the CO-Inhibited Form of the Fe-Only Hydrogenase from *Clostridium pasteurianum* I: Examination of its Light Sensitivity at Cryogenic Temperatures. *Biochemistry* **2002,** *41* (6), 2036–2043.
293. Silakov, A.; Wenk, B.; Reijerse, E.; Albracht, S. P.; Lubitz, W. Spin Distribution of the H-Cluster in the H(ox)-CO State of the [FeFe] Hydrogenase from *Desulfovibrio Desulfuricans*: HYSCORE and ENDOR Study of (14)N and (13)C Nuclear Interactions. *J. Biol. Inorg. Chem.* **2009,** *14* (2), 301–313.
294. Silakov, A.; Reijerse, E. J.; Albracht, S. P.; Hatchikian, E. C.; Lubitz, W. The Electronic Structure of the H-Cluster in the [FeFe]-Hydrogenase from *Desulfovibrio desulfuricans*: A Q-Band 57Fe-ENDOR and HYSCORE Study. *J. Am. Chem. Soc.* **2007,** *129* (37), 11447–11458.
295. Rumpel, S.; Ravera, E.; Sommer, C.; Reijerse, E.; Fares, C.; Luchinat, C.; Lubitz, W. (1)H NMR Spectroscopy of [FeFe] Hydrogenase: Insight into the Electronic Structure of the Active Site. *J. Am. Chem. Soc.* **2018,** *140* (1), 131–134.
296. Fiedler, A. T.; Brunold, T. C. Computational Studies of the H-Cluster of Fe-Only Hydrogenases: Geometric, Electronic, and Magnetic Properties and their Dependence on the [Fe4S4] Cubane. *Inorg. Chem.* **2005,** *44* (25), 9322–9334.
297. Sommer, C.; Adamska-Venkatesh, A.; Pawlak, K.; Birrell, J. A.; Rudiger, O.; Reijerse, E. J.; Lubitz, W. Proton Coupled Electronic Rearrangement within the H-Cluster as an Essential Step in the Catalytic Cycle of [FeFe] Hydrogenases. *J. Am. Chem. Soc.* **2017,** *139* (4), 1440–1443.
298. Volbeda, A.; Martin, L.; Cavazza, C.; Matho, M.; Faber, B. W.; Roseboom, W.; Albracht, S. P.; Garcin, E.; Rousset, M.; Fontecilla-Camps, J. C. Structural Differences between the Ready and Unready Oxidized States of [NiFe] Hydrogenases. *J. Biol. Inorg. Chem.* **2005,** *10* (3), 239–249.
299. Higuchi, Y.; Yagi, T.; Yasuoka, N. Unusual Ligand Structure in Ni-Fe Active Center and an Additional Mg Site in Hydrogenase Revealed by High Resolution X-Ray Structure Analysis. *Structure* **1997,** *5* (12), 1671–1680.
300. Ogata, H.; Mizoguchi, Y.; Mizuno, N.; Miki, K.; Adachi, S.; Yasuoka, N.; Yagi, T.; Yamauchi, O.; Hirota, S.; Higuchi, Y. Structural Studies of the Carbon Monoxide Complex of [NiFe]Hydrogenase from *Desulfovibrio vulgaris* Miyazaki F: Suggestion for the Initial Activation Site for Dihydrogen. *J. Am. Chem. Soc.* **2002,** *124* (39), 11628–11635.
301. Ogata, H.; Hirota, S.; Nakahara, A.; Komori, H.; Shibata, N.; Kato, T.; Kano, K.; Higuchi, Y. Activation Process of [NiFe] Hydrogenase Elucidated by High-Resolution X-Ray Analyses: Conversion of the Ready to the Unready State. *Structure* **2005,** *13* (11), 1635–1642.
302. Matias, P. M.; Soares, C. M.; Saraiva, L. M.; Coelho, R.; Morais, J.; Le Gall, J.; Carrondo, M. A. [NiFe] Hydrogenase from *Desulfovibrio desulfuricans* ATCC 27774: Gene Sequencing, Three-Dimensional Structure Determination and Refinement at 1.8 Å and Modelling Studies of its Interaction with the Tetrahaem Cytochrome c_3. *J. Biol. Inorg. Chem.* **2001,** *6* (1), 63–81.
303. Montet, Y.; Amara, P.; Volbeda, A.; Vernede, X.; Hatchikian, E. C.; Field, M. J.; Frey, M.; Fontecilla-Camps, J. C. Gas Access to the Active Site of Ni-Fe Hydrogenases Probed by X-Ray Crystallography and Molecular Dynamics. *Nat. Struct. Biol.* **1997,** *4* (7), 523–526.
304. Garcin, E.; Vernede, X.; Hatchikian, E. C.; Volbeda, A.; Frey, M.; Fontecilla-Camps, J. C. The Crystal Structure of a Reduced [NiFeSe] Hydrogenase Provides an Image of the Activated Catalytic Center. *Structure* **1999,** *7* (5), 557–566.
305. Page, C. C.; Moser, C. C.; Chen, X.; Dutton, P. L. Natural Engineering Principles of Electron Tunnelling in Biological Oxidation-Reduction. *Nature* **1999,** *402* (6757), 47–52.
306. Roberts, L. M.; Lindahl, P. A. Stoichiometric Reductive Titrations of *Desulfovibrio gigas* Hydrogenase. *J. Am. Chem. Soc.* **1995,** *117* (9), 2565–2572.
307. Tai, H.; Nishikawa, K.; Suzuki, M.; Higuchi, Y.; Hirota, S. Control of the Transition between Ni-C and Ni-SI(a) States by the Redox State of the Proximal Fe-S Cluster in the Catalytic Cycle of [NiFe] Hydrogenase. *Angew. Chem. Int. Ed. Engl.* **2014,** *53* (50), 13817–13820.
308. Vignais, P. M.; Billoud, B.; Meyer, J. Classification and Phylogeny of Hydrogenases. *FEMS Microbiol. Rev.* **2001,** *25* (4), 455–501.
309. Happe, R. P.; Roseboom, W.; Pierik, A. J.; Albracht, S. P.; Bagley, K. A. Biological Activation of Hydrogen. *Nature* **1997,** *385* (6612), 126.
310. Bleijlevens, B.; van Broekhuizen, F. A.; De Lacey, A. L.; Roseboom, W.; Fernandez, V. M.; Albracht, S. P. The Activation of the [NiFe]-Hydrogenase from *Allochromatium Vinosum*. An Infrared Spectro-Electrochemical Study. *J. Biol. Inorg. Chem.* **2004,** *9* (6), 743–752.
311. Fichtner, C.; Laurich, C.; Bothe, E.; Lubitz, W. Spectroelectrochemical Characterization of the [NiFe] Hydrogenase of *Desulfovibrio vulgaris* Miyazaki F. *Biochemistry* **2006,** *45* (32), 9706–9716.
312. Volbeda, A.; Garcin, E.; Piras, C.; deLacey, A. L.; Fernandez, V. M.; Hatchikian, E. C.; Frey, M.; FontecillaCamps, J. C. Structure of the [NiFe] Hydrogenase Active Site: Evidence for Biologically Uncommon Fe Ligands. *J. Am. Chem. Soc.* **1996,** *118* (51), 12989–12996.
313. Barilone, J. L.; Ogata, H.; Lubitz, W.; van Gastel, M. Structural Differences between the Active Sites of the Ni-A and Ni-B States of the [NiFe] Hydrogenase: An Approach by Quantum Chemistry and Single Crystal ENDOR Spectroscopy. *Phys. Chem. Chem. Phys.: PCCP* **2015,** *17* (24), 16204–16212.
314. Osuka, H.; Shomura, Y.; Komori, H.; Shibata, N.; Nagao, S.; Higuchi, Y.; Hirota, S. Photosensitivity of the Ni-a State of [NiFe] Hydrogenase from *Desulfovibrio vulgaris* Miyazaki F with Visible Light. *Biochem. Bioph. Res. Co* **2013,** *430* (1), 284–288.
315. van Gastel, M.; Stein, M.; Brecht, M.; Schroder, O.; Lendzian, F.; Bittl, R.; Ogata, H.; Higuchi, Y.; Lubitz, W. A Single-Crystal ENDOR and Density Functional Theory Study of the Oxidized States of the [NiFe] Hydrogenase from *Desulfovibrio vulgaris* Miyazaki F. *J. Biol. Inorg. Chem.* **2006,** *11* (1), 41–51.
316. Foerster, S.; van Gastel, M.; Brecht, M.; Lubitz, W. An Orientation-Selected ENDOR and HYSCORE Study of the Ni-C Active State of *Desulfovibrio vulgaris* Miyazaki F Hydrogenase. *J. Biol. Inorg. Chem.* **2005,** *10* (1), 51–62.
317. Pandelia, M. E.; Ogata, H.; Currell, L. J.; Flores, M.; Lubitz, W. Inhibition of the [NiFe] Hydrogenase from *Desulfovibrio vulgaris* Miyazaki F by Carbon Monoxide: An FTIR and EPR Spectroscopic Study. *Biochim. Biophys. Acta* **2010,** *1797* (2), 304–313.
318. Albracht, S. P. Nickel Hydrogenases: In Search of the Active Site. *Biochim. Biophys. Acta* **1994,** *1188* (3), 167–204.

319. Pandelia, M. E.; Ogata, H.; Lubitz, W. Intermediates in the Catalytic Cycle of [NiFe] Hydrogenase: Functional Spectroscopy of the Active Site. *Chemphyschem : a European journal of chemical physics and physical chemistry* **2010,** *11* (6), 1127–1140.
320. de Lacey, A. L.; Hatchikian, E. C.; Volbeda, A.; Frey, M.; Fontecilla-Camps, J. C.; Fernandez, V. M. Infrared-Spectroelectrochemical Characterization of the [NiFe] Hydrogenase of *Desulfovibrio gigas*. *J. Am. Chem. Soc.* **1997,** *119* (31), 7181–7189.
321. DeLacey, A. L.; Fernandez, V. M.; Rousset, M.; Cavazza, C.; Hatchikian, E. C. Spectroscopic and Kinetic Characterization of Active Site Mutants of *Desulfovibrio fructosovorans* Ni-Fe Hydrogenase. *J. Biol. Inorg. Chem.* **2003,** *8* (1-2), 129–134.
322. Dresselhaus, M. S.; Thomas, I. L. Alternative Energy Technologies. *Nature* **2001,** *414* (6861), 332–337.
323. Szczesny, J.; Markovic, N.; Conzuelo, F.; Zacarias, S.; Pereira, I. A. C.; Lubitz, W.; Plumere, N.; Schuhmann, W.; Ruff, A. A Gas Breathing Hydrogen/Air Biofuel Cell Comprising a Redox Polymer/Hydrogenase-Based Bioanode. *Nat. Commun.* **2018,** *9* (1), 4715.
324. Plumere, N.; Rudiger, O.; Oughli, A. A.; Williams, R.; Vivekananthan, J.; Poller, S.; Schuhmann, W.; Lubitz, W. A Redox Hydrogel Protects Hydrogenase from High-Potential Deactivation and Oxygen Damage. *Nat. Chem.* **2014,** *6* (9), 822–827.
325. Greene, B. L.; Vansuch, G. E.; Chica, B. C.; Adams, M. W. W.; Dyer, R. B. Applications of Photogating and Time Resolved Spectroscopy to Mechanistic Studies of Hydrogenases. *Acc. Chem. Res.* **2017,** *50* (11), 2718–2726.
326. Zhang, L. Y.; Beaton, S. E.; Carr, S. B.; Armstrong, F. A. Direct Visible Light Activation of a Surface Cysteine-Engineered [NiFe]-Hydrogenase by Silver Nanoclusters. *Energ. Environ. Sci.* **2018,** *11* (12), 3342–3348.
327. Shomura, Y.; Yoon, K. S.; Nishihara, H.; Higuchi, Y. Structural Basis for a [4Fe-3S] Cluster in the Oxygen-Tolerant Membrane-Bound [NiFe]-Hydrogenase. *Nature* **2011,** *479* (7372), 253–256.
328. Roessler, M. M.; Evans, R. M.; Davies, R. A.; Harmer, J.; Armstrong, F. A. EPR Spectroscopic Studies of the Fe-S Clusters in the O2-Tolerant [NiFe]-Hydrogenase Hyd-1 from *Escherichia coli* and Characterization of the Unique [4Fe-3S] Cluster by HYSCORE. *J. Am. Chem. Soc.* **2012,** *134* (37), 15581–15594.
329. Marques, M. C.; Coelho, R.; De Lacey, A. L.; Pereira, I. A.; Matias, P. M. The Three-Dimensional Structure of [NiFeSe] Hydrogenase from *Desulfovibrio Vulgaris* Hildenborough: A Hydrogenase without a Bridging Ligand in the Active Site in its Oxidised, "As-Isolated" State. *J. Mol. Biol.* **2010,** *396* (4), 893–907.
330. Marques, M. C.; Tapia, C.; Gutierrez-Sanz, O.; Ramos, A. R.; Keller, K. L.; Wall, J. D.; De Lacey, A. L.; Matias, P. M.; Pereira, I. A. C. The Direct Role of Selenocysteine in [NiFeSe] Hydrogenase Maturation and Catalysis. *Nat. Chem. Biol.* **2017,** *13* (5), 544–550.
331. Baltazar, C. S. A.; Marques, M. C.; Soares, C. M.; DeLacey, A. M.; Pereira, I. A. C.; Matias, P. M. Nickel–iron–selenium hydrogenases – An overview. *Eur. J. Inorg. Chem.* **2011,** *2011* (7), 948–962.
332. Teixeira, M.; Moura, I.; Fauque, G.; Dervartanian, D. V.; Legall, J.; Peck, H. D., Jr.; Moura, J. J.; Huynh, B. H. The iron-sulfur centers of the soluble [NiFeSe] hydrogenase, from *Desulfovibrio baculatus* (DSM 1743). EPR and Mossbauer Characterization. *Eur. J. Biochem.* **1990,** *189* (2), 381–386.
333. Parkin, A.; Goldet, G.; Cavazza, C.; Fontecilla-Camps, J. C.; Armstrong, F. A. The Difference a se Makes? Oxygen-Tolerant Hydrogen Production by the [NiFeSe]-Hydrogenase from *Desulfomicrobium baculatum*. *J. Am. Chem. Soc.* **2008,** *130* (40), 13410–13416.
334. Rüdiger, O.; Gutiérrez-Sánchez, C.; Olea, D.; Pereira, I. A. C.; Vélez, M.; Fernández, V. M.; De Lacey, A. L. Enzymatic Anodes for Hydrogen Fuel Cells Based on Covalent Attachment of Ni-Fe Hydrogenases and Direct Electron Transfer to SAM-Modified Gold Electrodes. *Electroanalysis* **2010,** *22* (7-8), 776–783.
335. Valente, F. M. A.; Oliveira, A. S. F.; Gnadt, N.; Pacheco, I.; Coelho, A. V.; Xavier, A. V.; Teixeira, M.; Soares, C. M.; Pereira, I. A. C. Hydrogenases in *Desulfovibrio Vulgaris* Hildenborough: Structural and Physiologic Characterisation of the Membrane-Bound [NiFeSe] Hydrogenase. *J. Biol. Inorg. Chem.* **2005,** *10* (6), 667–682.
336. Wombwell, C.; Caputo, C. A.; Reisner, E. [NiFeSe]-Hydrogenase Chemistry. *Acc. Chem. Res.* **2015,** *48* (11), 2858–2865.
337. Medina, M.; Claude Hatchikian, E.; Cammack, R. Studies of Light-Induced Nickel EPR Signals in Hydrogenase: Comparison of Enzymes with and without Selenium. *Biochim. Biophys. Acta* **1996,** *1275* (3), 227–236.
338. Riethausen, J.; Rudiger, O.; Gartner, W.; Lubitz, W.; Shafaat, H. S. Spectroscopic and Electrochemical Characterization of the [NiFeSe] Hydrogenase from *Desulfovibrio vulgaris* Miyazaki F: Reversible Redox Behavior and Interactions between Electron Transfer Centers. *ChemBioChem* **2013,** *14* (14), 1714–1719.
339. Teixeira, M.; Fauque, G.; Moura, I.; Lespinat, P. A.; Berlier, Y.; Prickril, B.; Peck, H. D., Jr.; Xavier, A. V.; Le Gall, J.; Moura, J. J. Nickel-[Iron-Sulfur]-Selenium-Containing Hydrogenases from *Desulfovibrio baculatus* (DSM 1743). Redox Centers and Catalytic Properties. *Eur. J. Biochem.* **1987,** *167* (1), 47–58.
340. Barbosa, T. M.; Baltazar, C. S. A.; Cruz, D. R.; Lousa, D.; Soares, C. M. Studying O_2 Pathways in [NiFe]- and [NiFeSe]-Hydrogenases. *Sci. Rep.* **2020,** *10* (1), 10540.
341. Gutierrez-Sanz, O.; Marques, M. C.; Baltazar, C. S.; Fernandez, V. M.; Soares, C. M.; Pereira, I. A.; De Lacey, A. L. Influence of the Protein Structure Surrounding the Active Site on the Catalytic Activity of [NiFeSe] Hydrogenases. *J. Biol. Inorg. Chem.* **2013,** *18* (4), 419–427.
342. Baltazar, C. S.; Teixeira, V. H.; Soares, C. M. Structural Features of [NiFeSe] and [NiFe] Hydrogenases Determining their Different Properties: A Computational Approach. *J. Biol. Inorg. Chem.* **2012,** *17* (4), 543–555.
343. Robb, F. T.; Techtmann, S. M. Life on the Fringe: Microbial Adaptation to Growth on Carbon Monoxide. *F1000Res* **2018,** 7.
344. Ferry, J. G. CO Dehydrogenase. *Annu. Rev. Microbiol.* **1995,** *49,* 305–333.
345. Ragsdale, S. W.; Kumar, M. Nickel-Containing Carbon Monoxide Dehydrogenase/Acetyl-CoA Synthase. *Chem. Rev.* **1996,** *96* (7), 2515–2540.
346. Ermler, U.; Grabarse, W.; Shima, S.; Goubeaud, M.; Thauer, R. K. Active Sites of Transition-Metal Enzymes with a Focus on Nickel. *Curr. Opin. Struct. Biol.* **1998,** *8* (6), 749–758.
347. Adam, P. S.; Borrel, G.; Gribaldo, S. Evolutionary History of Carbon Monoxide Dehydrogenase/Acetyl-CoA Synthase, One of the Oldest Enzymatic Complexes. *Proc. Natl. Acad. Sci. U. S. A.* **2018,** *115* (6), E1166–E1173.
348. Lindahl, P. A. The Ni-Containing Carbon Monoxide Dehydrogenase Family: Light at the End of the Tunnel? *Biochemistry* **2002,** *41* (7), 2097–2105.
349. Drennan, C. L.; Heo, J.; Sintchak, M. D.; Schreiter, E.; Ludden, P. W. Life on Carbon Monoxide: X-Ray Structure of *Rhodospirillum rubrum* Ni-Fe-S Carbon Monoxide Dehydrogenase. *Proc. Natl. Acad. Sci. U. S. A.* **2001,** *98* (21), 11973–11978.
350. Dobbek, H.; Svetlitchnyi, V.; Gremer, L.; Huber, R.; Meyer, O. Crystal Structure of a Carbon Monoxide Dehydrogenase Reveals a [Ni-4Fe-5S] Cluster. *Science* **2001,** *293* (5533), 1281–1285.
351. Wittenborn, E. C.; Guendon, C.; Merrouch, M.; Benvenuti, M.; Fourmond, V.; Leger, C.; Drennan, C. L.; Dementin, S. The Solvent-Exposed Fe-S D-Cluster Contributes to Oxygen-Resistance in *Desulfovibrio vulgaris* Ni-Fe Carbon Monoxide Dehydrogenase. *ACS Catal.* **2020,** *10* (13), 7328–7335.
352. Wittenborn, E. C.; Merrouch, M.; Ueda, C.; Fradale, L.; Leger, C.; Fourmond, V.; Pandelia, M. E.; Dementin, S.; Drennan, C. L. Redox-Dependent Rearrangements of the NiFeS Cluster of Carbon Monoxide Dehydrogenase. *Elife* **2018,** *7*.
353. Drennan, C. L.; Doukov, T. I.; Ragsdale, S. W. The Metalloclusters of Carbon Monoxide Dehydrogenase/Acetyl-CoA Synthase: A Story in Pictures. *J. Biol. Inorg. Chem.* **2004,** *9* (5), 511–515.
354. Kung, Y.; Drennan, C. L. A Role for Nickel-Iron Cofactors in Biological Carbon Monoxide and Carbon Dioxide Utilization. *Curr. Opin. Chem. Biol.* **2011,** *15* (2), 276–283.
355. Can, M.; Armstrong, F. A.; Ragsdale, S. W. Structure, Function, and Mechanism of the Nickel Metalloenzymes, CO Dehydrogenase, and Acetyl-CoA Synthase. *Chem. Rev.* **2014,** *114* (8), 4149–4174.
356. Craft, J. L.; Ludden, P. W.; Brunold, T. C. Spectroscopic Studies of Nickel-Deficient Carbon Monoxide Dehydrogenase from *Rhodospirillum rubrum*: Nature of the Iron-Sulfur Clusters. *Biochemistry* **2002,** *41* (5), 1681–1688.
357. Anderson, M. E.; Lindahl, P. A. Organization of Clusters and Internal Electron Pathways in CO Dehydrogenase from *Clostridium thermoaceticum*: Relevance to the Mechanism of Catalysis and Cyanide Inhibition. *Biochemistry* **1994,** *33* (29), 8702–8711.
358. Darnault, C.; Volbeda, A.; Kim, E. J.; Legrand, P.; Vernede, X.; Lindahl, P. A.; Fontecilla-Camps, J. C. Ni-Zn-[Fe4-S4] and Ni-Ni-[Fe4-S4] Clusters in Closed and Open Subunits of Acetyl-CoA Synthase/Carbon Monoxide Dehydrogenase. *Nat. Struct. Biol.* **2003,** *10* (4), 271–279.

359. Svetlitchnyi, V.; Dobbek, H.; Meyer-Klaucke, W.; Meins, T.; Thiele, B.; Romer, P.; Huber, R.; Meyer, O. A Functional Ni-Ni-[4Fe-4S] Cluster in the Monomeric Acetyl-CoA Synthase from *Carboxydothermus hydrogenoformans*. *Proc. Natl. Acad. Sci. U. S. A.* **2004,** *101* (2), 446–451.
360. Cohen, S. E.; Can, M.; Wittenborn, E. C.; Hendrickson, R. A.; Ragsdale, S. W.; Drennan, C. L. Crystallographic Characterization of the Carbonylated A-Cluster in Carbon Monoxide Dehydrogenase/Acetyl-CoA Synthase. *ACS Catal.* **2020,** *10* (17), 9741–9746.
361. Nicolet, Y.; Lemon, B. J.; Fontecilla-Camps, J. C.; Peters, J. W. A Novel FeS Cluster in Fe-Only Hydrogenases. *Trends Biochem. Sci.* **2000,** *25* (3), 138–143.
362. Doukov, T. I.; Iverson, T. M.; Seravalli, J.; Ragsdale, S. W.; Drennan, C. L. A Ni-Fe-Cu Center in a Bifunctional Carbon Monoxide Dehydrogenase/Acetyl-CoA Synthase. *Science* **2002,** *298* (5593), 567–572.
363. Gencic, S.; Grahame, D. A. Nickel in Subunit Beta of the Acetyl-CoA Decarbonylase/Synthase Multienzyme Complex in Methanogens. Catalytic Properties and Evidence for a Binuclear Ni-Ni Site. *J. Biol. Chem.* **2003,** *278* (8), 6101–6110.
364. Alfano, M.; Cavazza, C. Structure, Function, and Biosynthesis of Nickel-Dependent Enzymes. *Protein Sci.* **2020,** *29* (5), 1071–1089.
365. Merrouch, M.; Benvenuti, M.; Lorenzi, M.; Leger, C.; Fourmond, V.; Dementin, S. Maturation of the [Ni-4Fe-4S] Active Site of Carbon Monoxide Dehydrogenases. *J. Biol. Inorg. Chem.* **2018,** *23* (4), 613–620.
366. Lindahl, P. A.; Munck, E.; Ragsdale, S. W. CO Dehydrogenase from *Clostridium Thermoaceticum*. EPR and Electrochemical Studies in CO_2 and Argon Atmospheres. *J. Biol. Chem.* **1990,** *265* (7), 3873–3879.
367. Spangler, N. J.; Meyers, M. R.; Gierke, K. L.; Kerby, R. L.; Roberts, G. P.; Ludden, P. W. Substitution of Valine for Histidine 265 in Carbon Monoxide Dehydrogenase from *Rhodospirillum rubrum* Affects Activity and Spectroscopic States. *J. Biol. Chem.* **1998,** *273* (7), 4059–4064.
368. DeRose, V. J.; Telser, J.; Anderson, M. E.; Lindahl, P. A.; Hoffman, B. M. A Multinuclear ENDOR Study of the C-Cluster in CO Dehydrogenase from *Clostridium thermoaceticum*: Evidence for HxO and Histidine Coordination to the [Fe4S4] Center. *J. Am. Chem. Soc.* **1998,** *120* (34), 8767–8776.
369. Hu, Z. G.; Spangler, N. J.; Anderson, M. E.; Xia, J. Q.; Ludden, P. W.; Lindahl, P. A.; Munch, E. Nature of the C-Cluster in Ni-Containing Carbon Monoxide Dehydrogenases. *J. Am. Chem. Soc.* **1996,** *118* (4), 830–845.
370. Fraser, D. M.; Lindahl, P. A. Stoichiometric CO Reductive Titrations of Acetyl-CoA Synthase (Carbon Monoxide Dehydrogenase) from *Clostridium thermoaceticum*. *Biochemistry* **1999,** *38* (48), 15697–15705.
371. Russell, W. K.; Lindahl, P. A. CO/CO_2 Potentiometric Titrations of Carbon Monoxide Dehydrogenase from *Clostridium thermoaceticum* and the Effect of CO_2. *Biochemistry* **1998,** *37* (28), 10016–10026.
372. Fraser, D. M.; Lindahl, P. A. Evidence for a Proposed Intermediate Redox State in the CO/CO(2) Active Site of Acetyl-CoA Synthase (Carbon Monoxide Dehydrogenase) from *Clostridium thermoaceticum*. *Biochemistry* **1999,** *38* (48), 15706–15711.
373. Lindahl, P. A.; Ragsdale, S. W.; Munck, E. Mossbauer Study of CO Dehydrogenase from *Clostridium thermoaceticum*. *J. Biol. Chem.* **1990,** *265* (7), 3880–3888.
374. Seravalli, J.; Kumar, M.; Lu, W. P.; Ragsdale, S. W. Mechanism of CO Oxidation by Carbon Monoxide Dehydrogenase from *Clostridium thermoaceticum* and its Inhibition by Anions. *Biochemistry* **1995,** *34* (24), 7879–7888.
375. Fesseler, J.; Jeoung, J. H.; Dobbek, H. How the [NiFe4S4] Cluster of CO Dehydrogenase Activates CO_2 and NCO(−). *Angew. Chem. Int. Ed. Engl.* **2015,** *54* (29), 8560–8564.
376. Amara, P.; Mouesca, J. M.; Volbeda, A.; Fontecilla-Camps, J. C. Carbon Monoxide Dehydrogenase Reaction Mechanism: A Likely Case of Abnormal CO_2 Insertion to a Ni-H(−) Bond. *Inorg. Chem.* **2011,** *50* (5), 1868–1878.
377. Lindahl, P. A. Metal-Metal Bonds in Biology. *J. Inorg. Biochem.* **2012,** *106* (1), 172–178.
378. Wang, V. C.; Islam, S. T.; Can, M.; Ragsdale, S. W.; Armstrong, F. A. Investigations by Protein Film Electrochemistry of Alternative Reactions of Nickel-Containing Carbon Monoxide Dehydrogenase. *J. Phys. Chem. B* **2015,** *119* (43), 13690–13697.
379. Ciaccafava, A.; Tombolelli, D.; Domnik, L.; Fesseler, J.; Jeoung, J. H.; Dobbek, H.; Mroginski, M. A.; Zebger, I.; Hildebrandt, P. When the Inhibitor Tells More than the Substrate: The Cyanide-Bound State of a Carbon Monoxide Dehydrogenase. *Chem. Sci.* **2016,** *7* (5), 3162–3171.
380. Ciaccafava, A.; Tombolelli, D.; Domnik, L.; Jeoung, J. H.; Dobbek, H.; Mroginski, M. A.; Zebger, I.; Hildebrandt, P. Carbon monoxide dehydrogenase reduces cyanate to cyanide. *Angew. Chem. Int. Ed. Engl.* **2017,** *56* (26), 7398–7401.
381. Domnik, L.; Merrouch, M.; Goetzl, S.; Jeoung, J. H.; Leger, C.; Dementin, S.; Fourmond, V.; Dobbek, H. CODH-IV: A High-Efficiency CO-Scavenging CO Dehydrogenase with Resistance to O_2. *Angew. Chem. Int. Ed. Engl.* **2017,** *56* (48), 15466–15469.
382. Ragsdale, S. W.; Wood, H. G.; Antholine, W. E. Evidence that an Iron-Nickel-Carbon Complex Is Formed by Reaction of CO with the CO Dehydrogenase from *Clostridium thermoaceticum*. *Proc. Natl. Acad. Sci. U. S. A.* **1985,** *82* (20), 6811–6814.
383. Tucci, G. C.; Holm, R. H. Nickel-Mediated Formation of Thio Esters from Bound Methyl, Thiols, and Carbon Monoxide: A Possible Reaction Pathway of Acetyl-Coenzyme a Synthase Activity in Nickel-Containing Carbon Monoxide Dehydrogenases. *J. Am. Chem. Soc.* **1995,** *117* (24), 6489–6496.
384. Fan, C. L.; Gorst, C. M.; Ragsdale, S. W.; Hoffman, B. M. Characterization of the Ni-Fe-C Complex Formed by Reaction of Carbon Monoxide with the Carbon Monoxide Dehydrogenase from *Clostridium thermoaceticum* by Q-Band ENDOR. *Biochemistry* **1991,** *30* (2), 431–435.
385. Xia, J.; Hu, Z.; Popescu, C. V.; Lindahl, P. A.; Münck, E. Mössbauer and EPR Study of the Ni-Activated α-Subunit of Carbon Monoxide Dehydrogenase from *Clostridium thermoaceticum*. *J. Am. Chem. Soc.* **1997,** *119* (35), 8301–8312.
386. Russell, W. K.; Stalhandske, C. M. V.; Xia, J. Q.; Scott, R. A.; Lindahl, P. A. Spectroscopic, Redox, and Structural Characterization of the Ni-Labile and Nonlabile Forms of the Acetyl-CoA Synthase Active. Site of Carbon Monoxide Dehydrogenase. *J. Am. Chem. Soc.* **1998,** *120* (30), 7502–7510.
387. Shin, W.; Anderson, M. E.; Lindahl, P. A. Heterogeneous Nickel-Iron Environments in Carbon Monoxide Dehydrogenase from *Clostridium thermoaceticum*. *J. Am. Chem. Soc.* **1993,** *115* (13), 5522–5526.
388. McSkimming, A.; Sridharan, A.; Thompson, N. B.; Muller, P.; Suess, D. L. M. An $[Fe_4S_4]^{3+}$-Alkyl Cluster Stabilized by an Expanded Scorpionate Ligand. *J. Am. Chem. Soc.* **2020,** *142* (33), 14314–14323.
389. Moura, I.; Pauleta, S. R.; Moura, J. J. Enzymatic Activity Mastered by Altering Metal Coordination Spheres. *J. Biol. Inorg. Chem.* **2008,** *13* (8), 1185–1195.
390. Knappe, J.; Bohnert, E.; Brummer, W. S-Adenosyl-L-Methionine, a Component of the Clastic Dissimilation of Pyruvate in *Escherichia coli*. *Biochim. Biophys. Acta* **1965,** *107* (3), 603–605.
391. Chirpich, T. P.; Zappia, V.; Costilow, R. N.; Barker, H. A. Lysine 2,3-Aminomutase. Purification and Properties of a Pyridoxal Phosphate and S-Adenosylmethionine-Activated Enzyme. *J. Biol. Chem.* **1970,** *245* (7), 1778–1789.
392. Frey, P. A.; Hegeman, A. D.; Ruzicka, F. J. The Radical SAM Superfamily. *Crit. Rev. Biochem. Mol. Biol.* **2008,** *43* (1), 63–88.
393. Sofia, H. J.; Chen, G.; Hetzler, B. G.; Reyes-Spindola, J. F.; Miller, N. E. Radical SAM, a Novel Protein Superfamily Linking Unresolved Steps in Familiar Biosynthetic Pathways with Radical Mechanisms: Functional Characterization Using New Analysis and Information Visualization Methods. *Nucleic Acids Res.* **2001,** *29* (5), 1097–1106.
394. Holliday, G. L.; Akiva, E.; Meng, E. C.; Brown, S. D.; Calhoun, S.; Pieper, U.; Sali, A.; Booker, S. J.; Babbitt, P. C. Atlas of the Radical SAM Superfamily: Divergent Evolution of Function Using a "Plug and Play" Domain. *Methods Enzymol.* **2018,** *606,* 1–71.
395. Broderick, J. B.; Duffus, B. R.; Duschene, K. S.; Shepard, E. M. Radical S-Adenosylmethionine Enzymes. *Chem. Rev.* **2014,** *114* (8), 4229–4317.
396. Rivera-Serrano, E. E.; Gizzi, A. S.; Arnold, J. J.; Grove, T. L.; Almo, S. C.; Cameron, C. E. Viperin Reveals its True Function. *Annu. Rev. Virol.* **2020,** *7* (1), 421–446.
397. Hiratsuka, T.; Furihata, K.; Ishikawa, J.; Yamashita, H.; Itoh, N.; Seto, H.; Dairi, T. An Alternative Menaquinone Biosynthetic Pathway Operating in Microorganisms. *Science* **2008,** *321* (5896), 1670–1673.
398. Mahanta, N.; Hudson, G. A.; Mitchell, D. A. Radical S-Adenosylmethionine Enzymes Involved in RiPP Biosynthesis. *Biochemistry* **2017,** *56* (40), 5229–5244.
399. Mahanta, N.; Hudson, G. A.; Mitchell, D. A. Correction to Radical S-Adenosylmethionine Enzymes Involved in RiPP Biosynthesis. *Biochemistry* **2017,** *56* (45), 6072.
400. Jarrett, J. T. The Novel Structure and Chemistry of Iron-Sulfur Clusters in the Adenosylmethionine-Dependent Radical Enzyme Biotin Synthase. *Arch. Biochem. Biophys.* **2005,** *433* (1), 312–321.

401. Curatti, L.; Ludden, P. W.; Rubio, L. M. NifB-Dependent In Vitro Synthesis of the Iron-Molybdenum Cofactor of Nitrogenase. *Proc. Natl. Acad. Sci. U. S. A.* **2006,** *103* (14), 5297–5301.
402. Soboh, B.; Boyd, E. S.; Zhao, D.; Peters, J. W.; Rubio, L. M. Substrate Specificity and Evolutionary Implications of a NifDK Enzyme Carrying NifB-Co at Its Active Site. *FEBS Lett.* **2010,** *584* (8), 1487–1492.
403. Fajardo, A. S.; Legrand, P.; Paya-Tormo, L. A.; Martin, L.; Pellicer Marti Nez, M. T.; Echavarri-Erasun, C.; Vernede, X.; Rubio, L. M.; Nicolet, Y. Structural Insights into the Mechanism of the Radical SAM Carbide Synthase NifB, a Key Nitrogenase Cofactor Maturating Enzyme. *J. Am. Chem. Soc.* **2020,** *142* (25), 11006–11012.
404. Rubach, J. K.; Brazzolotto, X.; Gaillard, J.; Fontecave, M. Biochemical Characterization of the HydE and HydG Iron-Only Hydrogenase Maturation Enzymes from *Thermatoga maritima*. *FEBS Lett.* **2005,** *579* (22), 5055–5060.
405. Wu, W.; Booker, S.; Lieder, K. W.; Bandarian, V.; Reed, G. H.; Frey, P. A. Lysine 2,3-Aminomutase and Trans-4,5-Dehydrolysine: Characterization of an Allylic Analogue of a Substrate-Based Radical in the Catalytic Mechanism. *Biochemistry* **2000,** *39* (31), 9561–9570.
406. Quitterer, F.; List, A.; Eisenreich, W.; Bacher, A.; Groll, M. Crystal Structure of Methylornithine Synthase (PylB): Insights into the Pyrrolysine Biosynthesis. *Angew. Chem. Int. Ed. Engl.* **2012,** *51* (6), 1339–1342.
407. Cheek, J.; Broderick, J. B. Direct H Atom Abstraction from Spore Photoproduct C-6 Initiates DNA Repair in the Reaction Catalyzed by Spore Photoproduct Lyase: Evidence for a Reversibly Generated Adenosyl Radical Intermediate. *J. Am. Chem. Soc.* **2002,** *124* (12), 2860–2861.
408. Douglas, P.; Kriek, M.; Bryant, P.; Roach, P. L. Lipoyl Synthase Inserts Sulfur Atoms into an Octanoyl Substrate in a Stepwise Manner. *Angew. Chem. Int. Ed. Engl.* **2006,** *45* (31), 5197–5199.
409. Layer, G.; Verfurth, K.; Mahlitz, E.; Jahn, D. Oxygen-Independent Coproporphyrinogen-III Oxidase HemN from *Escherichia coli*. *J. Biol. Chem.* **2002,** *277* (37), 34136–34142.
410. Buis, J. M.; Broderick, J. B. Pyruvate Formate-Lyase Activating Enzyme: Elucidation of a Novel Mechanism for Glycyl Radical Formation. *Arch. Biochem. Biophys.* **2005,** *433* (1), 288–296.
411. Ollagnier, S.; Mulliez, E.; Gaillard, J.; Eliasson, R.; Fontecave, M.; Reichard, P. The Anaerobic *Escherichia coli* Ribonucleotide Reductase. Subunit Structure and Iron Sulfur Center. *J. Biol. Chem.* **1996,** *271* (16), 9410–9416.
412. Demick, J. M.; Lanzilotta, W. N. Radical SAM Activation of the B12-Independent Glycerol Dehydratase Results in Formation of 5′-Deoxy-5′-(Methylthio)Adenosine and Not 5′-Deoxyadenosine. *Biochemistry* **2011,** *50* (4), 440–442.
413. Selmer, T.; Pierik, A. J.; Heider, J. New Glycyl Radical Enzymes Catalysing Key Metabolic Steps in Anaerobic Bacteria. *Biol. Chem.* **2005,** *386* (10), 981–988.
414. Yu, L.; Blaser, M.; Andrei, P. I.; Pierik, A. J.; Selmer, T. 4-Hydroxyphenylacetate Decarboxylases: Properties of a Novel Subclass of Glycyl Radical Enzyme Systems. *Biochemistry* **2006,** *45* (31), 9584–9592.
415. Fang, Q.; Peng, J.; Dierks, T. Post-Translational Formylglycine Modification of Bacterial Sulfatases by the Radical S-Adenosylmethionine Protein AtsB. *J. Biol. Chem.* **2004,** *279* (15), 14570–14578.
416. Hernandez, H. L.; Pierrel, F.; Elleingand, E.; Garcia-Serres, R.; Huynh, B. H.; Johnson, M. K.; Fontecave, M.; Atta, M. MiaB, a Bifunctional Radical-S-Adenosylmethionine Enzyme Involved in the Thiolation and Methylation of tRNA, Contains Two Essential [4Fe-4S] Clusters. *Biochemistry* **2007,** *46* (17), 5140–5147.
417. Anton, B. P.; Saleh, L.; Benner, J. S.; Raleigh, E. A.; Kasif, S.; Roberts, R. J. RimO, a MiaB-Like Enzyme, Methylthiolates the Universally Conserved Asp88 Residue of Ribosomal Protein S12 in *Escherichia coli*. *Proc. Natl. Acad. Sci. U. S. A.* **2008,** *105* (6), 1826–1831.
418. Grove, T. L.; Radle, M. I.; Krebs, C.; Booker, S. J. Cfr and RlmN Contain a Single [4Fe-4S] cluster, which Directs Two Distinct Reactivities for S-Adenosylmethionine: Methyl Transfer by SN2 Displacement and Radical Generation. *J. Am. Chem. Soc.* **2011,** *133* (49), 19586–19589.
419. Chatterjee, A.; Li, Y.; Zhang, Y.; Grove, T. L.; Lee, M.; Krebs, C.; Booker, S. J.; Begley, T. P.; Ealick, S. E. Reconstitution of ThiC in Thiamine Pyrimidine Biosynthesis Expands the Radical SAM Superfamily. *Nat. Chem. Biol.* **2008,** *4* (12), 758–765.
420. Hanzelmann, P.; Schindelin, H. Binding of 5'-GTP to the C-Terminal FeS Cluster of the Radical S-Adenosylmethionine Enzyme MoaA Provides Insights into its Mechanism. *Proc. Natl. Acad. Sci. U. S. A.* **2006,** *103* (18), 6829–6834.
421. Nicolet, Y.; Amara, P.; Mouesca, J. M.; Fontecilla-Camps, J. C. Unexpected Electron Transfer Mechanism upon AdoMet Cleavage in Radical SAM Proteins. *Proc. Natl. Acad. Sci. U. S. A.* **2009,** *106* (35), 14867–14871.
422. Rettberg, L. A.; Wilcoxen, J.; Lee, C. C.; Stiebritz, M. T.; Tanifuji, K.; Britt, R. D.; Hu, Y. Probing the Coordination and Function of Fe4S4 Modules in Nitrogenase Assembly Protein NifB. *Nat. Commun.* **2018,** *9* (1), 2824.
423. Yokoyama, K.; Ohmori, D.; Kudo, F.; Eguchi, T. Mechanistic Study on the Reaction of a Radical SAM Dehydrogenase BtrN by Electron Paramagnetic Resonance Spectroscopy. *Biochemistry* **2008,** *47* (34), 8950–8960.
424. Duschene, K. S.; Broderick, J. B. The Antiviral Protein Viperin Is a Radical SAM Enzyme. *FEBS Lett.* **2010,** *584* (6), 1263–1267.
425. Zhang, Y.; Zhu, X.; Torelli, A. T.; Lee, M.; Dzikovski, B.; Koralewski, R. M.; Wang, E.; Freed, J.; Krebs, C.; Ealick, S. E.; Lin, H. Diphthamide Biosynthesis Requires an Organic Radical Generated by an Iron-Sulphur Enzyme. *Nature* **2010,** *465* (7300), 891–896.
426. Booker, S. J. Anaerobic Functionalization of Unactivated C-H Bonds. *Curr. Opin. Chem. Biol.* **2009,** *13* (1), 58–73.
427. Cosper, M. M.; Cosper, N. J.; Hong, W.; Shokes, J. E.; Broderick, W. E.; Broderick, J. B.; Johnson, M. K.; Scott, R. A. Structural Studies of the Interaction of S-Adenosylmethionine with the [4Fe-4S] Clusters in Biotin Synthase and Pyruvate Formate-Lyase Activating Enzyme. *Protein Sci.* **2003,** *12* (7), 1573–1577.
428. Chen, D.; Walsby, C.; Hoffman, B. M.; Frey, P. A. Coordination and Mechanism of Reversible Cleavage of S-Adenosylmethionine by the [4Fe-4S] Center in Lysine 2,3-Aminomutase. *J. Am. Chem. Soc.* **2003,** *125* (39), 11788–11789.
429. Cosper, M. M.; Jameson, G. N.; Davydov, R.; Eidsness, M. K.; Hoffman, B. M.; Huynh, B. H.; Johnson, M. K. The [4Fe-4S](2+) cluster in Reconstituted Biotin Synthase Binds S-Adenosyl-L-Methionine. *J. Am. Chem. Soc.* **2002,** *124* (47), 14006–14007.
430. Krebs, C.; Broderick, W. E.; Henshaw, T. F.; Broderick, J. B.; Huynh, B. H. Coordination of Adenosylmethionine to a Unique Iron Site of the [4Fe-4S] of Pyruvate Formate-Lyase Activating Enzyme: A Mossbauer Spectroscopic Study. *J. Am. Chem. Soc.* **2002,** *124* (6), 912–913.
431. Walsby, C. J.; Hong, W.; Broderick, W. E.; Cheek, J.; Ortillo, D.; Broderick, J. B.; Hoffman, B. M. Electron-Nuclear Double Resonance Spectroscopic Evidence that S-Adenosylmethionine Binds in Contact with the Catalytically Active [4Fe-4S](+) Cluster of Pyruvate Formate-Lyase Activating Enzyme. *J. Am. Chem. Soc.* **2002,** *124* (12), 3143–3151.
432. Walsby, C. J.; Ortillo, D.; Broderick, W. E.; Broderick, J. B.; Hoffman, B. M. An Anchoring Role for FeS Clusters: Chelation of the Amino Acid Moiety of S-Adenosylmethionine to the Unique Iron Site of the [4Fe-4S] Cluster of Pyruvate Formate-Lyase Activating Enzyme. *J. Am. Chem. Soc.* **2002,** *124* (38), 11270–11271.
433. Vey, J. L.; Drennan, C. L. Structural Insights into Radical Generation by the Radical SAM Superfamily. *Chem. Rev.* **2011,** *111* (4), 2487–2506.
434. Stephens, P. J.; Jollie, D. R.; Warshel, A. Protein Control of Redox Potentials of Iron-Sulfur Proteins. *Chem. Rev.* **1996,** *96* (7), 2491–2514.
435. Nicolet, Y.; Drennan, C. L. AdoMet Radical Proteins-from Structure to Evolution-Alignment of Divergent Protein Sequences Reveals Strong Secondary Structure Element Conservation. *Nucleic Acids Res.* **2004,** *32* (13), 4015–4025.
436. Layer, G.; Moser, J.; Heinz, D. W.; Jahn, D.; Schubert, W. D. Crystal Structure of Coproporphyrinogen III Oxidase Reveals Cofactor Geometry of Radical SAM Enzymes. *EMBO J.* **2003,** *22* (23), 6214–6224.
437. Grell, T. A.; Goldman, P. J.; Drennan, C. L. SPASM and Twitch Domains in S-Adenosylmethionine (SAM) Radical Enzymes. *J. Biol. Chem.* **2015,** *290* (7), 3964–3971.
438. Saichana, N.; Tanizawa, K.; Ueno, H.; Pechousek, J.; Novak, P.; Frebortova, J. Characterization of Auxiliary Iron-Sulfur Clusters in a Radical S-Adenosylmethionine Enzyme PqqE from *Methylobacterium extorquens* AM1. *FEBS Open Bio.* **2017,** *7* (12), 1864–1879.
439. Boggs, D. G.; Bridwell-Rabb, J. A Radical Exploration of the Cobalamin-Dependent Radical SAM Enzyme CysS. *Trends Chem.* **2020,** *2* (12), 1037–1040.
440. Cosper, N. J.; Booker, S. J.; Ruzicka, F.; Frey, P. A.; Scott, R. A. Direct FeS Cluster Involvement in Generation of a Radical in Lysine 2,3-Aminomutase. *Biochemistry* **2000,** *39* (51), 15668–15673.

441. Walsby, C. J.; Ortillo, D.; Yang, J.; Nnyepi, M. R.; Broderick, W. E.; Hoffman, B. M.; Broderick, J. B. Spectroscopic Approaches to Elucidating Novel Iron-Sulfur Chemistry in the "Radical-SAM" Protein Superfamily. *Inorg. Chem.* **2005,** *44* (4), 727–741.
442. Kamachi, T.; Kouno, T.; Doitomi, K.; Yoshizawa, K. Generation of Adenosyl Radical from S-Adenosylmethionine (SAM) in Biotin Synthase. *J. Inorg. Biochem.* **2011,** *105* (6), 850–857.
443. Birch, O. M.; Fuhrmann, M.; Shaw, N. M. Biotin Synthase from *Escherichia Coli*, an Investigation of the Low Molecular Weight and Protein Components Required for Activity *In Vitro*. *J. Biol. Chem.* **1995,** *270* (32), 19158–19165.
444. Tamarit, J.; Gerez, C.; Meier, C.; Mulliez, E.; Trautwein, A.; Fontecave, M. The Activating Component of the Anaerobic Ribonucleotide Reductase from *Escherichia coli*. An Iron-Sulfur Center with Only Three Cysteines. *J. Biol. Chem.* **2000,** *275* (21), 15669–15675.
445. Wan, J. T.; Jarrett, J. T. Electron Acceptor Specificity of Ferredoxin (Flavodoxin):NADP+ Oxidoreductase from *Escherichia coli*. *Arch. Biochem. Biophys.* **2002,** *406* (1), 116–126.
446. Marquet, A.; Bui, B. T.; Smith, A. G.; Warren, M. J. Iron-Sulfur Proteins as Initiators of Radical Chemistry. *Nat. Prod. Rep.* **2007,** *24* (5), 1027–1040.
447. Maiocco, S. J.; Walker, L. M.; Elliott, S. J. Determining Redox Potentials of the Iron-Sulfur Clusters of the AdoMet Radical Enzyme Superfamily. *Methods Enzymol.* **2018,** *606,* 319–339.
448. Ding, W.; Ji, X.; Zhong, Y.; Xu, K.; Zhang, Q. Adenosylation Reactions Catalyzed by the Radical S-Adenosylmethionine Superfamily Enzymes. *Curr. Opin. Chem. Biol.* **2020,** *55,* 86–95.
449. Song, K. B.; Frey, P. A. Molecular Properties of Lysine-2,3-Aminomutase. *J. Biol. Chem.* **1991,** *266* (12), 7651–7655.
450. Lepore, B. W.; Ruzicka, F. J.; Frey, P. A.; Ringe, D. The X-Ray Crystal Structure of Lysine-2,3-Aminomutase from *Clostridium subterminale*. *Proc. Natl. Acad. Sci. U. S. A.* **2005,** *102* (39), 13819–13824.
451. Frey, P. A.; Magnusson, O. T. S-Adenosylmethionine: A Wolf in sheep's Clothing, or a Rich man's Adenosylcobalamin? *Chem. Rev.* **2003,** *103* (6), 2129–2148.
452. Lieder, K. W.; Booker, S.; Ruzicka, F. J.; Beinert, H.; Reed, G. H.; Frey, P. A. S-Adenosylmethionine-Dependent Reduction of Lysine 2,3-Aminomutase and Observation of the Catalytically Functional Iron-Sulfur Centers by Electron Paramagnetic Resonance. *Biochemistry* **1998,** *37* (8), 2578–2585.
453. Frey, P. A.; Reed, G. H. Lysine 2,3-Aminomutase and the Mechanism of the Interconversion of Lysine and Beta-Lysine. *Adv. Enzymol. Relat. Areas Mol. Biol.* **1993,** *66,* 1–39.
454. Moss, M.; Frey, P. A. The Role of S-Adenosylmethionine in the Lysine 2,3-Aminomutase Reaction. *J. Biol. Chem.* **1987,** *262* (31), 14859–14862.
455. Horitani, M.; Byer, A. S.; Shisler, K. A.; Chandra, T.; Broderick, J. B.; Hoffman, B. M. Why Nature Uses Radical SAM Enzymes So Widely: Electron Nuclear Double Resonance Studies of Lysine 2,3-Aminomutase Show the 5′-dAdo* "Free Radical" Is Never Free. *J. Am. Chem. Soc.* **2015,** *137* (22), 7111–7121.
456. Ugulava, N. B.; Sacanell, C. J.; Jarrett, J. T. Spectroscopic Changes during a Single Turnover of Biotin Synthase: Destruction of a [2Fe-2S] Cluster Accompanies Sulfur Insertion. *Biochemistry* **2001,** *40* (28), 8352–8358.
457. Tse Sum Bui, B.; Florentin, D.; Marquet, A.; Benda, R.; Trautwein, A. X., Mossbauer Studies of *Escherichia coli* Biotin Synthase: Evidence for Reversible Interconversion between [2Fe-2S](2+) and [4Fe-4S](2+) Clusters. *FEBS Lett.* **1999,** *459* (3), 411–414.
458. Tse Sum Bui, B.; Benda, R.; Schunemann, V.; Florentin, D.; Trautwein, A. X.; Marquet, A. Fate of the (2Fe-2S)(2+) Cluster of *Escherichia coli* Biotin Synthase during Reaction: A Mossbauer Characterization. *Biochemistry* **2003,** *42* (29), 8791–8798.
459. Taylor, A. M.; Stoll, S.; Britt, R. D.; Jarrett, J. T. Reduction of the [2Fe-2S] Cluster Accompanies Formation of the Intermediate 9-Mercaptodethiobiotin in *Escherichia coli* Biotin Synthase. *Biochemistry* **2011,** *50* (37), 7953–7963.
460. Farrar, C. E.; Siu, K. K.; Howell, P. L.; Jarrett, J. T. Biotin Synthase Exhibits Burst Kinetics and Multiple Turnovers in the Absence of Inhibition by Products and Product-Related Biomolecules. *Biochemistry* **2010,** *49* (46), 9985–9996.
461. Choi-Rhee, E.; Cronan, J. E. Biotin Synthase Is Catalytic *In Vivo*, but Catalysis Engenders Destruction of the Protein. *Chem. Biol.* **2005,** *12* (4), 461–468.
462. McCarthy, E. L.; Booker, S. J. Destruction and Reformation of an Iron-Sulfur Cluster during Catalysis by Lipoyl Synthase. *Science* **2017,** *358* (6361), 373–377.
463. Knappe, J.; Neugebauer, F. A.; Blaschkowski, H. P.; Ganzler, M. Post-Translational Activation Introduces a Free Radical into Pyruvate Formate-Lyase. *Proc. Natl. Acad. Sci. U. S. A.* **1984,** *81* (5), 1332–1335.
464. Becker, A.; Fritz-Wolf, K.; Kabsch, W.; Knappe, J.; Schultz, S.; Volker Wagner, A. F. Structure and Mechanism of the Glycyl Radical Enzyme Pyruvate Formate-Lyase. *Nat. Struct. Biol.* **1999,** *6* (10), 969–975.
465. Broderick, J. B.; Duderstadt, R. E.; Fernandez, D. C.; Wojtuszewski, K.; Henshaw, T. F.; Johnson, M. K. Pyruvate Formate-Lyase Activating Enzyme Is an Iron-Sulfur Protein. *J. Am. Chem. Soc.* **1997,** *119* (31), 7396–7397.
466. Frey, M.; Rothe, M.; Wagner, A. F. V.; Knappe, J. Adenosylmethionine-Dependent Synthesis of the Glycyl Radical in Pyruvate Formate-Lyase by Abstraction of the Glycine C-2 pro-S Hydrogen-Atom - Studies of [H-2]Glycine-Substituted Enzyme and Peptides Homologous to the Glycine-734 Site. *J. Biol. Chem.* **1994,** *269* (17), 12432–12437.
467. Blaschkowski, H. P.; Neuer, G.; Ludwig-Festl, M.; Knappe, J. Routes of Flavodoxin and Ferredoxin Reduction in *Escherichia coli*. CoA-Acylating Pyruvate: Flavodoxin and NADPH: Flavodoxin Oxidoreductases Participating in the Activation of Pyruvate Formate-Lyase. *Eur. J. Biochem.* **1982,** *123* (3), 563–569.
468. Henshaw, T. F.; Cheek, J.; Broderick, J. B. The [4Fe-4S](1+) Cluster of Pyruvate Formate-Lyase Activating Enzyme Generates the Glycyl Radical on Pyruvate Formate-Lyase: EPR-Detected Single Turnover. *J. Am. Chem. Soc.* **2000,** *122* (34), 8331–8332.
469. Broderick, J. B.; Henshaw, T. F.; Cheek, J.; Wojtuszewski, K.; Smith, S. R.; Trojan, M. R.; McGhan, R. M.; Kopf, A.; Kibbey, M.; Broderick, W. E. Pyruvate Formate-Lyase-Activating Enzyme: Strictly Anaerobic Isolation Yields Active Enzyme Containing a [3Fe-4S](+) Cluster. *Biochem. Bioph. Res. Co* **2000,** *269* (2), 451–456.
470. Kulzer, R.; Pils, T.; Kappl, R.; Huttermann, J.; Knappe, J. Reconstitution and Characterization of the Polynuclear Iron-Sulfur Cluster in Pyruvate Formate-Lyase-Activating Enzyme. Molecular Properties of the Holoenzyme Form. *J. Biol. Chem.* **1998,** *273* (9), 4897–4903.
471. Krebs, C.; Henshaw, T. F.; Cheek, J.; Huynh, B. H.; Broderick, J. B. Conversion of 3Fe-4S to 4Fe-4S Clusters in Native Pyruvate Formate-Lyase Activating Enzyme: Mossbauer Characterization and Implications for Mechanism. *J. Am. Chem. Soc.* **2000,** *122* (50), 12497–12506.
472. Yang, J.; Naik, S. G.; Ortillo, D. O.; Garcia-Serres, R.; Li, M.; Broderick, W. E.; Huynh, B. H.; Broderick, J. B. The Iron-Sulfur Cluster of Pyruvate Formate-Lyase Activating Enzyme in Whole Cells: Cluster Interconversion and a Valence-Localized [4Fe-4S]2+ State. *Biochemistry* **2009,** *48* (39), 9234–9241.
473. Vey, J. L.; Yang, J.; Li, M.; Broderick, W. E.; Broderick, J. B.; Drennan, C. L. Structural Basis for Glycyl Radical Formation by Pyruvate Formate-Lyase Activating Enzyme. *Proc. Natl. Acad. Sci. U. S. A.* **2008,** *105* (42), 16137–16141.
474. Peng, Y.; Veneziano, S. E.; Gillispie, G. D.; Broderick, J. B. Pyruvate Formate-Lyase, Evidence for an Open Conformation Favored in the Presence of its Activating Enzyme. *J. Biol. Chem.* **2010,** *285* (35), 27224–27231.
475. Shisler, K. A.; Hutcheson, R. U.; Horitani, M.; Duschene, K. S.; Crain, A. V.; Byer, A. S.; Shepard, E. M.; Rasmussen, A.; Yang, J.; Broderick, W. E.; Vey, J. L.; Drennan, C. L.; Hoffman, B. M.; Broderick, J. B. Monovalent Cation Activation of the Radical SAM Enzyme Pyruvate Formate-Lyase Activating Enzyme. *J. Am. Chem. Soc.* **2017,** *139* (34), 11803–11813.
476. Long, K. S.; Poehlsgaard, J.; Kehrenberg, C.; Schwarz, S.; Vester, B. The Cfr rRNA Methyltransferase Confers Resistance to Phenicols, Lincosamides, Oxazolidinones, Pleuromutilins, and Streptogramin A Antibiotics. *Antimicrob. Agents Chemother.* **2006,** *50* (7), 2500–2505.
477. Giessing, A. M.; Jensen, S. S.; Rasmussen, A.; Hansen, L. H.; Gondela, A.; Long, K.; Vester, B.; Kirpekar, F. Identification of 8-Methyladenosine as the Modification Catalyzed by the Radical SAM Methyltransferase Cfr that Confers Antibiotic Resistance in Bacteria. *RNA* **2009,** *15* (2), 327–336.
478. Schwarz, S.; Werckenthin, C.; Kehrenberg, C. Identification of a Plasmid-Borne Chloramphenicol-Florfenicol Resistance Gene in *Staphylococcus sciuri*. *Antimicrob. Agents Chemother.* **2000,** *44* (9), 2530–2533.
479. Boal, A. K.; Grove, T. L.; McLaughlin, M. I.; Yennawar, N. H.; Booker, S. J.; Rosenzweig, A. C. Structural Basis for Methyl Transfer by a Radical SAM Enzyme. *Science* **2011,** *332* (6033), 1089–1092.

480. Yan, F.; LaMarre, J. M.; Rohrich, R.; Wiesner, J.; Jomaa, H.; Mankin, A. S.; Fujimori, D. G. RlmN and Cfr Are Radical SAM Enzymes Involved in Methylation of Ribosomal RNA. *J. Am. Chem. Soc.* **2010,** *132* (11), 3953–3964.
481. Yan, F.; Fujimori, D. G. RNA Methylation by Radical SAM Enzymes RlmN and Cfr Proceeds Via Methylene Transfer and Hydride Shift. *Proc. Natl. Acad. Sci. U. S. A.* **2011,** *108* (10), 3930–3934.
482. Grove, T. L.; Benner, J. S.; Radle, M. I.; Ahlum, J. H.; Landgraf, B. J.; Krebs, C.; Booker, S. J. A Radically Different Mechanism for S-Adenosylmethionine-Dependent Methyltransferases. *Science* **2011,** *332* (6029), 604–607.
483. Zhu, H.; Cong, J. P.; Shenk, T. Use of Differential Display Analysis to Assess the Effect of Human Cytomegalovirus Infection on the Accumulation of Cellular RNAs: Induction of Interferon-Responsive RNAs. *Proc. Natl. Acad. Sci. U. S. A.* **1997,** *94* (25), 13985–13990.
484. Ghosh, S.; Marsh, E. N. G. Viperin: An Ancient Radical SAM Enzyme Finds its Place in Modern Cellular Metabolism and Innate Immunity. *J. Biol. Chem.* **2020,** *295* (33), 11513–11528.
485. Lachowicz, J. C.; Gizzi, A. S.; Almo, S. C.; Grove, T. L. Structural Insight into the Substrate Scope of Viperin and Viperin-Like Enzymes from Three Domains of Life. *Biochemistry* **2021,** *60* (26), 2116–2129.
486. Fenwick, M. K.; Li, Y.; Cresswell, P.; Modis, Y.; Ealick, S. E. Structural Studies of Viperin, an Antiviral Radical SAM Enzyme. *Proc. Natl. Acad. Sci. U. S. A.* **2017,** *114* (26), 6806–6811.
487. Fenwick, M. K.; Su, D.; Dong, M.; Lin, H.; Ealick, S. E. Structural Basis of the Substrate Selectivity of Viperin. *Biochemistry* **2020,** *59* (5), 652–662.
488. Shaveta, G.; Shi, J.; Chow, V. T.; Song, J. Structural Characterization Reveals that Viperin Is a Radical S-Adenosyl-L-Methionine (SAM) Enzyme. *Biochem. Bioph. Res. Co* **2010,** *391* (3), 1390–1395.
489. Gizzi, A. S.; Grove, T. L.; Arnold, J. J.; Jose, J.; Jangra, R. K.; Garforth, S. J.; Du, Q.; Cahill, S. M.; Dulyaninova, N. G.; Love, J. D.; Chandran, K.; Bresnick, A. R.; Cameron, C. E.; Almo, S. C. A Naturally Occurring Antiviral Ribonucleotide Encoded by the Human Genome. *Nature* **2018,** *558* (7711), 610–614.
490. Mattheakis, L. C.; Sor, F.; Collier, R. J. Diphthamide Synthesis in *Saccharomyces cerevisiae*: Structure of the DPH2 Gene. *Gene* **1993,** *132* (1), 149–154.
491. Liu, S.; Milne, G. T.; Kuremsky, J. G.; Fink, G. R.; Leppla, S. H. Identification of the Proteins Required for Biosynthesis of Diphthamide, the Target of Bacterial ADP-Ribosylating Toxins on Translation Elongation Factor 2. *Mol. Cell. Biol.* **2004,** *24* (21), 9487–9497.
492. Moehring, J. M.; Moehring, T. J.; Danley, D. E. Posttranslational Modification of Elongation Factor 2 in Diphtheria-Toxin-Resistant Mutants of CHO-K1 Cells. *Proc. Natl. Acad. Sci. U. S. A.* **1980,** *77* (2), 1010–1014.
493. Ortiz, P. A.; Ulloque, R.; Kihara, G. K.; Zheng, H.; Kinzy, T. G. Translation Elongation Factor 2 Anticodon Mimicry Domain Mutants Affect Fidelity and Diphtheria Toxin Resistance. *J. Biol. Chem.* **2006,** *281* (43), 32639–32648.
494. Collier, R. J. Understanding the Mode of Action of Diphtheria Toxin: A Perspective on Progress during the 20th Century. *Toxicon* **2001,** *39* (11), 1793–1803.
495. Dong, M.; Su, X.; Dzikovski, B.; Dando, E. E.; Zhu, X.; Du, J.; Freed, J. H.; Lin, H. Dph3 Is an Electron Donor for Dph1-Dph2 in the First Step of Eukaryotic Diphthamide Biosynthesis. *J. Am. Chem. Soc.* **2014,** *136* (5), 1754–1757.
496. Zhu, X.; Dzikovski, B.; Su, X.; Torelli, A. T.; Zhang, Y.; Ealick, S. E.; Freed, J. H.; Lin, H. Mechanistic Understanding of *Pyrococcus horikoshii* Dph2, a [4Fe-4S] Enzyme Required for Diphthamide Biosynthesis. *Mol. Biosyst.* **2011,** *7* (1), 74–81.
497. Dong, M.; Kathiresan, V.; Fenwick, M. K.; Torelli, A. T.; Zhang, Y.; Caranto, J. D.; Dzikovski, B.; Sharma, A.; Lancaster, K. M.; Freed, J. H.; Ealick, S. E.; Hoffman, B. M.; Lin, H. Organometallic and Radical Intermediates Reveal Mechanism of Diphthamide Biosynthesis. *Science* **2018,** *359* (6381), 1247–1250.
498. Feng, J.; Shaik, S.; Wang, B. Spin-Regulated Electron Transfer and Exchange-Enhanced Reactivity in Fe_4S_4 -Mediated Redox Reaction of the Dph2 Enzyme during the Biosynthesis of Diphthamide. *Angew. Chem. Int. Ed. Engl.* **2021,** *60* (37), 20430–20436.
499. Sato, S.; Kudo, F.; Rohmer, M.; Eguchi, T. Characterization of Radical SAM Adenosylhopane Synthase, HpnH, which Catalyzes the 5′-Deoxyadenosyl Radical Addition to Diploptene in the Biosynthesis of C35 Bacteriohopanepolyols. *Angew. Chem. Int. Ed. Engl.* **2020,** *59* (1), 237–241.
500. Zhong, Y.; Ji, X.; Zhang, Q. Radical SAM-Dependent Adenosylation Involved in Bacteriohopanepolyol Biosynthesis. *Chin. J. Chem.* **2019,** *38* (1), 39–42.
501. Zhong, Y. T.; Ji, X. J. Adenosylhopane Biosynthesis by the Radical SAM Enzyme HpnH. *Chin. J. Chem.* **2020,** *38* (2), 218–219.
502. Mahanta, N.; Fedoseyenko, D.; Dairi, T.; Begley, T. P. Menaquinone Biosynthesis: Formation of Aminofutalosine Requires a Unique Radical SAM Enzyme. *J. Am. Chem. Soc.* **2013,** *135* (41), 15318–15321.
503. Joshi, S.; Mahanta, N.; Fedoseyenko, D.; Williams, H.; Begley, T. P. Aminofutalosine Synthase: Evidence for Captodative and Aryl Radical Intermediates Using Beta-Scission and SRN1 Trapping Reactions. *J. Am. Chem. Soc.* **2017,** *139* (32), 10952–10955.
504. Joshi, S.; Fedoseyenko, D.; Mahanta, N.; Begley, T. P. Aminofutalosine Synthase (MqnE): A New Catalytic Motif in Radical SAM Enzymology. *Methods Enzymol.* **2018,** *606,* 179–198.
505. Joshi, S.; Fedoseyenko, D.; Sharma, V.; Nesbit, M. A.; Britt, R. D.; Begley, T. P. Menaquinone Biosynthesis: New Strategies to Trap Radical Intermediates in the MqnE-Catalyzed Reaction. *Biochemistry* **2021,** *60* (21), 1642–1646.
506. Joshi, S.; Fedoseyenko, D.; Mahanta, N.; Ducati, R. G.; Feng, M.; Schramm, V. L.; Begley, T. P. Antibacterial Strategy against *H. pylori*: Inhibition of the Radical SAM Enzyme MqnE in Menaquinone Biosynthesis. *ACS Med. Chem. Lett.* **2019,** *10* (3), 363–366.
507. Xu, X. L.; Chen, S.; Grant, G. A. Kinetic, Mutagenic, and Structural Homology Analysis of L-Serine Dehydratase from *Legionella pneumophila*. *Arch. Biochem. Biophys.* **2011,** *515* (1-2), 28–36.
508. Flint, D. H. *Escherichia Coli* Fumarase a Catalyzes the Isomerization of Enol and Keto Oxalacetic Acid. *Biochemistry* **1993,** *32* (3), 799–805.
509. van Vugt-Lussenburg, B. M. A.; van der Weel, L.; Hagen, W. R.; Hagedoorn, P. L. Identification of Two [4Fe-4S]-Cluster-Containing Hydro-Lyases from *Pyrococcus furiosus*. *Microbiology* **2009,** *155* (Pt 9), 3015–3020.
510. Flint, D. H.; Emptage, M. H.; Finnegan, M. G.; Fu, W.; Johnson, M. K. The Role and Properties of the Iron-Sulfur Cluster in *Escherichia coli* Dihydroxy-Acid Dehydratase. *J. Biol. Chem.* **1993,** *268* (20), 14732–14742.
511. Muh, U.; Cinkaya, I.; Albracht, S. P.; Buckel, W. 4-Hydroxybutyryl-CoA Dehydratase from *Clostridium aminobutyricum*: Characterization of FAD and Iron-Sulfur Clusters Involved in an Overall Non-redox Reaction. *Biochemistry* **1996,** *35* (36), 11710–11718.
512. Rodriguez, M.; Wedd, A. G.; Scopes, R. K. 6-Phosphogluconate Dehydratase from *Zymomonas mobilis*: An Iron-Sulfur-Manganese Enzyme. *Biochem. Mol. Biol. Int.* **1996,** *38* (4), 783–789.
513. Flint, D. H.; Allen, R. M. Iron-Sulfur Proteins with Nonredox Functions. *Chem. Rev.* **1996,** *96* (7), 2315–2334.
514. Volbeda, A.; Fontecilla-Camps, J. C. Structural Basis for the Catalytic Activities of the Multifunctional Enzyme Quinolinate Synthase. *Coord. Chem. Rev.* **2020,** *417*.
515. Cherrier, M. V.; Chan, A.; Darnault, C.; Reichmann, D.; Amara, P.; Ollagnier de Choudens, S.; Fontecilla-Camps, J. C. The Crystal Structure of Fe(4)S(4) Quinolinate Synthase Unravels an Enzymatic Dehydration Mechanism that Uses Tyrosine and a Hydrolase-Type Triad. *J. Am. Chem. Soc.* **2014,** *136* (14), 5253–5256.
516. Esakova, O. A.; Silakov, A.; Grove, T. L.; Saunders, A. H.; McLaughlin, M. I.; Yennawar, N. H.; Booker, S. J. Structure of Quinolinate Synthase from *Pyrococcus horikoshii* in the Presence of its Product, Quinolinic Acid. *J. Am. Chem. Soc.* **2016,** *138* (23), 7224–7227.
517. Esakova, O. A.; Silakov, A.; Grove, T. L.; Warui, D. M.; Yennawar, N. H.; Booker, S. J. An Unexpected Species Determined by X-Ray Crystallography that May Represent an Intermediate in the Reaction Catalyzed by Quinolinate Synthase. *J. Am. Chem. Soc.* **2019,** *141* (36), 14142–14151.
518. Fenwick, M. K.; Ealick, S. E. Crystal Structures of the Iron-Sulfur Cluster-Dependent Quinolinate Synthase in Complex with Dihydroxyacetone Phosphate, Iminoaspartate Analogues, and Quinolinate. *Biochemistry* **2016,** *55* (30), 4135–4139.
519. Volbeda, A.; Saez Cabodevilla, J.; Darnault, C.; Gigarel, O.; Han, T. H.; Renoux, O.; Hamelin, O.; Ollagnier-de-Choudens, S.; Amara, P.; Fontecilla-Camps, J. C. Crystallographic Trapping of Reaction Intermediates in Quinolinic Acid Synthesis by NadA. *ACS Chem. Biol.* **2018,** *13* (5), 1209–1217.

520. Saez Cabodevilla, J.; Volbeda, A.; Hamelin, O.; Latour, J. M.; Gigarel, O.; Clemancey, M.; Darnault, C.; Reichmann, D.; Amara, P.; Fontecilla-Camps, J. C.; Ollagnier de Choudens, S. Design of Specific Inhibitors of Quinolinate Synthase Based on [4Fe-4S] Cluster Coordination. *Chem. Commun. (Camb.)* **2019,** *55* (26), 3725–3728.
521. Chan, A.; Clemancey, M.; Mouesca, J. M.; Amara, P.; Hamelin, O.; Latour, J. M.; Ollagnier de Choudens, S. Studies of Inhibitor Binding to the [4Fe-4S] Cluster of Quinolinate Synthase. *Angew. Chem. Int. Ed. Engl.* **2012,** *51* (31), 7711–7714.
522. Watanabe, S.; Murase, Y.; Watanabe, Y.; Sakurai, Y.; Tajima, K. Crystal Structures of Aconitase X Enzymes from Bacteria and Archaea Provide Insights into the Molecular Evolution of the Aconitase Superfamily. *Commun. Biol.* **2021,** *4* (1), 687.
523. Andberg, M.; Aro-Karkkainen, N.; Carlson, P.; Oja, M.; Bozonnet, S.; Toivari, M.; Hakulinen, N.; O'Donohue, M.; Penttila, M.; Koivula, A. Characterization and Mutagenesis of Two Novel Iron-Sulphur Cluster Pentonate Dehydratases. *Appl. Microbiol. Biotechnol.* **2016,** *100* (17), 7549–7563.
524. Rahman, M. M.; Andberg, M.; Koivula, A.; Rouvinen, J.; Hakulinen, N. The Crystal Structure of D-Xylonate Dehydratase Reveals Functional Features of Enzymes from the Ilv/ED Dehydratase Family. *Sci. Rep.* **2018,** *8* (1), 865.
525. Beinert, H.; Kennedy, M. C. 19th Sir Hans Krebs Lecture. Engineering of Protein Bound Iron-Sulfur Clusters. A Tool for the Study of Protein and Cluster Chemistry and Mechanism of Iron-Sulfur Enzymes. *Eur. J. Biochem.* **1989,** *186* (1-2), 5–15.
526. Lloyd, S. J.; Lauble, H.; Prasad, G. S.; Stout, C. D. The Mechanism of Aconitase: 1.8 Å Resolution Crystal Structure of the S642a:Citrate Complex. *Protein Sci.* **1999,** *8* (12), 2655–2662.
527. Kennedy, M. C.; Mende-Mueller, L.; Blondin, G. A.; Beinert, H. Purification and Characterization of Cytosolic Aconitase from Beef Liver and its Relationship to the Iron-Responsive Element Binding Protein. *Proc. Natl. Acad. Sci. U. S. A.* **1992,** *89* (24), 11730–11734.
528. Manikandan, K.; Geerlof, A.; Zozulya, A. V.; Svergun, D. I.; Weiss, M. S. Structural Studies on the Enzyme Complex Isopropylmalate Isomerase (LeuCD) from *Mycobacterium tuberculosis*. *Proteins* **2011,** *79* (1), 35–49.
529. Jang, S.; Imlay, J. A. Micromolar Intracellular Hydrogen Peroxide Disrupts Metabolism by Damaging Iron-Sulfur Enzymes. *J. Biol. Chem.* **2007,** *282* (2), 929–937.
530. Drevland, R. M.; Jia, Y.; Palmer, D. R.; Graham, D. E. Methanogen Homoaconitase Catalyzes both Hydrolyase Reactions in Coenzyme B Biosynthesis. *J. Biol. Chem.* **2008,** *283* (43), 28888–28896.
531. Muhlenhoff, U.; Richter, N.; Pines, O.; Pierik, A. J.; Lill, R. Specialized Function of Yeast Isa1 and Isa2 Proteins in the Maturation of Mitochondrial [4Fe-4S] Proteins. *J. Biol. Chem.* **2011,** *286* (48), 41205–41216.
532. Rocco, C. J.; Wetterhorn, K. M.; Garvey, G. S.; Rayment, I.; Escalante-Semerena, J. C. The PrpF Protein of *Shewanella Oneidensis* MR-1 Catalyzes the Isomerization of 2-Methyl-Cis-Aconitate during the Catabolism of Propionate Via the AcnD-Dependent 2-Methylcitric Acid Cycle. *PLoS One* **2017,** *12* (11), e0188130.
533. Grimek, T. L.; Escalante-Semerena, J. C. The acnD Genes of *Shewenella Oneidensis* and *Vibrio Cholerae* Encode a New Fe/S-Dependent 2-Methylcitrate Dehydratase Enzyme that Requires prpF Function *In Vivo*. *J. Bacteriol.* **2004,** *186* (2), 454–462.
534. Rouault, T. A.; Stout, C. D.; Kaptain, S.; Harford, J. B.; Klausner, R. D. Structural Relationship between an Iron-Regulated RNA-Binding Protein (IRE-BP) and Aconitase: Functional Implications. *Cell* **1991,** *64* (5), 881–883.
535. Zheng, L.; Kennedy, M. C.; Beinert, H.; Zalkin, H. Mutational Analysis of Active Site Residues in Pig Heart Aconitase. *J. Biol. Chem.* **1992,** *267* (11), 7895–7903.
536. Haile, D. J.; Rouault, T. A.; Tang, C. K.; Chin, J.; Harford, J. B.; Klausner, R. D. Reciprocal Control of RNA-Binding and Aconitase Activity in the Regulation of the Iron-Responsive Element Binding Protein: Role of the Iron-Sulfur Cluster. *Proc. Natl. Acad. Sci. U. S. A.* **1992,** *89* (16), 7536–7540.
537. Haile, D. J.; Rouault, T. A.; Harford, J. B.; Kennedy, M. C.; Blondin, G. A.; Beinert, H.; Klausner, R. D. Cellular Regulation of the Iron-Responsive Element Binding Protein: Disassembly of the Cubane Iron-Sulfur Cluster Results in High-Affinity RNA Binding. *Proc. Natl. Acad. Sci. U. S. A.* **1992,** *89* (24), 11735–11739.
538. Dickman, S. R.; Cloutier, A. A. Factors Affecting the Activity of Aconitase. *J. Biol. Chem.* **1951,** *188* (1), 379–388.
539. Kennedy, M. C.; Stout, C. D. Aconitase: An Iron-Sulfur Enzyme. In *Advances in Inorganic Chemistry;* Sykes, A. G., Ed.; vol. 38; Academic Press, 1992; pp 323–339.
540. Robbins, A. H.; Stout, C. D. The Structure of Aconitase. *Proteins* **1989,** *5* (4), 289–312.
541. Werst, M. M.; Kennedy, M. C.; Beinert, H.; Hoffman, B. M. 17O, 1H, and 2H Electron Nuclear Double Resonance Characterization of Solvent, Substrate, and Inhibitor Binding to the $[4Fe\text{-}4S]^{+}$ Cluster of Aconitase. *Biochemistry* **1990,** *29* (46), 10526–10532.
542. Werst, M. M.; Kennedy, M. C.; Houseman, A. L.; Beinert, H.; Hoffman, B. M. Characterization of the $[4Fe\text{-}4S]^{+}$ Cluster at the Active Site of Aconitase by ^{57}Fe, ^{33}S, and ^{14}N Electron Nuclear Double Resonance Spectroscopy. *Biochemistry* **1990,** *29* (46), 10533–10540.
543. Lauble, H.; Kennedy, M. C.; Beinert, H.; Stout, C. D. Crystal Structures of Aconitase with Trans-Aconitate and Nitrocitrate Bound. *J. Mol. Biol.* **1994,** *237* (4), 437–451.
544. Lauble, H.; Kennedy, M. C.; Beinert, H.; Stout, C. D. Crystal Structures of Aconitase with Isocitrate and Nitroisocitrate Bound. *Biochemistry* **1992,** *31* (10), 2735–2748.
545. Goodsell, D. S.; Lauble, H.; Stout, C. D.; Olson, A. J. Automated Docking in Crystallography: Analysis of the Substrates of Aconitase. *Proteins* **1993,** *17* (1), 1–10.
546. Rose, I. A.; O'Connell, E. L. Mechanism of Aconitase Action. I. the Hydrogen Transfer Reaction. *J. Biol. Chem.* **1967,** *242* (8), 1870–1879.
547. Schloss, J. V.; Emptage, M. H.; Cleland, W. W. pH Profiles and Isotope Effects for Aconitases from *Saccharomycopsis lipolytica*, Beef Heart, and Beef Liver. Alpha-Methyl-cis-Aconitate and Threo-Ds-Alpha-Methylisocitrate as Substrates. *Biochemistry* **1984,** *23* (20), 4572–4580.
548. Grawert, T.; Groll, M.; Rohdich, F.; Bacher, A.; Eisenreich, W. Biochemistry of the Non-mevalonate Isoprenoid Pathway. *Cell. Mol. Life Sci.* **2011,** *68* (23), 3797–3814.
549. Rohdich, F.; Bacher, A.; Eisenreich, W. Perspectives in Anti-Infective Drug Design. The Late Steps in the Biosynthesis of the Universal Terpenoid Precursors, Isopentenyl Diphosphate and Dimethylallyl Diphosphate. *Bioorg. Chem.* **2004,** *32* (5), 292–308.
550. Perez-Gil, J.; Rodriguez-Concepcion, M. Metabolic Plasticity for Isoprenoid Biosynthesis in Bacteria. *Biochem. J.* **2013,** *452* (1), 19–25.
551. Wang, W.; Oldfield, E. Bioorganometallic Chemistry with IspG and IspH: Structure, Function, and Inhibition of the [Fe(4)S(4)] Proteins Involved in Isoprenoid Biosynthesis. *Angew. Chem. Int. Ed. Engl.* **2014,** *53* (17), 4294–4310.
552. Zepeck, F.; Grawert, T.; Kaiser, J.; Schramek, N.; Eisenreich, W.; Bacher, A.; Rohdich, F. Biosynthesis of Isoprenoids. Purification and Properties of IspG Protein from *Escherichia coli*. *J. Org. Chem.* **2005,** *70* (23), 9168–9174.
553. Wang, W.; Li, J.; Wang, K.; Huang, C.; Zhang, Y.; Oldfield, E. Organometallic Mechanism of Action and Inhibition of the 4Fe-4S Isoprenoid Biosynthesis Protein GcpE (IspG). *Proc. Natl. Acad. Sci. U. S. A.* **2010,** *107* (25), 11189–11193.
554. Rekittke, I.; Jomaa, H.; Ermler, U. Structure of the GcpE (IspG)-MEcPP Complex from *Thermus thermophilus*. *FEBS Lett.* **2012,** *586* (19), 3452–3457.
555. Quitterer, F.; Frank, A.; Wang, K.; Rao, G.; O'Dowd, B.; Li, J.; Guerra, F.; Abdel-Azeim, S.; Bacher, A.; Eppinger, J.; Oldfield, E.; Groll, M. Atomic-Resolution Structures of Discrete Stages on the Reaction Coordinate of the [Fe4S4] Enzyme IspG (GcpE). *J. Mol. Biol.* **2015,** *427* (12), 2220–2228.
556. Rekittke, I.; Nonaka, T.; Wiesner, J.; Demmer, U.; Warkentin, E.; Jomaa, H.; Ermler, U. Structure of the E-1-Hydroxy-2-Methyl-but-2-Enyl-4-Diphosphate Synthase (GcpE) from *Thermus thermophilus*. *FEBS Lett.* **2011,** *585* (3), 447–451.
557. Rohdich, F.; Zepeck, F.; Adam, P.; Hecht, S.; Kaiser, J.; Laupitz, R.; Grawert, T.; Amslinger, S.; Eisenreich, W.; Bacher, A.; Arigoni, D. The Deoxyxylulose Phosphate Pathway of Isoprenoid Biosynthesis: Studies on the Mechanisms of the Reactions Catalyzed by IspG and IspH Protein. *Proc. Natl. Acad. Sci. U. S. A.* **2003,** *100* (4), 1586–1591.
558. Nyland, R. L., 2nd; Xiao, Y.; Liu, P.; Freel Meyers, C. L. IspG Converts an Epoxide Substrate Analogue to (E)-4-Hydroxy-3-Methylbut-2-Enyl Diphosphate: Implications for IspG Catalysis in Isoprenoid Biosynthesis. *J. Am. Chem. Soc.* **2009,** *131* (49), 17734–17735.
559. Xu, W.; Lees, N. S.; Adedeji, D.; Wiesner, J.; Jomaa, H.; Hoffman, B. M.; Duin, E. C. Paramagnetic Intermediates of (E)-4-Hydroxy-3-Methylbut-2-Enyl Diphosphate Synthase (GcpE/IspG) under Steady-State and Pre-Steady-State Conditions. *J. Am. Chem. Soc.* **2010,** *132* (41), 14509–14520.
560. Wang, W.; Wang, K.; Li, J.; Nellutla, S.; Smirnova, T. I.; Oldfield, E. An ENDOR and HYSCORE Investigation of a Reaction Intermediate in IspG (GcpE) Catalysis. *J. Am. Chem. Soc.* **2011,** *133* (22), 8400–8403.
561. Fay, A. W.; Blank, M. A.; Yoshizawa, J. M.; Lee, C. C.; Wiig, J. A.; Hu, Y.; Hodgson, K. O.; Hedman, B.; Ribbe, M. W. Formation of a Homocitrate-Free Iron-Molybdenum Cluster on NifEN: Implications for the Role of Homocitrate in Nitrogenase Assembly. *Dalton Trans.* **2010,** *39* (12), 3124–3130.

562. Wang, W.; Wang, K.; Liu, Y. L.; No, J. H.; Li, J.; Nilges, M. J.; Oldfield, E. Bioorganometallic Mechanism of Action, and Inhibition, of IspH. *Proc. Natl. Acad. Sci. U. S. A.* **2010,** *107* (10), 4522–4527.
563. Grawert, T.; Span, I.; Eisenreich, W.; Rohdich, F.; Eppinger, J.; Bacher, A.; Groll, M. Probing the Reaction Mechanism of IspH Protein by X-Ray Structure Analysis. *Proc. Natl. Acad. Sci. U. S. A.* **2010,** *107* (3), 1077–1081.
564. Rekittke, I.; Wiesner, J.; Rohrich, R.; Demmer, U.; Warkentin, E.; Xu, W.; Troschke, K.; Hintz, M.; No, J. H.; Duin, E. C.; Oldfield, E.; Jomaa, H.; Ermler, U. Structure of (E)-4-Hydroxy-3-Methyl-but-2-Enyl Diphosphate Reductase, the Terminal Enzyme of the Non-mevalonate Pathway. *J. Am. Chem. Soc.* **2008,** *130* (51), 17206–17207.
565. Grawert, T.; Rohdich, F.; Span, I.; Bacher, A.; Eisenreich, W.; Eppinger, J.; Groll, M. Structure of Active IspH Enzyme from *Escherichia coli* Provides Mechanistic Insights into Substrate Reduction. *Angew. Chem. Int. Ed. Engl.* **2009,** *48* (31), 5756–5759.
566. Xiao, Y.; Chu, L.; Sanakis, Y.; Liu, P. Revisiting the IspH Catalytic System in the Deoxyxylulose Phosphate Pathway: Achieving High Activity. *J. Am. Chem. Soc.* **2009,** *131* (29), 9931–9933.
567. Seemann, M.; Janthawornpong, K.; Schweizer, J.; Bottger, L. H.; Janoschka, A.; Ahrens-Botzong, A.; Tambou, E. N.; Rotthaus, O.; Trautwein, A. X.; Rohmer, M. Isoprenoid Biosynthesis Via the MEP Pathway: In Vivo Mossbauer Spectroscopy Identifies a [4Fe-4S]2+ Center with Unusual Coordination Sphere in the LytB Protein. *J. Am. Chem. Soc.* **2009,** *131* (37), 13184–13185.
568. Wolff, M.; Seemann, M.; Tse Sum Bui, B.; Frapart, Y.; Tritsch, D.; Garcia Estrabot, A.; Rodriguez-Concepcion, M.; Boronat, A.; Marquet, A.; Rohmer, M. Isoprenoid Biosynthesis Via the Methylerythritol Phosphate Pathway: The (E)-4-Hydroxy-3-Methylbut-2-Enyl Diphosphate Reductase (LytB/IspH) from *Escherichia coli* Is a [4Fe-4S] Protein. *FEBS Lett.* **2003,** *541* (1-3), 115–120.
569. Wang, K.; Wang, W.; No, J. H.; Zhang, Y.; Zhang, Y.; Oldfield, E. Inhibition of the Fe(4)S(4)-Cluster-Containing Protein IspH (LytB): Electron Paramagnetic Resonance, Metallacycles, and Mechanisms. *J. Am. Chem. Soc.* **2010,** *132* (19), 6719–6727.
570. Abdel-Azeim, S.; Jedidi, A.; Eppinger, J.; Cavallo, L. Mechanistic Insights into the Reductive Dehydroxylation Pathway for the Biosynthesis of Isoprenoids Promoted by the IspH Enzyme. *Chem. Sci.* **2015,** *6* (10), 5643–5651.
571. Wang, W.; Wang, K.; Span, I.; Jauch, J.; Bacher, A.; Groll, M.; Oldfield, E. Are Free Radicals Involved in IspH Catalysis? An EPR and Crystallographic Investigation. *J. Am. Chem. Soc.* **2012,** *134* (27), 11225–11234.
572. Blombach, B.; Eikmanns, B. J. Current Knowledge on Isobutanol Production with *Escherichia Coli*, *Bacillus subtilis* and *Corynebacterium glutamicum*. *Bioeng. Bugs* **2011,** *2* (6), 346–350.
573. Boer, H.; Andberg, M.; Pylkkanen, R.; Maaheimo, H.; Koivula, A. *In Vitro* Reconstitution and Characterisation of the Oxidative D-Xylose Pathway for Production of Organic Acids and Alcohols. *AMB Express* **2019,** *9* (1), 48.
574. Banares, A. B.; Nisola, G. M.; Valdehuesa, K. N. G.; Lee, W. K.; Chung, W. J. Understanding D-Xylonic Acid Accumulation: A Cornerstone for Better Metabolic Engineering Approaches. *Appl. Microbiol. Biotechnol.* **2021,** *105* (13), 5309–5324.
575. Guterl, J. K.; Garbe, D.; Carsten, J.; Steffler, F.; Sommer, B.; Reisse, S.; Philipp, A.; Haack, M.; Ruhmann, B.; Koltermann, A.; Kettling, U.; Bruck, T.; Sieber, V. Cell-Free Metabolic Engineering: Production of Chemicals by Minimized Reaction Cascades. *ChemSusChem* **2012,** *5* (11), 2165–2172.
576. Stephens, C.; Christen, B.; Fuchs, T.; Sundaram, V.; Watanabe, K.; Jenal, U. Genetic Analysis of a Novel Pathway for D-Xylose Metabolism in *Caulobacter crescentus*. *J. Bacteriol.* **2007,** *189* (5), 2181–2185.
577. Watanabe, S.; Shimada, N.; Tajima, K.; Kodaki, T.; Makino, K. Identification and Characterization of L-Arabonate Dehydratase, L-2-Keto-3-Deoxyarabonate Dehydratase, and L-Arabinolactonase Involved in an Alternative Pathway of L-Arabinose Metabolism. Novel Evolutionary Insight into Sugar Metabolism. *J. Biol. Chem.* **2006,** *281* (44), 33521–33536.
578. Watanabe, S.; Fukumori, F.; Nishiwaki, H.; Sakurai, Y.; Tajima, K.; Watanabe, Y. Novel Non-phosphorylative Pathway of Pentose Metabolism from Bacteria. *Sci. Rep.* **2019,** *9* (1), 155.
579. Flint, D. H.; Emptage, M. H. Dihydroxy Acid Dehydratase from Spinach Contains a [2Fe-2S] Cluster. *J. Biol. Chem.* **1988,** *263* (8), 3558–3564.
580. Rahman, M. M.; Andberg, M.; Thangaraj, S. K.; Parkkinen, T.; Penttila, M.; Janis, J.; Koivula, A.; Rouvinen, J.; Hakulinen, N. The Crystal Structure of a Bacterial L-Arabinonate Dehydratase Contains a [2Fe-2S] Cluster. *ACS Chem. Biol.* **2017,** *12* (7), 1919–1927.
581. Moss, J.; Vaughan, M. ADP-Ribosylation of Guanyl Nucleotide-Binding Regulatory Proteins by Bacterial Toxins. *Adv. Enzymol. Relat. Areas Mol. Biol.* **1988,** *61,* 303–379.
582. Corda, D.; Di Girolamo, M. Functional Aspects of Protein Mono-ADP-Ribosylation. *EMBO J.* **2003,** *22* (9), 1953–1958.
583. Catara, G.; Corteggio, A.; Valente, C.; Grimaldi, G.; Palazzo, L. Targeting ADP-Ribosylation as an Antimicrobial Strategy. *Biochem. Pharmacol.* **2019,** *167,* 13–26.
584. Castagnini, M.; Picchianti, M.; Talluri, E.; Biagini, M.; Del Vecchio, M.; Di Procolo, P.; Norais, N.; Nardi-Dei, V.; Balducci, E. Arginine-Specific Mono ADP-Ribosylation In Vitro of Antimicrobial Peptides by ADP-Ribosylating Toxins. *PLoS One* **2012,** *7* (8), e41417.
585. Munnur, D.; Ahel, I. Reversible Mono-ADP-Ribosylation of DNA Breaks. *FEBS J.* **2017,** *284* (23), 4002–4016.
586. Baysarowich, J.; Koteva, K.; Hughes, D. W.; Ejim, L.; Griffiths, E.; Zhang, K.; Junop, M.; Wright, G. D. Rifamycin Antibiotic Resistance by ADP-Ribosylation: Structure and Diversity of Arr. *Proc. Natl. Acad. Sci. U. S. A.* **2008,** *105* (12), 4886–4891.
587. Masignani, V.; Balducci, E.; Di Marcello, F.; Savino, S.; Serruto, D.; Veggi, D.; Bambini, S.; Scarselli, M.; Arico, B.; Comanducci, M.; Adu-Bobie, J.; Giuliani, M. M.; Rappuoli, R.; Pizza, M. NarE: A Novel ADP-Ribosyltransferase from *Neisseria meningitidis*. *Mol. Microbiol.* **2003,** *50* (3), 1055–1067.
588. Masignani, V.; Balducci, E.; Serruto, D.; Veggi, D.; Arico, B.; Comanducci, M.; Pizza, M.; Rappuoli, R. *In Silico* Identification of Novel Bacterial ADP-Ribosyltransferases. *Int. J. Med. Microbiol.* **2004,** *293* (7-8), 471–478.
589. Valeri, M.; Zurli, V.; Ayala, I.; Colanzi, A.; Lapazio, L.; Corda, D.; Soriani, M.; Pizza, M.; Rossi Paccani, S. The *Neisseria meningitidis* ADP-Ribosyltransferase NarE Enters Human Epithelial Cells and Disrupts Epithelial Monolayer Integrity. *PLoS One* **2015,** *10* (5), e0127614.
590. Del Vecchio, M.; Pogni, R.; Baratto, M. C.; Nobbs, A.; Rappuoli, R.; Pizza, M.; Balducci, E. Identification of an Iron-Sulfur Cluster that Modulates the Enzymatic Activity in NarE, a *Neisseria meningitidis* ADP-Ribosyltransferase. *J. Biol. Chem.* **2009,** *284* (48), 33040–33047.
591. Carlier, L.; Koehler, C.; Veggi, D.; Pizza, M.; Soriani, M.; Boelens, R.; Bonvin, A. M. NMR Resonance Assignments of NarE, a Putative ADP-Ribosylating Toxin from *Neisseria meningitidis*. *Biomol. NMR Assign.* **2011,** *5* (1), 35–38.
592. Del Vecchio, M.; Balducci, E. Opposite Regulatory Effects of Iron Ions on the *In Vitro* Catalytic Activities of NarE, the Toxin-like ADP-Ribosyltransferase from *Neisseria Meningitides*. *Biochem. Anal. Biochem.* **2015,** *04* (04).
593. Hedderich, R.; Hamann, N.; Bennati, M. Heterodisulfide Reductase from Methanogenic Archaea: A New Catalytic Role for an Iron-Sulfur Cluster. *Biol. Chem.* **2005,** *386* (10), 961–970.
594. Walters, E. M.; Johnson, M. K. Ferredoxin:Thioredoxin Reductase: Disulfide Reduction Catalyzed Via Novel Site-Specific [4Fe-4S] Cluster Chemistry. *Photosynth. Res.* **2004,** *79* (3), 249–264.
595. Yu, H.; Haja, D. K.; Schut, G. J.; Wu, C. H.; Meng, X.; Zhao, G.; Li, H.; Adams, M. W. W. Structure of the Respiratory MBS Complex Reveals Iron-Sulfur Cluster Catalyzed Sulfane Sulfur Reduction in Ancient Life. *Nat. Commun.* **2020,** *11* (1), 5953.
596. Tchong, S. I.; Xu, H.; White, R. H. L-Cysteine Desulfidase: An [4Fe-4S] Enzyme Isolated from *Methanocaldococcus jannaschii* that Catalyzes the Breakdown of L-Cysteine into Pyruvate, Ammonia, and Sulfide. *Biochemistry* **2005,** *44* (5), 1659–1670.
597. Mendez, J.; Reimundo, P.; Perez-Pascual, D.; Navais, R.; Gomez, E.; Guijarro, J. A. A Novel cdsAB Operon Is Involved in the Uptake of L-Cysteine and Participates in the Pathogenesis of *Yersinia ruckeri*. *J. Bacteriol.* **2011,** *193* (4), 944–951.
598. Loddeke, M.; Schneider, B.; Oguri, T.; Mehta, I.; Xuan, Z.; Reitzer, L. Anaerobic Cysteine Degradation and Potential Metabolic Coordination in *Salmonella enterica* and *Escherichia coli*. *J. Bacteriol.* **2017,** *199* (16).
599. Waldron, K. J.; Rutherford, J. C.; Ford, D.; Robinson, N. J. Metalloproteins and metal sensing. *Nature* **2009,** *460* (7257), 823–830.

600. Halliwell, B.; Gutteridge, J. M. Biologically Relevant Metal Ion-Dependent Hydroxyl Radical Generation. An Update. *FEBS Lett.* **1992,** *307* (1), 108–112.
601. Cairo, G.; Recalcati, S.; Pietrangelo, A.; Minotti, G. The Iron Regulatory Proteins: Targets and Modulators of Free Radical Reactions and Oxidative Damage. *Free Radic. Biol. Med.* **2002,** *32* (12), 1237–1243.
602. Rouault, T. A. The Role of Iron Regulatory Proteins in Mammalian Iron Homeostasis and Disease. *Nat. Chem. Biol.* **2006,** *2* (8), 406–414.
603. Hanson, E. S.; Leibold, E. A. Regulation of the Iron Regulatory Proteins by Reactive Nitrogen and Oxygen Species. *Gene Expr.* **1999,** *7* (4-6), 367–376.
604. Khan, M. A.; Walden, W. E.; Goss, D. J.; Theil, E. C. Direct Fe2+ Sensing by Iron-Responsive Messenger RNA:Repressor Complexes Weakens Binding. *J. Biol. Chem.* **2009,** *284* (44), 30122–30128.
605. Stys, A.; Galy, B.; Starzynski, R. R.; Smuda, E.; Drapier, J. C.; Lipinski, P.; Bouton, C. Iron Regulatory Protein 1 Outcompetes Iron Regulatory Protein 2 in Regulating Cellular Iron Homeostasis in Response to Nitric Oxide. *J. Biol. Chem.* **2011,** *286* (26), 22846–22854.
606. Jeffery, C. J. Moonlighting Proteins-an Update. *Mol. Biosyst.* **2009,** *5* (4), 345–350.
607. Leipuviene, R.; Theil, E. C. The Family of Iron Responsive RNA Structures Regulated by Changes in Cellular Iron and Oxygen. *Cell. Mol. Life Sci.* **2007,** *64* (22), 2945–2955.
608. Hentze, M. W.; Muckenthaler, M. U.; Galy, B.; Camaschella, C. Two to Tango: Regulation of Mammalian Iron Metabolism. *Cell* **2010,** *142* (1), 24–38.
609. Anderson, C. P.; Shen, M.; Eisenstein, R. S.; Leibold, E. A. Mammalian Iron Metabolism and Its Control by Iron Regulatory Proteins. *Biochim. Biophys. Acta* **2012,** *1823* (9), 1468–1483.
610. Meyron-Holtz, E. G.; Ghosh, M. C.; Rouault, T. A. Mammalian Tissue Oxygen Levels Modulate Iron-Regulatory Protein Activities *In Vivo*. *Science* **2004,** *306* (5704), 2087–2090.
611. Pantopoulos, K.; Hentze, M. W. Activation of Iron Regulatory Protein-1 by Oxidative Stress *In Vitro*. *Proc. Natl. Acad. Sci. U. S. A.* **1998,** *95* (18), 10559–10563.
612. Soum, E.; Brazzolotto, X.; Goussias, C.; Bouton, C.; Moulis, J. M.; Mattioli, T. A.; Drapier, J. C. Peroxynitrite and Nitric Oxide Differently Target the Iron-Sulfur Cluster and Amino Acid Residues of Human Iron Regulatory Protein 1. *Biochemistry* **2003,** *42* (25), 7648–7654.
613. Brazzolotto, X.; Gaillard, J.; Pantopoulos, K.; Hentze, M. W.; Moulis, J. M. Human Cytoplasmic Aconitase (Iron Regulatory Protein 1) Is Converted into its [3Fe-4S] Form by Hydrogen Peroxide In Vitro but Is Not Activated for Iron-Responsive Element Binding. *J. Biol. Chem.* **1999,** *274* (31), 21625–21630.
614. Brown, N. M.; Kennedy, M. C.; Antholine, W. E.; Eisenstein, R. S.; Walden, W. E. Detection of a [3Fe-4S] Cluster intermediate of Cytosolic Aconitase in Yeast Expressing Iron Regulatory Protein 1. Insights into the Mechanism of Fe-S Cluster Cycling. *J. Biol. Chem.* **2002,** *277* (9), 7246–7254.
615. Soum, E.; Drapier, J. C. Nitric Oxide and Peroxynitrite Promote Complete Disruption of the [4Fe-4S] Cluster of Recombinant Human Iron Regulatory Protein 1. *J. Biol. Inorg. Chem.* **2003,** *8* (1-2), 226–232.
616. Deck, K. M.; Vasanthakumar, A.; Anderson, S. A.; Goforth, J. B.; Kennedy, M. C.; Antholine, W. E.; Eisenstein, R. S. Evidence that Phosphorylation of Iron Regulatory Protein 1 at Serine 138 Destabilizes the [4Fe-4S] Cluster in Cytosolic Aconitase by Enhancing 4Fe-3Fe Cycling. *J. Biol. Chem.* **2009,** *284* (19), 12701–12709.
617. Clarke, S. L.; Vasanthakumar, A.; Anderson, S. A.; Pondarre, C.; Koh, C. M.; Deck, K. M.; Pitula, J. S.; Epstein, C. J.; Fleming, M. D.; Eisenstein, R. S. Iron-Responsive Degradation of Iron-Regulatory Protein 1 Does Not Require the Fe-S Cluster. *EMBO J.* **2006,** *25* (3), 544–553.
618. Walden, W. E.; Selezneva, A. I.; Dupuy, J.; Volbeda, A.; Fontecilla-Camps, J. C.; Theil, E. C.; Volz, K. Structure of Dual Function Iron Regulatory Protein 1 Complexed with Ferritin IRE-RNA. *Science* **2006,** *314* (5807), 1903–1908.
619. Samaniego, F.; Chin, J.; Iwai, K.; Rouault, T. A.; Klausner, R. D. Molecular Characterization of a Second Iron-Responsive Element Binding Protein, Iron Regulatory Protein 2. Structure, Function, and Post-Translational Regulation. *J. Biol. Chem.* **1994,** *269* (49), 30904–30910.
620. Theil, E. C.; Goss, D. J. Living with Iron (and Oxygen): Questions and Answers about Iron Homeostasis. *Chem. Rev.* **2009,** *109* (10), 4568–4579.
621. Salahudeen, A. A.; Thompson, J. W.; Ruiz, J. C.; Ma, H. W.; Kinch, L. N.; Li, Q.; Grishin, N. V.; Bruick, R. K. An E3 Ligase Possessing an Iron-Responsive Hemerythrin Domain Is a Regulator of Iron Homeostasis. *Science* **2009,** *326* (5953), 722–726.
622. Vashisht, A. A.; Zumbrennen, K. B.; Huang, X.; Powers, D. N.; Durazo, A.; Sun, D.; Bhaskaran, N.; Persson, A.; Uhlen, M.; Sangfelt, O.; Spruck, C.; Leibold, E. A.; Wohlschlegel, J. A. Control of Iron Homeostasis by an Iron-Regulated Ubiquitin Ligase. *Science* **2009,** *326* (5953), 718–721.
623. Wang, H.; Shi, H.; Rajan, M.; Canarie, E. R.; Hong, S.; Simoneschi, D.; Pagano, M.; Bush, M. F.; Stoll, S.; Leibold, E. A.; Zheng, N. FBXL5 Regulates IRP2 Stability in Iron Homeostasis Via an Oxygen-Responsive [2Fe2S] Cluster. *Mol. Cell* **2020,** *78* (1), 31-41 e5.
624. Chollangi, S.; Thompson, J. W.; Ruiz, J. C.; Gardner, K. H.; Bruick, R. K. Hemerythrin-Like Domain within F-Box and Leucine-Rich Repeat Protein 5 (FBXL5) Communicates Cellular Iron and Oxygen Availability by Distinct Mechanisms. *J. Biol. Chem.* **2012,** *287* (28), 23710–23717.
625. Thompson, J. W.; Salahudeen, A. A.; Chollangi, S.; Ruiz, J. C.; Brautigam, C. A.; Makris, T. M.; Lipscomb, J. D.; Tomchick, D. R.; Bruick, R. K. Structural and Molecular Characterization of Iron-Sensing Hemerythrin-like Domain within F-Box and Leucine-Rich Repeat Protein 5 (FBXL5). *J. Biol. Chem.* **2012,** *287* (10), 7357–7365.
626. Shu, C.; Sung, M. W.; Stewart, M. D.; Igumenova, T. I.; Tan, X.; Li, P. The Structural Basis of Iron Sensing by the Human F-Box Protein FBXL5. *ChemBioChem* **2012,** *13* (6), 788–791.
627. Erlitzki, R.; Long, J. C.; Theil, E. C. Multiple, Conserved Iron-Responsive Elements in the 3′-Untranslated Region of Transferrin Receptor mRNA Enhance Binding of Iron Regulatory Protein 2. *J. Biol. Chem.* **2002,** *277* (45), 42579–42587.
628. Smith, S. R.; Ghosh, M. C.; Ollivierre-Wilson, H.; Hang Tong, W.; Rouault, T. A. Complete Loss of Iron Regulatory Proteins 1 and 2 Prevents Viability of Murine Zygotes beyond the Blastocyst Stage of Embryonic Development. *Blood Cells Mol. Dis.* **2006,** *36* (2), 283–287.
629. Meyron-Holtz, E. G.; Ghosh, M. C.; Iwai, K.; LaVaute, T.; Brazzolotto, X.; Berger, U. V.; Land, W.; Ollivierre-Wilson, H.; Grinberg, A.; Love, P.; Rouault, T. A. Genetic Ablations of Iron Regulatory Proteins 1 and 2 Reveal why Iron Regulatory Protein 2 Dominates Iron Homeostasis. *EMBO J.* **2004,** *23* (2), 386–395.
630. Zhang, D. L.; Ghosh, M. C.; Rouault, T. A. The Physiological Functions of Iron Regulatory Proteins in Iron Homeostasis - An Update. *Front. Pharmacol.* **2014,** *5,* 124.
631. Terzi, E. M.; Sviderskiy, V. O.; Alvarez, S. W.; Whiten, G. C.; Possemato, R. Iron-Sulfur Cluster Deficiency Can Be Sensed by IRP2 and Regulates Iron Homeostasis and Sensitivity to Ferroptosis Independent of IRP1 and FBXL5. *Sci. Adv.* **2021,** *7* (22).
632. Sun, F.; Ji, Q.; Jones, M. B.; Deng, X.; Liang, H.; Frank, B.; Telser, J.; Peterson, S. N.; Bae, T.; He, C. AirSR, a [2Fe-2S] Cluster-Containing Two-Component System, Mediates Global Oxygen Sensing and Redox Signaling in *Staphylococcus aureus*. *J. Am. Chem. Soc.* **2012,** *134* (1), 305–314.
633. Poor, C. B.; Wegner, S. V.; Li, H.; Dlouhy, A. C.; Schuermann, J. P.; Sanishvili, R.; Hinshaw, J. R.; Riggs-Gelasco, P. J.; Outten, C. E.; He, C. Molecular Mechanism and Structure of the *Saccharomyces cerevisiae* Iron Regulator Aft2. *Proc. Natl. Acad. Sci. U. S. A.* **2014,** *111* (11), 4043–4048.
634. Li, H.; Outten, C. E. The Conserved CDC Motif in the Yeast Iron Regulator Aft2 Mediates Iron-Sulfur Cluster Exchange and Protein-Protein Interactions with Grx3 and Bol2. *J. Biol. Inorg. Chem.* **2019,** *24* (6), 809–815.
635. Mettert, E. L.; Kiley, P. J. Fe-S Proteins that Regulate Gene Expression. *Biochim. Biophys. Acta* **2015,** *1853* (6), 1284–1293.
636. Shepard, W.; Soutourina, O.; Courtois, E.; England, P.; Haouz, A.; Martin-Verstraete, I. Insights into the Rrf2 Repressor Family-the Structure of CymR, the Global Cysteine Regulator of *Bacillus subtilis*. *FEBS J.* **2011,** *278* (15), 2689–2701.
637. Schwartz, C. J.; Giel, J. L.; Patschkowski, T.; Luther, C.; Ruzicka, F. J.; Beinert, H.; Kiley, P. J. IscR, an Fe-S Cluster-Containing Transcription Factor, Represses Expression of *Escherichia coli* Genes Encoding Fe-S Cluster Assembly Proteins. *Proc. Natl. Acad. Sci. U. S. A.* **2001,** *98* (26), 14895–14900.
638. Yeo, W. S.; Lee, J. H.; Lee, K. C.; Roe, J. H. IscR Acts as an Activator in Response to Oxidative Stress for the Suf Operon Encoding Fe-S Assembly Proteins. *Mol. Microbiol.* **2006,** *61* (1), 206–218.
639. Xu, X. M.; Moller, S. G. Iron-Sulfur Cluster Biogenesis Systems and their Crosstalk. *ChemBioChem* **2008,** *9* (15), 2355–2362.
640. Giel, J. L.; Rodionov, D.; Liu, M.; Blattner, F. R.; Kiley, P. J. IscR-Dependent Gene Expression Links Iron-Sulphur Cluster Assembly to the Control of O_2-Regulated Genes in *Escherichia coli*. *Mol. Microbiol.* **2006,** *60* (4), 1058–1075.
641. Rajagopalan, S.; Teter, S. J.; Zwart, P. H.; Brennan, R. G.; Phillips, K. J.; Kiley, P. J. Studies of IscR Reveal a Unique Mechanism for Metal-Dependent Regulation of DNA Binding Specificity. *Nat. Struct. Mol. Biol.* **2013,** *20* (6), 740–747.

642. Zeng, J.; Zhang, X.; Wang, Y.; Ai, C.; Liu, Q.; Qiu, G. Glu43 Is an Essential Residue for Coordinating the [Fe2S2] Cluster of IscR from *Acidithiobacillus ferrooxidans*. *FEBS Lett.* **2008,** *582* (28), 3889–3892.
643. Fleischhacker, A. S.; Stubna, A.; Hsueh, K. L.; Guo, Y.; Teter, S. J.; Rose, J. C.; Brunold, T. C.; Markley, J. L.; Munck, E.; Kiley, P. J. Characterization of the [2Fe-2S] Cluster of *Escherichia coli* Transcription Factor IscR. *Biochemistry* **2012,** *51* (22), 4453–4462.
644. Todd, J. D.; Wexler, M.; Sawers, G.; Yeoman, K. H.; Poole, P. S.; Johnston, A. W. B. RirA, an Iron-Responsive Regulator in the Symbiotic Bacterium *Rhizobium leguminosarum*. *Microbiology* **2002,** *148* (Pt 12), 4059–4071.
645. Chao, T. C.; Buhrmester, J.; Hansmeier, N.; Puhler, A.; Weidner, S. Role of the Regulatory Gene *rirA* in the Transcriptional Response of *Sinorhizobium meliloti* to Iron Limitation. *Appl. Environ. Microbiol.* **2005,** *71* (10), 5969–5982.
646. Todd, J. D.; Sawers, G.; Johnston, A. W. Proteomic Analysis Reveals the Wide-Ranging Effects of the Novel, Iron-Responsive Regulator RirA in *Rhizobium leguminosarum* Bv. Viciae. *Mol. Genet. Genomics* **2005,** *273* (2), 197–206.
647. Johnston, A. W.; Todd, J. D.; Curson, A. R.; Lei, S.; Nikolaidou-Katsaridou, N.; Gelfand, M. S.; Rodionov, D. A. Living without Fur: The Subtlety and Complexity of Iron-Responsive Gene Regulation in the Symbiotic Bacterium *Rhizobium* and Other Alpha-Proteobacteria. *Biometals* **2007,** *20* (3-4), 501–511.
648. Rodionov, D. A.; Gelfand, M. S.; Todd, J. D.; Curson, A. R.; Johnston, A. W. Computational Reconstruction of Iron- and Manganese-Responsive Transcriptional Networks in Alpha-Proteobacteria. *PLoS Comput. Biol.* **2006,** *2* (12), e163.
649. Pellicer Martinez, M. T.; Martinez, A. B.; Crack, J. C.; Holmes, J. D.; Svistunenko, D. A.; Johnston, A. W. B.; Cheesman, M. R.; Todd, J. D.; Le Brun, N. E. Sensing Iron Availability Via the Fragile [4Fe-4S] Cluster of the Bacterial Transcriptional Repressor RirA. *Chem. Sci.* **2017,** *8* (12), 8451–8463.
650. Pellicer Martinez, M. T.; Crack, J. C.; Stewart, M. Y.; Bradley, J. M.; Svistunenko, D. A.; Johnston, A. W.; Cheesman, M. R.; Todd, J. D.; Le Brun, N. E. Mechanisms of Iron- and O2-Sensing by the [4Fe-4S] Cluster of the Global Iron Regulator RirA. *Elife* **2019,** *8*.
651. Behringer, M.; Plotzky, L.; Baabe, D.; Zaretzke, M. K.; Schweyen, P.; Broring, M.; Jahn, D.; Hartig, E. RirA of *Dinoroseobacter shibae* Senses Iron Via a $[3Fe\text{-}4S]^{1+}$ Cluster Co-Ordinated by Three Cysteine Residues. *Biochem. J.* **2020,** *477* (1), 191–212.
652. Chhabra, S.; Spiro, S. Inefficient Translation of *nsrR* Constrains Behaviour of the NsrR Regulon in *Escherichia coli*. *Microbiology* **2015,** *161* (10), 2029–2038.
653. Tucker, N. P.; Le Brun, N. E.; Dixon, R.; Hutchings, M. I. There's NO Stopping NsrR, a Global Regulator of the Bacterial NO Stress Response. *Trends Microbiol.* **2010,** *18* (4), 149–156.
654. Bonamore, A.; Boffi, A. Flavohemoglobin: Structure and Reactivity. *IUBMB Life* **2008,** *60* (1), 19–28.
655. Gilberthorpe, N. J.; Poole, R. K. Nitric Oxide Homeostasis in *Salmonella typhimurium*: Roles of Respiratory Nitrate Reductase and Flavohemoglobin. *J. Biol. Chem.* **2008,** *283* (17), 11146–11154.
656. Crack, J. C.; Svistunenko, D. A.; Munnoch, J.; Thomson, A. J.; Hutchings, M. I.; Le Brun, N. E. Differentiated, Promoter-Specific Response of [4Fe-4S] NsrR DNA Binding to Reaction with Nitric Oxide. *J. Biol. Chem.* **2016,** *291* (16), 8663–8672.
657. Yukl, E. T.; Elbaz, M. A.; Nakano, M. M.; Moenne-Loccoz, P. Transcription Factor NsrR from *Bacillus subtilis* Senses Nitric Ooxide with a 4Fe-4S Cluster. *Biochemistry* **2008,** *47* (49), 13084–13092.
658. Tucker, N. P.; Hicks, M. G.; Clarke, T. A.; Crack, J. C.; Chandra, G.; Le Brun, N. E.; Dixon, R.; Hutchings, M. I. The Transcriptional Repressor Protein NsrR Senses Nitric Oxide Directly Via a [2Fe-2S] Cluster. *PLoS One* **2008,** *3* (11), e3623.
659. Partridge, J. D.; Bodenmiller, D. M.; Humphrys, M. S.; Spiro, S. NsrR Targets in the *Escherichia coli* Genome: New Insights into DNA Sequence Requirements for Binding and a Role for NsrR in the Regulation of Motility. *Mol. Microbiol.* **2009,** *73* (4), 680–694.
660. Gilberthorpe, N. J.; Lee, M. E.; Stevanin, T. M.; Read, R. C.; Poole, R. K. NsrR: A Key Regulator Circumventing *Salmonella Enterica* Serovar Typhimurium Oxidative and Nitrosative Stress In Vitro and in IFN-Gamma-Stimulated J774.2 Macrophages. *Microbiology* **2007,** *153* (Pt 6), 1756–1771.
661. Rock, J. D.; Thomson, M. J.; Read, R. C.; Moir, J. W. Regulation of Denitrification Genes in *Neisseria meningitidis* by Nitric Oxide and the Repressor NsrR. *J. Bacteriol.* **2007,** *189* (3), 1138–1144.
662. Isabella, V. M.; Lapek, J. D., Jr.; Kennedy, E. M.; Clark, V. L. Functional Analysis of NsrR, a Nitric Oxide-Sensing Rrf2 Repressor in *Neisseria gonorrhoeae*. *Mol. Microbiol.* **2009,** *71* (1), 227–239.
663. Beaumont, H. J.; Lens, S. I.; Reijnders, W. N.; Westerhoff, H. V.; van Spanning, R. J. Expression of Nitrite Reductase in *Nitrosomonas europaea* Involves NsrR, a Novel Nitrite-Sensitive Transcription Repressor. *Mol. Microbiol.* **2004,** *54* (1), 148–158.
664. Couture, M. M.; Colbert, C. L.; Babini, E.; Rosell, F. I.; Mauk, A. G.; Bolin, J. T.; Eltis, L. D. Characterization of BphF, a Rieske-Type Ferredoxin with a Low Reduction Potential. *Biochemistry* **2001,** *40* (1), 84–92.
665. Kommineni, S.; Yukl, E.; Hayashi, T.; Delepine, J.; Geng, H.; Moenne-Loccoz, P.; Nakano, M. M. Nitric Oxide-Sensitive and -Insensitive Interaction of *Bacillus subtilis* NsrR with a ResDE-Controlled Promoter. *Mol. Microbiol.* **2010,** *78* (5), 1280–1293.
666. Crack, J. C.; Munnoch, J.; Dodd, E. L.; Knowles, F.; Al Bassam, M. M.; Kamali, S.; Holland, A. A.; Cramer, S. P.; Hamilton, C. J.; Johnson, M. K.; Thomson, A. J.; Hutchings, M. I.; Le Brun, N. E. NsrR from *Streptomyces coelicolor* Is a Nitric Oxide-Sensing [4Fe-4S] Cluster Protein with a Specialized Regulatory Function. *J. Biol. Chem.* **2015,** *290* (20), 12689–12704.
667. Volbeda, A.; Dodd, E. L.; Darnault, C.; Crack, J. C.; Renoux, O.; Hutchings, M. I.; Le Brun, N. E.; Fontecilla-Camps, J. C. Crystal Structures of the NO Sensor NsrR Reveal how its Iron-Sulfur Cluster Modulates DNA Binding. *Nat. Commun.* **2017,** *8,* 15052.
668. Crack, J. C.; Le Brun, N. E. Biological Iron-Sulfur Clusters: Mechanistic Insights from Mass Spectrometry. *Coord. Chem. Rev.* **2021,** 448.
669. Crack, J. C.; Le Brun, N. E. Mass Spectrometric Identification of [4Fe-4S](NO)x Intermediates of Nitric Oxide Sensing by Regulatory Iron-Sulfur Cluster Proteins. *Chemistry* **2019,** *25* (14), 3675–3684.
670. Crack, J. C.; Hamilton, C. J.; Le Brun, N. E. Mass Spectrometric Detection of Iron Nitrosyls, Sulfide Oxidation and Mycothiolation during Nitrosylation of the NO Sensor [4Fe-4S] NsrR. *Chem. Commun. (Camb.)* **2018,** *54* (47), 5992–5995.
671. Serrano, P. N.; Wang, H.; Crack, J. C.; Prior, C.; Hutchings, M. I.; Thomson, A. J.; Kamali, S.; Yoda, Y.; Zhao, J.; Hu, M. Y.; Alp, E. E.; Oganesyan, V. S.; Le Brun, N. E.; Cramer, S. P. Nitrosylation of Nitric-Oxide-Sensing Regulatory Proteins Containing [4Fe-4S] Clusters Gives Rise to Multiple Iron-Nitrosyl Complexes. *Angew. Chem. Int. Ed. Engl.* **2016,** *55* (47), 14575–14579.
672. Munnoch, J. T.; Martinez, M. T.; Svistunenko, D. A.; Crack, J. C.; Le Brun, N. E.; Hutchings, M. I. Characterization of a Putative NsrR Homologue in *Streptomyces venezuelae* Reveals a New Member of the Rrf2 Superfamily. *Sci. Rep.* **2016,** *6,* 31597.
673. Crack, J. C.; Gaskell, A. A.; Green, J.; Cheesman, M. R.; Le Brun, N. E.; Thomson, A. J. Influence of the Environment on the [4Fe-4S]2+ to [2Fe-2S]2+ Cluster Switch in the Transcriptional Regulator FNR. *J. Am. Chem. Soc.* **2008,** *130* (5), 1749–1758.
674. Green, J.; Paget, M. S. Bacterial Redox Sensors. *Nat. Rev. Microbiol.* **2004,** *2* (12), 954–966.
675. Salmon, K.; Hung, S. P.; Mekjian, K.; Baldi, P.; Hatfield, G. W.; Gunsalus, R. P. Global Gene Expression Profiling in *Escherichia coli* K12. The Effects of Oxygen Availability and FNR. *J. Biol. Chem.* **2003,** *278* (32), 29837–29855.
676. Tolla, D. A.; Savageau, M. A. Regulation of Aerobic-to-Anaerobic Transitions by the FNR Cycle in *Escherichia coli*. *J. Mol. Biol.* **2010,** *397* (4), 893–905.
677. Lazazzera, B. A.; Beinert, H.; Khoroshilova, N.; Kennedy, M. C.; Kiley, P. J. DNA Binding and Dimerization of the Fe-S-Containing FNR Protein from *Escherichia coli* Are Regulated by Oxygen. *J. Biol. Chem.* **1996,** *271* (5), 2762–2768.
678. Cruz-Ramos, H.; Crack, J.; Wu, G.; Hughes, M. N.; Scott, C.; Thomson, A. J.; Green, J.; Poole, R. K. NO Sensing by FNR: Regulation of the *Escherichia Coli* NO-Detoxifying Flavohaemoglobin, Hmp. *EMBO J.* **2002,** *21* (13), 3235–3244.
679. Crack, J. C.; Le Brun, N. E. Redox-Sensing Iron-Sulfur Cluster Regulators. *Antioxid. Redox Signal.* **2018,** *29* (18), 1809–1829.

680. Jervis, A. J.; Crack, J. C.; White, G.; Artymiuk, P. J.; Cheesman, M. R.; Thomson, A. J.; Le Brun, N. E.; Green, J. The O2 Sensitivity of the Transcription Factor FNR Is Controlled by Ser24 Modulating the Kinetics of [4Fe-4S] to [2Fe-2S] Conversion. *Proc. Natl. Acad. Sci. U. S. A.* **2009,** *106* (12), 4659–4664.
681. Crack, J.; Green, J.; Thomson, A. J. Mechanism of Oxygen Sensing by the Bacterial Transcription Factor Fumarate-Nitrate Reduction (FNR). *J. Biol. Chem.* **2004,** *279* (10), 9278–9286.
682. Crack, J. C.; Green, J.; Cheesman, M. R.; Le Brun, N. E.; Thomson, A. J. Superoxide-Mediated Amplification of the Oxygen-Induced Switch from [4Fe-4S] to [2Fe-2S] Clusters in the Transcriptional Regulator FNR. *Proc. Natl. Acad. Sci. U. S. A.* **2007,** *104* (7), 2092–2097.
683. Crack, J. C.; Green, J.; Le Brun, N. E.; Thomson, A. J. Detection of Sulfide Release from the Oxygen-Sensing [4Fe-4S] Cluster of FNR. *J. Biol. Chem.* **2006,** *281* (28), 18909–18913.
684. Crack, J. C.; Thomson, A. J.; Le Brun, N. E. Mass Spectrometric Identification of Intermediates in the O_2-Driven [4Fe-4S] to [2Fe-2S] Cluster Conversion in FNR. *Proc. Natl. Acad. Sci. U. S. A.* **2017,** *114* (16), E3215–E3223.
685. Zhang, B.; Crack, J. C.; Subramanian, S.; Green, J.; Thomson, A. J.; Le Brun, N. E.; Johnson, M. K. Reversible Cycling between Cysteine Persulfide-Ligated [2Fe-2S] and Cysteine-Ligated [4Fe-4S] Clusters in the FNR Regulatory Protein. *Proc. Natl. Acad. Sci. U. S. A.* **2012,** *109* (39), 15734–15739.
686. Reinhart, F.; Achebach, S.; Koch, T.; Unden, G. Reduced Apo-Fumarate Nitrate Reductase Regulator (apoFNR) as the Major Form of FNR in Aerobically Growing *Escherichia coli*. *J. Bacteriol.* **2008,** *190* (3), 879–886.
687. Jervis, A. J.; Green, J. In Vivo Demonstration of FNR Dimers in Response to Lower O(2) Availability. *J. Bacteriol.* **2007,** *189* (7), 2930–2932.
688. Popescu, C. V.; Bates, D. M.; Beinert, H.; Munck, E.; Kiley, P. J. Mossbauer Spectroscopy as a Tool for the Study of Activation/Inactivation of the Transcription Regulator FNR in Whole Cells of *Escherichia coli*. *Proc. Natl. Acad. Sci. U. S. A.* **1998,** *95* (23), 13431–13435.
689. Moore, L. J.; Kiley, P. J. Characterization of the Dimerization Domain in the FNR Transcription Factor. *J. Biol. Chem.* **2001,** *276* (49), 45744–45750.
690. Moore, L. J.; Mettert, E. L.; Kiley, P. J. Regulation of FNR Dimerization by Subunit Charge Repulsion. *J. Biol. Chem.* **2006,** *281* (44), 33268–33275.
691. Volbeda, A.; Darnault, C.; Renoux, O.; Nicolet, Y.; Fontecilla-Camps, J. C. The Crystal Structure of the Global Anaerobic Transcriptional Regulator FNR Explains its Extremely Fine-Tuned Monomer-Dimer Equilibrium. *Sci. Adv.* **2015,** *1* (11), e1501086.
692. Mettert, E. L.; Kiley, P. J. Reassessing the Structure and Function Relationship of the O_2 Sensing Transcription Factor FNR. *Antioxid. Redox Signal.* **2018,** *29* (18), 1830–1840.
693. Crack, J. C.; Le Brun, N. E.; Thomson, A. J.; Green, J.; Jervis, A. J. Reactions of Nitric Oxide and Oxygen with the Regulator of Fumarate and Nitrate Reduction, a Global Transcriptional Regulator, during Anaerobic Growth of *Escherichia coli*. *Methods Enzymol.* **2008,** *437,* 191–209.
694. Pullan, S. T.; Gidley, M. D.; Jones, R. A.; Barrett, J.; Stevanin, T. M.; Read, R. C.; Green, J.; Poole, R. K. Nitric Oxide in Chemostat-Cultured *Escherichia coli* Is Sensed by Fnr and Other Global Regulators: Unaltered Methionine Biosynthesis Indicates Lack of S Nitrosation. *J. Bacteriol.* **2007,** *189* (5), 1845–1855.
695. Justino, M. C.; Vicente, J. B.; Teixeira, M.; Saraiva, L. M. New Genes Implicated in the Protection of Anaerobically Grown *Escherichia coli* against Nitric Oxide. *J. Biol. Chem.* **2005,** *280* (4), 2636–2643.
696. Hutchings, M. I.; Crack, J. C.; Shearer, N.; Thompson, B. J.; Thomson, A. J.; Spiro, S. Transcription Factor FnrP from *Paracoccus denitrificans* Contains an Iron-Sulfur Cluster and Is Activated by Anoxia: Identification of Essential Cysteine Residues. *J. Bacteriol.* **2002,** *184* (2), 503–508.
697. Edwards, J.; Cole, L. J.; Green, J. B.; Thomson, M. J.; Wood, A. J.; Whittingham, J. L.; Moir, J. W. Binding to DNA Protects *Neisseria meningitidis* Fumarate and Nitrate Reductase Regulator (FNR) from Oxygen. *J. Biol. Chem.* **2010,** *285* (2), 1105–1112.
698. Wu, G.; Hill, S.; Kelly, M. J. S.; Sawers, G.; Poole, R. K. The *cydR* Gene Product, Required for Regulation of Cytochrome *bd* Expression in the Obligate Aerobe *Azotobacter vinelandii*, Is an Fnr-Like Protein. *Microbiology* **1997,** *143* (Pt 7), 2197–2207.
699. Wu, G.; Cruz-Ramos, H.; Hill, S.; Green, J.; Sawers, G.; Poole, R. K. Regulation of Cytochrome *bd* Expression in the Obligate Aerobe *Azotobacter Vinelandii* by CydR (Fnr). Sensitivity to Oxygen, Reactive Oxygen Species, and Nitric Oxide. *J. Biol. Chem.* **2000,** *275* (7), 4679–4686.
700. Gruner, I.; Fradrich, C.; Bottger, L. H.; Trautwein, A. X.; Jahn, D.; Hartig, E. Aspartate 141 Is the Fourth Ligand of the Oxygen-Sensing $[4Fe\text{-}4S]^{2+}$ Cluster of *Bacillus subtilis* Transcriptional Regulator Fnr. *J. Biol. Chem.* **2011,** *286* (3), 2017–2021.
701. Reents, H.; Gruner, I.; Harmening, U.; Bottger, L. H.; Layer, G.; Heathcote, P.; Trautwein, A. X.; Jahn, D.; Hartig, E. *Bacillus subtilis* Fnr Senses Oxygen Via a [4Fe-4S] Cluster Coordinated by Three Cysteine Residues without Change in the Oligomeric State. *Mol. Microbiol.* **2006,** *60* (6), 1432–1445.
702. Sawers, R. G. Identification and Molecular Characterization of a Transcriptional Regulator from Pseudomonas Aeruginosa PAO1 Exhibiting Structural and Functional Similarity to the FNR Protein of *Escherichia coli*. *Mol. Microbiol.* **1991,** *5* (6), 1469–1481.
703. Zimmermann, A.; Reimmann, C.; Galimand, M.; Haas, D. Anaerobic Growth and Cyanide Synthesis of *Pseudomonas Aeruginosa* Depend on *Anr*, a Regulatory Gene Homologous with *Fnr* of *Escherichia coli*. *Mol. Microbiol.* **1991,** *5* (6), 1483–1490.
704. Ray, A.; Williams, H. D. The Effects of Mutation of the Anr Gene on the Aerobic Respiratory Chain of *Pseudomonas aeruginosa*. *FEMS Microbiol. Lett.* **1997,** *156* (2), 227–232.
705. Ugidos, A.; Morales, G.; Rial, E.; Williams, H. D.; Rojo, F. The Coordinate Regulation of Multiple Terminal Oxidases by the *Pseudomonas putida* ANR Global Regulator. *Environ. Microbiol.* **2008,** *10* (7), 1690–1702.
706. Schreiber, K.; Krieger, R.; Benkert, B.; Eschbach, M.; Arai, H.; Schobert, M.; Jahn, D. The Anaerobic Regulatory Network Required for *Pseudomonas aeruginosa* Nitrate Respiration. *J. Bacteriol.* **2007,** *189* (11), 4310–4314.
707. Trunk, K.; Benkert, B.; Quack, N.; Munch, R.; Scheer, M.; Garbe, J.; Jansch, L.; Trost, M.; Wehland, J.; Buer, J.; Jahn, M.; Schobert, M.; Jahn, D. Anaerobic Adaptation in *Pseudomonas aeruginosa*: Definition of the Anr and Dnr Regulons. *Environ. Microbiol.* **2010,** *12* (6), 1719–1733.
708. Tribelli, P. M.; Lujan, A. M.; Pardo, A.; Ibarra, J. G.; Fernandez Do Porto, D.; Smania, A.; Lopez, N. I. Core Regulon of the Global Anaerobic Regulator ANR Targets Central Metabolism Functions in *Pseudomonas* Species. *Sci. Rep.* **2019,** *9* (1), 9065.
709. Yoon, S. S.; Karabulut, A. C.; Lipscomb, J. D.; Hennigan, R. F.; Lymar, S. V.; Groce, S. L.; Herr, A. B.; Howell, M. L.; Kiley, P. J.; Schurr, M. J.; Gaston, B.; Choi, K. H.; Schweizer, H. P.; Hassett, D. J. Two-Pronged Survival Strategy for the Major Cystic Fibrosis Pathogen, *Pseudomonas aeruginosa*, Lacking the Capacity to Degrade Nitric Oxide during Anaerobic Respiration. *EMBO J.* **2007,** *26* (15), 3662–3672.
710. Ibrahim, S. A.; Crack, J. C.; Rolfe, M. D.; Borrero-de Acuna, J. M.; Thomson, A. J.; Le Brun, N. E.; Schobert, M.; Stapleton, M. R.; Green, J. Three *Pseudomonas putida* FNR Family Proteins with Different Sensitivities to O_2. *J. Biol. Chem.* **2015,** *290* (27), 16812–16823.
711. Ding, H.; Hidalgo, E.; Demple, B. The Redox State of the [2Fe-2S] Clusters in SoxR Protein Regulates its Activity as a Transcription Factor. *J. Biol. Chem.* **1996,** *271* (52), 33173–33175.
712. Seo, S. W.; Kim, D.; Szubin, R.; Palsson, B. O. Genome-Wide Reconstruction of OxyR and SoxRS Transcriptional Regulatory Networks under Oxidative Stress in *Escherichia coli* K-12 MG1655. *Cell Rep.* **2015,** *12* (8), 1289–1299.
713. Pomposiello, P. J.; Bennik, M. H.; Demple, B. Genome-Wide Transcriptional Profiling of the *Escherichia coli* Responses to Superoxide Stress and Sodium Salicylate. *J. Bacteriol.* **2001,** *183* (13), 3890–3902.
714. Blanchard, J. L.; Wholey, W. Y.; Conlon, E. M.; Pomposiello, P. J. Rapid Changes in Gene Expression Dynamics in Response to Superoxide Reveal SoxRS-Dependent and Independent Transcriptional Networks. *PLoS One* **2007,** *2* (11), e1186.
715. Palma, M.; Zurita, J.; Ferreras, J. A.; Worgall, S.; Larone, D. H.; Shi, L.; Campagne, F.; Quadri, L. E. *Pseudomonas aeruginosa* SoxR Does Not Conform to the Archetypal Paradigm for SoxR-Dependent Regulation of the Bacterial Oxidative Stress Adaptive Response. *Infect. Immun.* **2005,** *73* (5), 2958–2966.
716. Dietrich, L. E.; Price-Whelan, A.; Petersen, A.; Whiteley, M.; Newman, D. K. The Phenazine Pyocyanin Is a Terminal Signalling Factor in the Quorum Sensing Network of *Pseudomonas aeruginosa*. *Mol. Microbiol.* **2006,** *61* (5), 1308–1321.

717. Dietrich, L. E.; Teal, T. K.; Price-Whelan, A.; Newman, D. K. Redox-Active Antibiotics Control Gene Expression and Community Behavior in Divergent Bacteria. *Science* **2008,** *321* (5893), 1203–1206.
718. Singh, A. K.; Shin, J. H.; Lee, K. L.; Imlay, J. A.; Roe, J. H. Comparative Study of SoxR Activation by Redox-Active Compounds. *Mol. Microbiol.* **2013,** *90* (5), 983–996.
719. Naseer, N.; Shapiro, J. A.; Chander, M. RNA-Seq Analysis Reveals a Six-Gene SoxR Regulon in *Streptomyces coelicolor*. *PLoS One* **2014,** *9* (8), e106181.
720. Shin, J. H.; Singh, A. K.; Cheon, D. J.; Roe, J. H. Activation of the SoxR Regulon in *Streptomyces coelicolor* by the Extracellular Form of the Pigmented Antibiotic Actinorhodin. *J. Bacteriol.* **2011,** *193* (1), 75–81.
721. Park, W.; Pena-Llopis, S.; Lee, Y.; Demple, B. Regulation of Superoxide Stress in *Pseudomonas putida* KT2440 Is Different from the SoxR Paradigm in *Escherichia coli*. *Biochem. Bioph. Res. Co* **2006,** *341* (1), 51–56.
722. Kobayashi, K.; Tagawa, S. Activation of SoxR-Dependent Transcription in *Pseudomonas aeruginosa*. *J. Biochem.* **2004,** *136* (5), 607–615.
723. Bradley, T. M.; Hidalgo, E.; Leautaud, V.; Ding, H.; Demple, B. Cysteine-to-Alanine Replacements in the *Escherichia coli* SoxR Protein and the Role of the [2Fe-2S] Centers in Transcriptional Activation. *Nucleic Acids Res.* **1997,** *25* (8), 1469–1475.
724. Hidalgo, E.; Demple, B. An Iron-Sulfur Center Essential for Transcriptional Activation by the Redox-Sensing SoxR Protein. *EMBO J.* **1994,** *13* (1), 138–146.
725. Hidalgo, E.; Bollinger, J. M., Jr.; Bradley, T. M.; Walsh, C. T.; Demple, B. Binuclear [2Fe-2S] Clusters in the *Escherichia coli* SoxR Protein and Role of the Metal Centers in Transcription. *J. Biol. Chem.* **1995,** *270* (36), 20908–20914.
726. Kobayashi, K.; Fujikawa, M.; Kozawa, T. Binding of Promoter DNA to SoxR Protein Decreases the Reduction Potential of the [2Fe-2S] Cluster. *Biochemistry* **2015,** *54* (2), 334–339.
727. Gorodetsky, A. A.; Dietrich, L. E.; Lee, P. E.; Demple, B.; Newman, D. K.; Barton, J. K. DNA Binding Shifts the Redox Potential of the Transcription Factor SoxR. *Proc. Natl. Acad. Sci. U. S. A.* **2008,** *105* (10), 3684–3689.
728. Watanabe, S.; Kita, A.; Kobayashi, K.; Miki, K. Crystal Structure of the [2Fe-2S] Oxidative-Stress Sensor SoxR Bound to DNA. *Proc. Natl. Acad. Sci. U. S. A.* **2008,** *105* (11), 4121–4126.
729. Hassan, H. M.; Fridovich, I. Superoxide Radical and the Oxygen Enhancement of the Toxicity of Paraquat in *Escherichia coli*. *J. Biol. Chem.* **1978,** *253* (22), 8143–8148.
730. Hassan, H. M.; Fridovich, I. Paraquat and *Escherichia coli*. Mechanism of Production of Extracellular Superoxide Radical. *J. Biol. Chem.* **1979,** *254* (21), 10846–10852.
731. Gu, M.; Imlay, J. A. The SoxRS Response of *Escherichia coli* Is Directly Activated by Redox-Cycling Drugs Rather than by Superoxide. *Mol. Microbiol.* **2011,** *79* (5), 1136–1150.
732. de Paiva, S. R.; Figueiredo, M. R.; Aragao, T. V.; Kaplan, M. A. Antimicrobial Activity *In Vitro* of Plumbagin Isolated from Plumbago Species. *Mem. Inst. Oswaldo Cruz* **2003,** *98* (7), 959–961.
733. Gerstel, A.; Zamarreno Beas, J.; Duverger, Y.; Bouveret, E.; Barras, F.; Py, B. Oxidative Stress Antagonizes Fluoroquinolone Drug Sensitivity Via the SoxR-SUF Fe-S Cluster Homeostatic Axis. *PLoS Genet.* **2020,** *16* (11), e1009198.
734. Koo, M. S.; Lee, J. H.; Rah, S. Y.; Yeo, W. S.; Lee, J. W.; Lee, K. L.; Koh, Y. S.; Kang, S. O.; Roe, J. H. A Reducing System of the Superoxide Sensor SoxR in *Escherichia coli*. *EMBO J.* **2003,** *22* (11), 2614–2622.
735. Kobayashi, K.; Tagawa, S. Isolation of Reductase for SoxR that Governs an Oxidative Response Regulon from *Escherichia coli*. *FEBS Lett.* **1999,** *451* (3), 227–230.
736. Krapp, A. R.; Humbert, M. V.; Carrillo, N. The soxRS Response of *Escherichia coli* Can Be Induced in the Absence of Oxidative Stress and Oxygen by Modulation of NADPH Content. *Microbiology* **2011,** *157* (Pt 4), 957–965.
737. Kobayashi, K. Sensing Mechanisms in the Redox-Regulated, [2Fe-2S] Cluster-Containing, Bacterial Transcriptional Factor SoxR. *Acc. Chem. Res.* **2017,** *50* (7), 1672–1678.
738. Fujikawa, M.; Kobayashi, K.; Kozawa, T. Redox-Dependent DNA Distortion in a SoxR Protein-Promoter Complex Studied Using Fluorescent Probes. *J. Biochem.* **2015,** *157* (5), 389–397.
739. Fujikawa, M.; Kobayashi, K.; Tsutsui, Y.; Tanaka, T.; Kozawa, T. Rational Tuning of Superoxide Sensitivity in SoxR, the [2Fe-2S] Transcription Factor: Implications of Species-Specific Lysine Residues. *Biochemistry* **2017,** *56* (2), 403–410.
740. Ding, H.; Demple, B. Direct Nitric Oxide Signal Transduction Via Nitrosylation of Iron-Sulfur Centers in the SoxR Transcription Activator. *Proc. Natl. Acad. Sci. U. S. A.* **2000,** *97* (10), 5146–5150.
741. Chander, M.; Demple, B. Functional Analysis of SoxR Residues Affecting Transduction of Oxidative Stress Signals into Gene Expression. *J. Biol. Chem.* **2004,** *279* (40), 41603–41610.
742. Fujikawa, M.; Kobayashi, K.; Kozawa, T. Mechanistic Studies on Formation of the Dinitrosyl Iron Complex of the [2Fe-2S] Cluster of SoxR Protein. *J. Biochem.* **2014,** *156* (3), 163–172.
743. Lo, F. C.; Lee, J. F.; Liaw, W. F.; Hsu, I. J.; Tsai, Y. F.; Chan, S. I.; Yu, S. S. The Metal Core Structures in the Recombinant *Escherichia coli* Transcriptional Factor SoxR. *Chemistry* **2012,** *18* (9), 2565–2577.
744. Imlay, J. A. Transcription Factors that Defend Bacteria against Reactive Oxygen Species. *Annu. Rev. Microbiol.* **2015,** *69,* 93–108.
745. Soliveri, J. A.; Gomez, J.; Bishai, W. R.; Chater, K. F. Multiple Paralogous Genes Related to the *Streptomyces coelicolor* Developmental Regulatory Gene *whiB* Are Present in *Streptomyces* and Other Actinomycetes. *Microbiology* **2000,** *146* (Pt 2), 333–343.
746. Bush, M. J. The Actinobacterial WhiB-Like (Wbl) Family of Transcription Factors. *Mol. Microbiol.* **2018,** *110* (5), 663–676.
747. Rybniker, J.; Nowag, A.; van Gumpel, E.; Nissen, N.; Robinson, N.; Plum, G.; Hartmann, P. Insights into the Function of the WhiB-Like Protein of Mycobacteriophage TM4-a Transcriptional Inhibitor of WhiB2. *Mol. Microbiol.* **2010,** *77* (3), 642–657.
748. Fowler-Goldsworthy, K.; Gust, B.; Mouz, S.; Chandra, G.; Findlay, K. C.; Chater, K. F. The Actinobacteria-Specific Gene wblA Controls Major Developmental Transitions in *Streptomyces coelicolor* A3(2). *Microbiology* **2011,** *157* (Pt 5), 1312–1328.
749. den Hengst, C. D.; Buttner, M. J. Redox Control in Actinobacteria. *Biochim. Biophys. Acta* **2008,** *1780* (11), 1201–1216.
750. Mehta, M.; Singh, A. *Mycobacterium tuberculosis* WhiB3 Maintains Redox Homeostasis and Survival in Response to Reactive Oxygen and Nitrogen Species. *Free Radic. Biol. Med.* **2019,** *131,* 50–58.
751. Alam, M. S.; Garg, S. K.; Agrawal, P. Studies on Structural and Functional Divergence among Seven WhiB Proteins of *Mycobacterium tuberculosis* H37Rv. *FEBS J.* **2009,** *276* (1), 76–93.
752. Smith, L. J.; Stapleton, M. R.; Fullstone, G. J.; Crack, J. C.; Thomson, A. J.; Le Brun, N. E.; Hunt, D. M.; Harvey, E.; Adinolfi, S.; Buxton, R. S.; Green, J. *Mycobacterium tuberculosis* WhiB1 Is an Essential DNA-Binding Protein with a Nitric Oxide-Sensitive Iron-Sulfur Cluster. *Biochem. J.* **2010,** *432* (3), 417–427.
753. Singh, A.; Guidry, L.; Narasimhulu, K. V.; Mai, D.; Trombley, J.; Redding, K. E.; Giles, G. I.; Lancaster, J. R., Jr.; Steyn, A. J. *Mycobacterium tuberculosis* WhiB3 Responds to O2 and Nitric Oxide Via its [4Fe-4S] Cluster and Is Essential for Nutrient Starvation Survival. *Proc. Natl. Acad. Sci. U. S. A.* **2007,** *104* (28), 11562–11567.
754. Jakimowicz, P.; Cheesman, M. R.; Bishai, W. R.; Chater, K. F.; Thomson, A. J.; Buttner, M. J. Evidence that the *Streptomyces* Developmental Protein WhiD, a Member of the WhiB Family, Binds a [4Fe-4S] Cluster. *J. Biol. Chem.* **2005,** *280* (9), 8309–8315.
755. Wan, T.; Horova, M.; Beltran, D. G.; Li, S.; Wong, H. X.; Zhang, L. M. Structural Insights into the Functional Divergence of WhiB-Like Proteins in *Mycobacterium tuberculosis*. *Mol. Cell* **2021,** *81* (14), 2887–2900 e5.
756. Kudhair, B. K.; Hounslow, A. M.; Rolfe, M. D.; Crack, J. C.; Hunt, D. M.; Buxton, R. S.; Smith, L. J.; Le Brun, N. E.; Williamson, M. P.; Green, J. Structure of a Wbl Protein and Implications for NO Sensing by *M. tuberculosis*. *Nat. Commun.* **2017,** *8* (1), 2280.
757. Crack, J. C.; Smith, L. J.; Stapleton, M. R.; Peck, J.; Watmough, N. J.; Buttner, M. J.; Buxton, R. S.; Green, J.; Oganesyan, V. S.; Thomson, A. J.; Le Brun, N. E. Mechanistic Insight into the Nitrosylation of the [4Fe-4S] Cluster of WhiB-Like Proteins. *J. Am. Chem. Soc.* **2011,** *133* (4), 1112–1121.
758. Ramon-Garcia, S.; Ng, C.; Jensen, P. R.; Dosanjh, M.; Burian, J.; Morris, R. P.; Folcher, M.; Eltis, L. D.; Grzesiek, S.; Nguyen, L.; Thompson, C. J. WhiB7, an Fe-S-Dependent Transcription Factor that Activates Species-Specific Repertoires of Drug Resistance Determinants in Actinobacteria. *J. Biol. Chem.* **2013,** *288* (48), 34514–34528.

759. Crack, J. C.; den Hengst, C. D.; Jakimowicz, P.; Subramanian, S.; Johnson, M. K.; Buttner, M. J.; Thomson, A. J.; Le Brun, N. E. Characterization of [4Fe-4S]-Containing and Cluster-Free Forms of *Streptomyces* WhiD. *Biochemistry* **2009,** *48* (51), 12252–12264.
760. Wan, T.; Li, S.; Beltran, D. G.; Schacht, A.; Zhang, L.; Becker, D. F.; Zhang, L. Structural Basis of Non-canonical Transcriptional Regulation by the sigmaA-Bound Iron-Sulfur Protein WhiB1 in *M. tuberculosis*. *Nucleic Acids Res.* **2020,** *48* (2), 501–516.
761. Guo, M.; Feng, H.; Zhang, J.; Wang, W.; Wang, Y.; Li, Y.; Gao, C.; Chen, H.; Feng, Y.; He, Z. G. Dissecting Transcription Regulatory Pathways through a New Bacterial One-Hybrid Reporter System. *Genome Res.* **2009,** *19* (7), 1301–1308.
762. Schlag, S.; Fuchs, S.; Nerz, C.; Gaupp, R.; Engelmann, S.; Liebeke, M.; Lalk, M.; Hecker, M.; Gotz, F. Characterization of the Oxygen-Responsive NreABC Regulon of *Staphylococcus aureus*. *J. Bacteriol.* **2008,** *190* (23), 7847–7858.
763. Barth, C.; Weiss, M. C.; Roettger, M.; Martin, W. F.; Unden, G. Origin and Phylogenetic Relationships of [4Fe-4S]-Containing O2 Sensors of Bacteria. *Environ. Microbiol.* **2018,** *20* (12), 4567–4586.
764. Fedtke, I.; Kamps, A.; Krismer, B.; Gotz, F. The Nitrate Reductase and Nitrite Reductase Operons and the narT Gene of *Staphylococcus carnosus* Are Positively Controlled by the Novel Two-Component System NreBC. *J. Bacteriol.* **2002,** *184* (23), 6624–6634.
765. Kamps, A.; Achebach, S.; Fedtke, I.; Unden, G.; Gotz, F. Staphylococcal NreB: An O(2)-Sensing Histidine Protein Kinase with an O(2)-Labile Iron-Sulphur Cluster of the FNR Type. *Mol. Microbiol.* **2004,** *52* (3), 713–723.
766. Unden, G.; Klein, R. Sensing of O_2 and Nitrate by Bacteria: Alternative Strategies for Transcriptional Regulation of Nitrate Respiration by O_2 and Nitrate. *Environ. Microbiol.* **2021,** *23* (1), 5–14.
767. Klein, R.; Kretzschmar, A. K.; Unden, G. Control of the Bifunctional O_2-Sensor Kinase NreB of *Staphylococcus carnosus* by the Nitrate Sensor NreA: Switching from Kinase to Phosphatase State. *Mol. Microbiol.* **2020,** *113* (2), 369–380.
768. Nilkens, S.; Koch-Singenstreu, M.; Niemann, V.; Gotz, F.; Stehle, T.; Unden, G. Nitrate/Oxygen Co-Sensing by an NreA/NreB Sensor Complex of *Staphylococcus carnosus*. *Mol. Microbiol.* **2014,** *91* (2), 381–393.
769. Mullner, M.; Hammel, O.; Mienert, B.; Schlag, S.; Bill, E.; Unden, G. A PAS Domain with an Oxygen Labile [4Fe-4S](2+) Cluster in the Oxygen Sensor Kinase NreB of *Staphylococcus carnosus*. *Biochemistry* **2008,** *47* (52), 13921–13932.
770. Reinhart, F.; Huber, A.; Thiele, R.; Unden, G. Response of the Oxygen Sensor NreB to Air In Vivo: Fe-S-Containing NreB and Apo-NreB in Aerobically and Anaerobically Growing *Staphylococcus carnosus*. *J. Bacteriol.* **2010,** *192* (1), 86–93.
771. Dong, G.; Witcher, S.; Outten, F. W.; Pilon, M. FeS Cluster Assembly: SUF System in Bacteria, Plastids and Archaea. In *Encyclopedia of Inorganic and Bioinorganic Chemistry;* 2017; pp 1–16.
772. Cheng, Y.; Lyu, M.; Yang, R.; Wen, Y.; Song, Y.; Li, J.; Chen, Z. SufR, a [4Fe-4S] Cluster-Containing Transcription Factor, Represses the *sufRBDCSU* Operon in *Streptomyces avermitilis* Iron-Sulfur Cluster Assembly. *Appl. Environ. Microbiol.* **2020,** *86* (18).
773. Anand, K.; Tripathi, A.; Shukla, K.; Malhotra, N.; Jamithireddy, A. K.; Jha, R. K.; Chaudhury, S. N.; Rajmani, R. S.; Ramesh, A.; Nagaraja, V.; Gopal, B.; Nagaraju, G.; Narain Seshayee, A. S.; Singh, A. *Mycobacterium tuberculosis* SufR Responds to Nitric Oxide Via its 4Fe-4S Cluster and regulates Fe-S Cluster Biogenesis for Persistence in Mice. *Redox Biol.* **2021,** *46*, 102062.
774. Maiti, B. K.; Moura, I.; Moura, J. J. G.; Pauleta, S. R. The Small Iron-Sulfur Protein from the ORP Operon Binds a [2Fe-2S] Cluster. *Biochim. Biophys. Acta* **2016,** *1857* (9), 1422–1429.
775. Fievet, A.; My, L.; Cascales, E.; Ansaldi, M.; Pauleta, S. R.; Moura, I.; Dermoun, Z.; Bernard, C. S.; Dolla, A.; Aubert, C. The Anaerobe-Specific Orange Protein Complex of *Desulfovibrio vulgaris* Hildenborough Is Encoded by Two Divergent Operons Coregulated by sigma54 and a Cognate Transcriptional Regulator. *J. Bacteriol.* **2011,** *193* (13), 3207–3219.
776. Fievet, A.; Merrouch, M.; Brasseur, G.; Eve, D.; Biondi, E. G.; Valette, O.; Pauleta, S. R.; Dolla, A.; Dermoun, Z.; Burlat, B.; Aubert, C. OrpR Is a Sigma(54) -Dependent Activator Using an Iron-Sulfur Cluster for Redox Sensing in *Desulfovibrio vulgaris* Hildenborough. *Mol. Microbiol.* **2021,** *116* (1), 231–244.
777. Pardoux, R.; Fievet, A.; Carreira, C.; Brochier-Armanet, C.; Valette, O.; Dermoun, Z.; Py, B.; Dolla, A.; Pauleta, S. R.; Aubert, C. The Bacterial MrpORP Is a Novel Mrp/NBP35 Protein Involved in Iron-Sulfur Biogenesis. *Sci. Rep.* **2019,** *9* (1), 712.
778. Carepo, M. S.; Carreira, C.; Grazina, R.; Zakrzewska, M. E.; Dolla, A.; Aubert, C.; Pauleta, S. R.; Moura, J. J.; Moura, I. Orange Protein from *Desulfovibrio alaskensis* G20: Insights into the Mo-Cu Cluster Protein-Assisted Synthesis. *J. Biol. Inorg. Chem.* **2016,** *21* (1), 53–62.
779. Carepo, M. S.; Pauleta, S. R.; Wedd, A. G.; Moura, J. J.; Moura, I. Mo-cu Metal Cluster Formation and Binding in an Orange Protein Isolated from *Desulfovibrio gigas*. *J. Biol. Inorg. Chem.* **2014,** *19* (4-5), 605–614.
780. Neca, A. J.; Soares, R.; Carepo, M. S.; Pauleta, S. R. Resonance Assignment of DVU2108 that Is Part of the Orange Protein Complex in *Desulfovibrio vulgaris* Hildenborough. *Biomol. NMR Assign.* **2016,** *10* (1), 117–120.
781. Pauleta, S. R.; Duarte, A. G.; Carepo, M. S.; Pereira, A. S.; Tavares, P.; Moura, I.; Moura, J. J. NMR Assignment of the Apo-Form of a *Desulfovibrio gigas* Protein Containing a Novel Mo-Cu Cluster. *Biomol. NMR Assign.* **2007,** *1* (1), 81–83.
782. Imlay, J. A. Iron-Sulphur Clusters and the Problem with Oxygen. *Mol. Microbiol.* **2006,** *59* (4), 1073–1082.
783. Rudolf, J.; Makrantoni, V.; Ingledew, W. J.; Stark, M. J.; White, M. F. The DNA Repair Helicases XPD and FancJ Have Essential Iron-Sulfur Domains. *Mol. Cell* **2006,** *23* (6), 801–808.
784. Liu, H.; Rudolf, J.; Johnson, K. A.; McMahon, S. A.; Oke, M.; Carter, L.; McRobbie, A. M.; Brown, S. E.; Naismith, J. H.; White, M. F. Structure of the DNA Repair Helicase XPD. *Cell* **2008,** *133* (5), 801–812.
785. Wolski, S. C.; Kuper, J.; Hanzelmann, P.; Truglio, J. J.; Croteau, D. L.; Van Houten, B.; Kisker, C. Crystal Structure of the FeS Cluster-Containing Nucleotide Excision Repair Helicase XPD. *PLoS Biol.* **2008,** *6* (6), e149.
786. Fan, L.; Fuss, J. O.; Cheng, Q. J.; Arvai, A. S.; Hammel, M.; Roberts, V. A.; Cooper, P. K.; Tainer, J. A. XPD Helicase Structures and Activities: Insights into the Cancer and Aging Phenotypes from XPD Mutations. *Cell* **2008,** *133* (5), 789–800.
787. Pugh, R. A.; Honda, M.; Spies, M. Ensemble and Single-Molecule Fluorescence-Based Assays to Monitor DNA Binding, Translocation, and Unwinding by Iron-Sulfur Cluster Containing Helicases. *Methods* **2010,** *51* (3), 313–321.
788. Ren, B.; Duan, X.; Ding, H. Redox Control of the DNA Damage-Inducible Protein DinG Helicase Activity Via its Iron-Sulfur Cluster. *J. Biol. Chem.* **2009,** *284* (8), 4829–4835.
789. Yeeles, J. T.; Cammack, R.; Dillingham, M. S. An Iron-Sulfur Cluster Is Essential for the Binding of Broken DNA by AddAB-Type Helicase-Nucleases. *J. Biol. Chem.* **2009,** *284* (12), 7746–7755.
790. Hirata, A.; Klein, B. J.; Murakami, K. S. The X-Ray Crystal Structure of RNA Polymerase from Archaea. *Nature* **2008,** *451* (7180), 851–854.
791. Hirata, A.; Murakami, K. S. Archaeal RNA Polymerase. *Curr. Opin. Struct. Biol.* **2009,** *19* (6), 724–731.
792. Korkhin, Y.; Unligil, U. M.; Littlefield, O.; Nelson, P. J.; Stuart, D. I.; Sigler, P. B.; Bell, S. D.; Abrescia, N. G. Evolution of Complex RNA Polymerases: The Complete Archaeal RNA Polymerase Structure. *PLoS Biol.* **2009,** *7* (5), e1000102.
793. Netz, D. J.; Stith, C. M.; Stumpfig, M.; Kopf, G.; Vogel, D.; Genau, H. M.; Stodola, J. L.; Lill, R.; Burgers, P. M.; Pierik, A. J. Eukaryotic DNA Polymerases Require an Iron-Sulfur Cluster for the Formation of Active Complexes. *Nat. Chem. Biol.* **2011,** *8* (1), 125–132.
794. Klinge, S.; Hirst, J.; Maman, J. D.; Krude, T.; Pellegrini, L. An Iron-Sulfur Domain of the Eukaryotic Primase Is Essential for RNA Primer Synthesis. *Nat. Struct. Mol. Biol.* **2007,** *14* (9), 875–877.
795. Weiner, B. E.; Huang, H.; Dattilo, B. M.; Nilges, M. J.; Fanning, E.; Chazin, W. J. An Iron-Sulfur Cluster in the C-Terminal Domain of the p58 Subunit of Human DNA Primase. *J. Biol. Chem.* **2007,** *282* (46), 33444–33451.

796. Sauguet, L.; Klinge, S.; Perera, R. L.; Maman, J. D.; Pellegrini, L. Shared Active Site Architecture between the Large Subunit of Eukaryotic Primase and DNA Photolyase. *PLoS One* **2010,** *5* (4), e10083.
797. Greenwood, C.; Selth, L. A.; Dirac-Svejstrup, A. B.; Svejstrup, J. Q. An Iron-Sulfur Cluster Domain in Elp3 Important for the Structural Integrity of Elongator. *J. Biol. Chem.* **2009,** *284* (1), 141–149.
798. Pokharel, S.; Campbell, J. L. Cross Talk between the Nuclease and Helicase Activities of Dna2: Role of an Essential Iron-Sulfur Cluster Domain. *Nucleic Acids Res.* **2012,** *40* (16), 7821–7830.
799. White, M. F.; Dillingham, M. S. Iron-Sulphur Clusters in Nucleic Acid Processing Enzymes. *Curr. Opin. Struct. Biol.* **2012,** *22* (1), 94–100.
800. Fu, W.; O'Handley, S.; Cunningham, R. P.; Johnson, M. K. The Role of the Iron-Sulfur Cluster in *Escherichia coli* Endonuclease III. A Resonance Raman Study. *J. Biol. Chem.* **1992,** *267* (23), 16135–16137.
801. Moe, E.; Sezer, M.; Hildebrandt, P.; Todorovic, S. Surface Enhanced Vibrational Spectroscopic Evidence for an Alternative DNA-Independent Redox Activation of Endonuclease III. *Chem. Commun. (Camb.)* **2015,** *51* (15), 3255–3257.
802. Hassan, A.; Macedo, L. J. A.; Souza, J. C. P.; Lima, F.; Crespilho, F. N. A Combined Far-FTIR, FTIR Spectromicroscopy, and DFT Study of the Effect of DNA Binding on the [4Fe4S] Cluster Site in EndoIII. *Sci. Rep.* **2020,** *10* (1), 1931.
803. Moe, E.; Rollo, F.; Silveira, C. M.; Sezer, M.; Hildebrandt, P.; Todorovic, S. Spectroelectrochemical Insights into Structural and Redox Properties of Immobilized Endonuclease III and its Catalytically Inactive Mutant. *Spectrochim. Acta A* **2018,** *188,* 149–154.
804. Boal, A. K.; Yavin, E.; Barton, J. K. DNA Repair Glycosylases with a [4Fe-4S] Cluster: A Redox Cofactor for DNA-Mediated Charge Transport? *J. Inorg. Biochem.* **2007,** *101* (11 − 12), 1913–1921.
805. Fuss, J. O.; Tsai, C. L.; Ishida, J. P.; Tainer, J. A. Emerging Critical Roles of Fe-S Clusters in DNA Replication and Repair. *Biochim. Biophys. Acta* **2015,** *1853* (6), 1253–1271.
806. Hinks, J. A.; Evans, M. C.; De Miguel, Y.; Sartori, A. A.; Jiricny, J.; Pearl, L. H. An Iron-Sulfur Cluster in the Family 4 Uracil-DNA Glycosylases. *J. Biol. Chem.* **2002,** *277* (19), 16936–16940.
807. David, S. S.; Williams, S. D. Chemistry of Glycosylases and Endonucleases Involved in Base-Excision Repair. *Chem. Rev.* **1998,** *98* (3), 1221–1262.
808. Krokan, H. E.; Bjoras, M. Base Excision Repair. *Cold Spring Harb. Perspect. Biol.* **2013,** *5* (4), a012583.
809. Dalhus, B.; Laerdahl, J. K.; Backe, P. H.; Bjoras, M. DNA base repair–recognition and initiation of catalysis. *FEMS Microbiol. Rev.* **2009,** *33* (6), 1044–1078.
810. Golinelli, M. P.; Chmiel, N. H.; David, S. S. Site-Directed Mutagenesis of the Cysteine Ligands to the [4Fe-4S] Cluster of *Escherichia coli* MutY. *Biochemistry* **1999,** *38* (22), 6997–7007.
811. Boal, A. K.; Yavin, E.; Lukianova, O. A.; O'Shea, V. L.; David, S. S.; Barton, J. K. DNA-Bound Redox Activity of DNA Repair Glycosylases Containing [4Fe-4S] Clusters. *Biochemistry* **2005,** *44* (23), 8397–8407.
812. Hoseki, J.; Okamoto, A.; Masui, R.; Shibata, T.; Inoue, Y.; Yokoyama, S.; Kuramitsu, S. Crystal Structure of a Family 4 Uracil-DNA Glycosylase from *Thermus thermophilus* HB8. *J. Mol. Biol.* **2003,** *333* (3), 515–526.
813. Yang, H.; Fitz-Gibbon, S.; Marcotte, E. M.; Tai, J. H.; Hyman, E. C.; Miller, J. H. Characterization of a Thermostable DNA Glycosylase Specific for U/G and T/G Mismatches from the Hyperthermophilic Archaeon *Pyrobaculum aerophilum*. *J. Bacteriol.* **2000,** *182* (5), 1272–1279.
814. Lee, C. H.; Kim, S. H.; Choi, J. I.; Choi, J. Y.; Lee, C. E.; Kim, J. Electron Paramagnetic Resonance Study Reveals a Putative Iron-Sulfur Cluster in Human rpS3 Protein. *Mol. Cells* **2002,** *13* (1), 154–156.
815. Guan, Y.; Manuel, R. C.; Arvai, A. S.; Parikh, S. S.; Mol, C. D.; Miller, J. H.; Lloyd, S.; Tainer, J. A. MutY Catalytic Core, Mutant and Bound Adenine Structures Define Specificity for DNA Repair Enzyme Superfamily. *Nat. Struct. Biol.* **1998,** *5* (12), 1058–1064.
816. Kuo, C. F.; McRee, D. E.; Fisher, C. L.; O'Handley, S. F.; Cunningham, R. P.; Tainer, J. A. Atomic Structure of the DNA Repair [4Fe-4S] Enzyme Endonuclease III. *Science* **1992,** *258* (5081), 434–440.
817. Fromme, J. C.; Verdine, G. L. Structure of a Trapped Endonuclease III-DNA Covalent Intermediate. *EMBO J.* **2003,** *22* (13), 3461–3471.
818. Chepanoske, C. L.; Golinelli, M. P.; Williams, S. D.; David, S. S. Positively Charged Residues within the Iron-Sulfur Cluster Loop of *E. coli* MutY Participate in Damage Recognition and Removal. *Arch. Biochem. Biophys.* **2000,** *380* (1), 11–19.
819. Cunningham, R. P.; Asahara, H.; Bank, J. F.; Scholes, C. P.; Salerno, J. C.; Surerus, K.; Munck, E.; McCracken, J.; Peisach, J.; Emptage, M. H. Endonuclease III Is an Iron-Sulfur Protein. *Biochemistry* **1989,** *28* (10), 4450–4455.
820. Porello, S. L.; Cannon, M. J.; David, S. S. A Substrate Recognition Role for the [4Fe-4S]2+ Cluster of the DNA Repair Glycosylase MutY. *Biochemistry* **1998,** *37* (18), 6465–6475.
821. Boon, E. M.; Livingston, A. L.; Chmiel, N. H.; David, S. S.; Barton, J. K. DNA-Mediated Charge Transport for DNA Repair. *Proc. Natl. Acad. Sci. U. S. A.* **2003,** *100* (22), 12543–12547.
822. Yavin, E.; Stemp, E. D.; O'Shea, V. L.; David, S. S.; Barton, J. K. Electron Trap for DNA-Bound Repair Enzymes: A Strategy for DNA-Mediated Signaling. *Proc. Natl. Acad. Sci. U. S. A.* **2006,** *103* (10), 3610–3614.
823. Barton, J. K.; Silva, R. M. B.; O'Brien, E. Redox Chemistry in the Genome: Emergence of the [4Fe4S] Cofactor in Repair and Replication. *Annu. Rev. Biochem.* **2019,** *88,* 163–190.
824. Bartels, P. L.; Zhou, A.; Arnold, A. R.; Nunez, N. N.; Crespilho, F. N.; David, S. S.; Barton, J. K. Electrochemistry of the [4Fe4S] Cluster in Base Excision Repair Proteins: Tuning the Redox Potential with DNA. *Langmuir* **2017,** *33* (10), 2523–2530.
825. Gorodetsky, A. A.; Boal, A. K.; Barton, J. K. Direct Electrochemistry of Endonuclease III in the Presence and Absence of DNA. *J. Am. Chem. Soc.* **2006,** *128* (37), 12082–12083.
826. Tse, E. C. M.; Zwang, T. J.; Barton, J. K. The Oxidation State of [4Fe4S] Clusters Modulates the DNA-Binding Affinity of DNA Repair Proteins. *J. Am. Chem. Soc.* **2017,** *139* (36), 12784–12792.
827. Silva, R. M. B.; Zhou, A.; Grodick, M. A.; Barton, J. K. DNA-Mediated Redox Signaling in Bacterial Nucleotide Excision Eepair by UvrC. *Biophys. J.* **2016,** *110* (3), 62a–63a.
828. Bartels, P. L.; Stodola, J. L.; Burgers, P. M. J.; Barton, J. K. A Redox Role for the [4Fe4S] Cluster of Yeast DNA Polymerase Delta. *J. Am. Chem. Soc.* **2017,** *139* (50), 18339–18348.
829. O'Brien, E.; Holt, M. E.; Thompson, M. K.; Salay, L. E.; Ehlinger, A. C.; Chazin, W. J.; Barton, J. K. The [4Fe4S] Cluster of Human DNA Primase Functions as a Redox Switch Using DNA Charge Transport. *Science* **2017,** *355* (6327).
830. Mui, T. P.; Fuss, J. O.; Ishida, J. P.; Tainer, J. A.; Barton, J. K. ATP-Stimulated, DNA-Mediated Redox Signaling by XPD, a DNA Repair and Transcription Helicase. *J. Am. Chem. Soc.* **2011,** *133* (41), 16378–16381.
831. Sontz, P. A.; Mui, T. P.; Fuss, J. O.; Tainer, J. A.; Barton, J. K. DNA Charge Transport as a First Step in Coordinating the Detection of Lesions by Repair Proteins. *Proc. Natl. Acad. Sci. U. S. A.* **2012,** *109* (6), 1856–1861.
832. Ekanger, L. A.; Oyala, P. H.; Moradian, A.; Sweredoski, M. J.; Barton, J. K. Nitric Oxide Modulates Endonuclease III Redox Activity by a 800 mV Negative Shift upon [Fe4S4] Cluster Nitrosylation. *J. Am. Chem. Soc.* **2018,** *140* (37), 11800–11810.
833. Boal, A. K.; Barton, J. K. Electrochemical Detection of Lesions in DNA. *Bioconjug. Chem.* **2005,** *16* (2), 312–321.
834. Hall, D. B.; Holmlin, R. E.; Barton, J. K. Oxidative DNA Damage through Long-Range Electron Transfer. *Nature* **1996,** *382* (6593), 731–735.
835. Genereux, J. C.; Boal, A. K.; Barton, J. K. DNA-Mediated Charge Transport in Redox Sensing and Signaling. *J. Am. Chem. Soc.* **2010,** *132* (3), 891–905.
836. Ye, H.; Rouault, T. A. Human Iron-Sulfur Cluster Assembly, Cellular Iron Homeostasis, and Disease. *Biochemistry* **2010,** *49* (24), 4945–4956.
837. Sheftel, A.; Stehling, O.; Lill, R. Iron-Sulfur Proteins in Health and Disease. *Trends Endocrinol. Metab.* **2010,** *21* (5), 302–314.

838. Read, A. D.; Bentley, R. E.; Archer, S. L.; Dunham-Snary, K. J. Mitochondrial Iron-Sulfur Clusters: Structure, Function, and an Emerging Role in Vascular Biology. *Redox Biol.* **2021,** *47*, 102164.
839. Kung, W. M.; Lin, M. S. The NFkappaB Antagonist CDGSH Iron-Sulfur Domain 2 Is a Promising Target for the Treatment of Neurodegenerative Diseases. *Int. J. Mol. Sci.* **2021,** *22* (2).
840. Liao, H. Y.; Liao, B.; Zhang, H. H. CISD2 Plays a Role in Age-Related Diseases and Cancer. *Biomed. Pharmacother.* **2021,** *138*, 111472.
841. Berndt, C.; Christ, L.; Rouhier, N.; Muhlenhoff, U. Glutaredoxins with Iron-Sulphur Clusters in Eukaryotes - Structure, Function and Impact on Disease. *Biochim. Biophys. Acta Bioenerg.* **2021,** *1862* (1), 148317.